

UNCLASSIFIED

AD NUMBER

ADB012970

LIMITATION CHANGES

TO:

Approved for public release; distribution is unlimited.

FROM:

Distribution authorized to U.S. Gov't. agencies only; Test and Evaluation; MAR 1976. Other requests shall be referred to Air Force Flight Dynamics Laboratory, Wright-Patterson AFB, OH 45433. This document contains export-controlled technical data.

AUTHORITY

AFWAL ltr, 12 Dec 1986

THIS PAGE IS UNCLASSIFIED

AD Bo 12 970

AUTHORITY:

AFWAL etc.,

12 Dec 86





ADB012970

AFFTC

AD No. \_\_\_\_\_  
DDC FILE COPY

AFFTC-TR-76-8 ✓



**HANDLING QUALITIES  
AND  
STABILITY DERIVATIVES  
OF THE  
X-24B RESEARCH AIRCRAFT**

**MARCH 1976**

**FINAL REPORT**

Distribution limited to U. S. Government agencies only (Test and Evaluation), March 1976. Other requests for this document must be referred to AFFDL (FXS), Wright-Patterson AFB, Ohio 45433.

Controlling Office: FDL/FXS  
Wright-Patterson AFB, Ohio 45433

**AIR FORCE FLIGHT TEST CENTER  
EDWARDS AIR FORCE BASE, CALIFORNIA  
AIR FORCE SYSTEMS COMMAND  
UNITED STATES AIR FORCE**

DDC  
APPROVED  
AUG 23 1976  
RECEIVED

This technical report was submitted under Job Order Number 1366AO by the Deputy Commander for Operations of the Air Force Flight Test Center, Edwards AFB, California 93521.

Foreign announcement and dissemination by the Defense Documentation Center are not authorized because of the technology restrictions of the U.S. Export Control Acts as implemented by AFR 400-10.

Prepared by:

This report has been reviewed  
and is approved for publications:

*Christopher J. Nagy*  
CHRISTOPHER J. NAGY  
Aerospace Engineer

*Thomas P. Stafford*  
THOMAS P. STAFFORD  
Major General, USAF  
Commander

*Paul W. Kirsten*  
PAUL W. KIRSTEN  
Aerospace Engineer

*Joseph A. Guthrie*  
JOSEPH A. GUTHRIE  
Colonel, USAF  
Deputy Commander for Operations

Qualified requesters may obtain copies of this report from the Defense Documentation Center, Cameron Station, Alexandria, Virginia 22314. Department of Defense contractors must be established for DDC services, or have "need to know" certified by cognizant military agency of their project or contract.

DDC release to NTIS is not authorized

When U.S. Government drawings, specifications, or other data are used for any purpose other than a definitely related government procurement operation, the government thereby incurs no responsibility nor any obligation whatsoever; and the fact that the government may have formulated, furnished, or in any way supplied the said drawings, specifications, or any other data is not to be regarded by implication or otherwise, as in any manner licensing the holder or any other person or corporation or conveying any rights or permission to manufacture, use or sell any patented invention that may in any way be related thereto.

Do not return this copy; retain or destroy.

ACCESSION IN	White Section	<input type="checkbox"/>
RTS	Red Section	<input type="checkbox"/>
DDC	Blue Section	<input type="checkbox"/>
UNCLASSIFIED		
JUSTIFICATION		
BY	DISTRIBUTION AVAILABILITY CODES	
DATE	AVAIL. at 1st SP. CAL	
		B

UNCLASSIFIED

SECURITY CLASSIFICATION OF THIS PAGE (When Data Entered)

REPORT DOCUMENTATION PAGE		READ INSTRUCTIONS BEFORE COMPLETING FORM
1. REPORT NUMBER AFTIC-TR-76-8 ✓	2. GOVT ACCESSION NO.	3. RECIPIENT'S CATALOG NUMBER
4. TITLE (and Subtitle) Handling Qualities and Stability Derivatives of the X-24B Research Aircraft.	5. TYPE OF REPORT & PERIOD COVERED Final report. 1 Aug 73 - 26 Nov 75	6. PERFORMING ORG. REPORT NUMBER
7. AUTHOR(s) Christopher J. Nagy Paul W. Kirsten	8. CONTRACT OR GRANT NUMBER(s)	9. PROGRAM ELEMENT, PROJECT, TASK AREA & WORK UNIT NUMBERS JON 1366AO
10. CONTROLLING OFFICE NAME AND ADDRESS Deputy Commander of Operations Air Force Flight Test Center Edwards AFB, CA 93523	11. REPORT DATE March 1976	12. NUMBER OF PAGES 275
13. CONTROLLING OFFICE NAME AND ADDRESS ASD/FXS Wright-Patterson AFB, Ohio 45433	14. SECURITY CLASS. (of this report) UNCLASSIFIED	15a. DECLASSIFICATION/DOWNGRADING SCHEDULE
14. MONITORING AGENCY NAME & ADDRESS (if different from Controlling Office) 12272p.	16. DISTRIBUTION STATEMENT (of this Report) Distribution limited to U.S. Government agencies only (Test and Evaluation), March 1976. Other requests for this document must be referred to AFFDL(FXS), Wright-Patterson AFB, Ohio 45433	
17. DISTRIBUTION STATEMENT (of the abstract entered in Block 20, if different from Report)		
18. SUPPLEMENTARY NOTES		
19. KEY WORDS (Continue on reverse side if necessary and identify by block number) X-24B                      research vehicle                      lifting body glide flight                      flight test                      wind tunnel handling qualities                      flying qualities                      stability and control parameter identification                      flight control systems                      limit cycle		
20. ABSTRACT (Continue on reverse side if necessary and identify by block number) This reports presents the handling qualities and stability derivatives of the X-24B research aircraft. Handling qualities were excellent for the subsonic flight and the approach and landing task. For transonic and supersonic flight, the rocket engine had a significant effect on flying qualities. Handling qualities with the rocket engine off were adequate to good. Power-on flying qualities were degraded by low directional stability. Roll and pitch control was adequate or good for all phases of flight.		

DD FORM 1 JAN 73 1473

EDITION OF 1 NOV 65 IS OBSOLETE

UNCLASSIFIED

SECURITY CLASSIFICATION OF THIS PAGE (When Data Entered)

D12 100

mt



UNCLASSIFIED

SECURITY CLASSIFICATION OF THIS PAGE(When Data Entered)

Block 19 continued:

rocket powered aircraft simulation derivative extraction  
structural resonance

Block 20 continued:

Predictions of the stability derivatives were accurate in most cases. Longitudinal stability derivatives were lower than predicted subsonically but agreed well at transonic and most supersonic Mach numbers. Sideslip derivatives agreed well except for the subsonic, mid-angle of attack range, where directional stability was higher than predicted, and the supersonic, mid-angle of attack range, where directional stability was lower than predicted. Power effects from the rocket engine produced significant degradations in sideslip derivatives. Control derivatives were equal to or slightly higher than predicted except for yaw-due-to-aileron, which was lower than wind tunnel estimates. Damping derivative data were scattered but generally agreed with pre-flight calculations.

SECURITY CLASSIFICATION OF THIS PAGE(When Data Entered)

## SUMMARY

This report discusses the handling qualities of the X-24B research aircraft and those design features which contributed to aircraft handling characteristics. These include a description of the aircraft, flight control system, and a discussion of wind tunnel and flight test stability derivatives of the aircraft.

Handling qualities, with a few minor exceptions, were excellent for subsonic flight and the approach and landing task. Handling qualities with the rocket engine off were adequate-to-good for the transonic and supersonic areas. Power-on flying qualities were degraded by low directional stability. Roll and pitch control was adequate or good for all phases of flight. Pilot-induced-oscillations in pitch and roll were nonexistent with the augmentation system on and present only at limited conditions with the augmentation system off.

Predictions of the stability derivatives were accurate in most cases. Values of angle of attack derivatives were lower than predicted subsonically but agreed well at transonic and supersonic Mach numbers. Sideslip derivatives agreed well except for the subsonic, mid-angle of attack range, where directional stability was higher than predicted, and the supersonic, high-angle of attack range where directional stability was lower than predicted. Power effects from the rocket engine were found to cause significant degradations in sideslip derivatives. Control derivatives were equal to or slightly higher than predicted except for yaw-due-to aileron, which was lower than wind tunnel estimates. Damping derivative data were scattered but generally agreed with pre-flight calculations.

Much of the flight control system was common to that used in the X-24A, and hence the design of new flight control system components was limited. New features included the addition of ailerons and the modification of the X-24A variable lower flap gearing to a fixed gain system. Specifications for these designs were determined by five degree-of-freedom simulator studies performed at the Air Force Flight Test Center. Performance of the flight control system was excellent. This was attributed, in part, to the use of subsystems that had already been developed and proven during the X-24A program.

## PREFACE

This report is written as one of several documenting the flight test program of the X-24B research aircraft. Other aspects of the test program are detailed in references 1, 2, and 11. The X-24B program was accomplished in a joint effort between the Air Force Flight Dynamics Laboratory (AFFDL), the Air Force Flight Test Center (AFFTC) and the National Aeronautics and Space Administration Dryden Flight Research Center (NASA-DFRC). Participation in the X-24B program was authorized by Project Directive 73-87 and was accomplished under JON 1366AO.

The authors wish to thank the hundreds of people who contributed to the success of the X-24B program. The teamwork and cooperation exhibited by members of AFFDL, AFFTC, and NASA-DFRC serve as an excellent model for future programs. Special acknowledgement and appreciation are extended to those who contributed to the publication of this report. Mr. David F. Richardson determined the longitudinal trim curves for the X-24B and is responsible for Appendix B. Capt. Dennis Penka performed some of the handling qualities analyses and developed the wind shear techniques discussed in Appendix C. Alex G. Sim, of NASA-DFRC extracted many of the flight test derivatives found in this report.

# table of contents

	Page No.
INTRODUCTION	11
Program Description	11
Vehicle Description	11
Aerodynamic Shape	11
Flight Control System	13
Configurations	13
X-24B HANDLING QUALITIES	21
General Handling Qualities	21
Test Methods	21
Pilot Ratings and Mission Tasks	21
Preflight Simulator Studies	27
Flight Test Handling Qualities	29
Launch Transient	29
Subsonic Handling Qualities (Mach = 0.3 - 0.6)	29
Longitudinal	29
Lateral-Directional	31
Transonic Handling Qualities (Mach = 0.6 - 1.0)	34
Longitudinal	37
Lateral-Directional	39
Supersonic Handling Qualities (Mach = 1.0 - 1.7)	41
Longitudinal	41
Lateral-Directional	41
Final Approach and Landing	44
Pilot Checkout Program	49

Confirmation of Preflight Simulator Predictions	Page No. 53
Pitchup Boundary	53
PIO Sensitivity	53
Handling Qualities Boundaries	53
STABILITY DERIVATIVE RESULTS	57
Method	57
Wind Tunnel Data	64
Data Plots and Points	64
Longitudinal Derivatives	67
Subsonic Configuration	67
Transonic Configuration	69
Lateral-Directional Derivatives	70
Subsonic Configuration	70
Transonic Configuration	73
Power Effects	76
Longitudinal Derivatives	76
Lateral-Directional Derivatives	79
Power Effects Flight	79
Aileron and Rudder Bias Effects	79
Aileron Bias	81
Rudder Bias	81
CONCLUSIONS	83
REFERENCES	85
Appendix A - Stability Derivatives	87
Appendix B - Longitudinal Trim Curves	177
Appendix C - Wind Shear Techniques	197
Appendix D - Flight Control System	207



System Description

System Performance

Faired Test Data

Appendix E - Preflight Simulator Studies

233

Aileron Authority and Rate Limit Determination

Pitch Gearing

Derivative Sensitivity

Lateral-Directional PIO Sensitivity

Aileron and Rudder Roll Reversal

Handling Qualities Study in the Gear Down Configuration

Aileron-To-Rudder Interconnect (KRA) Determination

SAS Gale Determination

## list of figures

	Page No.
1. X-24B Three-View Drawing	12
2. Aerodynamic Surfaces and Control Surface Definition	14
3. X-24B Configurations	18
4. Sideslip Derivatives at $4^\circ$ Angle of Attack	22
5. Sideslip Derivatives at $8^\circ$ Angle of Attack	23
6. Sideslip Derivatives at $12^\circ$ Angle of Attack	24
7. Cooper-Harper Rating Scale	26
8. Launch Transient Time History	28
9. Stick Fixed Configuration Change	30
10. SAS-On Configuration Change	32
11. SAS-Off Configuration Change	33
12. Transonic Longitudinal Trim Change	36
13. Pitchup Boundary	38
14. Supersonic Sideslip Time History	42
15. Elevator Crossover	46
16. Crosswind Landing	48
17. Flight-Measured Pitchup Boundary	52
18. Predicted Controllability Boundaries	55
19. Actual Controllability Boundaries	56
20. Longitudinal Derivative Extraction Test Conditions	58
21. Lateral-Directional Derivative Extraction Test Conditions	59
22. Derivatives Extracted from a PIO Maneuver	61-63
23. Pitching Moment Derivatives - $M = 0.4 - 0.6$ , Correlation Between Cornell and AFIT Wind Tunnel Data	66
24. Pitching Moment Derivatives - $M = 0.8$ , Correlation Between Cornell and AEDC Wind Tunnel Data	68
25. Sideslip Derivatives - $M = 0.4$ , Reynolds Number Effects	72

26. Tip Fin Separation Effects	Page No. 74
27. Power Effects Flight Results	78

#### Appendix A

A1-A26 Pitching Moment and Normal Force Derivatives	89-114
A27-A87 Sideslip, Aileron, Rudder, and Damping Derivatives	115-175

#### Appendix B

B1-B12 Longitudinal Trim Curves	179-190
B13 Longitudinal Trim Curves-Aileron Bias	191
B14 Longitudinal Trim Curves-Landing Gear Down	192
B15-B17 Longitudinal Trim Curves-Rocket Engine On	193-195

#### Appendix C

C1 Sidewinds Obtained by Computed Technique and Rawinsonde Measurement	199
C2 Sidewinds Obtained During Two Different Flight Phases	200
C3 Sidewinds Obtained by Computed Technique and Contrail Film Method	202
C4 Sidewinds Obtained by Several Different Techniques	204

#### Appendix D

D1 Flight Control System Schematic (Pitch and Roll)	208
D2 Flight Control System Schematic (Yaw)	210
D3 Control System Block Diagram	211
D4 Longitudinal Stick Characteristics	218
D5 Lateral Stick Characteristics	220
D6 Rudder Pedal Characteristics	221
D7 Rudder Bias, Lower Flap, and Full Pitch Deflections Versus Upper Flap Bias	222
D8 Aileron-to-Rudder Interconnect	223
D9 SAS Rate Feedback Gains and Authorities	224

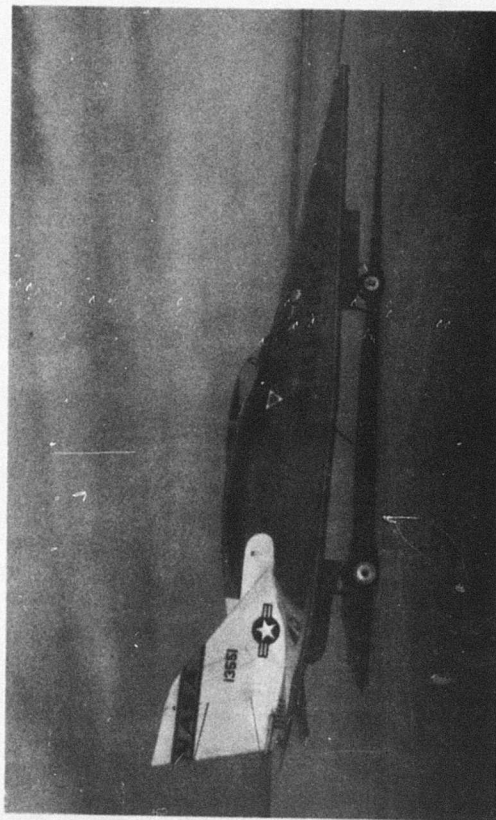
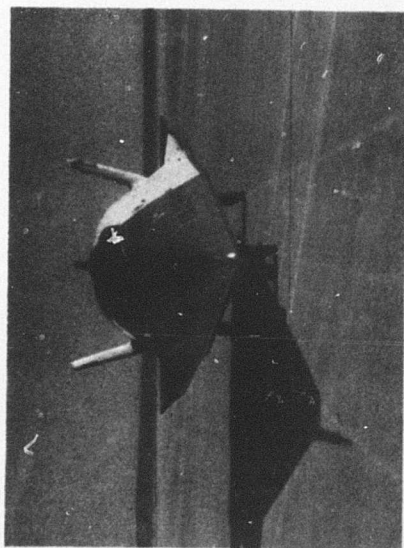
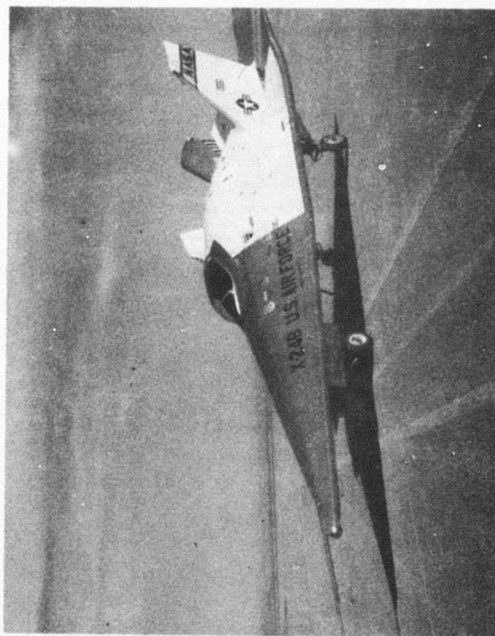
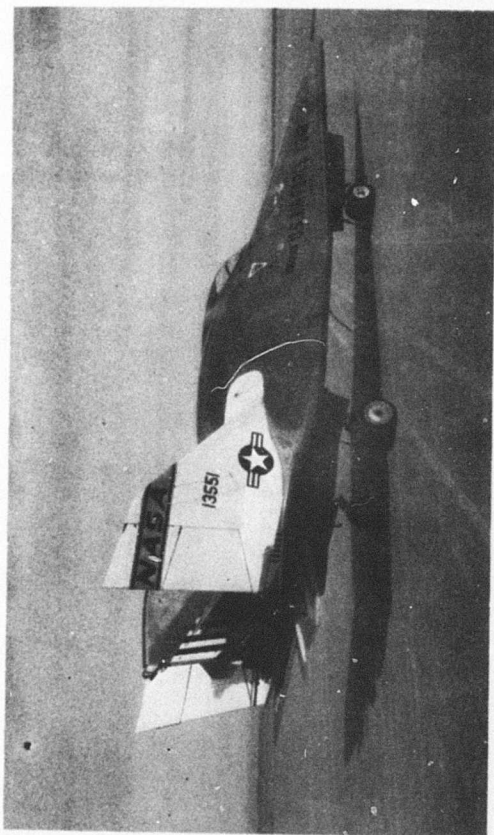
D10	Pitch Limit Cycle Characteristics	Page No. 226
D11	Roll Limit Cycle Characteristics	228
D12	Yaw Limit Cycle Characteristics	229
D13	Aileron Mechanical Resonance	230

#### Appendix E

E1	Aileron Surface Authority Determination	234
E2	Aileron Surface Rate Limit Determination	236
E3	Aileron Design Requirements	237
E4	Aileron Actuator Characteristics	238
E5	Pitch Surface Authority Determination	240
E6-E11	Derivative Sensitivity Results	242-248
E12-E14	Predicted Roll Performance	250-252
E15	Predicted Lateral-Directional PIO Boundaries (SAS Off)	253
E16	Predicted Lateral-Directional PIO Boundaries (SAS On)	254
E17	Predicted Roll Reversal Boundaries	256
E18	Landing Gear Effects on Handling Qualities	258
E19	Aileron-to-Rudder Interconnect Schedules	260
E20	Dutch Roll Root Locus Characteristics	262

## **list of tables**

	<b>Page No.</b>
1. X-24B Dimensions and Mass Characteristics	16&17
2. X-24B Pilot Ratings Summary	25
3. Pilot Ratings from Checkout Flights	50,51
4. Wind Tunnel Sources	65
5. Power Effect Flight Comparison	80
6. Aileron Bias and Lower Flap Pitching Moment Effectiveness	82
7. Rudder Bias Pitch Effectiveness	82





# INTRODUCTION

## Program Description

The task of designing an aircraft with reasonable hypersonic, supersonic, and subsonic performance is difficult, but when the additional requirement of adequate stability and good handling qualities is given, the task becomes a formidable challenge. The FDL-8 aerodynamic shape, from which the X-24B evolved, was designed to address this challenge, and the X-24B program proved the success of the design at subsonic and supersonic flight conditions.

The X-24B free flight tests were conducted between 1 August 1973 and 26 November 1975. The basic research flight program was primarily an incremental Mach number and angle of attack envelope expansion program requiring 6 glide flights and 24 powered flights. A typical mission began after launch from an NB-52B mothership. The rocket engine was ignited, and the aircraft accelerated to the planned maximum Mach number and altitude. After the rocket engine was shut down, the aircraft glided back to a landing on the Rogers Dry Lake. The total time for each powered flight was about seven minutes of which from three to four minutes were devoted to handling qualities, performance, and derivative extraction maneuvers. After completion of the 30-flight research program, 6 additional glide flights were flown to checkout 3 new pilots.

Two of the key objectives of the test program were: (1) to evaluate the aircraft's handling qualities and (2) to assess the ability of ground prediction techniques to accurately predict the flight characteristics of this unusual aerodynamic shape.<sup>1</sup> An overview of the flight test program is presented in reference 1.<sup>1</sup>

This report will discuss the X-24B handling qualities, which were good in most areas. Stability derivatives, which were extracted from flight test data, will be presented along with the corresponding wind tunnel predictions. The flight control system and its performance will also be discussed in some detail.

## Vehicle Description

### Aerodynamic Shape

The X-24B was a piloted, rocket-powered research aircraft with a double delta planform. The sweep of the planform was 78° on the forebody of the aircraft and 72° on the aft portion. The double delta configuration was adopted to provide the required static margin for adequate longitudinal stability by moving the aerodynamic center of pressure aft.

<sup>1</sup>Reference 1: Armstrong, Johnny G., Flight Planning and Conduct of the X-24B Research Aircraft Flight Test Program, AFFTC-TR-76-4, Air Force Flight Test Center, Edwards AFB, California, to be published.

The aircraft featured a flat bottom for increased hypersonic lift-to-drag ratio, with a  $30^\circ$  forebody ramp for hypersonic trim. The aircraft sides were sloped at  $60^\circ$  to maintain heating predictability and to add negative dihedral effect. The top of the aircraft was rounded and connected the two slanted sides. Directional stability was provided by two outboard vertical fins and a center fin. In addition to directional stability, the outboard fins also contributed a large positive dihedral effect. A three view drawing of the X-24B is shown in figure 1, and some typical mass and dimensional numbers are given in table 1. A more detailed discussion of the method of determining mass characteristics is contained in reference 1.

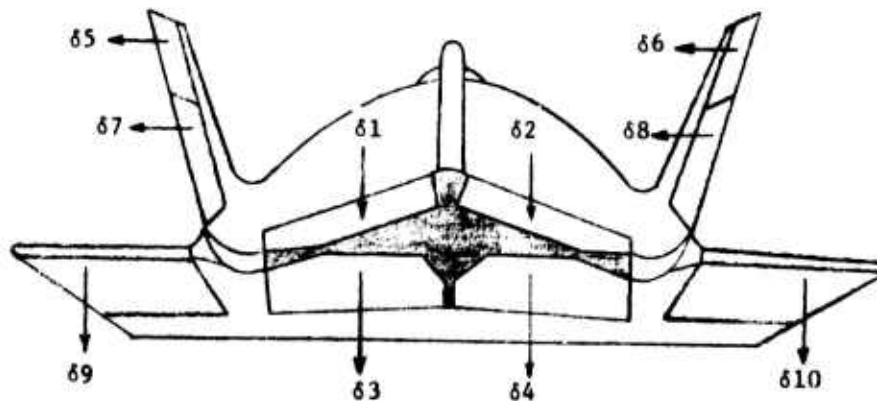
#### Flight Control System

The X-24B control system was basically a modification of the X-24A system. Ten surfaces were available for aerodynamic control of the X-24B. These consisted of the following: two upper flaps, two lower flaps, two upper rudders, two lower rudders, and two ailerons. These surfaces are depicted in figure 2. The two upper flaps were moved symmetrically as an upper flap bias ( $\delta U_p$ ). The two lower flaps also moved symmetrically and provided primary pitch control ( $\delta e_L$ ). When the lower flaps retracted to zero, pitch control was transferred mechanically to the upper flaps ( $\delta e_U$ ). All four rudders could be biased symmetrically as a rudder bias ( $\delta R_p$ ), and only the upper rudders ( $\delta r$ ) provided yaw control. The rudder bias differed from a rudder trim in that all four rudder biased inward or outward together; the rudder bias did not cause a yawing moment on the aircraft. The aileron surfaces could be deflected differentially ( $\delta a$ ) for roll control or could be biased symmetrically ( $\delta A_p$ ) for additional pitch trimming. Pilot inputs were provided through a conventional center stick for pitch and roll, and rudder pedals for yaw. The aircraft was artificially stabilized in all three axes by a triply-redundant, rate-feedback stability augmentation system (SAS). The SAS feedback gain for each axis was controlled by the pilot via a seven position rotary switch and a zero-gain mode switch. In addition to the pilot and SAS commands, two other inputs were made for yaw control. An aileron-to-rudder interconnect was provided to minimize adverse sideslip during aileron inputs, and, midway through the test program, a lateral acceleration feedback system was installed to help control steady-state-sideslip at transonic and supersonic Mach numbers with the rocket engine on. A complete description of the flight control system is included in Appendix D along with a review of system performance during the conduct of the flight program.

#### Configurations

The aircraft was flown in basically two configurations with minor variations on each. The high speed configuration was called the "transonic" configuration and was flown with the upper flaps bias at  $-40^\circ$ , the rudder bias at  $0^\circ$ , and the aileron bias at  $7^\circ$ . The low speed or "subsonic" configuration was used for approach and landing. The biases for this configuration were: upper flap bias at  $-20^\circ$ , rudder bias at  $-10^\circ$ , and aileron bias at  $7^\circ$ . These two configurations are shown in figure 3. The two configurations provided a trade-off between stability





$$\delta A_B = \frac{\delta 9 + \delta 10}{2}$$

$$\delta a = \delta 9 - \delta 10$$

$$\delta e_L = \frac{\delta 3 + \delta 4}{2}$$

$$\delta R_B = \frac{\delta 5 - \delta 6 + \delta 7 - \delta 8}{4}$$

$$\delta r = \frac{\delta 5 + \delta 6}{2}$$

$$\delta U_B = \frac{\delta 1 + \delta 2}{2}$$

Note: Arrows indicate positive deflection

Figure 2. Aerodynamic Surfaces and Control Surface Definition.

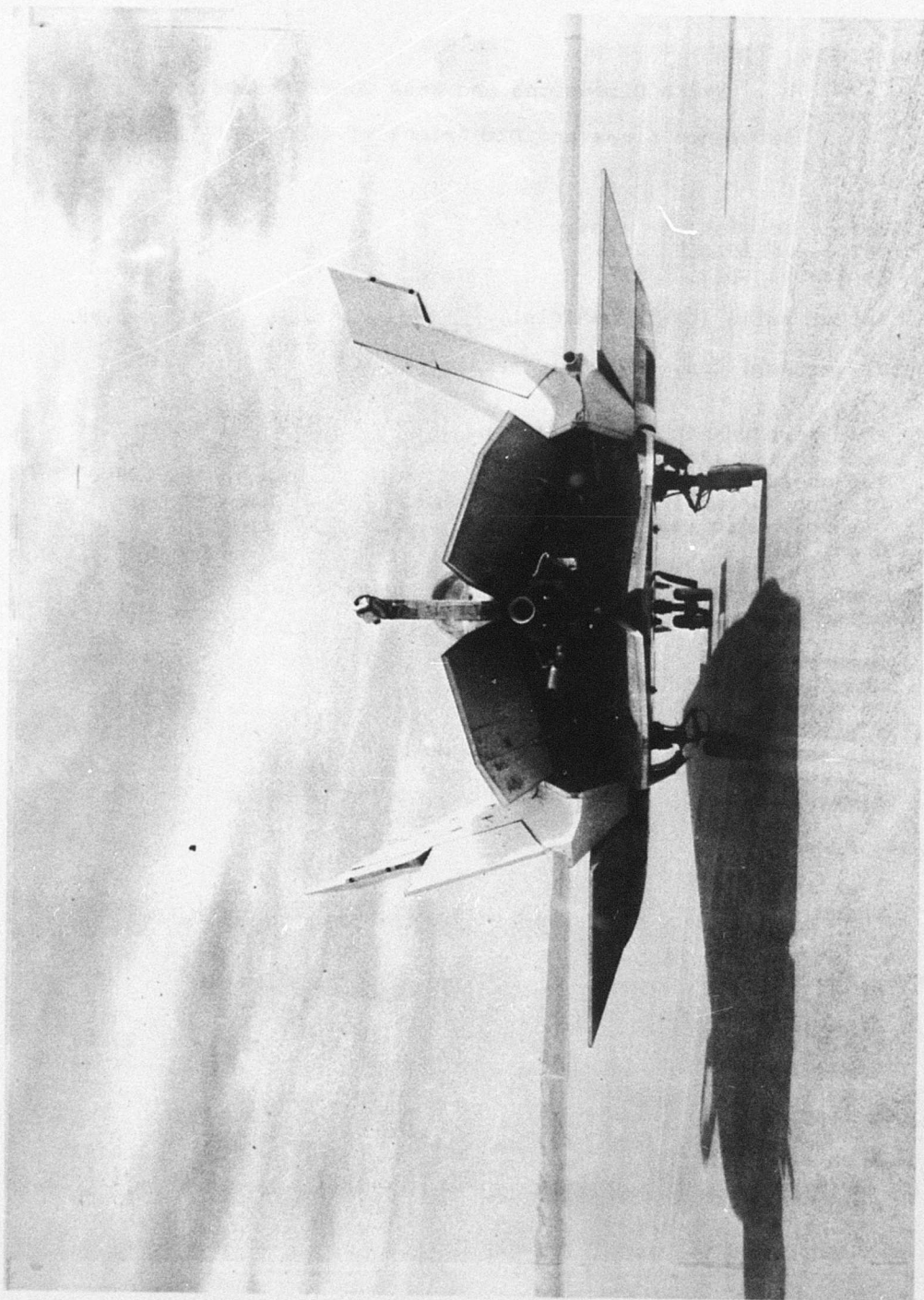


Table 1

## X-24B Dimensions and Mass Characteristics

## Reference Areas and Dimensions of the X-24B Vehicle

## Body -

Reference planform area, (ft <sup>2</sup> )	330.5
Reference length, (ft)	37.5
Reference span, (ft)	19.0
Aspect ratio (basic vehicle), $\frac{b^2}{S}$	1.09

## Center vertical fin, (airfoil stabilizer) -

Area, (ft <sup>2</sup> )	14.70
Mean aerodynamic chord, (in)	57.90
Root chord, (in)	73.90
Tip chord, (in)	38.00
Distance between root chord and mean aerodynamic center, (in)	17.30
Span, (in)	38.80

## Outboard vertical fin (airfoil cambered with leading edge droop) -

Area each, (ft <sup>2</sup> )	25.9
Mean aerodynamic chord, (in)	75.7
Root chord, (in)	101.5
Tip chord, (in)	41.5
Distance between root chord and mean aerodynamic chord, (in)	20.8
Span, (in)	50.1

## Upper rudder -

Area each, (ft <sup>2</sup> )	4.99
Chord, (in)	29.60
Span, (in)	24.20

## Lower rudder -

Area each, (ft <sup>2</sup> )	6.67
Chord, (in)	29.60
Span, (in)	34.20

## Upper flap -

Area each, (ft <sup>2</sup> )	10.82
Chord, (in)	34.10
Span, (in)	45.70

Table 1 (Concluded)

Lower flap -

Area each, (ft <sup>2</sup> )	13.99
Chord, (in)	44.90
Span, (in)	44.90

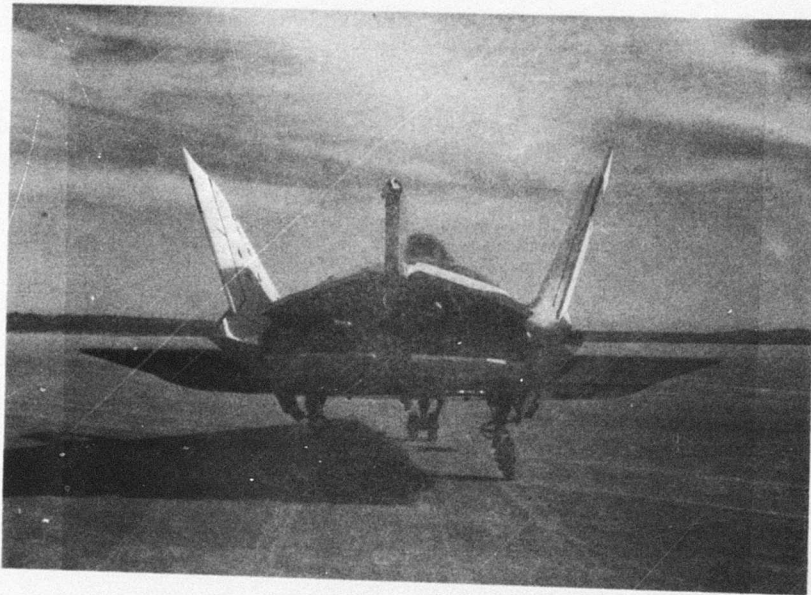
Typical Mass Characteristics of the X-24B Vehicle

Empty Aircraft

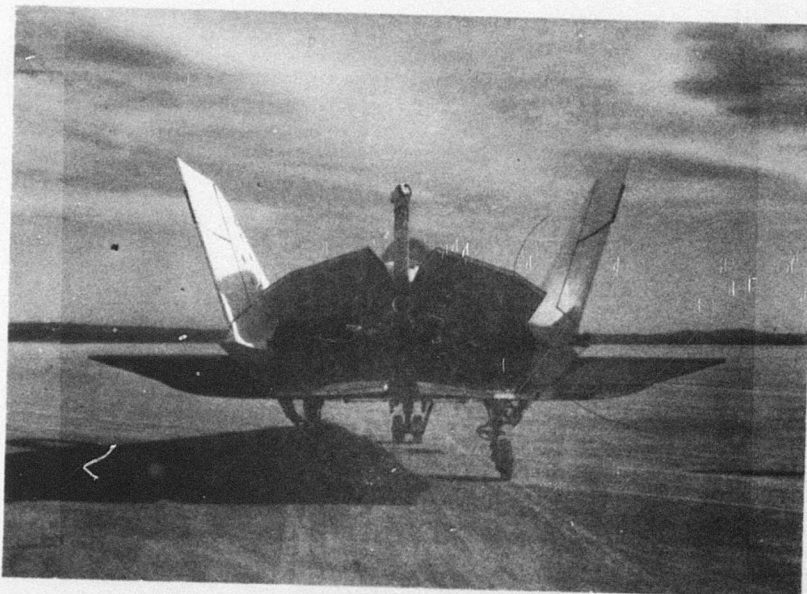
Weight (lb)	8500
x-cg (in)	126.0 (64%)
y-cg (in)	-0.5
z-cg (in)	22.5
I <sub>x</sub> (slug-ft <sup>2</sup> )	2700
I <sub>y</sub> (slug-ft <sup>2</sup> )	23500
I <sub>z</sub> (slug-ft <sup>2</sup> )	24000
I <sub>xz</sub> (slug-ft <sup>2</sup> )	700

Full Aircraft

Weight (lb)	14000
x-cg (in)	136.0 (66.2%)
y-cg (in)	-0.8
z-cg (in)	28.0
I <sub>x</sub> (slug-ft <sup>2</sup> )	3200
I <sub>y</sub> (slug-ft <sup>2</sup> )	25000
I <sub>z</sub> (slug-ft <sup>2</sup> )	25500
I <sub>xz</sub> (slug-ft <sup>2</sup> )	830



Subsonic Configuration -  $\delta U_B = -20^\circ$ ,  $\delta R_B = -10^\circ$ ,  $\delta A_B = 7^\circ$



Transonic Configuration -  $\delta U_B = -40^\circ$ ,  $\delta R_B = 0^\circ$ ,  $\delta A_B = 7^\circ$

Figure 3. X-24B Configurations



and performance. The subsonic configuration provided the lift-to-drag ratio required to flare and land the aircraft but did not have adequate stability for flight at Mach numbers much above 0.7. The transonic configuration provided satisfactory stability for transonic and supersonic flight but resulted in inadequate performance for landing. In addition, some perturbations of these configurations were flown during the test program to assess their effect on handling qualities, performance, and stability derivatives. These included moving the rudder bias to  $5^\circ$  with  $-40^\circ$  upper flap bias, flying with  $3^\circ$  and  $11^\circ$  on the aileron bias, and flying with the upper flap bias at  $-30^\circ$ . During the test program, the nominal upper flap bias settings were  $20^\circ$ ,  $25^\circ$  and  $28^\circ$ . These various bias settings were used to investigate landing approaches and different lift-to-drag ratios. Intermediate biases served as speedbrakes for energy management and glide path control. A discussion of these results is provided in reference 2.<sup>2</sup>

<sup>2</sup>Reference 2: Stuart, John L., Analysis of the Approach, Flare, and Landing Characteristics of the X-24B Research Aircraft, AFFTC-TR-76-9, Air Force Flight Test Center, Edwards AFB, California, to be published.



# **X-24B HANDLING QUALITIES**

## **General Handling Qualities**

The power-off handling qualities of the X-24B were good over most of the Mach angle of attack envelope. Most pilot ratings for X-24B mission tasks were between two and four. Considerable time was spent evaluating the SAS-off handling qualities at low Mach numbers, and pilots stated that the aircraft flew excellently. Some degradations occurred during the powered portion of flight when the rocket engine caused significantly lower levels of directional stability and relatively low values of dynamic pressure decreased control effectiveness. Figures 4 thru 6 show the primary derivatives which reflect the lateral-directional stability of the aircraft for three different angles of attack. The levels of stability as the Mach number changes present an excellent picture of the aircraft's handling qualities, and the strong influence of the rocket engine is apparent. The two areas of poor handling qualities were the transonic area at high angles of attack with the power on and the supersonic area above  $M=1.3$  at moderate angles of attack. Both of these areas were marked by low values of  $C_{n\beta}$  and  $C_{n\beta}^*$ .<sup>3</sup> Pilot rating develops for specific tasks during the X-24B mission are summarized in table 2.

## **Test Methods**

Due to flight profile control requirements and the relatively limited amount of stabilized flight time, many of the classical handling qualities maneuvers were not performed. The evaluation of the X-24B handling qualities was based on a study of time histories and the gathering of pilot comments and ratings.<sup>4</sup> Parameters describing the aircraft's stability and control were displayed in real time and were available for immediate observation. A pilot debriefing was held after each flight and the pilot was asked to comment and rate various phases and maneuvers of that flight. Pilots tended to evaluate the aircraft based on the ability to control angle of attack, heading angle, bank angle, rate of sink, etc. A good correlation could usually be made between the pilot's comments and the aircraft time histories. Most of the handling qualities descriptions in this report will be done via one or more of these modes of expression.

## **Pilot Ratings and Mission Tasks**

Since many of the handling qualities discussions in this report are enhanced by Cooper-Harper pilot ratings, it is essential to understand the tasks for which the pilot ratings were given. Almost all of the

<sup>3</sup> $C_{n\beta}^*$  or dynamic  $C_{n\beta}$  is a measure of dynamic dutch roll stability. Negative values of  $C_{n\beta}^*$  are conducive to a non-oscillatory directional divergence (nose slice) and loss of control.  $C_{n\beta}^*$  includes components of both  $C_{n\beta}$  and  $C_{l\beta}$  and is defined by the equation:

$$C_{n\beta}^* = C_{n\beta} \cos \alpha - (I_z/I_x) C_{l\beta} \sin \alpha - (I_{xz}/I_z)(C_{n\beta} \sin \alpha - C_{l\beta} \cos \alpha)$$

<sup>4</sup>All pilot ratings contained in this report are based on the Cooper-Harper scale shown in figure 7.



$\delta\alpha_0 = -40^\circ$ ,  $\delta\beta_0 = 0^\circ$ ,  $\delta\gamma_0 = 7^\circ$ ,  $c_g = 66\%$

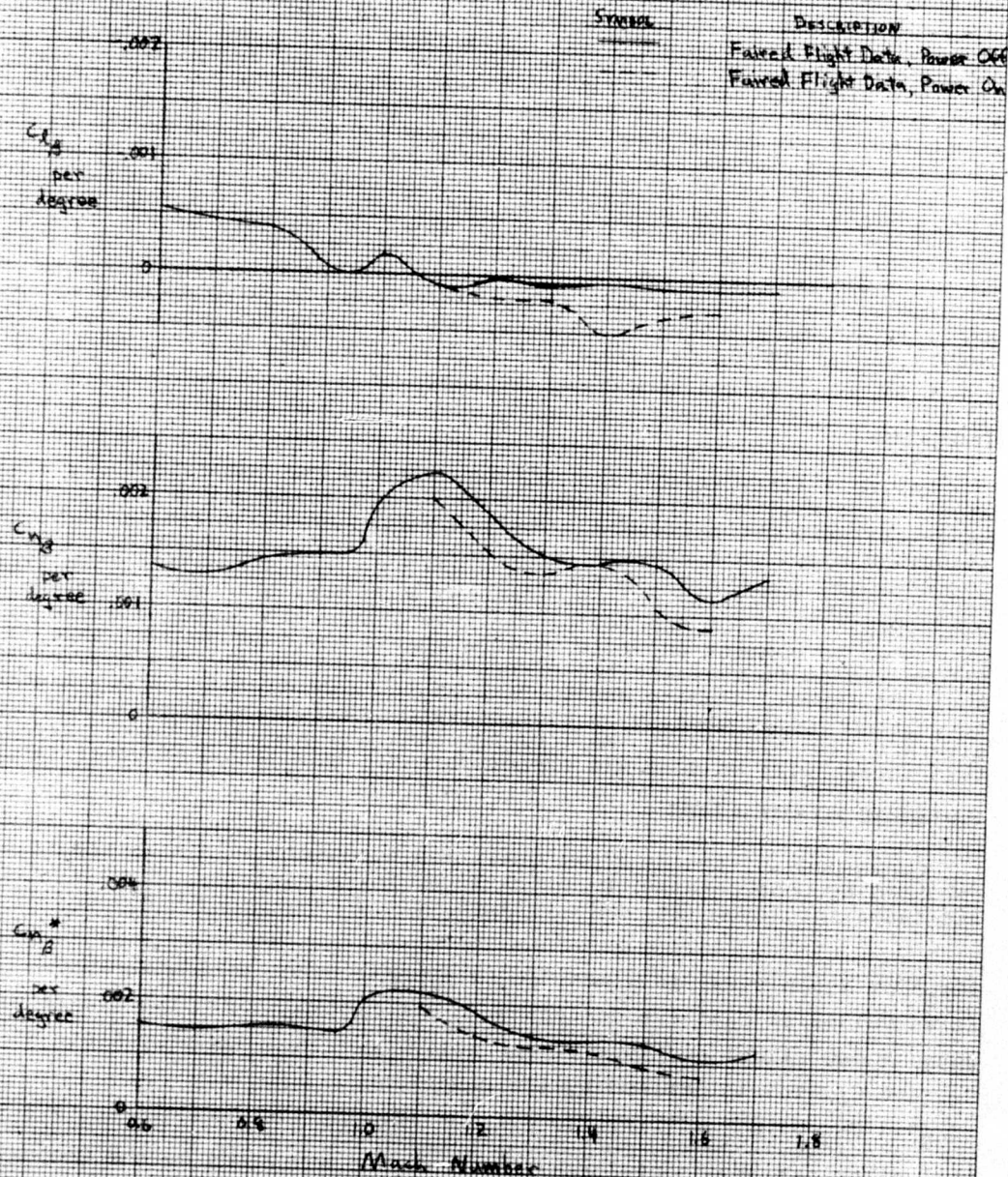


Figure 4 - Sideslip Derivatives At 4° Angle of Attack

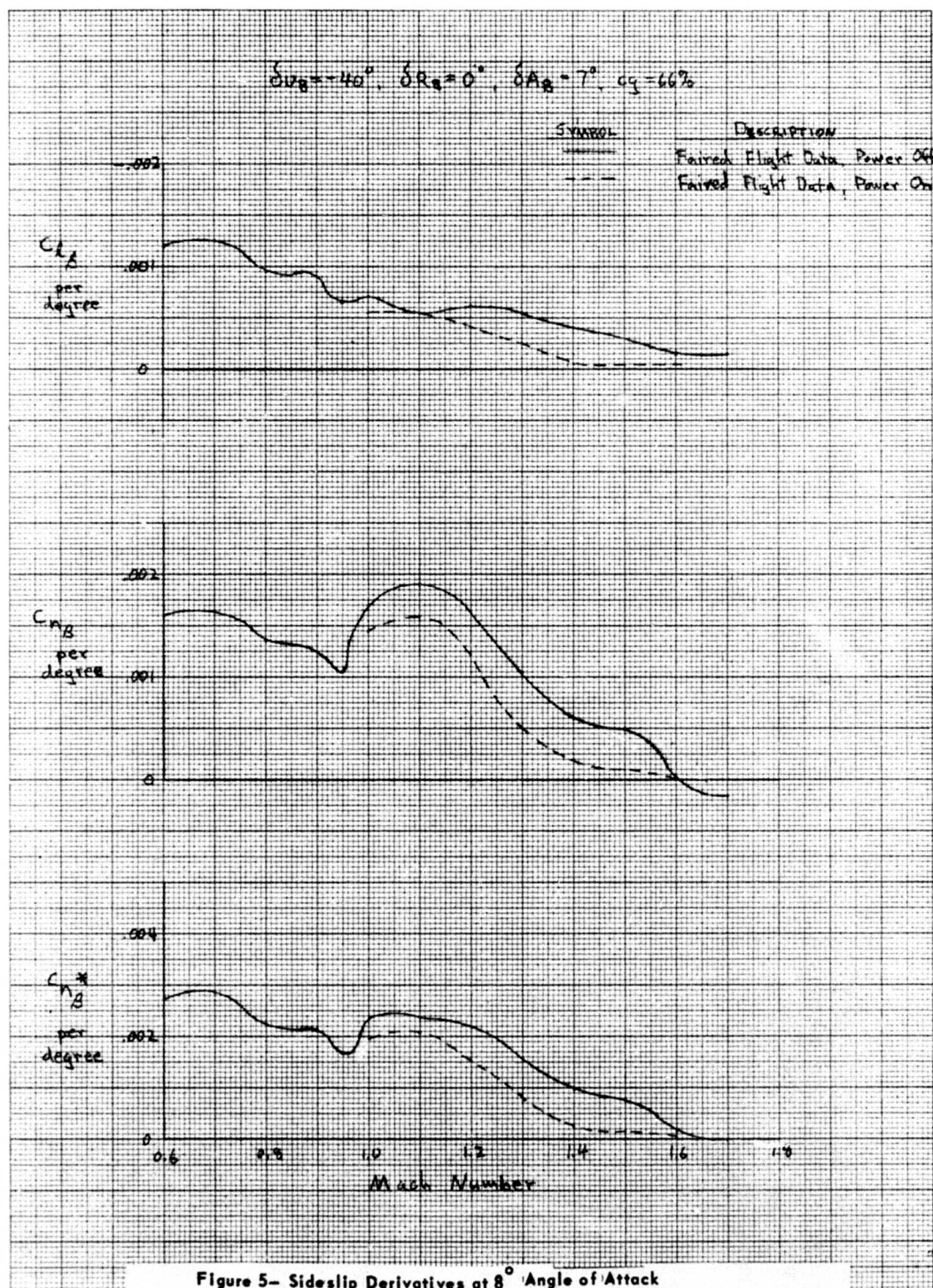


Figure 5- Sideslip Derivatives at  $8^\circ$  Angle of Attack



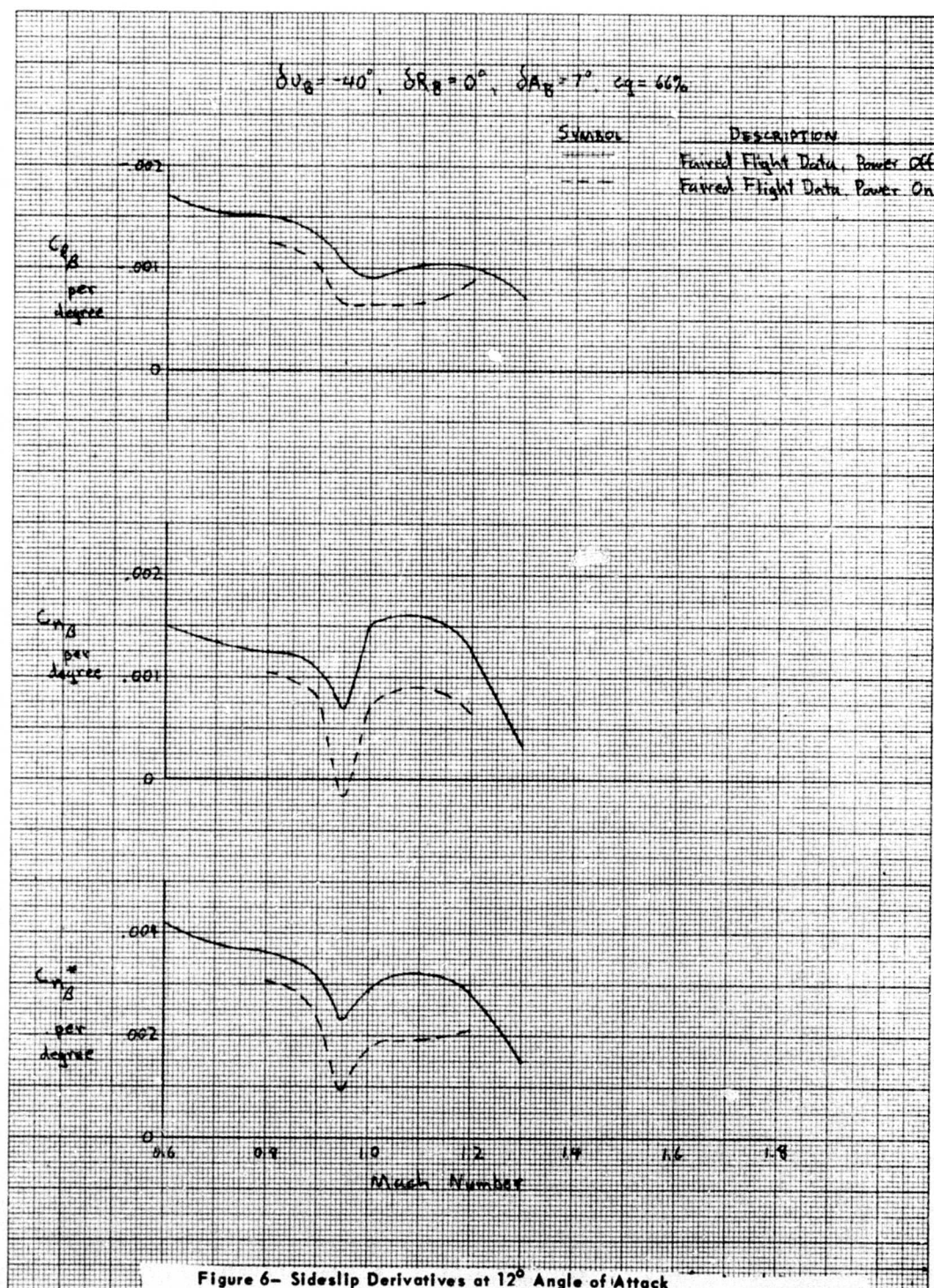
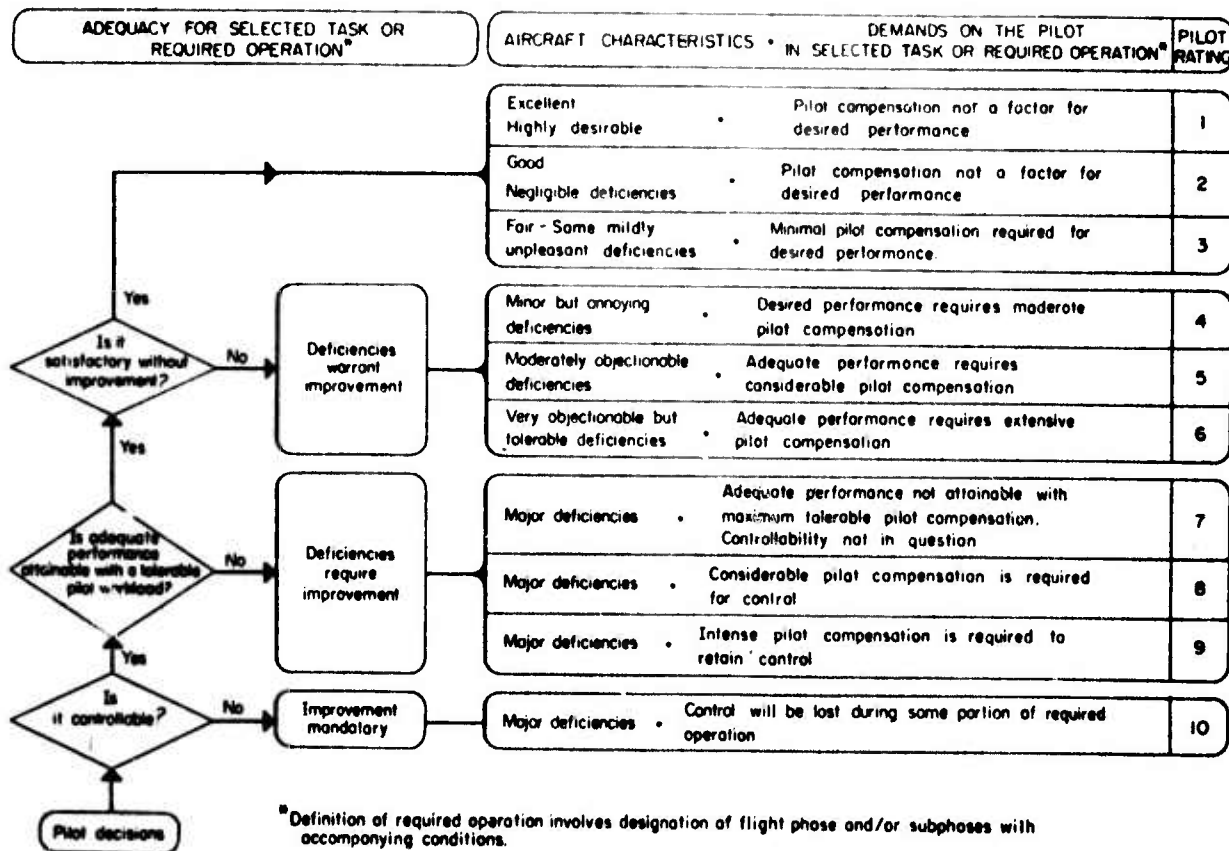


Figure 6- Sideslip Derivatives at 12° Angle of Attack

Table 2

## X-24B PILOT RATING

Launch Transient Recovery	
Pitch _____	3.0
Roll _____	3.0
Subsonic Handling Qualities	
Pitch _____	2.5
Roll/Yaw _____	2.0-2.5
Transonic Handling Qualities	
Pitch	
M=0.6-0.8 _____	2.0-2.5
M=0.8-1.0 _____	3.0-3.5
M=0.8-1.0 with yaw task _____	4.0
M=0.8-1.0 after experience _____	2.0-2.5
Low Dynamic pressure _____	0.5-1.0 degraded
Roll/Yaw	
M=0.6-0.8 _____	2.0-2.5
Transonic sideslip excursions (power-on) _____	4.5-6.0
Transonic sideslip excursions after improvement (power-on) _____	2.5
PIO (with aileron deadband) _____	4.0
M=0.8-1.0 (power-off) _____	2.0-2.5
Supersonic Handling Qualities	
Pitch _____	2.0-2.5
Roll/Yaw (power-on) _____	6.0
Final Approach and Landing	
Flare _____	1.0-2.0
Landing _____	2.0-3.0
Ground handling _____	3.0



**Figure 7- Cooper-Harper Rating Scale**

ratings were based on the tasks associated with the pilot maintaining the flight control parameters to achieve the required flight profile for each mission. After launch and engine light, the pilot established the specified angle of attack to arrest the descent and to establish the desired climb angle. During the climb, a lower angle of attack was maintained between 0.85 and 1.2 Mach number for lateral-directional stability reasons. At about 1.2 Mach number, a low angle of attack was established to allow the aircraft to accelerate to the planned maximum Mach number for the flight. During the powered boost portion of the flight, maintaining angle of attack was the primary task. Heading corrections, control of uncommand sideslip and roll excursions, and controlling the aircraft subsystems were tasks which demanded the pilots attention during this time, thereby increasing the difficulty of the primary task. The primary items utilized by the pilot for profile and ground track control were angle of attack (or pitch angle), altitude, indicated Mach number, engine burn time, and radio calls from the ground controller. In addition, some stability and control maneuvers were performed during this time to obtain data with the rocket engine on.

After the rocket engine was shut down (or burned out) the aircraft glided to "low key" where the landing approach pattern was initiated. This deceleration period was the prime time for flight data maneuvers. The primary piloting task during this time was to arrive at the desired Mach number and angle of attack combinations and to perform stability and control, performance, and structural loads maneuvers as required. In addition to these maneuvers, the pilot performed energy management tasks as recommended by the ground controller. Just prior to low key, the configuration change was performed.

After low key, data maneuvers were curtailed, and the primary task was to perform a power-off landing. The landing pattern consisted of a 180° turn from the low key position of 20,000 to 25,000 feet. Airspeed was allowed to increase during the turn such that a nominal airspeed of 300 knots was established on final approach. The flare began at about 1000 feet above the ground with the aircraft coming almost level at 75 to 100 feet. At 240 knots, the pilot deployed the landing gear and touchdown occurred at about 180 knots.

Occasionally, pilots would rate the handling qualities over a time period of sufficient duration for the pilot to assess the overall flight characteristics. Implied in such a rating is the ability to control angle of attack, airspeed, bank angle, and/or heading angle for profile control, energy management, or other mission task.

#### **Preflight Simulator Studies**

An extensive simulator investigation was conducted prior to the first flight of the X-24B. The first portion of the simulation effort concentrated on designing the portion of the X-24B control system which differed from the X-24A control system. The second portion defined the predicted handling qualities characteristics and stability boundaries. Due to the critical flight profile for this type of aircraft, it is extremely important, from a flight safety standpoint, to conduct a



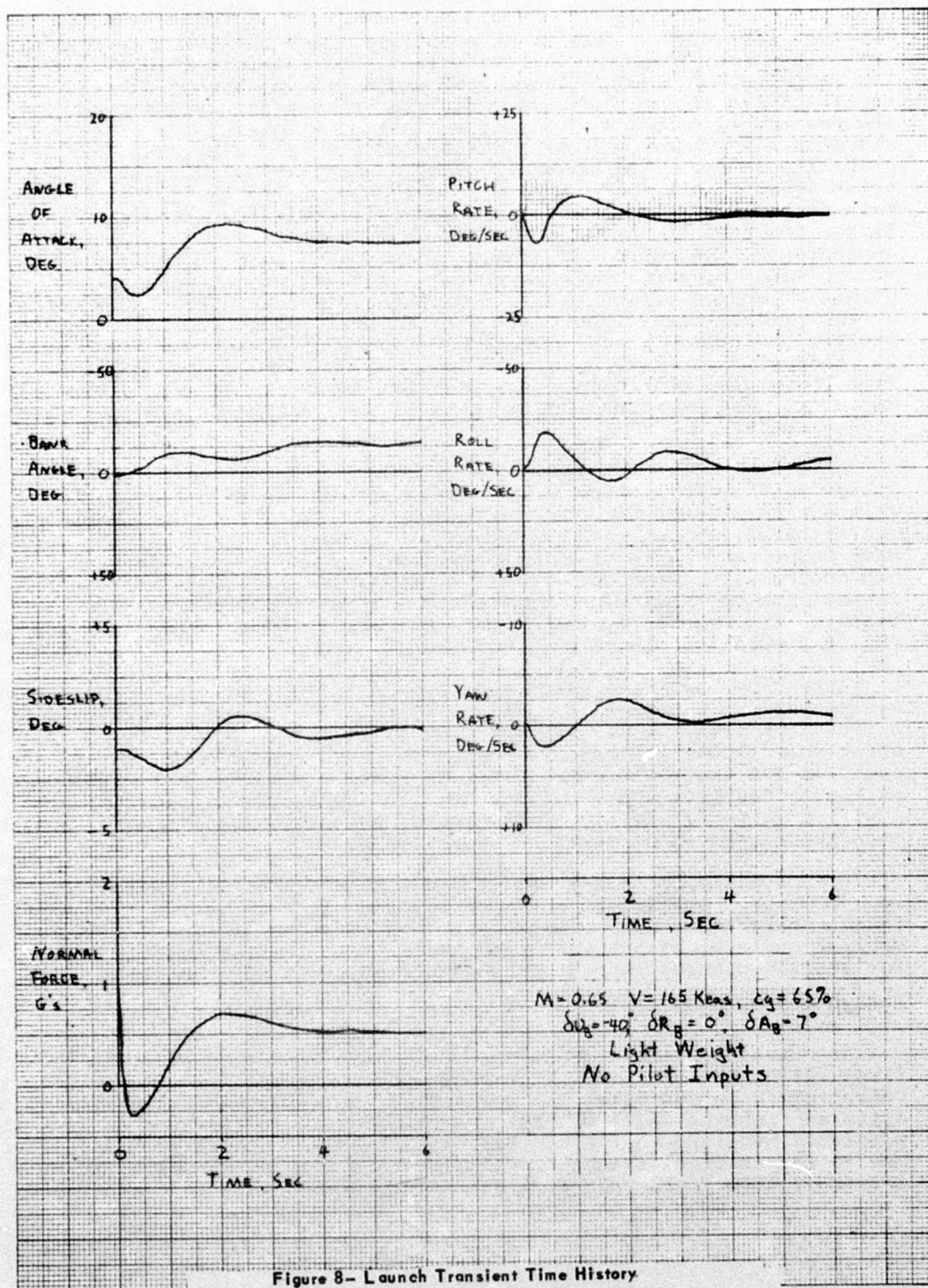


Figure 8- Launch Transient Time History

thorough preflight simulator investigation to eliminate as many unknowns and surprises as possible. It is also very desirable to maintain a large margin between first flight conditions and areas of known instabilities. The specific simulation studies performed for the X-24B are listed and discussed in detail in Appendix E. A comparison of flight results with these simulator studies is contained in the section entitled "Confirmation of Preflight Simulator Predictions".

## **Flight Test Handling Qualities**

### Launch Transient

Recovery from the launch transient was always the initial task that the pilot had to perform on any X-24B flight. The lower flaps however, were set to provide the desired trim angle of attack after launch. The pilot could then perform a hands-off launch and the aircraft would trim at the desired angle of attack. Most launches, however, were not hands-off, but the pilot did not attempt the transient immediately after launch. Since the X-24B was carried at a low angle of attack to insure clean separation, the initial part of the transient was close to zero lift. This was followed by an increase in angle of attack and lift as the trim angle of attack was attained. Sidewash from the B-52 caused an initial sideslip condition of  $-2^\circ$  and a roll-off to the left after launch. Pilots who had never experienced an air launch were unanimous in their opinion that it was certainly a surprise. However, a pilot with previous lifting body experience commented after his first flight "That's probably the smoothest launch I've ever had on a lifting body." Pilot ratings were obtained from the first five launches for the task to recover from the launch transient to wings-level flight at  $10^\circ$  angle of attack. Average pilot ratings for this task were 3.0 for both pitch and roll; no pilot inputs in yaw were required. A time history of a typical launch is shown in figure 8. The heavy weight launches performed on powered flights exhibited little difference from the lightweight launches.

### Subsonic Handling Qualities (Mach = 0.3 - 0.6)

The subsonic area as defined by this report, will cover the Mach number range of 0.3 to 0.6. Since the configuration change usually occurred at about 0.6 Mach number, the handling qualities discussed in the section will be for the subsonic configuration. All flying in this area was accomplished in the 64% to 65% cg range. A discussion of longitudinal characteristics during the configuration change will also be presented. Handling qualities with the landing gear down, the landing itself, and ground handling will be discussed in the "Final Approach and Landing" section.

### Longitudinal

The longitudinal handling qualities of the aircraft with the SAS on were generally good in the subsonic area. Although pitch stability was less than predicted (1.0% to 1.5% static margin) and the aircraft was slightly less stable than desired, pitch damping and control were good. Short period frequency and damping ratios were approximately 0.4 cyc/sec



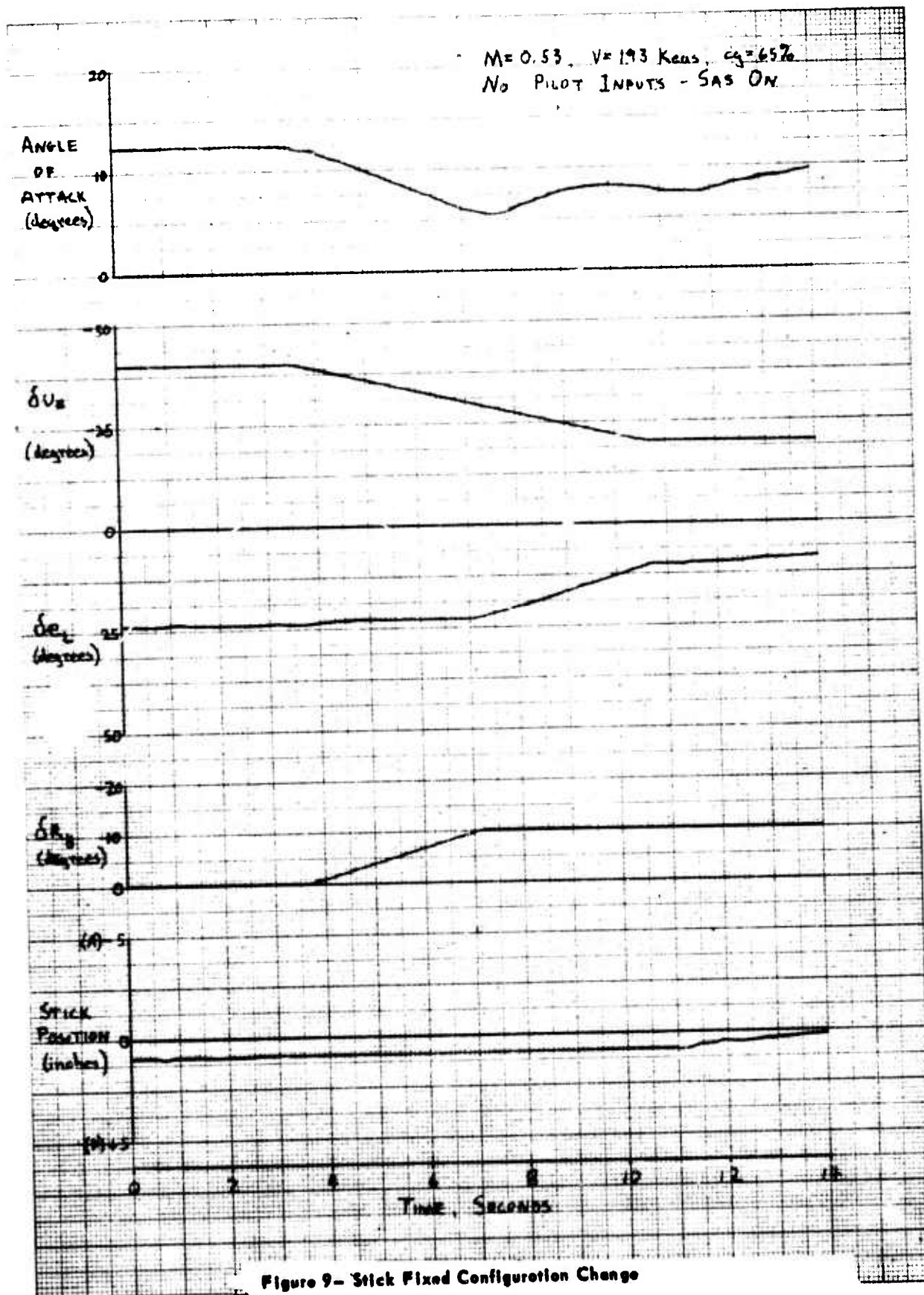


Figure 9- Stick Fixed Configuration Change

and 0.86 respectively. Average pilot ratings for maintaining angle of attack control in this area were 2.5. Longitudinal trim curves are shown in figures B1 and B2.

The X-24B showed some degradation in longitudinal control when the pitch SAS was turned off. Pilots commented that the stick sensitivity was greater and that overshoots in angle of attack became noticeable. Pilot inputs made through the stick trim system posed no problems, but normal stick inputs resulted in mild overshoots and small amplitude pitch oscillations. Pilot ratings for controlling angle of attack with the pitch damper off were 3.0-4.0. At no time were any longitudinal PIO tendencies reported, and pilots agreed that the X-24B flew well with the pitch SAS off in the subsonic region.

The configuration change was unique since three controls, all with major pitching moment effects, were moving at the same time. The upper flaps produced a strong nose down pitch change as they closed from  $-40^\circ$  to  $-20^\circ$ . Nose up trim changes were caused by closing the lower flap and biasing the rudders inward. A "hands-off" configuration change time history is shown in figure 9. The trim change caused by the surfaces moving is apparent. Note the automatic scheduling of the rudders and lower flaps sequentially to offset the effect of the upper flap. Figure 10 shows a time history of a configuration change where the pilot was asked to hold angle of attack. Pilot ratings for this maneuver were 2.0-3.0. Figure 11 shows the same task performed with the pitch SAS off. The pilot rating here was a 4.0. One comment voiced unanimously by the pilots was that the configuration change was easier to perform in the aircraft than it was in the simulator. This was probably due to a lack of visual and motion cues in the fixed-base simulator.

The entire Mach/angle of attack envelope of the X-24B was bounded at high angles of attack by a pitchup boundary where  $C_{m\alpha}$  decreased to zero. In the subsonic area this boundary occurred at about  $25^\circ$  angle of attack, much higher than the angle of attack required for operational maneuvering. Since the pitchup boundary affected primarily the boost portion of the profile, the discussion of the boundary will be deferred to the "Transonic Handling Qualities" section.

#### Lateral-Directional

Handling qualities in the lateral-directional axis were very good subsonically and consistently received ratings of 2.0 - 2.5 for the task of flying the landing pattern and maneuvering to final approach. Pilots were particularly pleased with the roll response and control, and the directional stability. One pilot remarked, "In fact, there was no roll overshoot in the airplane. If I wanted to stop at  $30^\circ$  (bank angle), I stopped it there. I thought it was a nice handling airplane in roll." Another pilot described the roll characteristics as "a very positive control and just about the right roll rate for a given stick deflection." Directional stability and damping were considered good. Typical dutch roll frequencies varied with dynamic pressure but were on the order of 0.4 cyc/sec. SAS-on damping ratios were on the order of 0.26. Characteristics of the dutch roll varied directly with the value of  $C_{\ell\beta}$  (See

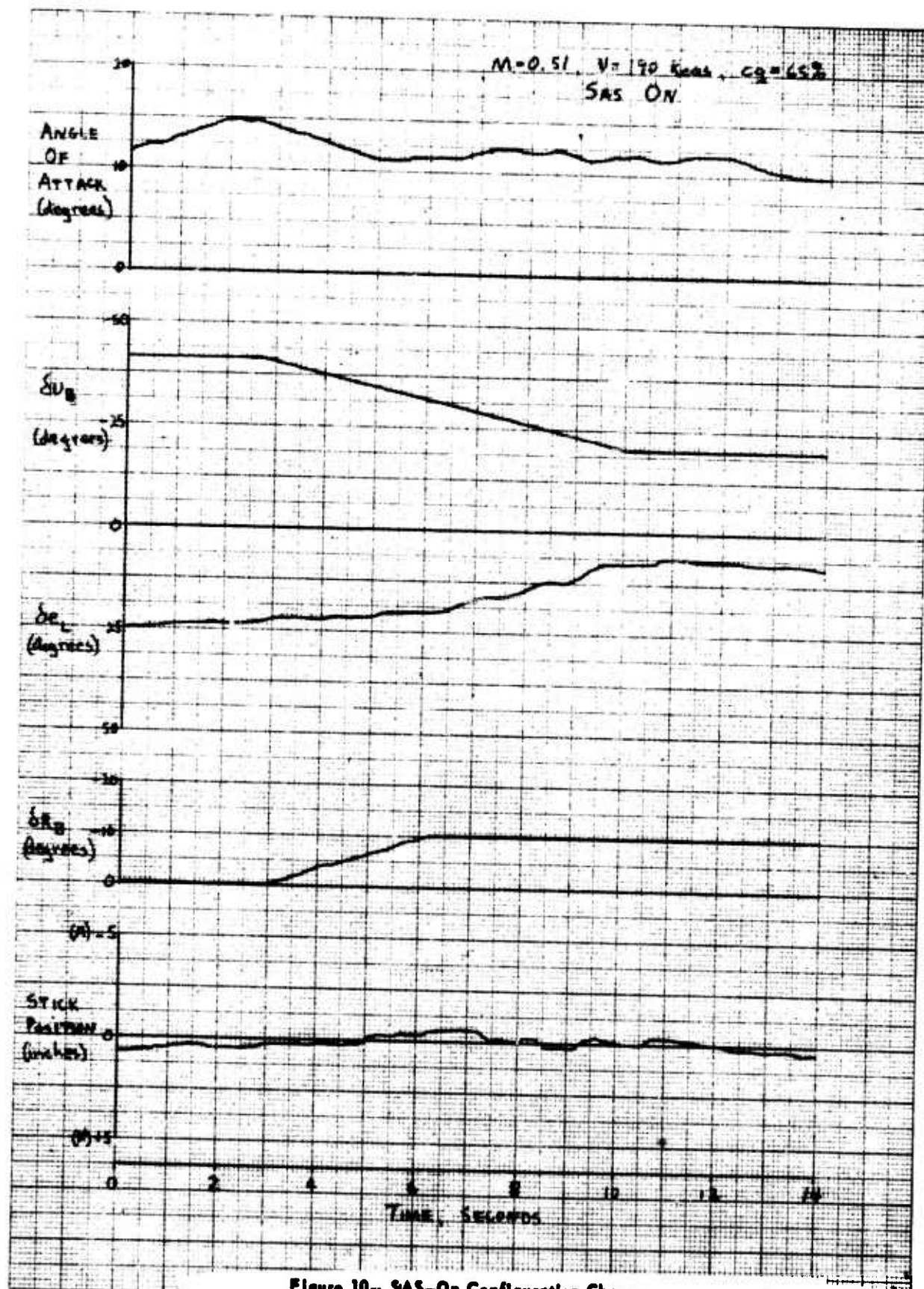


Figure 10-- SAS-On Configuration Change

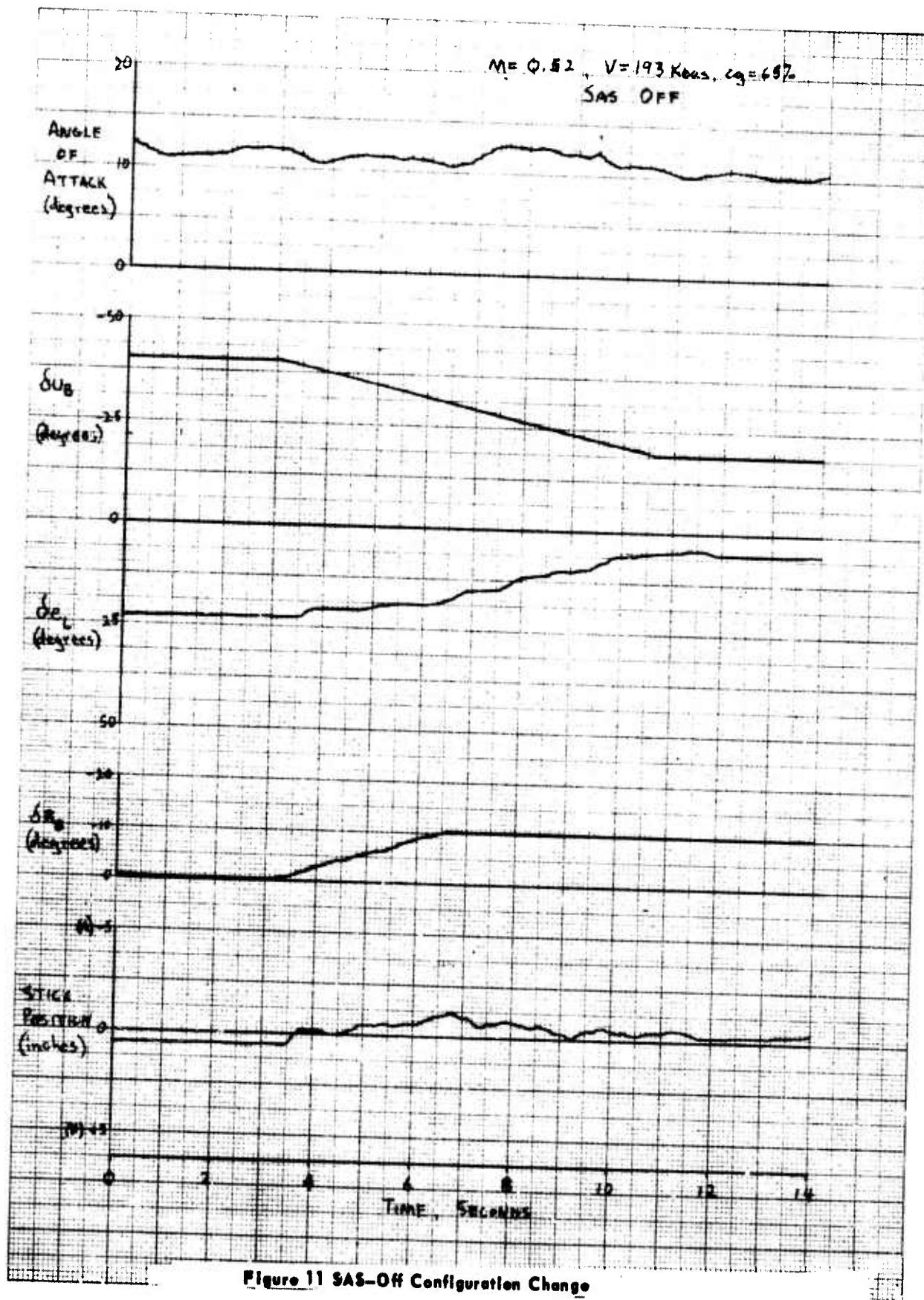


Figure 11 SAS-Off Configuration Change



figures A28 and A29). At low angles of attack where  $C_{L\delta}$  was small, the dutch roll was a flat, "snaky" type of motion. When the  $C_{L\delta}$  was large, roll-to-yaw ratios associated with an oscillation became larger. In the angle of attack range most often flown after the configuration change (80-120) the roll damper was the most effective means of attenuating the dutch roll oscillations. Yaw rates generated during an oscillation were usually not large because of the high yaw inertia, and consequently the yaw damper contributed little to dutch roll damping. Pilots commented that they could see little or no effect of the yaw damper.

SAS-off lateral-directional handling qualities were excellent in comparison to previous lifting bodies. Although some precision in the control of angle of attack and bank angle was sacrificed, pilots were still pleased with the way the aircraft flew. One pilot's comments were "It really flew well, you don't see anything in yaw, you know, unless you boot the rudder. You can sit there and fly it and roll, and the nifty part was I felt there was some roll damping (aerodynamic) in the airplane with the dampers off." Dutch roll damping ratios with the SAS off were about 0.11, and the characteristics discussed in the previous paragraph are applicable.

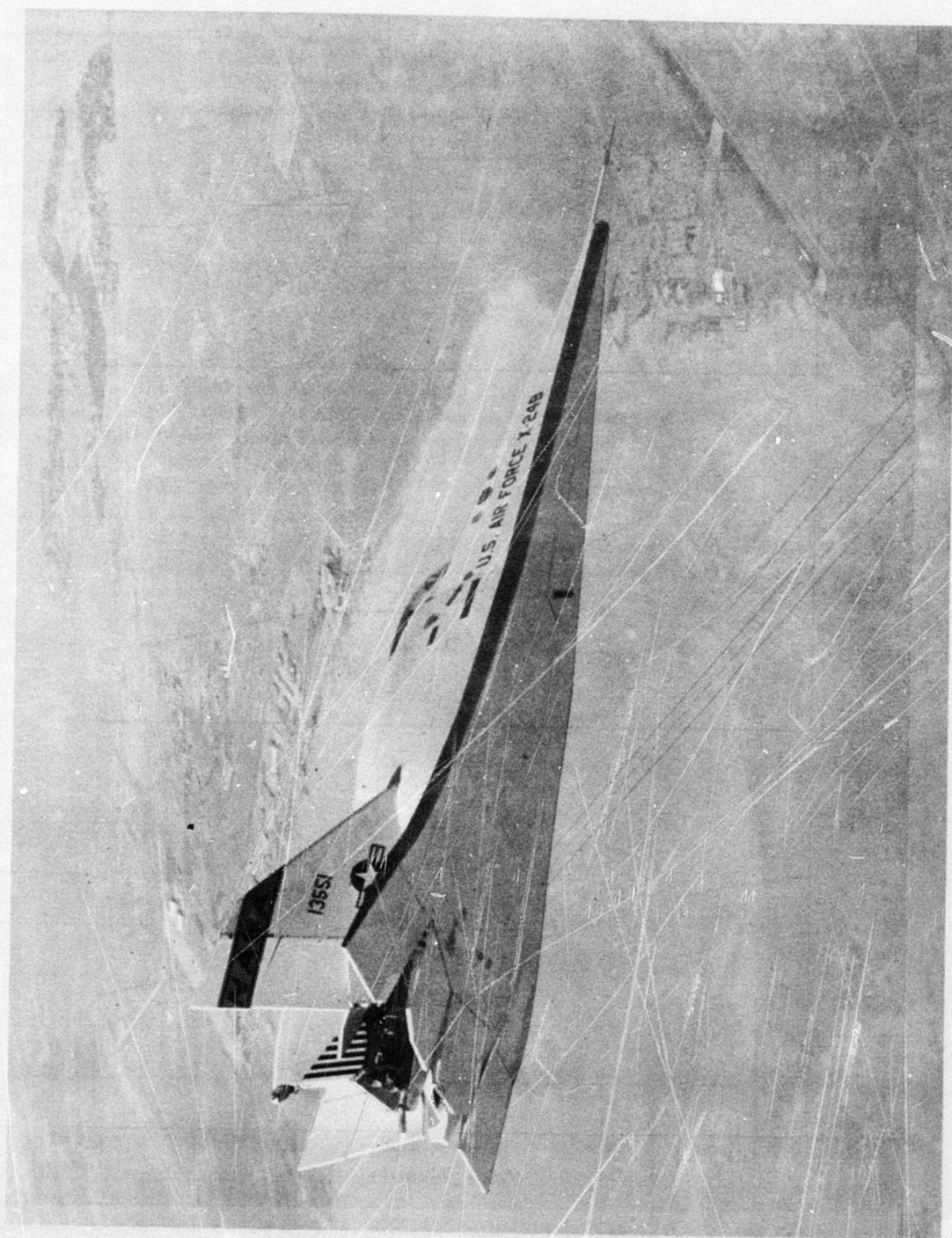
Aileron-to-rudder interconnect ratios for the subsonic configuration were investigated on one flight and it appeared that the low schedule (see figure D8) was close to optimum. The pilot reported however that the interconnect ratio was not as critical as earlier simulator studies had predicted. Interconnect values of zero gave only slightly degraded roll performance, and no PIO tendencies were exhibited with the SAS off. PIO sensitive areas, predicted by preflight simulator studies, were not encountered in actual flight. This was attributed to the fact that the pilots responded more to roll rate than to bank angle and also to favorable differences between predicted and actual lateral-directional derivatives (see "Lateral-Direction PIO Sensitivity" section in Appendix D).

From time to time the X-24B encountered buffet in the subsonic configuration. The buffet was caused by separation of one or both outboard vertical fins (tip fins). The separation boundary was a function of both Mach number on angle of attack and is pictured in figure 26. Since the X-24B used the same tip fins as the X-24A, it was assumed that the separation boundary established during that program would be valid for the X-24B. This boundary has been confirmed by buffet, hinge moment changes, fin pressure changes, tuft photos, and step changes in the values of  $C_{n\delta}$ . The buffet encountered was described by one pilot, "I might mention that up in the 100 angle of attack area, there was a noticeable buffet in the airplane, nothing like a F-104 buffet when you pull it back hard with takeoff flaps or with flaps up, but it was noticeable...." The buffet region was investigated on several occasions, and no adverse handling qualities were reported.

#### Transonic Handling Qualities (Mach: 0.5 - 1.0)

The transonic Mach number regime extends from about 0.6 to 1.0 and all of this area was flown in the transonic configuration. Flight





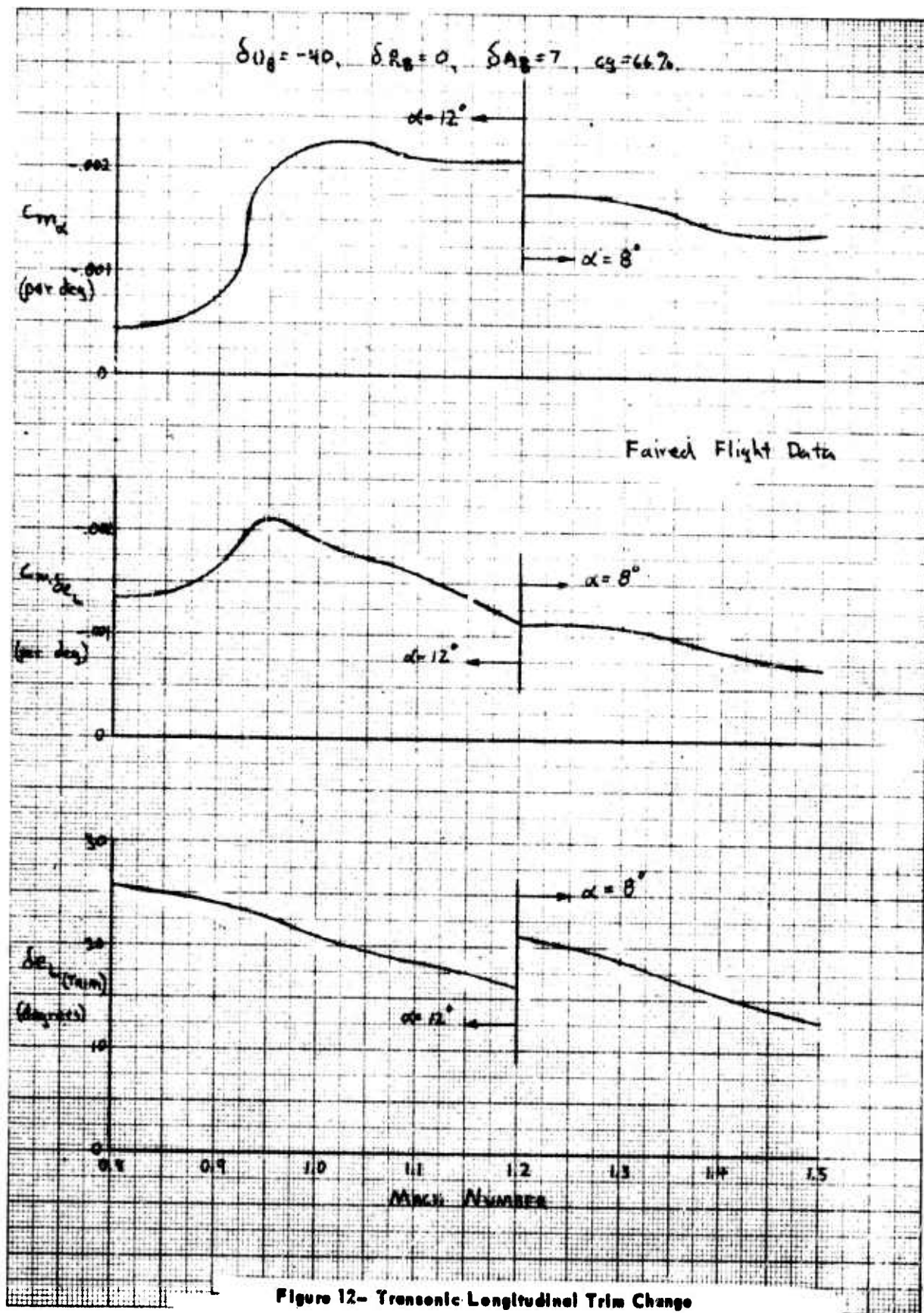


Figure 12- Transonic Longitudinal Trim Change

at these Mach numbers was almost always of a transient nature, since the aircraft was either accelerating or decelerating rapidly. Evaluation time was severely limited and stabilized flight at all but the lowest Mach numbers (0.6, 0.7) was never obtained. Flying in this area was done at 65-66% c.g. with the power on and 64% c.g. with the power off.

#### Longitudinal

Longitudinal handling qualities at Mach numbers of 0.6 to 0.8 were similar to those described for the subsonic configuration. Angle of attack control was described as being a little better in the transonic configuration and this is probably attributable to somewhat higher pitch damping (see figures A 2 and A 5). Pilot ratings for this Mach number area were 2.0 to 2.5 based primarily on the ability to capture and maintain angle of attack. Longitudinal trim curves are shown in figures B3 through B7.

Longitudinal handling qualities from Mach 0.8 to Mach 1.0 were fair but were degraded by several minor problems. The first was the rapid trim change as the aircraft accelerated or decelerated through this area. The trim change (illustrated in figure 12) made it more difficult to control angle of attack or pitch angle, especially if other tasks were involved. About the task to maintain  $30^\circ \theta$  during the boost, one pilot said, "But if a guy was to fly a good solid  $\theta$  task, and not have to make heading changes and things like that, it would still present a bit of a task because we are still getting trim changes. Since we changed Mach number in this area, I'd rate that a 3.0 to 3.5." On another flight where the pilot was required to perform a yaw trim task concurrent with the pitch task, this area was rated 4.5. The pilot rating improved to 2.0 to 2.5 during later flights when the pilots had flown the task several times and pitch control was the primary task being performed.

The second problem occurred during the portions of powered flight where dynamic pressure and airspeed were low. Pilot commented that the pitch task became more difficult when the dynamic pressure decreased to approximately 75 psf or below as it always did during the climb and acceleration. Pilot ratings for the low dynamic pressure area were typically degraded .5 to 1.0 from those obtained at higher dynamic pressures. This problem was not encountered during the glide portion of the flight since dynamic pressure was higher.

Another area of concern, especially on early powered flights, was a pitchup predicted at moderately high angles of attack (figure 13). The simulator showed a very mild entry into the pitchup region, and that control could be maintained several degrees higher than the angle of attack at which  $C_{m\alpha}$  was zero. Although pilots never mentioned an area of instability (the pitch boundary was never intentionally violated), extrapolated values of flight measured derivatives verified its existence (see section entitled "Confirmation of Preflight Simulator Predictions"). The predicted existence of the pitchup boundary led to the installation of a stick shaker warning device prior to the first flight and close monitoring of angle of attack during all flights.



$\delta \alpha_B = -20^\circ$ ,  $\delta \beta_B = 0^\circ$ ,  $\delta \gamma_B = 7^\circ$ ,  $C_M = 66\%$

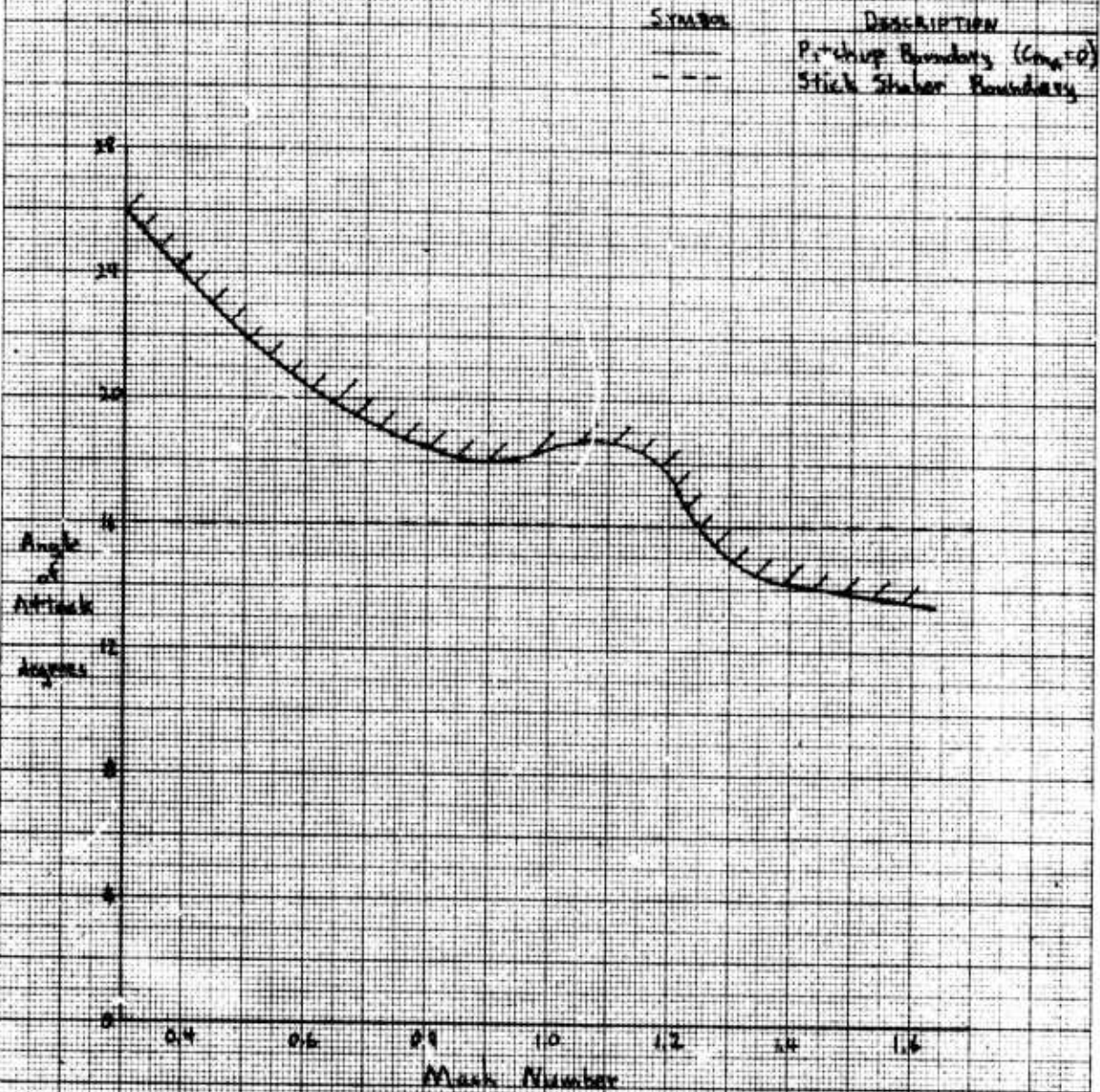


Figure 13- Pitchup Boundary

SAS-off longitudinal handling qualities were again similar to those of the subsonic configuration. The aircraft was lightly damped, and overshoots were common during normal maneuvering. Pilot ratings for this condition were not obtained.

#### Lateral-Directional

Lateral-directional handling qualities in the low transonic Mach region, power off, were similar to those of the subsonic configuration. Directional stability and roll response were considered good and received pilot ratings of 2.0 to 2.5. SAS-off handling qualities for this area were characterized by lack of precise control of aircraft attitude as was noted for the subsonic configuration. Lateral-directional SAS-off conditions were investigated only below a Mach number of 0.8.

Handling qualities with the rocket engine on were seriously degraded by low levels of directional stability. Figures A38 through A40 show the effect of the rocket engine on  $C_{l\delta}$  and  $C_{n\delta}$ . Flight planning performance requirements dictated that the powered boost be flown at high angles of attack, and, therefore, all handling qualities investigations in the transonic area with the power on were conducted at angles of attack greater than  $10^\circ$ . As these angles of attack increased, the directional stability decreased, and the further reduction due to the rocket engine could cause  $C_{n\delta}$  to be zero or even negative. The low levels of stability were further aggravated by two other phenomena which produced sideslip motion. The first was caused by passing through lateral wind shears at high climb rates. This caused an uncommanded sideslip and made the aircraft appear to be directionally unstable. Wind shears are discussed in some detail in Appendix C. The second problem was a misalignment of the rocket engine. Before the first powered flight an attempt was made to align the rocket engine through a slightly offset lateral c.g. Measurements made after Flight 25 showed that the engine had been over-corrected such that a nose right moment was caused whenever the rocket was on. This caused a steady state sideslip of  $1^\circ$  to  $3^\circ$  depending on the level of directional stability. Since this level of sideslip was not observed when the rocket engine was off, the power-on aircraft appeared initially to the pilot to be marginally stable in the directional axis. The area of low stability was particularly restrictive at Mach 0.95 and  $12^\circ$  angle of attack (see figure A40). The low directional stability became the limiting factor for high angle of attack flight in that region.

During the latter portion of the flight test program, several improvements were made in an attempt to reduce the sideslip encountered in flight. Since the rudders were very effective throughout the area of low stability, an  $\dot{a}_y$  feedback loop was added to the flight control system after flight 19 to reduce the steady state sideslip. In the transonic area, however, the  $\dot{a}_y$  feedback was only partially effective since low values of dynamic pressure made the values of  $\dot{a}_y$  (and hence the fixed-gain rudder signal) small. The biggest improvement, however, was the realignment of the rocket engine prior to flight 26. It is worthwhile noting that the engine realignment was only  $0.5^\circ$  but signifi-



cant reduction of steady state sideslip values resulted. This illustrates that the primary problem was the low value of  $C_{n\delta}$  with the rocket engine on, and not the small misalignment of the rocket engine.

Pilot ratings for the initial encounter with this low directional stability ranged from 4.5 to 6.0. With the improvements to the aircraft (a<sub>y</sub> feedback and engine realignment) and the confidence obtained on subsequent flights that the aircraft would not depart in yaw, pilot ratings were improved to 2.5.

The low level of stability also provided the only area of pilot induced oscillation (PIO) sensitivity encountered during the flight test program. On the first powered flight, the pilot reported a mild PIO or wing rock during the boost at 14° angle of attack. Post flight pilot comments relating to the wing rock were, "I had no problem controlling heading and the basic bank angle, but I did have this wing rock problem that I called out to you..... I didn't feel it was going to diverge. It never felt like a hazardous or dangerous situation. It was there and it got my attention a few times..... Because of this little problem, I would rate it a 4." Examination of the flight records revealed an aileron deadband which is further discussed in Appendix D. Since for small aileron commands only one aileron surface had been moving, the effective roll SAS gain had been half of what it was programmed to be. On the next flight the roll SAS gain was increased and PIO areas were not encountered again. Roll response was considered good for this type of aircraft in this Mach regime. The primary roll task for this portion of the flight was to maintain wings level and make occasional heading corrections.

Handling qualities with the power off were markedly improved. Not only was the directional stability higher, but the misaligned engine no longer caused the steady state sideslip. A pilot commented, "This is essentially the same area we flew before ( $M=.95$ ,  $\alpha=12^\circ$ ), but this time with the power off.... I felt better about the directional stability at this point; I could tell the difference in directional stability. It was no longer a concern from a hazard standpoint. Even though the stability is a little low here, I could feel that the airplane was directionally stable." Pilots were generally pleased with the handling qualities, even at moderately high angles of attack. Asked to evaluate the handling qualities at 12° angle of attack while decelerating from Mach 1.0 to Mach 0.85, one pilot said, "What I did see at 12° angle of attack looked very much like the simulator. The airplane flies like a champ in that area. When you put in an aileron input, you can see the beta swing out. It swings out about a degree or a degree and a half, but it does that in the simulator, and comes right back again. It's a beautiful airplane to fly. I'd rate it at 2.0 or 2.5 in that area."

Due to the low stability at the Mach numbers of 0.85 to 1.0, SAS-off characteristics were never investigated.

### Supersonic Handling Qualities (Mach 1.0 - 1.7)

The supersonic area covered handling qualities between a Mach number of 1.0 and the aircraft's maximum Mach number of 1.76. Evaluation time, as in the transonic case, was very limited and stabilized cruise time was not possible. The center of gravity at these Mach numbers was 64% to 65%.

#### Longitudinal

Longitudinal handling qualities were excellent in the supersonic Mach range. Dynamic pressures at these Mach numbers were high enough to provide excellent control and damping. One pilot commented, "As I mentioned before, in pitch it's a real solid airplane. The pitch sensitivity of course, changes considerably with Mach number in this area, but it's real solid..." The change in lower flap effectiveness mentioned by the pilot and the associated trim change were the only detractors. Discussing the trim change with Mach number, the same pilot said, "Here again the airplane flies nicely in this area. I felt real good about my 7° angle of attack this time. You still have to trim like gangbusters because the trim change is really fast in this area. You have to move it back all the way, but I felt good about holding 7° angle of attack, and I'd rate that a 2.0 to 2.5. Very nice flying, and the only thing that would keep it from being a solid 2.0 was the fact that you have to trim it all the time. You have to work at it, and it takes quite a bit of attention just to fly angle of attack; if one should encounter a severe lateral-directional task, why, then the pitch task would become more difficult because it requires about 90% of your time." The factors governing this trim change are shown in figure 12. All pilot ratings given in this area for the task of maintaining angle of attack were 2.0 to 2.5. Pilots were unable to detect any differences between the power-on and power-off aircraft in pitch. No pitch transients were associated with rocket engine shutdown. Values of  $C_m$  for Mach numbers of 1.1, 1.2 and 1.3 show a degradation of pitch stability with the rocket engine on, but the level of power-on stability is still high. Frequencies for the short period in this area were 0.7 cyc/sec and damping ratios for the aircraft with the SAS on were about 0.64. Longitudinal trim curves for this area are shown in figures B8 through B12.

SAS-off frequency and damping were investigated briefly by performing several pitch pulses with the pitch gain at zero. Pitch damping was considered adequate with a damping ratio of 0.10. After performing two SAS-off pitch pulses at Mach numbers of 1.4 and 1.5, one pilot commented, "Just as the simulator shows, the pitch damping at this speed is excellent. You could fly this airplane with the pitch damper off without any problem."

#### Lateral-Directional

Power-on lateral-directional handling qualities were good at lower supersonic Mach numbers, but increasing Mach numbers brought decreasing directional stability and sideslip problems similar to those encountered in the transonic Mach region. Levels of dutch roll stability are presented in figures 4 through 6.

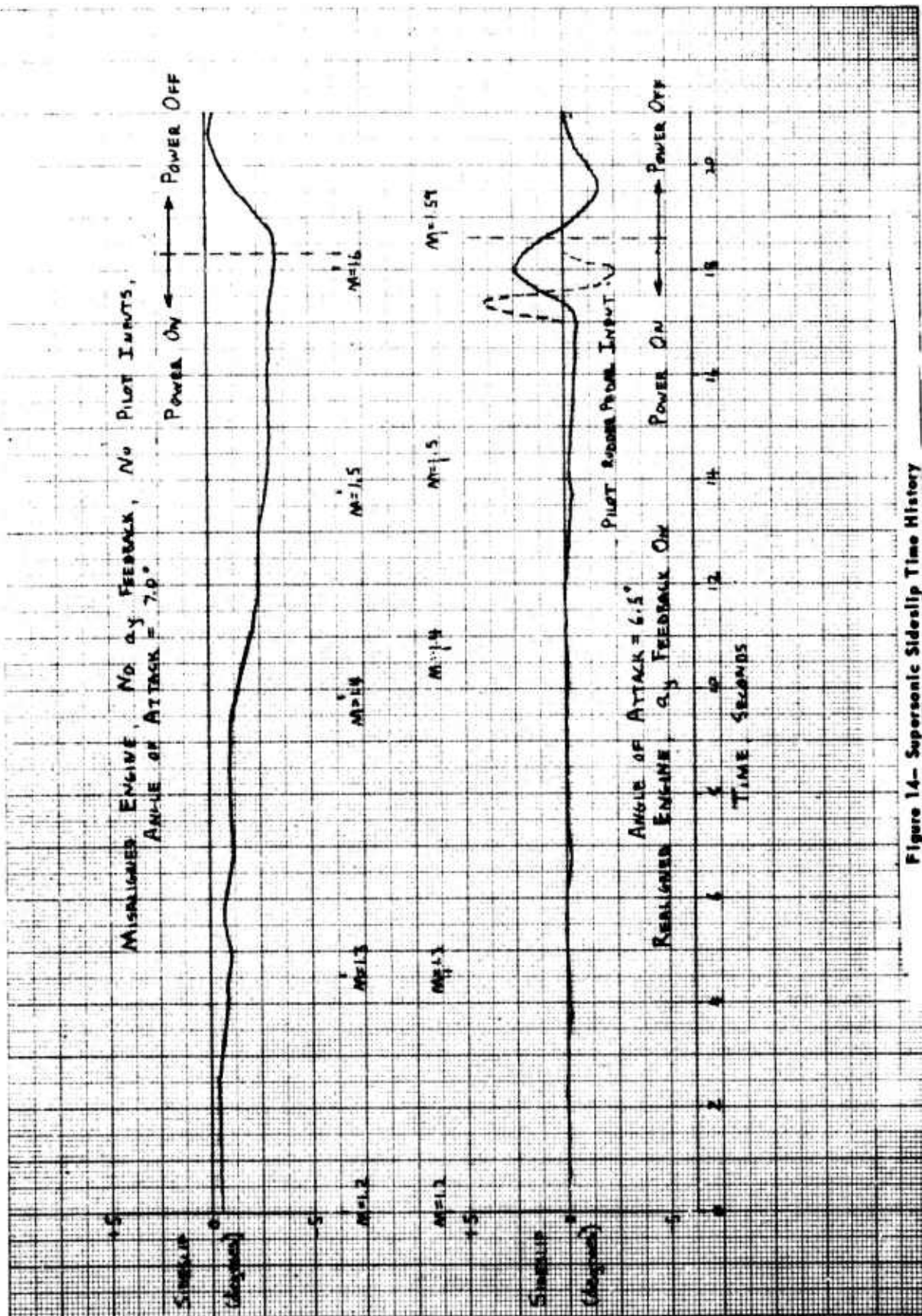


Figure 14- Supersonic Sideslip Time History

For supersonic Mach numbers between 1.0 and 1.3, stability was good. As one pilot commented, "Once you get beyond the transonic beta excursion, it's a pretty good airplane to fly." As the Mach number increased above 1.3, directional stability decreased. At 4° to 5° angle of attack with the rocket engine on, directional stability was acceptable up to 1.76 Mach number. But at 7° angle of attack, values of  $C_{n\beta}$ \* approached zero as the aircraft approached its maximum Mach number (figure 5). The effects of low directional stability were especially apparent before the rocket engine was realigned. Figure 14 shows a typical time history of sideslip before and after the engine realignment. The three degrees of sideslip shown in figure 14 was typical of flight at 7° angle of attack above 1.4 Mach number. Note the reduction in sideslip when the engine was shut down. The amount of sideslip generated was a strong function of angle of attack. When asked to discuss the handling qualities above 1.2 Mach number at 8° angle of attack with the power on (before realignment), a pilot replied, "Right above 1.2 no real problem, but as it shows in the simulator, once you get to 1.3, you can start noticing the reduced directional stability. And as we got out to 1.5 directional stability was considerably reduced. It is definitely less in the airplane than the simulator. The pilot rating out here is based on the pulses at 1.3 and 1.5. Beta slipped out to the left again, and I remember it going out to at least about 3 to 4 degrees. I do remember coming in with left rudder to bring it back. This area as a result of the pulse, would have to be rated 6.0 in yaw." Asked the same question about 5° angle of attack on subsequent flights the pilot said, "The airplane is considerably better at 5° angle of attack above 1.2 than it is at 7° angle of attack. I was very confident that beta (sideslip angle) was not going to take off and cause me a lot of worry. Beta does move out to the left, just like it has before, but it only gets out to somewhere between 1 and 2 degrees. I got the impression that that's where it wanted to sit, and it probably wouldn't go out anymore. So once or twice, somewhere in here, I pushed it in with the rudder and then didn't worry about it anymore. I'd rate it somewhere around 3.0." Flight measured values of  $C_{n\beta}$  (figures A45 through A48) confirm these pilot comments.

The reduced directional stability with power on above 1.3 Mach number and 6° angle of attack was not readily apparent to the pilot unless he noted the visual sideslip display. There was no uncommanded roll mistrim since the dihedral effect at these conditions was negligible. Sideforce at the pilot's station was sufficiently low as to be easily unnoticed when concentrating on the task other than directional stability. The reduction in stability was considered a hazard and treated as a stability boundary. In addition to the  $\dot{a}_y$  feedback system discussed earlier, an audible warning system was mechanized which notified the pilot when the sideslip exceeded 3.5 degrees.

Power-off handling qualities in the supersonic area were improved over those with the power on. Again, the removal of the rocket engine moment and increased levels of directional stability with the rocket off were the primary reasons. Pilots flew as high as 12° angle of attack at Mach 1.4 (aft stick limit) and reported no problems. Most of the supersonic time, after engine shutdown, was spent performing data maneuvers, and no lateral-directional handling qualities evaluations were done. Pilots, however, never had any complaints about the way the aircraft flew supersonically with the power off.



SAS-off handling qualities were not investigated for the supersonic area.

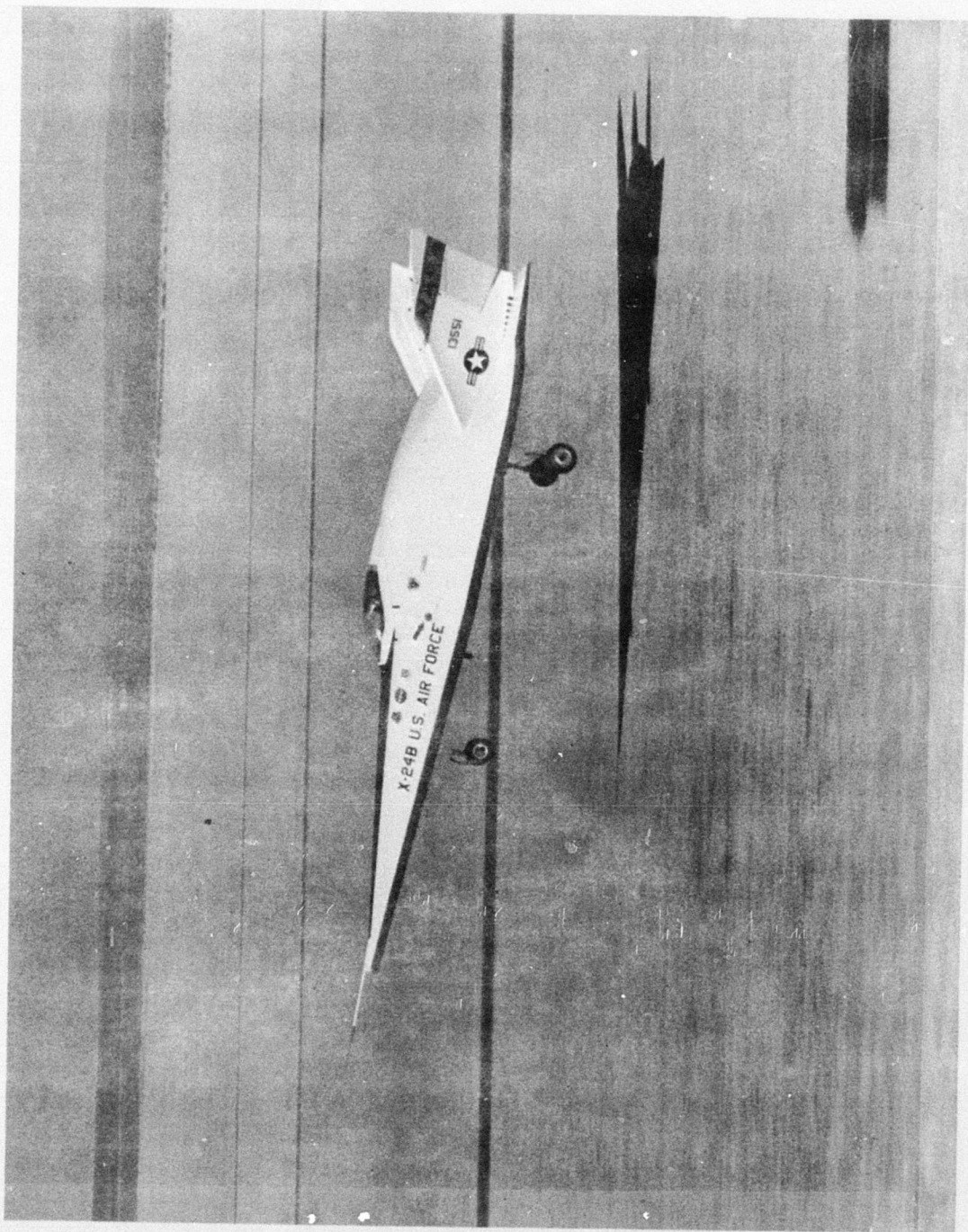
#### Final Approach and Landing

Handling qualities for both the longitudinal and lateral-directional axes were excellent during the final portion of the flight. The handling qualities of the aircraft compared favorably with fighter class aircraft and led to the first conventional runway landings for an aircraft of this type. Pilot ratings for flaring the aircraft ranged from 1.0 to 2.0. Ratings for landing the aircraft were 2.0 to 3.0. One pilot with extensive lifting body experience, summarized the flare and landing characteristics by saying "If we were to look at the airplane from the start of flare through touchdown, in the two flights I've seen, this airplane is far superior to any of the other airplanes (lifting bodies)." Roll response was considered good for heading and bank angle control, and no PIO sensitive areas were ever encountered. Control effectiveness, in general, was very good down to the low airspeeds encountered at touchdown. Some of the specific items which affected the handling qualities are discussed below.

Turbulence was not a problem for the X-24B because of the relatively low dihedral effect. The response in turbulence was compared to an F-104 and was characterized by small "choppy" inputs in sideforce. Earlier lifting bodies had experienced very sharp, low magnitude roll inputs in turbulence. These were caused by a very high dihedral effect and were described by the pilots as a very uncomfortable feeling that the aircraft was about to roll over. The low values of  $C_{l\delta}$  on the X-24B eliminated the roll inputs and provided a much nicer flying aircraft in turbulence. This was a very significant improvement over earlier lifting bodies!

Another pleasant surprise for former lifting body pilots was the lack of a landing gear transient. For performance considerations, the landing gear on the X-24B and the lifting bodies was deployed after the flare at approximately 50 feet above the runway. This occurred between 6 and 15 seconds prior to touchdown (gear extension time was approximately 1 second). Some of the previous lifting bodies (notably the X-24A) exhibited a noticeable pitch down at gear extension which resulted in an annoying longitudinal disturbance. The increased drag load below the aircraft cg played a small part in the pitch down, but the fact that both main and nose gear deployed forward, thereby shifting the longitudinal cg forward, was the major contributor. During the modification of the X-24A to the X-24B, the nose gear was designed such that it deployed aft and the nose gear door was designed to produce less drag. The resultant cg shift then was negligible, and the nosedown trim change at gear extension essentially disappeared. The predicted aerodynamic effect on pitching moment was small, which was confirmed in flight (figure B14). Although a reduction in  $C_{n\delta}$  (see figure A27) was due to gear extension measured in flight, it was not apparent to the pilot and did not result in a degradation in handling qualities.





$M=0.59$ ,  $V=240$  Knts, Altitude = 24000 ft  
 $\delta V_B = -20^\circ$ ,  $\delta R_B = -10^\circ$ ,  $\delta A_B = 7^\circ$ ,  $c_q = 64\%$

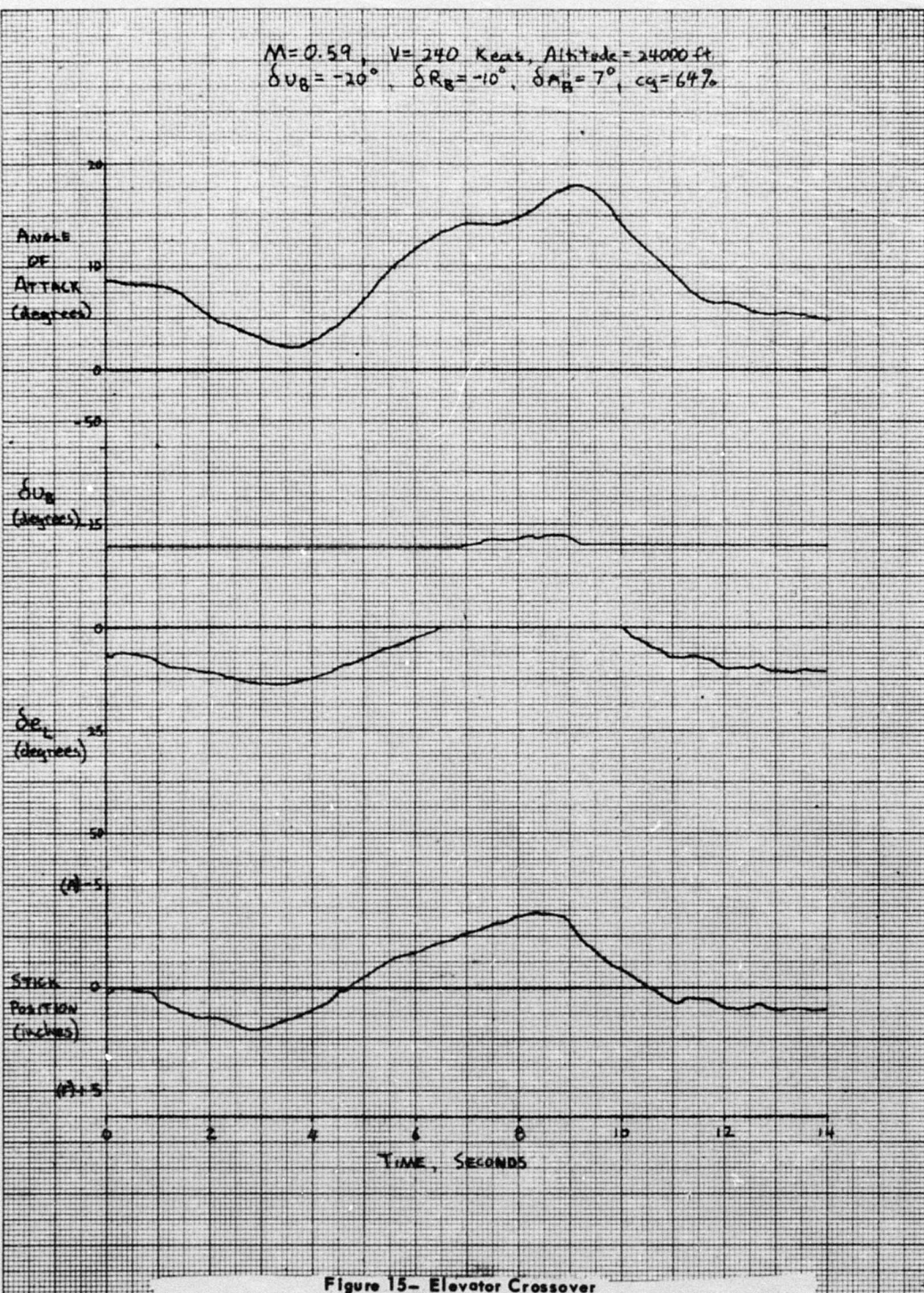


Figure 15- Elevator Crossover



An apparent ground effect was detected in the time between gear extension and touchdown. This manifested itself as a relaxation of longitudinal stick forces as the aircraft came in close proximity with the ground. Thus, pilots were required to relax back pressure on the stick to maintain angle of attack, or experience an increase in angle of attack if stick position were held constant (see figure B14). The pilots were not concerned with this phenomenon because the aircraft responded well to pilot commands. Pitch control close to the ground was good.

As mentioned previously, pitch control was transferred from the lower flaps to the upper flaps when the lower flap closed to zero. Associated with this control transfer was a deadband equivalent to one half inch of stick travel. Thus the pilot could move the stick one half inch and neither upper or lower flap would move. This deadband was encountered on many flights just before touchdown. Comments from the pilots indicated they were often not aware they were flying in the deadband region and could not detect any decrease in pitch control because of it. On one flight a pull-up maneuver at high altitude was performed to pull into the crossover. Figure 15 shows a time history of that maneuver. The pilot mentioned that the only problem associated with the deadband was gauging the size of the stick input required to pull through it.

Another unique feature of the X-24B landing was that the nose could not be held off after the main gear touched down, because the cg was considerably forward of the main gear. The average time between main gear touchdown and nose gear touchdown was approximately 1.5 seconds. This characteristic was a very impressive experience to the pilots. After the first flight in the aircraft, the pilot remarked, "The nose comes through very rapidly, as everybody told me it would. There's nothing you can do about it. It seems like it's going to go all the way into the lakebed." After several flights, pilots became accustomed to the rate (20deg/sec) and accepted the characteristic. This rapid nose slap down was perhaps a contributor to undesirable lateral-directional deviations during crosswind landing.

Crosswind landings represented the only facet of the landing where the aircraft handling was not good. A ten knot crosswind limit was in effect for most X-24B operations and two landings were made at or near that limit. On the first crosswind landing the pilot commented, "Okay, because of a little right crosswind, I was holding a little right-wing down and I touched down on the right gear first, and as it touched down, I got the impression that the nose had sliced rather than come straight down. While it was doing this, the other gear came down." On the second crosswind landing the pilot gave this account. "I felt I touched on both mains. As the airplane started to settle, the left main settled a lot faster than the right, giving me the impression that the left main was collapsing. I reached up and grabbed the gear handle again just as a reflex action, and about that time the nose got to the ground. I started to control it with rudder and possibly aileron. I got the nose gear steering armed as soon as I got the nose on the ground,

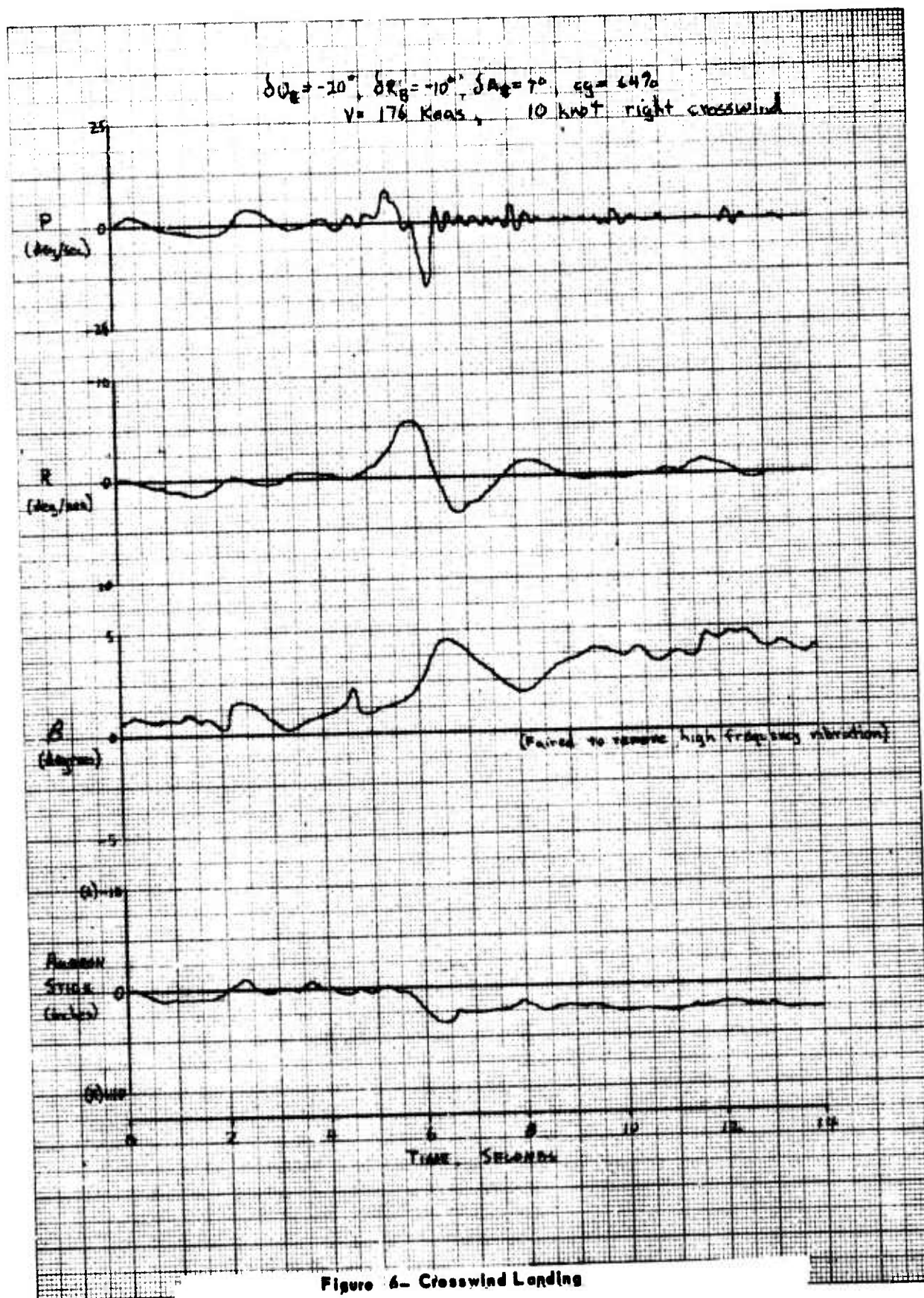


Figure 4- Crosswind Landing

opened the flaps and then became aware that it was time to really start steering because I was starting to drift left really rapidly with the right crosswind." (Rate the airplane during the upset at touchdown). "The airplane touchdown was very smooth and I'd rate it a two, it really felt nice. From touchdown until both mains deflected to the same degree, the airplane would have to be called uncontrollable because I couldn't control it. From mains touching to nose touching down you don't have any control over the airplane and I certainly didn't have any control over the roll rate. Once the roll had quit and I realized that the mains were ok, then the airplane became a very controllable airplane. Nice qualities with that amount of crosswind; I'd rate it a three." Figure 16 shows a time history of the second landing. Neither landing resulted in any damage to the aircraft, but both were uncomfortable experiences for the pilots involved.

The ground handling characteristics of the X-24B were considered excellent for this type of aircraft. A total of four types of steering could be used for directional control on the ground. Above 100 knots both aileron and rudders were effective in steering the aircraft. Their effectiveness, however, decreased markedly once the airspeed dropped below 100 knots. Nosewheel steering was used at that point and worked very well. The following quote from the second crosswind landing serves to illustrate the effectiveness of the nosewheel steering, "I got the nose gear steering armed as soon as I got the nose on the ground, opened the flaps, and then became aware that it was about time to really start steering because I was starting to drift left really rapidly with the right crosswind. I got the nose gear steering engaged and stuck in some rudder (rudder pedals controlled the nose gear steering) to control that left drift; I got very good response, no problem controlling the airplane. I had to put in enough so I did feel some sideforce and felt that certainly the mains were taking some wear on the tires, but I felt that at no time was I in any danger of rolling over. Nice qualities with that amount of crosswind; I'd rate it a three." In addition to the nose wheel steering, differential braking was used on some occasions, but the braking on the aircraft, both differential and total, proved to be less effective than desired.

#### **Pilot Checkout Program**

At the end of the X-24B basic research program, a six-flight pilot checkout program was conducted. Three pilots, without previous lifting body or X-24B experience, were given two glide flights each to gain experience with procedural considerations and handling qualities for this type of aircraft. Each flight was conducted with several typical data maneuvers and evaluation time for SAS-on and SAS-off handling qualities. The Mach numbers covered were 0.7 and below, both transonic and subsonic configurations were flown, and the longitudinal cg was fixed at 64.5%.

Since the envelope involved in the checkout program had been explored previously, no startling revelations or problems came out of the checkout program. Their flights, however, did provide additional independent evaluations from experienced test pilots, with various flying background. Table 3 summarizes the pilot ratings and comments obtained from these flights.



Table 3  
PILOT RATINGS FROM CHECKOUT FLIGHTS

Task <sup>5</sup>	Pilot Ratings			Comments
	Pilot A	Pilot B	Pilot C	
Recover from launch and acquire $10^\circ \alpha$	1.5	2.0	2.5	Not much trimming required.
Recover from launch and acquire $50^\circ \alpha$	3.0	3.0	2.0	
Pullup and capture $12^\circ \alpha$	2.5	3.0	2.0	
Handling qualities with $-40^\circ \delta U_B$ ( $M=0.6$ , $\alpha=10^\circ$ )	3.0P 2.0R	---	3.0	Good bank angle control, pitch stability light
Pitch handling qualities with $-40^\circ \delta U_B$ and pitch SAS-off ( $M=0.6$ , $\alpha=10^\circ$ )	4.0	4.5 3.0	2.0	Poorer ratings for $\alpha$ tracking tasks - aircraft is sensitive in pitch. Better ratings for trimming tasks.
Pitch handling qualities during pushover-pullup maneuvers ( $\delta U_B=-40$ , $M=0.6$ )	3.0	---	3.0	
Configuration change while maintaining $\pm 10^\circ \alpha$ .	Sat	3.0	2.0	Easier than simulator
Pitch SAS-off configuration change while maintaining $\pm 10^\circ \alpha$ .	4.0	5.0	3.0	Hard to keep angle of attack from "bobbling"
Handling qualities with $-20^\circ \delta U_B$ ( $M=0.5$ , $\alpha=10^\circ$ )	2.0	---	2.0	Good handling qualities in pitch and roll
Handling qualities with $-20^\circ \delta U_B$ and all SAS-off ( $M=0.5$ , $\alpha=10^\circ$ )	3.0	4.0P 2.0R 4.0Y	3.0P 4.0R 3.0Y	Lightly damped. Lack of precise control - some overshoots. No PIO tendencies

Key: P=Pitch R=Roll Y=Yaw Sat=Satisfactory (1, 2, or 3)

<sup>5</sup>All tasks are performed with the SAS system on unless other wise noted.

Table 3 (Concluded)

## PILOT RATINGS FROM CHECKOUT FLIGHTS

Task <sup>5</sup>	Pilot Ratings			Comments
	Pilot A	Pilot B	Pilot C	
Handling qualities in landing pattern (M=0.5, $\alpha=80^\circ$ )	---	2.0	2.0P 3.0R	Spiral stability a minor problem. Pitch stability is light.
Handling qualities in landing pattern with all the SAS off (M=0.5, $\alpha=80^\circ$ )	3.0	3.5	3.0P 4.0R 3.0Y	Spiral stability a problem in the turn. SAS-on is a generally tighter aircraft.
Landing flare ( $K_Q=.54$ )	1.0	---	---	
Landing flare ( $K_Q=.38$ )	1.0	4.0	2.5	Flare slightly over-controlled. Pitch damping noticeably lighter with the lower SAS gain.
Landing ( $K_Q=.54$ )	---	3.0	2.5	Sensitive in pitch.
Landing ( $K_Q=.38$ )	2.0	3.0	3.5	Liked better than the landing with $K_Q=.54$ but the pitch axis is a little loose.

Key: P=Pitch R=Roll Y=Yaw Sat=Satisfactory (1, 2, or 3)

$$\delta u_g = -40, \delta R_g = 0, \delta A_g = 7, c_g = 66\%$$

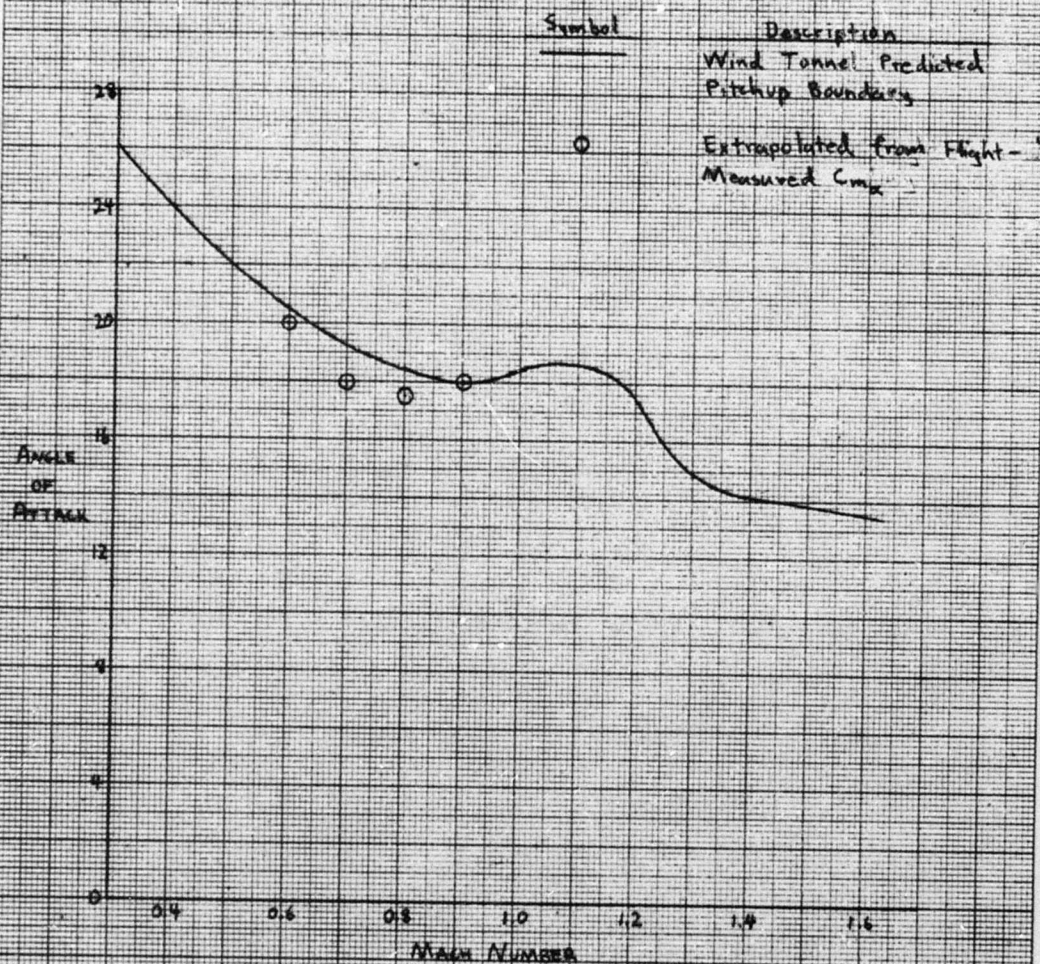


Figure 17- Flight-Measured Pitchup Boundary

## Confirmation of Preflight Simulator Predictions

This section will present a comparison between information extracted from flight test results and data obtained from the simulator studies performed before first flight. The comparison is not intended to be comprehensive and will only highlight some of the more interesting findings.

### Pitchup Boundary

Figure 17 shows the pitchup boundary as defined before first flight and several data points confirming its existence. The data points have been determined by extrapolating measure values of  $C_{m_\alpha}$  over one or two degrees angle of attack. The pitchup boundary was never intentionally crossed, and pilots never reported flying an unstable aircraft in pitch. Agreement between the predicted pitchup boundary and the extrapolate flight test data point is good. At supersonic Mach numbers, extrapolation of data to zero  $C_{m_\alpha}$  is not possible, but high angle of attack  $C_{m_\alpha}$ 's are higher than predicted. It is probable then, that the predicted pitchup boundary is conservative in this area.

### PIO Sensitivity

The PIO sensitive area predicted by the simulator (see Appendix E) caused some concern, and so early in the flight test program the actual SAS off lateral-directional PIO tendencies were investigated. The flight conditions at which the investigation occurred are shown in figure D15. The pilots found no PIO tendencies whatsoever during flight. This tends to confirm the simulator results obtained using aileron to roll rate pilot transfer functions and indicates the pilots responded to roll rate in flight. In other words, because of motion cues, they responded much quicker during actual flight than they did using a fixed base simulator.

A second factor contributing to the absence of PIO sensitivity was the change of several derivatives which play a key role in the determination of PIO tendencies. For example,  $C_{n_\delta}$  was 25% higher than predicted in the mid-angle of attack range and  $C_{n_{\delta a}}$  was 30% to 50% less than predicted. Both of these changes would contribute to reduced PIO sensitivity.

For this vehicle, simulator results were conservative in that the PIO tendencies shown on the simulator did not occur in flight. If the tendencies had been reversed such that the vehicle were PIO sensitive to a/P transfer functions (such as might be the case with a vehicle with a high  $C_{l_\delta}$  to  $C_{n_\delta}$  ratio), a fixed based simulator would probably not predict PIO tendencies which might occur in flight.

### Handling Qualities Boundaries

One of the most useful ways of describing the flight envelope of an aircraft like the X-24B is with a Mach/angle of attack plot. On this plot the handling qualities or stability and control characteristics which



limit flight are represented as boundaries. Figure 18 shows the handling qualities boundaries which were developed before first flight. Note that the prime limiting factor over the major part of the Mach number range was expected to be the avoidance of the pitchup boundary ( $C_{m_\alpha}=0$ ). In the Mach number range between 1.1 and 1.4 it was predicted that the maximum attainable angles of attack would be limited by full aft stick deflection ( $\delta e_L=0$ ) and would be below the pitchup boundary as shown. With the exception of zero directional stability above sixteen degrees angle of attack in the transonic region, all lateral-directional limiting conditions were at angles of attack above the pitchup boundary and, therefore, were not of major concern.

The boundaries defined after analysis of all available flight test data are shown in figure 19. These boundaries are presented for the reference cg of 66% to be consistent with the data comparisons made throughout this report. During flight the cg varied from 66% at launch to 64% at maximum Mach number as propellant was consumed. Therefore the actual limiting angle of attack during flight were somewhat higher than the values shown. A discussion of these boundaries with respect to the actual cg during flight is contained in reference 1. In many cases these boundaries were based on conservative extrapolations of the flight test data to the limiting values. As previously discussed, the angles of attack where  $C_{m_\alpha}$  was zero were close to predicted between 0.6 and 0.9 Mach number. (Insufficient data was available at all other Mach numbers to define  $C_{m_\alpha}=0$ .) The maximum attainable angle of attack with full aft stick was different from predictions. As can be seen by comparing figures 18 and 19, these angles of attack were significantly lower than expected above 1.4 Mach number but higher than predicted between 1.4 Mach number. Lateral-directional handling qualities boundaries were defined based on extrapolated values of sideslip derivatives. Although zero  $C_{n_\beta}$  was not a limiting boundary per se, flight in areas where  $C_{n_\beta}$  approached zero was explored with caution in an incremental manner. With the rocket engine off,  $C_{n_\beta}$  was zero (at angles of attack below pitchup) above 1.3 Mach number only. An even larger area of negative  $C_{n_\beta}$  was defined over the transonic and supersonic Mach range as a result of aerodynamic effects due to the rocket exhaust. Boundaries for potential loss of directional control ( $C_{n_\beta}^*=0$ ) were conservatively estimated based on flight test results above 1.3 Mach number both with and without rocket engine on. As can be seen in figure 19, these boundaries significantly reduced the usable angle of attack. Neither of the  $C_{n_\beta}^*=0$  boundaries were violated during test program.

No power-on  $C_{n_\beta}$  boundaries are shown on the predicted boundary plot. After power effects had been discovered on the X-24A, wind tunnel tests were conducted to predict these effects for the X-24B. Although modeling of the rocket exhaust conditions was not exact (hence the resulting data was not considered to be accurate), the results were used as guidelines to evaluate the potential loss of stability with the rocket engine on.

The comparison of the handling qualities boundaries before and after the flight test program exemplifies the need for an incremental envelope expansion approach to flight test of new aircraft. Boundaries determined by actual lateral-directional stability were considerably more restrictive than they were predicted to be. Although power-on wind tunnel test did indicate an effect of the rocket engine, tests of this nature are not conducted for most test programs.

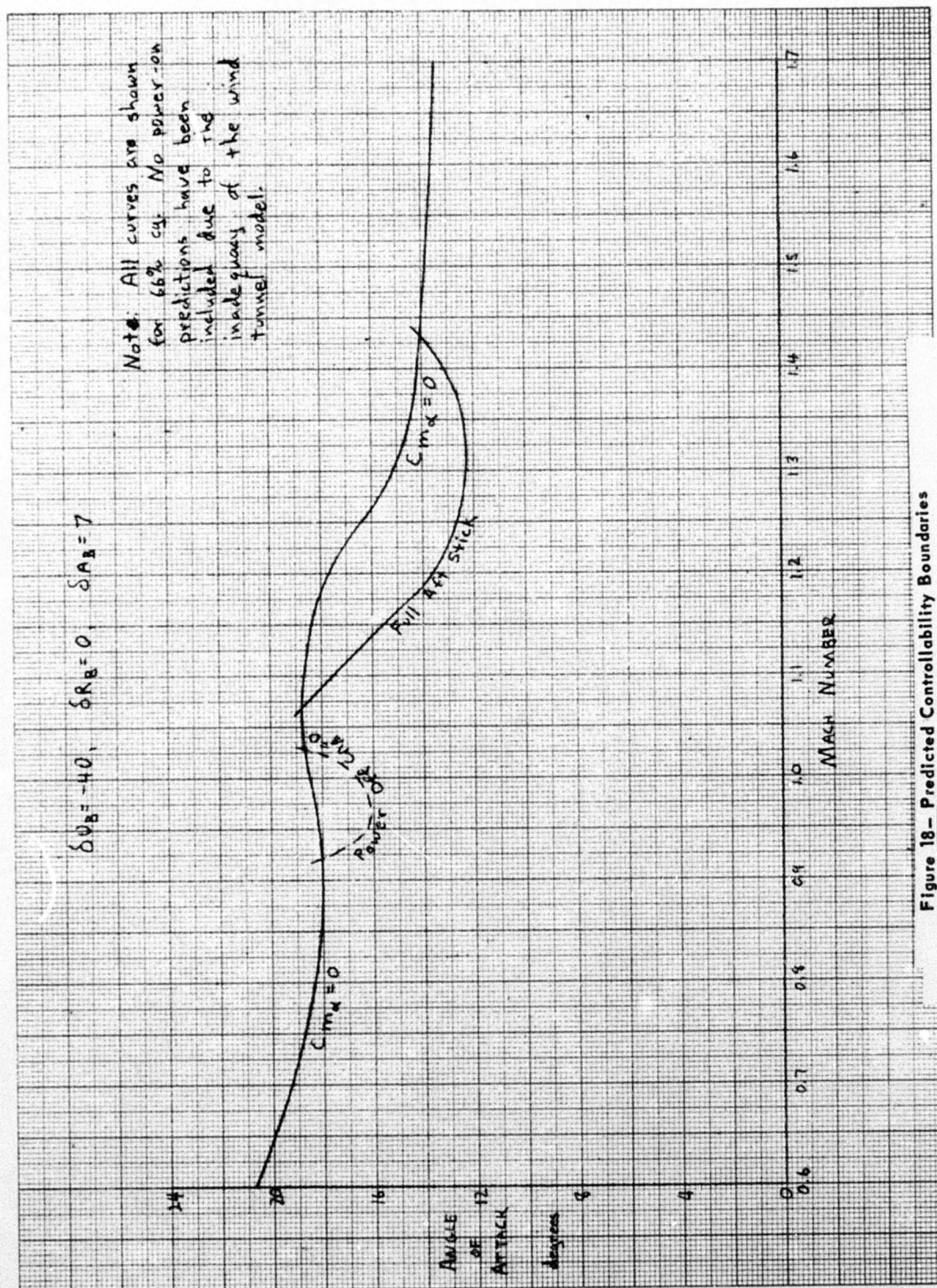


Figure 18— Predicted Controllability Boundaries



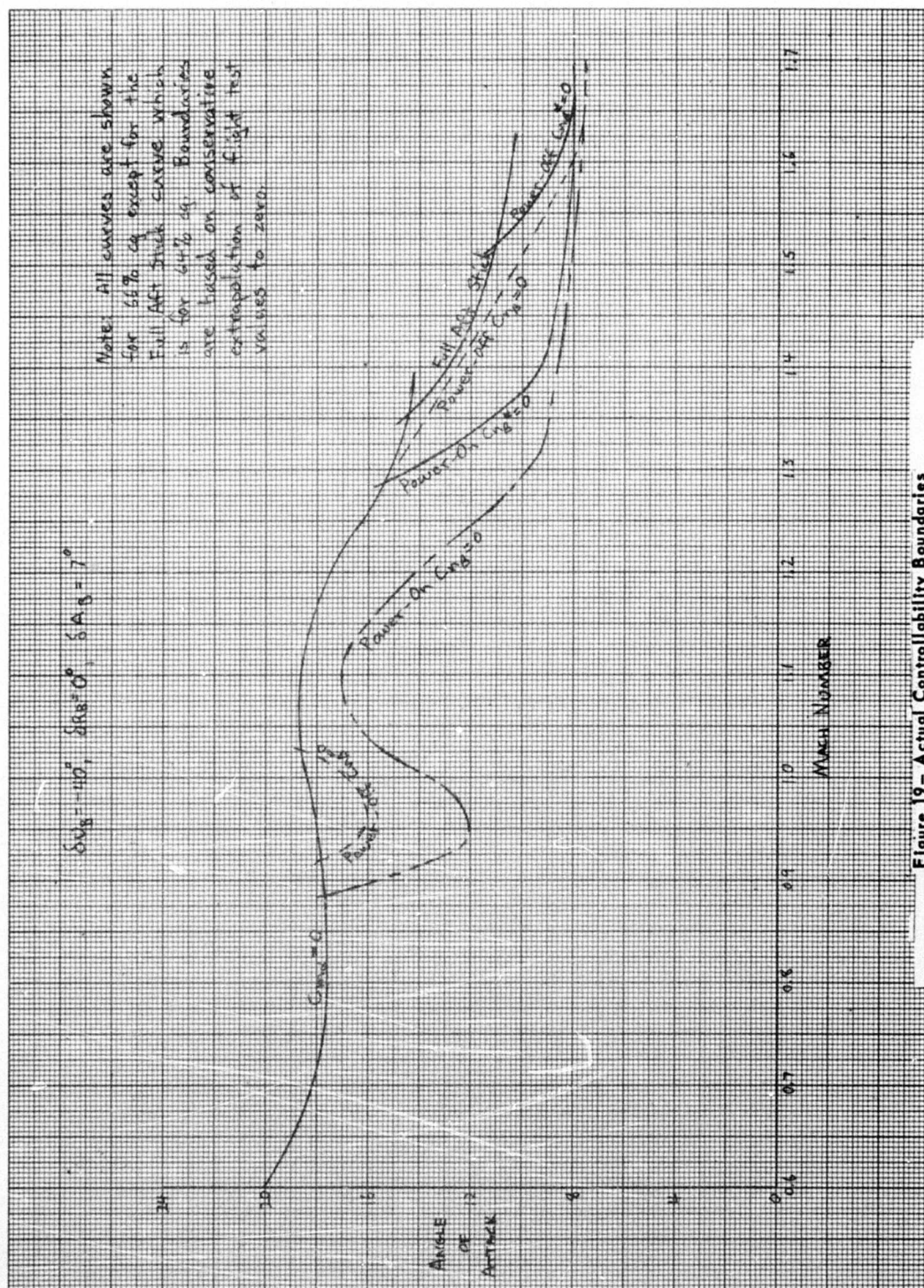


Figure 19 - Actual Controllability Boundaries

## STABILITY DERIVATIVE RESULTS

Stability derivatives were extracted from flight test data as both a research objective and a means to insure a safe flight envelope expansion. A knowledge of the aerodynamic derivatives simplified the analysis of aircraft motions and made the task of pinpointing problem areas much easier. In addition, the heavy reliance of the test program on the simulator made authenticity mandatory, and revision of the simulator with flight determined derivatives was the most accurate method of insuring simulator fidelity.

### Method

Two methods of extracting stability derivatives were used on the X-24B flight test program. The Modified Maximum Likelihood Estimator (MMLE) is an all-digital computer program that was used for routine processing of data. MMLE is an output error program that uses a modified Newton-Raphson technique to attain convergence. Features of the program include a signal noise weighting function (noise covariance matrix) and an a priori weighting scheme. Both features were used to determine flight-measured derivatives. The ease and speed of setup and execution made derivative results available within a day after the engineering units tape (which contained flight time histories) was received.

The second method was a hybrid matching technique named STABDIV. This was a sophisticated manual matching process that allowed greater accuracy in less time than obtained with earlier analog matching techniques. A digital computer is used to store and recall time histories of measured control surface inputs and aircraft response. Equations of motion are solved by an analog computer in a repetitive operation mode, and the computed and measured responses are shown as standing waves on a cathode ray tube. The effect of changing a derivative can be seen instantaneously by viewing the standing waves on the cathode ray tube. While the hybrid technique represents a marked improvement over conventional analog methods, it still requires more time and expertise than the MMLE program. The advantage of STABDIV lies in the fact that the operator may quickly assess the accuracy of the derivative he is determining. The sensitivity of the match to particular derivatives and other derivative trade-offs is readily apparent, and the accuracy of any one derivative for a single case is better known. For this reason, STABDIV was used in conjunction with MMLE during the early phases of the flight test program to determine results from "envelope expansion" maneuvers. Once the available envelope had been explored, the use of STABDIV was discontinued.

Test conditions were selected to determine the effects of angle of attack, Mach number, power, control system biases, and Reynolds number. For the purpose of derivative extraction, the X-24B was assumed to be rigid. Due to the boost/glide nature of the flights, test time in a trimmed and stabilized condition was minimal. The derivative extraction maneuvers performed, however, were usually short in duration (5 to 10 seconds), and the flight conditions usually did not change appreciably in that time. Most of the results presented in this



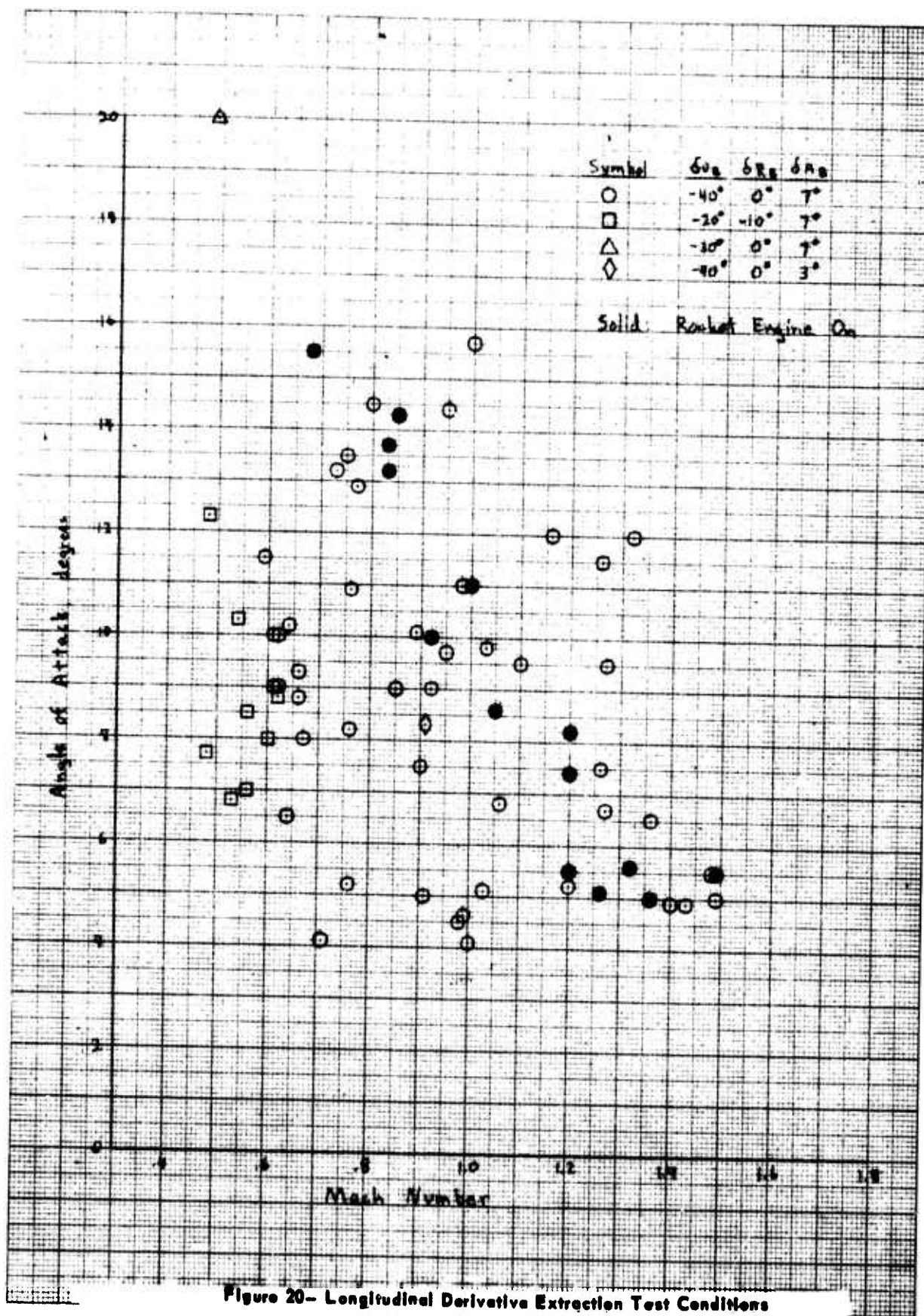


Figure 20- Longitudinal Derivative Extraction Test Conditions

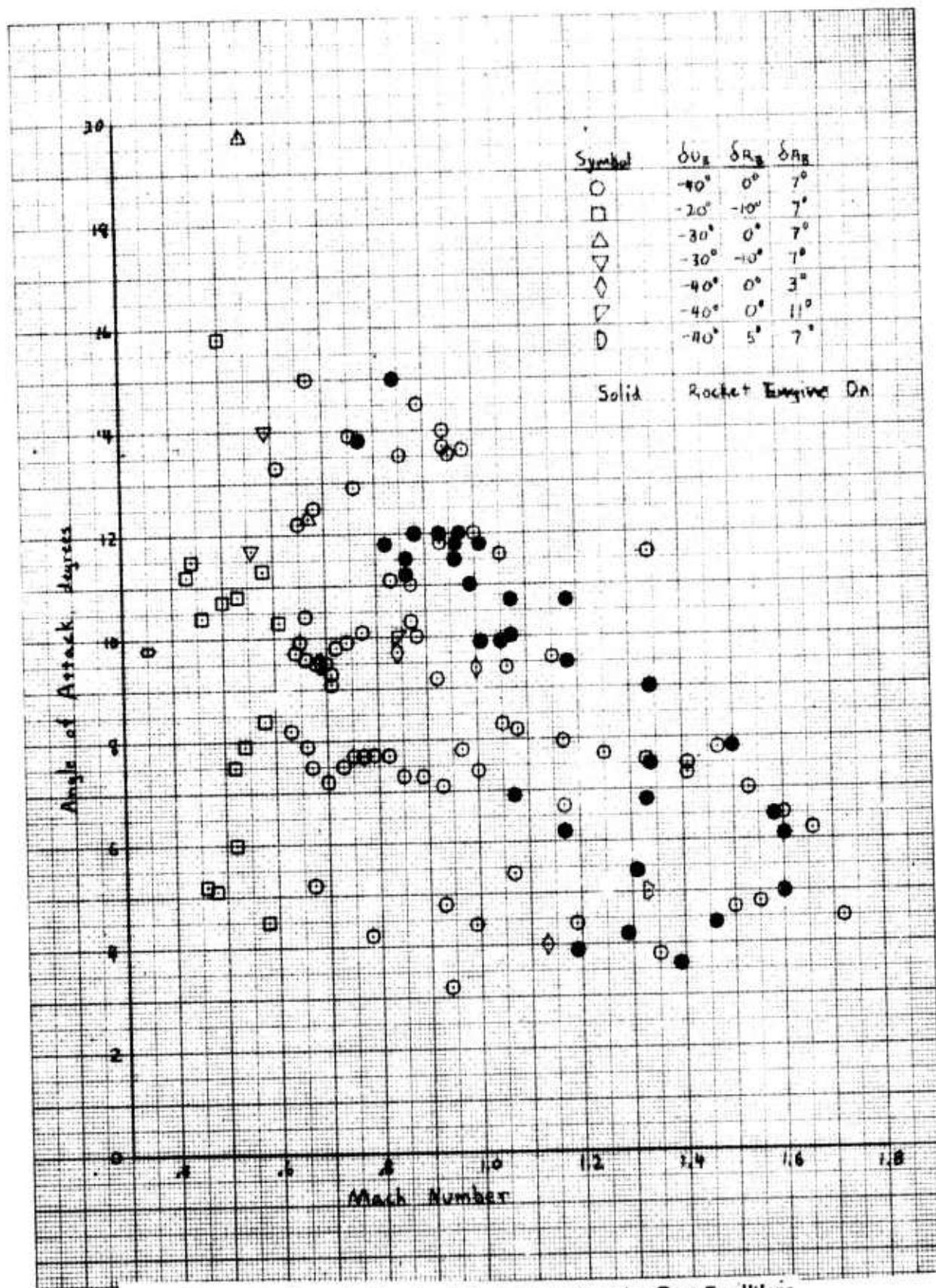


Figure 21- Lateral-Directional Derivative Extraction Test Conditions

report are from maneuvers performed with the SAS on. While derivatives obtained from SAS-off data are usually more accurate, low lateral-directional stability in some areas and the time required to revert from SAS-on to SAS-off flight conditions resulted in most of the inputs being performed with the SAS on. Flight conditions for maneuvers performed during the program are shown in figures 20 and 21.

Inputs consisted of control surface pulses and doublets initiated through the pilots control stick and rudder pedals. Sharp doublets and pulses were essential for obtaining accurate derivatives, as they allowed separation of the control inputs from the aircraft response. This prevented the trade-offs between control and damping derivatives that often occur with a slow maneuver. A longitudinal maneuver consisted of one or two rapid elevator pulses followed by a period of stick free oscillation. A lateral-directional maneuver was initiated by a sharp rudder doublet followed by two to three seconds of free oscillation, and terminated by an aileron doublet. Doublets were preferred over pulses because a doublet would aid in keeping the aircraft at wings-level flight. Some unplanned maneuvers such as a pilot induced oscillation (PIO) and several sideslip excursions were also matched, and, although the time history matches were often good, it was obvious that the derivative values were very misleading. Subsequent data analysis revealed poor correlation between data obtained from doublet maneuvers and data taken from non-doublet maneuvers. Figure 22 shows one example of this type of maneuver and the corresponding derivative extraction results.

Instrumentation was provided and maintained by NASA personnel. Aircraft accelerations, rotational rates, and angles were measured by accelerometers, gyros and an attitude platform, respectively. Angles of attack and sideslip were measured by nose boom mounted vanes. The nose boom also measured static and total pressure used in the calculation of altitude, airspeed, Mach number and dynamic pressure. These data were transmitted via a PCM telemetry system. Calibrations were made and the data was written onto a magnetic tape at 50 samples per second. All data except for bank angle and pitch angle were relatively free of noise, transients, and phase lag. Bank angle and pitch angle had a noticeable phase lag associated with them, but these parameters are probably the least important in the derivative extraction process. Weight, cg, and inertias were determined experimentally prior to first flight and then calculated for each succeeding flight based on current aircraft equipment and propellant usage. Greater detail concerning these items may be found in reference 1.

It is intended that the previous discussion give only an overview of the techniques and considerations required for a successful derivative extraction effort. A complete discussion of these techniques and the two programs involved may be found in reference 3.<sup>6</sup> Additional discussion on the STABDIV program is provided in reference 4.<sup>7</sup>

<sup>6</sup>Reference 3: Nagy, Christopher J., A New Method for Test and Analysis of Dynamic Stability and Control, AFFTC-TD-75-4, Air Force Flight Test Center, Edwards AFB, California, November 1975.

<sup>7</sup>Reference 4: Kirsten, Paul W. and Ash, Lawrence G., A Comparison and Evaluation of Two Methods of Extracting Stability Derivatives from Flight Test Data, AFFTC-TD-73-5, Air Force Flight Test Center, Edwards AFB, California, May 1974.



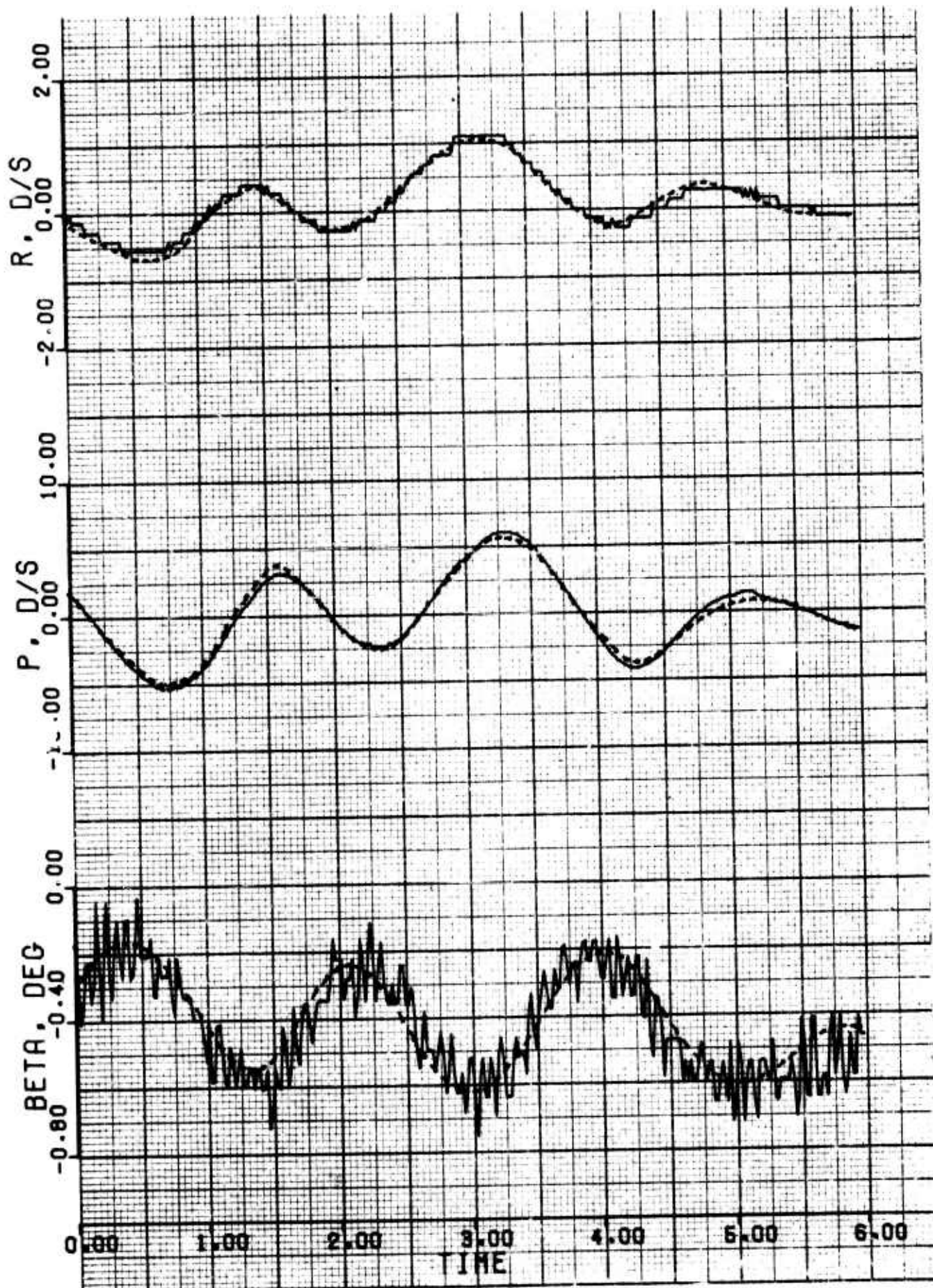
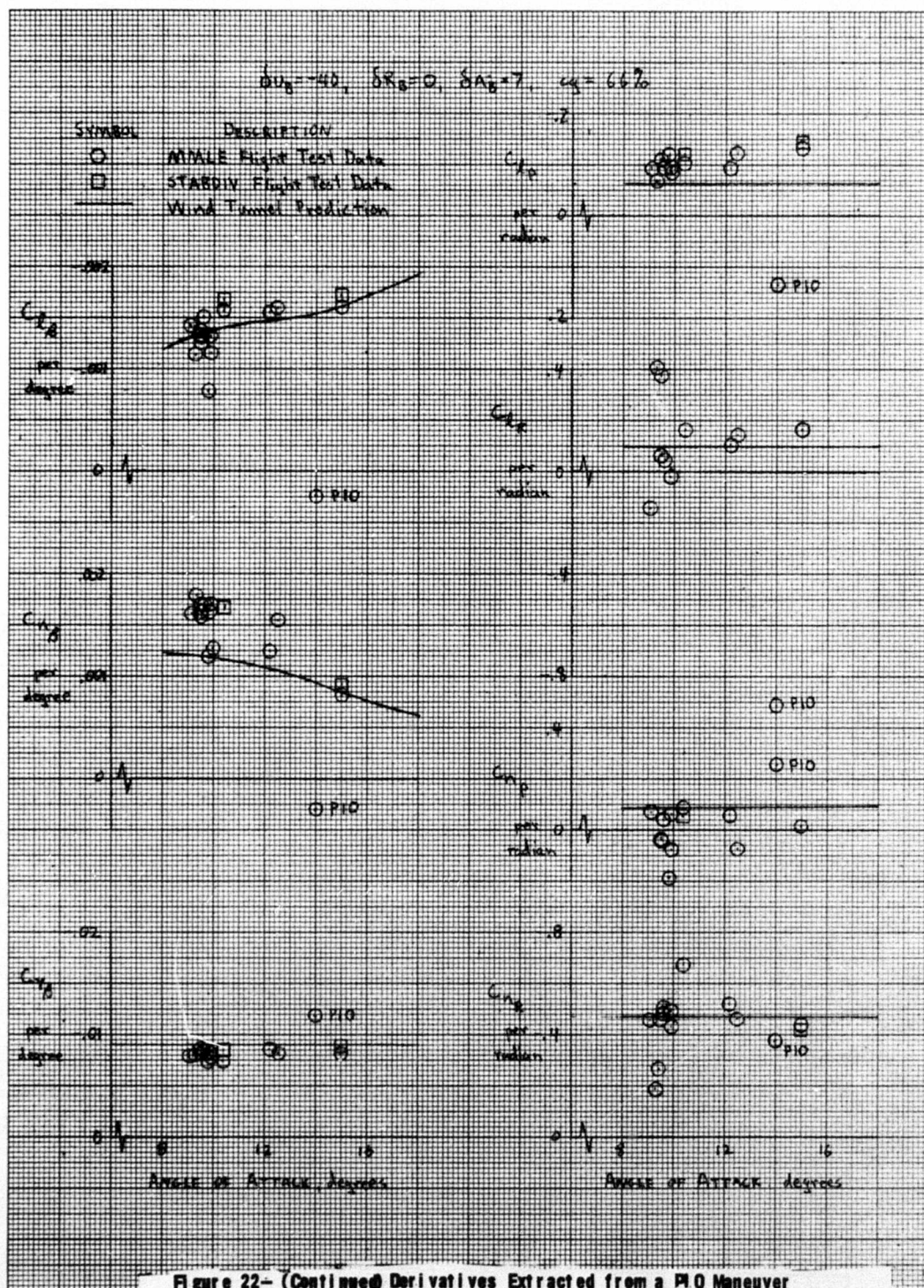


Figure 22- Derivatives Extracted from a PIO Maneuver





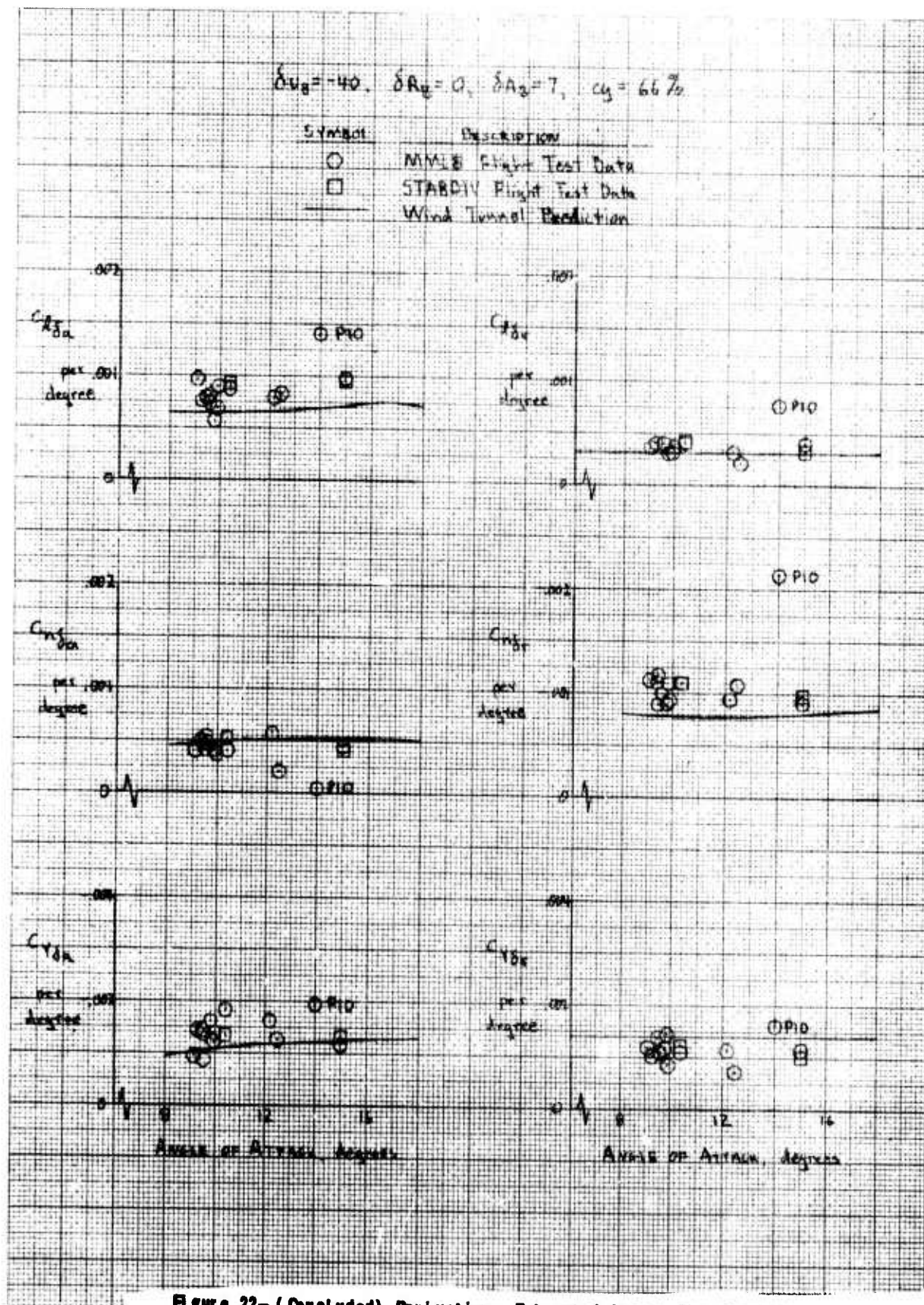


Figure 22- (Concluded) Derivatives Extracted from a PIO Manuever

## Wind Tunnel Data

All flight test derivatives will be presented with the appropriate wind tunnel or predicted estimate. Wind tunnel predictions are taken from several major tests run prior to and during the flight test program. The source of each wind tunnel curve (unless otherwise noted) may be identified using table 4. Most of the wind tunnel data shown on the figures and in table 4 were obtained from tests run fairly early in the program. As the program progressed, additional wind tunnel studies were completed. While the data from these tests were analyzed and used for simulator updates, manpower limitations precluded their presentation in this report. Additional test included transonic tests performed by Arnold Engineering Development Center (AEDC) in 1974<sup>8</sup> (source for the AEDC data in figure 24), supersonic tests performed by Langley Research Center in 1973<sup>9</sup> and some transonic tests made by AEDC in 1973.<sup>10</sup> Since all flight derivatives were obtained in a trimmed configuration, corrections have been made to the wind tunnel data for the effects of upper flaps, lower flaps, aileron bias, etc. where applicable. The derivatives  $C_{L\beta}$ ,  $C_{L\dot{\alpha}}$ , and  $C_{Y\dot{\alpha}}$  are shown as functions of Mach number only. Wind tunnel data for these derivatives showed small variations as angle of attack changed but none large enough to void the approximation. All wind tunnel predictions are shown for the reference center of gravity of 66 per cent. It should be noted that wind tunnel data for Mach number of 1.1 and 1.2 were interpolated from Mach numbers of 1.0, 1.15 and 1.3. Similarly, data at Mach numbers of 1.4, 1.6 and 1.7 were derived from tests conducted at Mach numbers of 1.3, 1.5 and 1.76. For some Mach numbers, a power-on wind tunnel prediction has been shown. These data are from tests in which it was not possible to match the exact rocket exhaust conditions encountered in flight. Hence these power-on curves should be used to indicate trends only and are in no way intended to match the power-on flight test results.

## Data Plots and Points

Derivative plots will not be shown in the body of the report unless they contribute significantly to the explanation of a handling qualities degradation or other specific effect; however, the complete set of derivatives values is contained in Appendix A. Each data point depicted on the plots comes from a maneuver where all pertinent derivatives have been determined or fixed at reasonable values. This technique prevents major derivatives from being affected by large errors in minor derivatives.

<sup>8</sup>Reference 5: Whorric, J.M., Aerodynamic Characteristics of a 5.5 Percent Scale Model of the AFFDL X-24B Flight Test Vehicle, AEDC-TR-75-10, Arnold Engineering Development Center, Arnold AFS, Tennessee, February 1975.

<sup>9</sup>Reference 6: Norris, Richard B., Summary of Supersonic Aerodynamic Characteristics of the X-24B Lifting Body, Air Force Flight Dynamics Laboratory, Wright-Patterson AFB, Ohio, to be published.

<sup>10</sup>Reference 7: White, Warren E., Documentation of Wind Tunnel Test Data From a 0.08- Scale Model of the X-24B at Mach Numbers From 0.6 to 1.3, AEDC-DR-73-18, Arnold Engineering Development Center, Arnold AFS, Tennessee, October 1973.



Table 4

## Wind Tunnel Sources

Derivative Description	Mach Range	Source
All power-off stability derivatives except damping derivatives	0.4 - 1.3	Cornell Aeronautical Laboratory, 8-Ft Transonic Wind Tunnel <sup>11</sup>
All power-off lateral-directional stability derivatives except damping derivatives	1.5 - 1.76	Arnold Engineering Development Center VKF Supersonic Wind Tunnel <sup>12</sup>
All power-off longitudinal stability derivatives except damping derivatives	1.5 - 1.76	Arnold Engineering Development Center VKF Supersonic Wind Tunnel <sup>13</sup>
All power-on derivatives	0.8 - 1.2	NASA Langley 16-foot Transonic Tunnel <sup>14</sup>
All damping derivatives	0.4 - 2.0	Calculated estimate <sup>15</sup>
All gear down derivatives	0.17	Air Force Institute of Technology Five-Foot Subsonic Tunnel <sup>16</sup>

<sup>11</sup>Reference 8: DeKuyper, R.E., Transonic Wind Tunnel Tests on a .08 Scale Model of the FDL-8 Lifting Body, Vol 1-4, Report No. AA-4024-W-2, Cornell Aeronautical Laboratory, Inc., Buffalo, New York, January-March 1971.

<sup>12</sup>Reference 9: Jenke, Leroy M., Wind Tunnel Tests of an FDL-8X Double-Delta Spacecraft Model at Mach Numbers From 1.5 to 8.0, AEDC-TR-71-218, Arnold Engineering Development Center, Arnold AFS, Tennessee, October 1971.

<sup>13</sup>Reference 10: Lindsay E. Earl, Aerodynamic Characteristics of the AFFDL X-24B Configuration at Mach Numbers From 1.5 to 5.0, AEDC-TR-74-87, Arnold Engineering Development Center, Arnold AFS, Tennessee, September 1974.

<sup>14</sup>Reference 11: Selegan, D.R. et. al., Effects of Rocket Exhaust on the Aerodynamics of the X-24A and X-24B Lifting Bodies, AFFDL-TM-75-29-FXS, Air Force Flight Dynamics Laboratory, Wright-Patterson AFB, Ohio, May 1975.

<sup>15</sup>Damping derivatives were obtained from a computer program developed by AFFDL. These data were originally calculated for the FDL-7 aerodynamic shape.

<sup>16</sup>Reference 12: Norris, Richard B., et. al., Parametric Study of an 8 $\frac{1}{2}$  Scale Model of the X-24B in the Landing Configuration, AFFDL-TM-73-21-FXS, Air Force Flight Dynamics Laboratory, Wright-Patterson AFB, Ohio April 1973.



$\delta U_B = -20^\circ$ ,  $\delta R_B = -10^\circ$ ,  $\delta A_B = 7^\circ$ ,  $CG = 66\%$

SYMBOL

DESCRIPTION

○

Flight Test Data ( $M = 0.4 - 0.6$ )

—

Cornell Wind Tunnel Prediction ( $M = 0.4$ )

- - -

AFIT Wind Tunnel Prediction ( $M = 0.47$ )

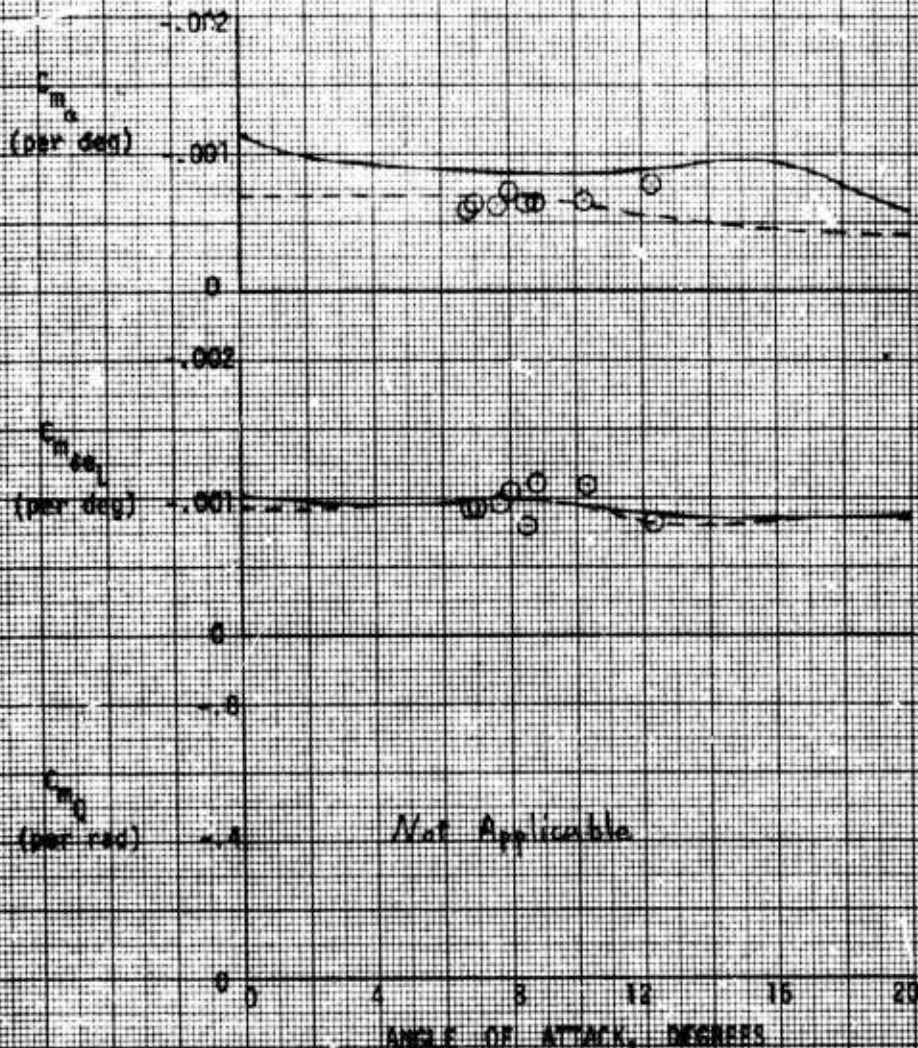


FIGURE 23 PITCHING MOMENT DERIVATIVES  $M = 0.4 - 0.6$

Correlation Between Cornell and AFIT Wind Tunnel Data

For example,  $C_{n\delta r}$  obtained from a maneuver where  $C_{nR}$  was off by a factor of 100 would not be used. In some cases the program was unable to determine a realistic value for one or more derivatives (usually damping derivatives). These maneuvers were rerun holding the indeterminate derivatives fixed at values obtained from previous test results. In these cases the particular derivative held fixed will not be shown on the derivative plots. A final note is that in many cases an MMLE data point and a STABDIV data point will be shown at the same angle of attack with similar derivative values. It should be understood that these are simply two different analysis methods performed on the same maneuver, and similar derivative values would be expected.

#### Longitudinal Derivatives

Longitudinal derivative plots are shown in figures A1 through A26. Both MMLE and STABDIV were run in a two degree of freedom mode to extract pitching moment and normal force derivatives. Determination of chordforce derivatives entailed more setup work and were not of primary interest for this program; hence they were not determined. Complete performance data may be found in reference 13.<sup>17</sup>

#### Subsonic Configuration

Derivatives for this configuration are shown on figures A1 through A4. One of the early surprises of the test program is shown on the pitching moment plots.  $C_{m\alpha}$  was consistently 20% to 30% below Cornell wind tunnel predictions. After this discrepancy was discovered, a great deal of effort was spent rechecking the longitudinal cg and pitch inertia to insure that an error in one of these parameters was not responsible for the  $C_{m\alpha}$  discrepancy. No error could be found;  $C_{m\alpha}$  was definitely lower than predicted. This has also confirmed by the longitudinal trim curves (figures B1 and B2). Figure 23 shows a  $C_{m\alpha}$  comparison between flight data, the Cornell wind tunnel values and  $C_{m\alpha}$  measured by the AFIT wind tunnel test described in reference 12. It may be seen that the AFIT data is closer to the flight-measured data. There are, however, large differences in Mach number and Reynolds number between the flight data and the AFIT wind tunnel data. The AFIT test was conducted at a Mach number of 0.17 (flight data at 0.4 to 0.6) and a total Reynolds number of  $3.3 \times 10^6$  (flight data at  $50 \times 10^6$ ).

The lower flap effectiveness derivative,  $C_{m\delta e_L}$ , agreed well with wind tunnel predictions at both Mach numbers. This fact assures that the difference in the slope of the pitch trim curve is, indeed, attributable to the difference in  $C_{m\alpha}$ .

<sup>17</sup>Reference 13: Richardson, David F., Flight Test and Wind Tunnel Performance of the X-24B Research Aircraft, AFFTC-TR-76-10, Air Force Flight Test Center, Edwards AFB, California, to be published.

$\delta U_B = -40^\circ$ ,  $\delta R_B = 0^\circ$ ,  $\delta A_B = 7^\circ$ ,  $c_g = 66\%$

SYMBOL

DESCRIPTION

○  
—  
---

Flight Test Data  
Cornell Wind Tunnel Prediction ( $M=0.8$ )  
AEDC Wind Tunnel Prediction ( $M=0.8$ )

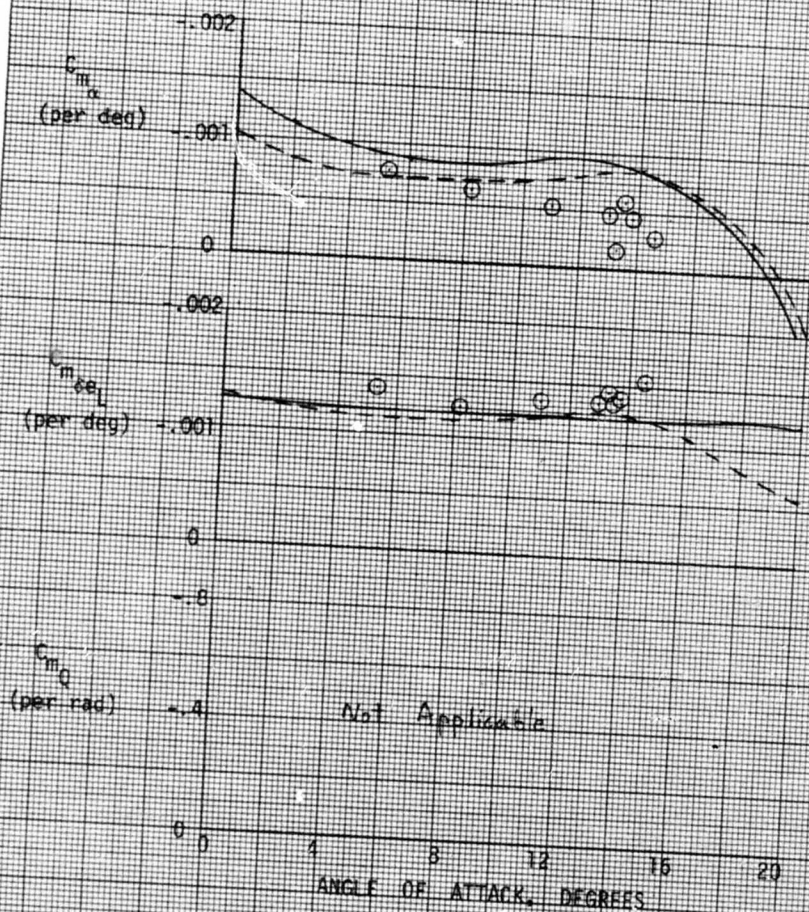


FIGURE 24 PITCHING MOMENT DERIVATIVES  $M=0.8$   
Correlation Between Cornell and AEDC Wind Tunnel Data



Pitch damping is generally less than the calculated prediction, although there is some scatter in the  $C_{m_Q}$  values. Many of these data points come from SAS-on maneuvers where  $C_{m_Q}$  is difficult to identify.

Normal force derivatives were in general agreement with predicted values, although the normal force curve slope,  $C_{N_\alpha}$ , was consistently slightly less than the wind tunnel value. The slight decrease in  $C_{N_\alpha}$  was also detected on the plots of  $C_L$  vs angle of attack (reference 13).  $C_{N_{\delta_{er}}}$  was scattered around the wind tunnel line.

#### Transonic Configuration

The pitch stability derivative,  $C_{m_\alpha}$ , exhibited a continued degradation in the transonic configuration (figures A5 through A7). This trend was most apparent through Mach 0.8. Concern over this degradation led to a short wind tunnel study to try to predict correct values of  $C_{m_\alpha}$  in the wind tunnel. The study was run at AEDC (reference 5) and used a model which corrected some minor deficiencies in the original model. Figure 24 shows a comparison of this data with Cornell data and flight test values. It may be seen that the AEDC data is closer to flight measured values of  $C_{m_\alpha}$  in some areas but was not in complete agreement.

Values of  $C_{m_\alpha}$  for Mach numbers of 0.9 and 0.95 (figures A8 and A10) show reasonable agreement with predictions except at high angles of attack. Wind tunnel data in this Mach number region, however, are subject to interpretation, and small shifts in the measured value of  $C_m$  could lead to considerably different values of  $C_{m_\alpha}$  at high angles of attack. One data point on the  $M=0.9$  curve reflects the rapidly changing values of  $C_{m_\alpha}$  with Mach number. The data point at  $\alpha=9.0^\circ$  was taken at a Mach number of 0.95, and it is indeed about halfway between the  $M=0.9$  and  $M=0.95$  curves.<sup>18</sup>

Power off values of  $C_{m_\alpha}$  at Mach numbers of 1.0 to 1.3 are slightly less than wind tunnel predictions except at high angles of attack. These data are shown in Figures A10 through A13. Much of the scatter evident in these data may be due to unsteady flow at these Mach numbers. In many cases it was impossible to determine accurate values of all pitch derivatives in the area. Power-on values of  $C_{m_\alpha}$  exhibit a significant downward trend. This effect will be discussed in the "Power Effects" section.

Flight values for  $C_{m_\alpha}$  at  $M=1.4$  (figure A14) were close to wind tunnel estimates, but values of  $C_{m_\alpha}$  at  $M=1.5$  (figure A15) were up to 60% higher than predicted. The angle of attack range at these Mach numbers was severely limited by low lateral-directional stability and other flight planning considerations (reference 1).

<sup>18</sup>Several Mach effects of these type will be seen throughout the report. They occur because wind tunnels are capable of testing at stabilized, even increments of Mach number and rocket/glide research vehicles are not. Mach number for data shown in this report have been rounded to the nearest available Mach number where a plot is presented.



Values of  $C_{m\delta e_L}$  were slightly higher than predicted at all Mach numbers. Some of the apparent scatter in the data may be explained by Mach effects. For example, at  $M=0.9$  the three low values of  $C_{m\delta e_L}$  were determined at Mach numbers of 0.85 to 0.87. All other values of  $C_{m\delta e_L}$  on that plot were measured at Mach numbers of 0.90 to 0.92. By observing the data values and wind tunnel curves, it can be seen that  $C_{m\delta e_L}$  changes rapidly with Mach number throughout the transonic and supersonic region.

Longitudinal trim curves for transonic and supersonic Mach numbers (figure B5 through B12) continue to show reduced pitch stability. This is consistent with the slight reduction in  $C_{m\alpha}$  at many Mach numbers and angles of attack combined with the increase in  $C_{m\delta e_L}$ .

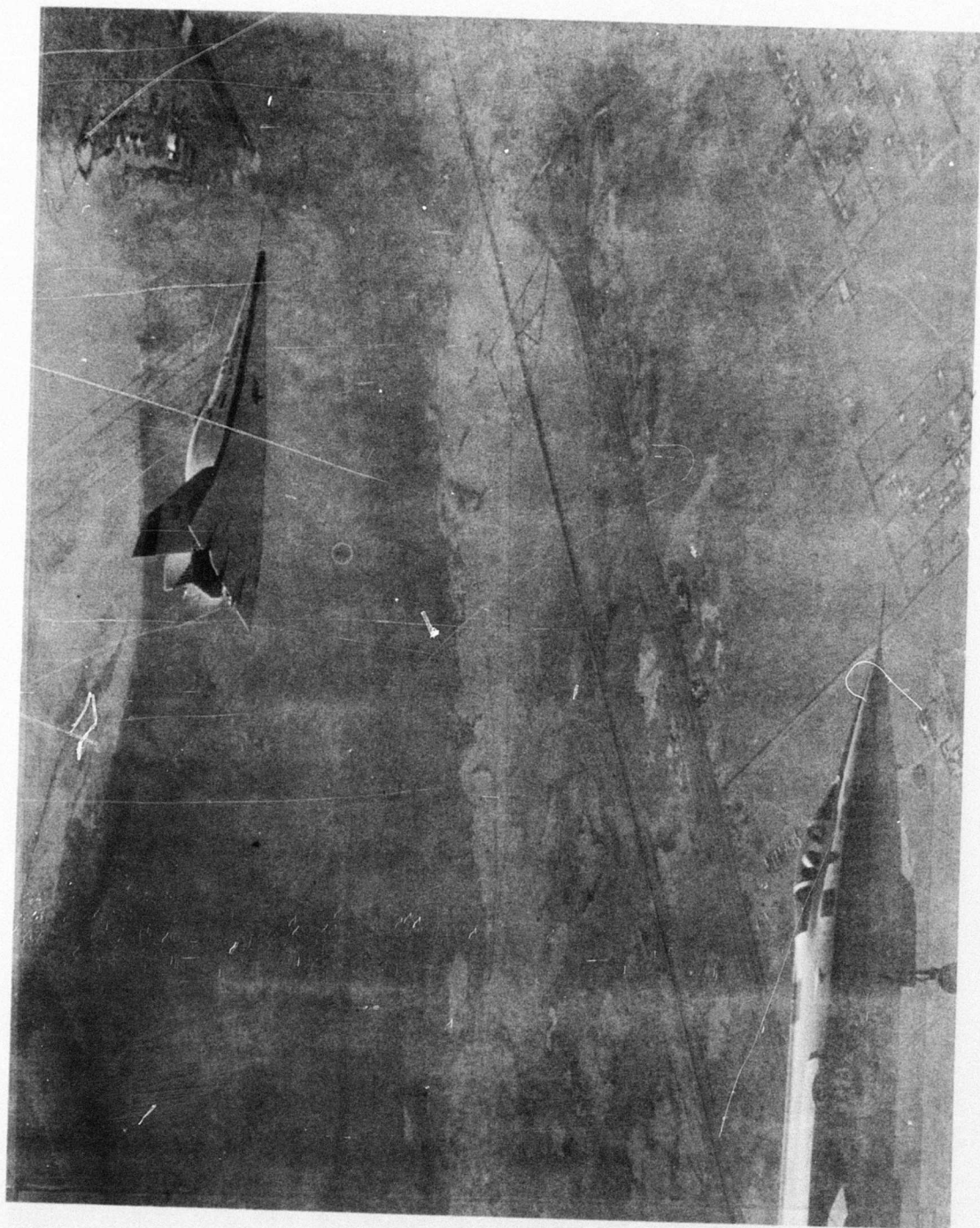
The pitch damping derivative data are scattered around the preflight prediction. It will be noted that fewer  $C_{m_Q}$  data points are shown than for the other pitch derivatives. Values of  $C_{m_Q}$  were held fixed at the predicted value for some of the SAS-on maneuvers where reasonable values of  $C_{m_Q}$  were unattainable. (The derivative  $C_{m_Q}$  is difficult to identify when it is overshadowed by large values of  $C_{m\delta e_L}$  and  $C_{m\alpha}$ .) In addition the larger values of velocity at high Mach number ( $>0.8$ ) tend to make the contribution of  $C_{m_Q}$  small, since velocity is in the denominator of the  $C_{m_Q}$  dimensionalization factor. This is not true for the other pitching moment derivatives. All the values of  $C_{m_Q}$  which have been shown have been weighted toward the calculated prediction by the a priori scheme in MMLE.

Normal force derivatives,  $C_{N\alpha}$  and  $C_{N\delta e_L}$  are shown in figures A16 through A26. Predictions of both derivatives were generally good. As was the case with the subsonic configuration, flight measured values of  $C_{N\alpha}$  in the transonic configuration were 5% to 10% lower than predicted values at some Mach numbers.

#### Lateral-Directional Derivatives

##### Subsonic Configuration

Figure A27 shows sideslip derivatives for the landing gear down configuration. The flight value of  $C_{n\beta}$  is considerably above the value predicted by the AFIT test with the gear down. Notice, however, that the gear up prediction by the AFIT tunnel is substantially less than that of the Cornell tunnel. Comparison of the gear down flight value of  $C_{n\beta}$  with the gear up flight values (figure A28) shows that the AFIT predicted increment in  $C_{n\beta}$  due to the landing gear is approximately correct. The lower values of  $C_{n\beta}$  on both of the AFIT curves are thought



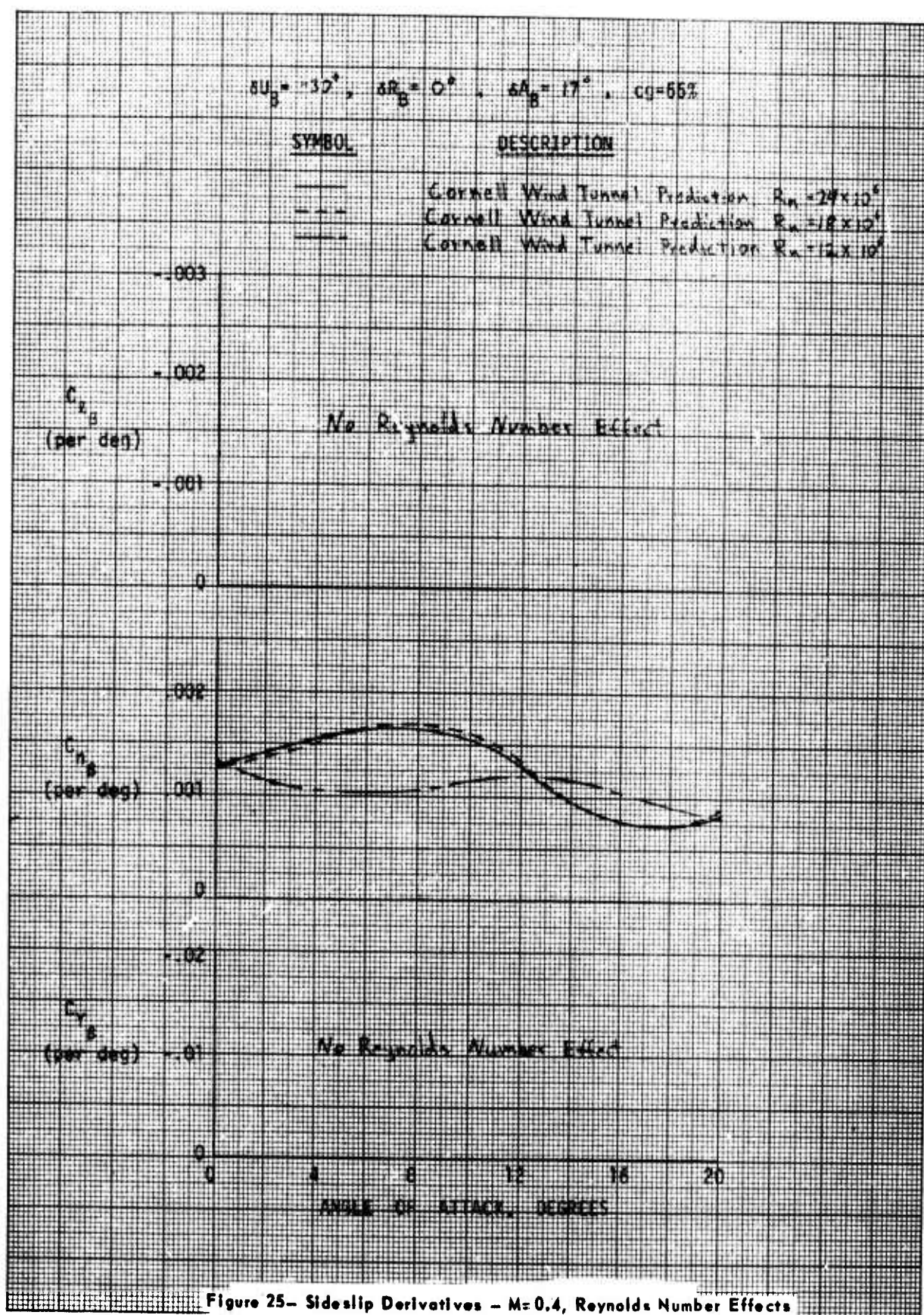


Figure 25- Sideslip Derivatives -  $M=0.4$ , Reynolds Number Effects



to be a Reynolds number effect. The Reynolds number for the AFIT test was  $3.3 \times 10^6$ . The Cornell test was run at  $23.2 \times 10^6$  and the flight data is about  $50 \times 10^6$ . Data obtained at Mach numbers of 0.4 indicate a lower  $C_{N\beta}$  at lower Reynolds numbers.

Sideslip derivatives in the subsonic configuration (figures A28 and A29) agree well with wind tunnel prediction except  $C_{N\beta}$  in the mid-angle of attack range. The increase in the flight measured values of  $C_{N\beta}$  was possibly due to higher Reynolds number effects. Figure 25 shows  $C_{N\beta}$  for several different Reynolds numbers. Considerable changes in  $C_{N\beta}$  can be seen as the Reynolds number is increased. Much of the apparent scatter in  $C_{L\beta}$  at high angles of attack is due to the Mach effects between  $M=0.4$  and  $M=0.6$ .

Aileron, rudder, and damping derivatives are shown in figures A30 through A35. The following observations can be made:  $C_{L\delta a}$  was generally higher than predicted,  $C_{N\delta a}$  was generally lower than predicted,  $C_{N\delta r}$  was generally higher than predicted. While the differences between wind tunnel and flight measured values of these derivatives was small in each case, the combined influence on the aircraft handling qualities was noticeable. This effect will be discussed in Appendix E. Other differences between flight measured and predicted derivatives were observed;  $C_{Y\delta r}$  was less than predicted, and  $C_{Lp}$  exhibited a trend to increase with increasing angle of attack. The increased scatter in the damping derivative data is typical for this type of aircraft using SAS-on doublet maneuvers as inputs. Gear down data are shown with the gear up data since no aileron or rudder wind tunnel derivatives were obtained in the gear down configuration.

#### Transonic Configuration

Sideslip derivatives for Mach numbers of 0.6 and 0.7 in the transonic configuration (figures A36 and A37) exhibit the same trends as those of the subsonic configurations. Agreement of  $C_{L\beta}$  and  $C_{Y\beta}$  data points with wind tunnel predictions is good.  $C_{N\beta}$  shows the same tendency to be high at mid-range angles of attack at  $M=0.6$ . At  $M=0.7$  an interesting phenomenon was observed. Figure 26 shows a number of  $C_{N\beta}$  values obtained from a series of maneuvers performed at 7.5 and 9.5 degrees angle of attack as the Mach number was decreasing. A step change may be seen as the Mach number passes through 0.74 and 0.715 respectively. It had been observed that the pressure data from orifices on the inside of the outboard fins were exhibiting a large step change as the aircraft decelerated through approximately 0.7 Mach number. Analysis of onboard motion pictures of tufts placed on the inside of the fin confirmed that a sudden change in flow was taking place. In addition, it was found that this step change was also a function of angle of attack. The Mach number and angle of attack conditions at which these pressure changes occurred were catalogued and used to define the flow separation boundary shown in figure 26. It was then decided to perform a set of data maneuvers through this region to determine if



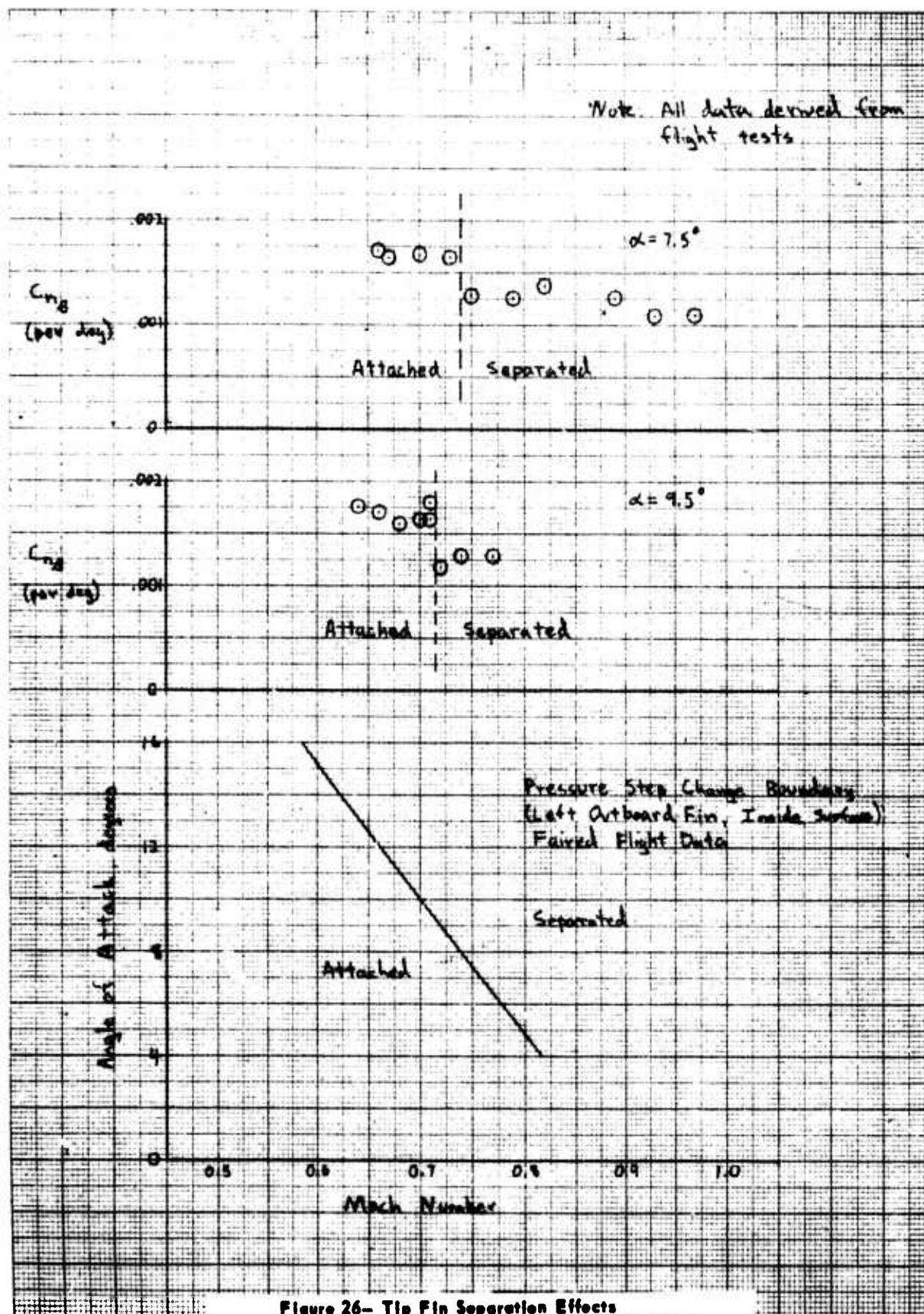


Figure 26- Tip Fin Separation Effects

the directional stability was being affected. As the  $C_{n_\beta}$  plots show, a measurable step change was detected.

Figures A38 through A43 show sideslip derivatives for the transonic and low supersonic Mach numbers ( $0.8 \leq M \leq 1.2$ ). Agreement between wind tunnel and flight measured values of power-off derivatives is generally good except for the  $M=0.95$  data. Values of  $C_{n_\beta}$  are consistently lower than predicted at 0.95 Mach numbers. Part of the scatter in  $C_{l_\beta}$  can be explained by Mach number effects, but much is believed to be the result of unsteady transonic flow. Wind tunnel testing and flight testing in this area have always been hampered by this problem. Of special interest are the data at 4.8 degrees angle of attack (figure A40). The value of  $C_{l_\beta}$  is much higher than wind tunnel predictions, and much effort has been spent trying to assess the accuracy of the data. Nothing could be found to indicate any reason to doubt either the maneuver or the results.

These figures (A38 through A43) also serve to introduce the destabilizing effect of the rocket engine in the transonic region as reflected in the reduction of  $C_{l_\beta}$  and  $C_{n_\beta}$ . Power-on data will be discussed in the "Power Effects" section. Some maneuvers were performed with different values of aileron bias and rudder bias to assess their effects on lateral-directional stability. These maneuvers will be discussed in the "Aileron and Rudder Bias Effects" section.

Supersonic sideslip derivatives are shown in figures A44 through A48 ( $1.3 \leq M \leq 1.7$ ). Agreement between flight values and wind tunnel curves is good for power-off  $C_{l_\beta}$ 's,  $C_{y_\beta}$ 's, and low-angle-of-attack  $C_{n_\beta}$ 's. Values of  $C_{n_\beta}$  measured at the mid-angle-of-attack range ( $60-120^\circ$ ) show a degradation from predictions. As the Mach number is increased, the degradation occurs at lower angles of attack and becomes more severe. There are at least two possible explanations for this. Wind tunnel data at lower Mach numbers predicted a decrease in  $C_{n_\beta}$  as the lower flaps were closed to zero. At these angles of attack supersonically, trim flap deflections are very close to zero and it is possible that this effect is stronger than predicted. A second explanation is suggested by the agreement between power-off and power-on data at these angles of attack. It is obvious that the rocket engine caused a flow change that reduced  $C_{l_\beta}$  and  $C_{n_\beta}$ . This reduction may be seen at all Mach numbers greater than 0.8. At Mach numbers above 1.3 and moderate angle of attack, it is possible that the flow change had already started to occur due to the high Mach number. The rocket engine then would not have additional effect since the slow change had already occurred. In either case the values of  $C_{n_\beta}$  at high Mach numbers and moderate angles of attack were substantially less than predicted.

Aileron derivatives are shown in figures A49 through A61. As was the case for the subsonic configuration,  $C_{l_{\delta a}}$  for the transonic configuration was slightly higher than predicted, and  $C_{n_{\delta a}}$  was from 0% to 50% lower than

predicted. Values of  $C_{Y\delta a}$  were generally higher than wind tunnel predictions. Values of  $C_{l\delta a}$ ,  $C_{n\delta a}$ , and  $C_{Y\delta a}$  were remarkably unvarying with Mach number and angle of attack.

Rudder effectiveness derivatives,  $C_{l\delta r}$ ,  $C_{n\delta r}$ , and  $C_{Y\delta r}$  are depicted in figures A62 through A74. Values of  $C_{l\delta r}$  are the same as, or slightly higher than those predicted by the wind tunnel.  $C_{n\delta r}$  was found to be about 30% higher than predicted transonically, about the same as predicted from  $M=1.1$  to  $M=1.3$ , and less than predicted above  $M=1.4$ . Wind tunnel data above  $M=1.4$  came from a different source, which may explain the shift. Flight test values of  $C_{Y\delta r}$  agree well with predictions transonically, but are up to 50% less supersonically.

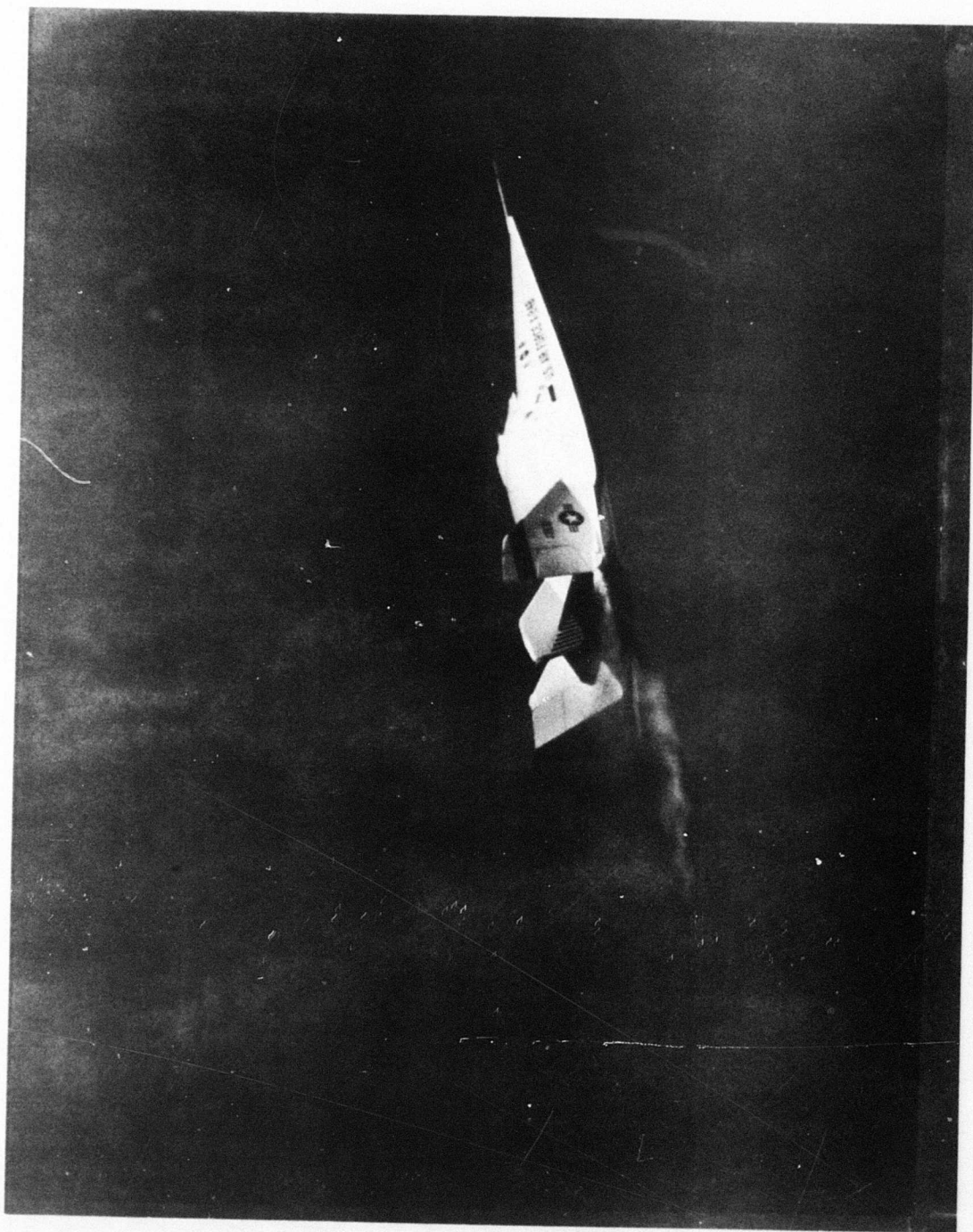
Damping derivatives (figures A75 through A87) show considerable scatter around the calculated predictions. Many of these data points, however, have been considerably influenced by the a priori weighting in MMLE, and it is probable that only  $C_{lp}$  and  $C_{np}$ , to a lesser extent, are accurate. One of the reasons for the large amount of scatter is the decreasing effect of aerodynamic damping on the vehicle as the speed increases. Since velocity is in the denominator of the dimensionalization terms (as was the case with  $C_{mQ}$ ), the effect of damping derivatives becomes negligible in the transonic and supersonic region.

#### Power Effects

One of the most significant results of the X-24B derivative study was the identification of significant derivative changes when the rocket engine was on. These occurred primarily in the lateral-directional axis but some effects were also identified longitudinally. It should be reemphasized that, due to the inability of the wind tunnel to match flight rocket exhaust conditions precisely, the wind tunnel power-on data presented in this section should be used to indicate trends only.

#### Longitudinal Derivatives

Power effects on the longitudinal derivatives were identified only at Mach numbers of 1.1 through 1.3. Figures A11 through A13 show reduced values of  $C_{m\alpha}$  for power-on maneuvers. When the derivatives were extracted, it was discovered that large trades could be made, especially between  $C_{m\alpha}$  and  $C_{mQ}$ . For example,  $C_{m\alpha}$  could be made to agree with power-off data but values of  $C_{mQ}$  would be very large negative numbers. Since SAS-off maneuvers had already established the power-off  $C_{mQ}$  as being close to predicted, it was decided to fix  $C_{mQ}$  (and sometimes  $C_{m\delta a}$ ) at values established by the wind tunnel or previous data values. These runs yielded the values of  $C_{m\alpha}$  shown in the figures. Longitudinal derivative values in this region were not well defined by the extraction program, so the conclusion about the power effect on





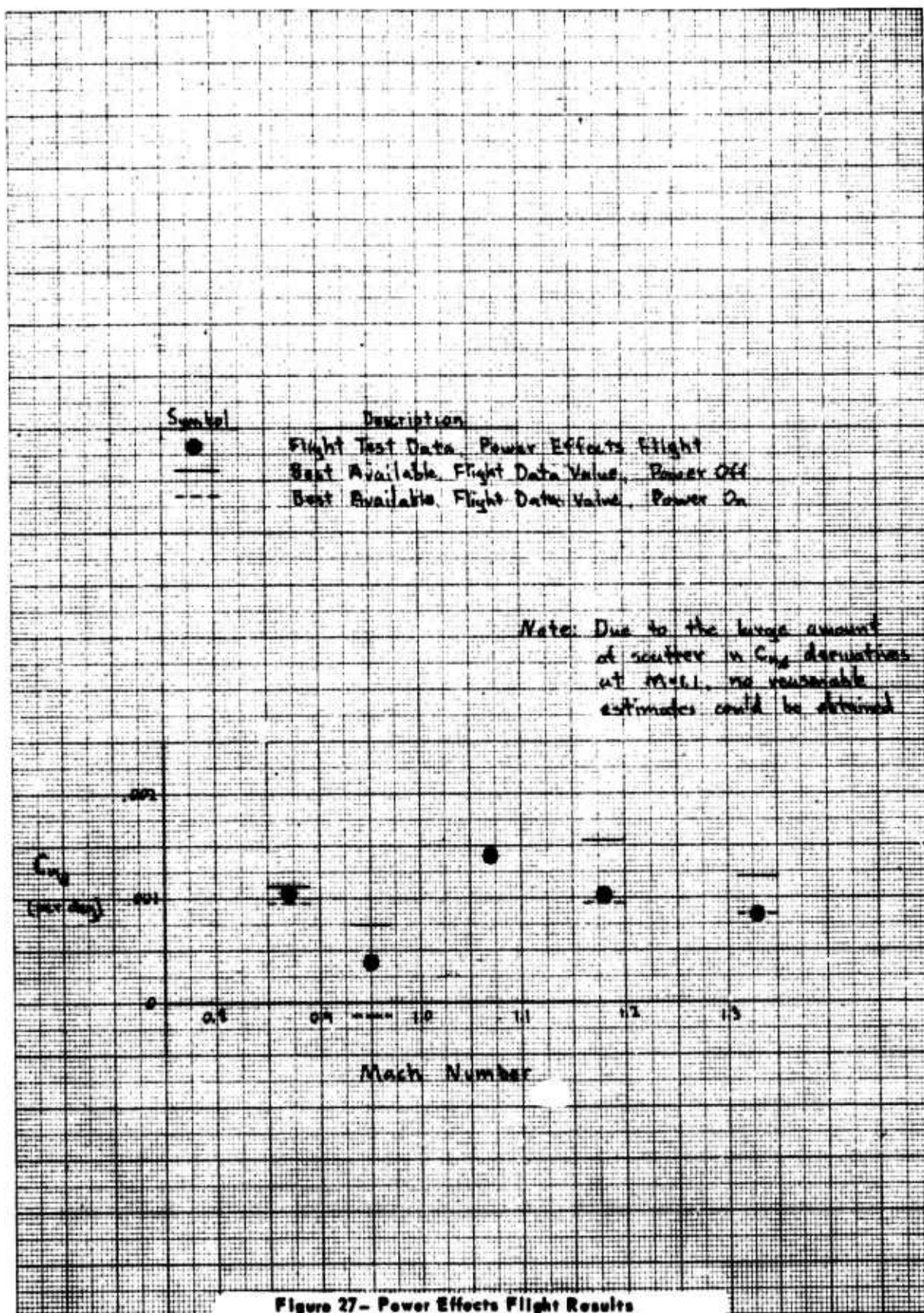


Figure 27- Power Effects Flight Results

$C_{m\alpha}$  is not well supported. No other pitching moment or normal force derivative showed consistent effects of the rocket engine. The power-on longitudinal trim curve at  $M=1.15$  (figure B16) shows a reduced pitch stability which tends to confirm the reduced values of  $C_{m\alpha}$  in this Mach region.

#### Lateral-Directional Derivatives

Power effects on lateral-directional derivatives were experienced during the X-24A flight test program. The effects were further confirmed during the X-24B program and appeared as degradations in  $C_{l\beta}$  and  $C_{n\beta}$ . These were present, in varying degrees, at Mach numbers from 0.8 to 1.7. Power effects can be seen on figures A38 through A47. In general, the power effect on  $C_{l\beta}$  was a small biasing in the destabilizing direction, and was not a strong function of angle of attack. The power effect on  $C_{n\beta}$  was small at low angles of attack (where  $C_{n\beta}$  was high). The effect was usually largest where  $C_{n\beta}$  was lowest (at higher angles of attack). The worst degradation with the power on occurred at  $M=0.95$  (figure A40). At  $12^\circ$  angle of attack and  $M=0.95$ , the rocket not only caused a degradation in  $C_{l\beta}$  and  $C_{n\beta}$  but allowed sideslip excursions into a region of non-linear sideslip derivatives. The two power-on data points near  $12^\circ$  angle of attack ( $C_{l\beta}=-.00065$ ,  $C_{n\beta}=-.00013$ ) were extracted from a maneuver where the sideslip was less than two degrees. The power-on points at the same angle of attack showing decreased stability ( $C_{l\beta}=-.00035$ ,  $C_{n\beta}=-.00055$ ) came from a maneuver where the sideslip reached six degrees. Cornell wind tunnel data (power-off) at this condition had predicted a non-linear  $C_{n\beta}$  but only when sideslip was greater than six degrees. The increased directional stability with the rocket engine off resulted in sideslip excursions of less than 4 degrees for normal inputs. For this reason, non-linear values of  $C_{n\beta}$  were not noticed when the rocket engine was off. No other lateral-directional derivative exhibited any effects of power.

#### Power Effects Flight

Discussion of the power effects with aerodynamicists at the Air Force Flight Dynamics Laboratory led to the theory (based on wind tunnel results) that power effects might be reduced by flying at a higher Reynolds number and dynamic pressure. To test this hypothesis, one flight was planned to duplicate five Mach/angle of attack conditions encountered on previous flights. The new test points, however, would be flown at a lower altitude, thus increasing dynamic pressure and Reynolds number. Table 5 shows a comparison between the test conditions. Figure 27 shows the results of this test along with the best available flight data for power-off and power-on values of  $C_{n\beta}$ . It can be seen that the higher dynamic pressure and Reynolds number alleviated the power effects only at 0.95 Mach number.

#### Aileron and Rudder Bias Effects

Wind tunnel tests had predicted some effects of both rudder and aileron

Table 5

## POWER EFFECT FLIGHT COMPARISON

Type of Flight	Mach Number	Angle of Attack Degrees	Dynamic Pressure psf	Reynold's Number	Velocity ft/sec	Altitude ft
Power Effects	0.86	11.5	145	$46.7 \times 10^6$	835	48600
Normal	0.88	12.0	86	$29.1 \times 10^6$	853	58800
Power Effects	0.96	11.8	141	$39.6 \times 10^6$	930	54400
Normal	0.93	12.0	109	$30.4 \times 10^6$	890	57000
Power Effects	1.07	10.0	154	$40.1 \times 10^6$	1040	56300
Normal	1.08	10.7	80	$21.0 \times 10^6$	1050	68900
Power Effects	1.18	9.5	174	$40.3 \times 10^6$	1155	58100
Normal	1.18	10.7	89	$21.3 \times 10^6$	1145	70200
Power Effects	1.33	6.8	205	$42.4 \times 10^6$	1280	59000
Normal	1.34	7.5	107	$22.6 \times 10^6$	1293	71300

bias on  $C_{l\beta}$  and  $C_{n\beta}$  in addition to their effects on pitch trim. To test for this, several data maneuvers were performed with off-nominal values of rudder bias and aileron bias.

#### Aileron Bias

Several maneuvers were performed with the aileron bias at 3° and 11°. Results of these tests may be found on figures A8, A37, A38, A40, A41, and A42. No effect was discernable on the longitudinal stability derivative  $C_{m\alpha}$ . The wind tunnel had predicted that decreased aileron bias would produce higher values of  $C_{n\beta}$ . No effect, however, could be seen on either  $C_{n\beta}$  or  $C_{l\beta}$ .

In addition to the effect on sideslip derivatives, the wind tunnel also predicted a pitching moment effectiveness of the aileron bias. While the aileron bias moved too slowly to produce a dynamic maneuver analyzable by MMLE, it was possible to determine its effectiveness by calculating the amount of elevator required to retrim the vehicle at the same angle of attack. This has been done for several conditions and the results are presented in Table 6. The results indicated that the aileron bias was somewhat more effective in pitch than predicted and generally more effective than the lower flap.

#### Rudder Bias

The rudder bias could be biased inward from zero to obtain the subsonic configuration or outward to obtain a predicted increase in directional stability at high Mach numbers. Only one maneuver with outboard bias was performed and the results are shown in figure A44. It is very difficult to verify any increase in  $C_{n\beta}$  from this data point, however, the predicted increase from +5°  $\delta R_{\beta}$  at this condition was small (+.00015).

The rudder bias, like the aileron bias, was also capable of causing a significant pitching moment effect. The outward bias at  $M=1.3$  had a negligible effect on pitch trim but the pitch change of the inward bias at low speeds was significant. Pitching moment effectiveness of the rudder bias was calculated the same way as the aileron bias, and the results are presented in Table 7.



Table 6

## AILERON BIAS AND LOWER FLAP PITCHING MOMENT EFFECTIVENESS

Mach Number	Angle of Attack degrees	Predicted $C_{m\delta AB}$ per degree	Measured $C_{m\delta AB}$ per degree	Measured $C_{m\delta e_L}$ per degree
0.6	6° - 12°	-.00106	-.00115	-.00125
0.9	4° - 8°	-.00155	-.00210	-.00175
1.25	4° - 6°	-.00130	-.00140	-.00110

Table 7

## RUDDER BIAS PITCHING MOMENT EFFECTIVENESS

Bias Rudder Setting Degrees	Mach Number	Angle of Attack degrees	Measured $C_{m\delta RB}$ per degree	Predicted $C_{m\delta RB}$ per degree
+5(outbrd)	1.4	5°	0	-.00008
-10(inbrd)	0.6	5° - 13°	-.00059	-.00050

## CONCLUSIONS

The handling qualities and the factors which contribute to handling qualities were determined for the X-24B to a Mach number of 1.76. Although flight test time was limited and stabilized flight was difficult to achieve, a comprehensive picture of the aircraft's flight characteristics was developed. This was accomplished by utilizing a combination of pilot ratings and comments in conjunction with analysis of time histories and flight-determined stability derivatives.

The X-24B was an aerodynamic shape optimized for efficient hypersonic flight which exhibited good handling qualities over much of the flight envelope tested. The design resulted in two areas of significant improvement in lateral-directional handling qualities over some of previous lifting bodies. A low dihedral effect resulted in a reduction of the sharp roll response to sideslip excursions that had been characteristic of the lifting bodies, particularly in turbulence during final approach. The low dihedral effect also caused the aircraft to be less PIO sensitive in the lateral-directional axis. The addition of outboard ailerons provided excellent roll power. This alleviated strong dependence on an aileron-to-rudder interconnect for roll control. This excellent roll power also provided a roll SAS which was very effective in stabilizing the aircraft throughout the flight envelope. The high effectiveness of the aileron control surface meant that relatively small values for control surface authority and rate limits could be used.

The handling qualities of the X-24B were generally good with the rocket engine off. Subsonic handling was excellent in both the longitudinal and lateral-directional axes. Longitudinal stability was considered to be excellent at transonic and supersonic speeds. However, the obtainable angle of attack with full aft stick was significantly limited above 1.4 Mach number. Lateral-directional handling qualities in the same Mach range were generally considered to be satisfactory over the limited angle of attack range flown. Although the primary tasks performed at these conditions were transient data maneuvers the pilot never reported any lateral-directional control deficiencies. With the power off, the aircraft exhibited no PIO tendencies in pitch or roll, and at no time was pitch or roll control a problem.

Handling qualities with the rocket engine on were considerably degraded at some conditions. Transonic and supersonic characteristics were good or fair depending, primarily, on the level of directional stability. The level of directional stability was often a good indicator of the change in lateral-directional handling qualities as the Mach number increased. Most of the adverse comments associated with flight at transonic and supersonic speeds were directed at uncommanded sideslip excursions. Steady-state-sideslip and a wandering sideslip were caused by low directional stability and aggravated by wind shears and a misaligned rocket engine.

Handling qualities in the approach and landing phases were excellent. Due to relatively low values of dihedral effect the aircraft rode turbulence very well. The large pitchdown associated with gear deployment

on the X-24A was eliminated on the X-24B. The pilots were favorably impressed with the capability for control while in ground effect just prior to touchdown. Crosswind contributed to some uncomfortable landings since the nose sliced and the aircraft rolled sharply as the nose fell through after main gear touchdown. The aircraft could be steered with ailerons, rudders, differential braking, or nose wheel steering. Pilots considered the ground directional control to be excellent. Deceleration from braking was considered poor but adequate for the aircraft mission.

Most of the predicted stability derivatives were reasonably accurate with the rocket engine off. The major exception for the longitudinal case was subsonic values of  $C_{m\alpha}$  which were consistently 20% and 30% below wind tunnel predictions. Three significant areas of deviation from predicted directional stability were determined. At subsonic Mach number and mid-range angles of attack,  $C_{n\beta}$  was 25% above predicted estimates. At 0.95 Mach number,  $C_{n\beta}$  was somewhat less than predicted. Above 1.5 Mach number, the values of  $C_{n\beta}$  were considerably below predictions as the angle of attack increased above  $6^\circ$ .

A flow change associated with the rocket engine produced a significant change in several major derivatives. In the Mach range of 1.1 to 1.3, the values of  $C_{m\alpha}$  showed a measurable reduction with the rocket on. Both  $C_{l\beta}$  and  $C_{n\beta}$  showed reduction above Mach 0.8. The incremental reduction of  $C_{n\beta}$  generally increased as the angle of attack increased.

Flight control system performance was excellent during the test program. Since much of the system was carried over from the X-24A vehicle, most of the components were proven items. Design criteria for the new aileron system was established on the AFFTC five degree-of-freedom simulator. The resulting design performed satisfactorily during the test program.

## REFERENCES

1. Armstrong, Johnny G., Flight Planning and Conduct of the X-24B Research Aircraft Flight Test Program, AFFTC-TR-76-11, Air Force Flight Test Center, Edwards AFB, California, to be published.
2. Stuart, John S., Analysis of the Approach, Flare, and Landing Characteristics of the X-24B Research Aircraft, AFFTC-TR-76-9, Air Force Flight Test Center, Edwards AFB, California, to be published.
3. Nagy, Christopher J., A New Method for Test and Analysis of Dynamic Stability and Control, AFFTC-TD-75-4, Air Force Flight Test Center, Edwards AFB, California, November 1975.
4. Kirsten, Paul W. and Ash, Lawrence G., A Comparison and Evaluation of Two Methods of Extracting Stability Derivatives From Flight Test Data, AFFTC-TD-73-5, Air Force Flight Test Center, Edwards AFB, California, May 1974.
5. Whorric, J.M., Aerodynamic Characteristics of a 5.5 Percent Scale Model of the AFFDL X-24B Flight Test Vehicle, AEDC-TR-75-10, Arnold Engineering Development Center, Arnold AFS, Tennessee, February 1975.
6. Norris, Richard B., Summary of Supersonic Aerodynamic Characteristics of the X-24B Lifting Body, Air Force Flight Dynamics Laboratory, Wright-Patterson AFB, Ohio, to be published.
7. White, Warren E., Documentation of Wind Tunnel Test Data From a 0.08-Scale Model of the X-24B at Mach Numbers From 0.6 to 1.3, AEDC-DR-73-18, Arnold Engineering Development Center, Arnold AFS, Tennessee, October 1973.
8. DeKuyper, R.E., Transonic Wind Tunnel Tests on a .08 Scale Model of the FDL-8 Lifting Body, Vol. 1-4, Report No. AA-4042-W-2, Cornell Aeronautical Laboratory, Inc., Buffalo, New York, January-March 1971.
9. Jenke, Leroy M., Wind Tunnel Tests of an FDL-8X Double-Delta Spacecraft Model at Mach Numbers From 1.5 to 8.0, AEDC-TR-71-218, Arnold Engineering Development Center, Arnold AFS, Tennessee, October 1971.
10. Lindsay, E. Earl, Aerodynamic Characteristics of the AFFDL X-24B Configuration at Mach Numbers from 1.5 to 5.0, AEDC-TR-74-87, Arnold Engineering Development Center, Arnold AFS, Tennessee, September 1974.
11. Selegan, D.R. et al., Effects of Rocket Exhaust on the Aerodynamics of the X-24A and X-24B Lifting Bodies, AFFDL-TM-75-29-FXS, Air Force Flight Dynamics Laboratory, Wright-Patterson AFB, Ohio, May 1975.
12. Norris, Richard B., et al., Parametric Study of an 8% Scale Model of the X-24B in the Landing Configuration, AFFDL-TM-73-21-FXS, Air Force Flight Dynamics Laboratory, Wright-Patterson AFB, Ohio, April 1973.

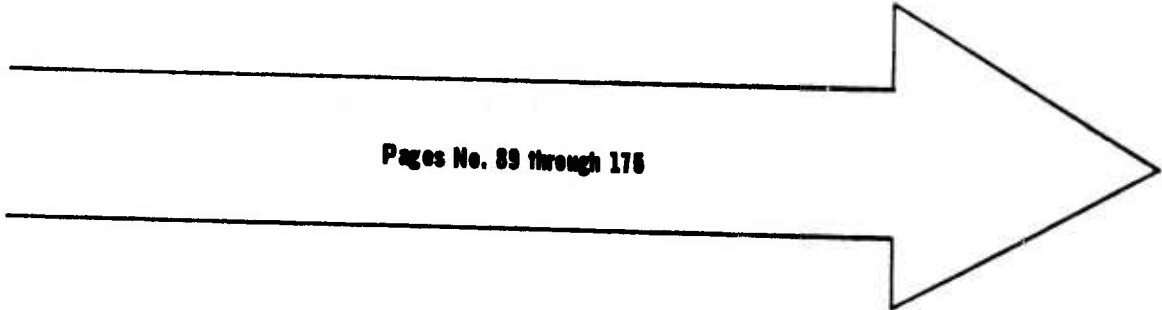


13. Richardson, David F., Flight Test and Wind Tunnel Performance Characteristics of the X-24B Research Aircraft, AFFTC-TR-76-10, Air Force Flight Test Center, Edwards AFB, California, to be published.
14. Anon., Reliability of Meteorological Data, Meteorological Working Group, Inter-Range Instrumentation Group, Document 110-71, Secretariat, Range Commanders Council, White Sand Missile Range, New Mexico, March 1971.
15. Hoey, Robert G., Flight Test Handling Qualities of the X-24A Lifting Body, AFFTC-TD-71-11, Air Force Flight Test Center, Edwards AFB, California, February 1973.
16. Kirsten, Paul W., Measured Characteristics of the X-24A Lifting Body Flight Control System, AFFTC-TD-71-12, Air Force Flight Test Center, Edwards AFB, California, October 1972.
17. DiFranco, Dante A. and Mitchell, John F., Preliminary Handling Qualities Requirements for Lifting Re-Entry Vehicles During Terminal Flight, AFFDL-TR-71-64, Air Force Flight Dynamics Laboratory, Wright-Patterson AFB, Ohio, August 1971.

## **APPENDIX A**

## **APPENDIX A STABILITY DERIVATIVES**

As was stated previously, some data points (particularly damping derivatives) are missing from the data plots. For example, figure A10 shows no  $C_{mQ}$  values even though two maneuvers were analyzed. In cases like these, it was not possible to obtain a reasonable value for the missing derivative(s), so the maneuver was reanalyzed holding the indeterminate derivative(s) fixed at pre-flight estimates. See the section entitled "Data Plots and Points".



Pages No. 89 through 176

$\delta U_B = -20^\circ$ ,  $\delta R_B = -12^\circ$ ,  $\delta A_B = 7^\circ$ ,  $co=56\%$

SYMBOL

DESCRIPTION

○

MMLE Flight Test Data  
Wind Tunnel Prediction

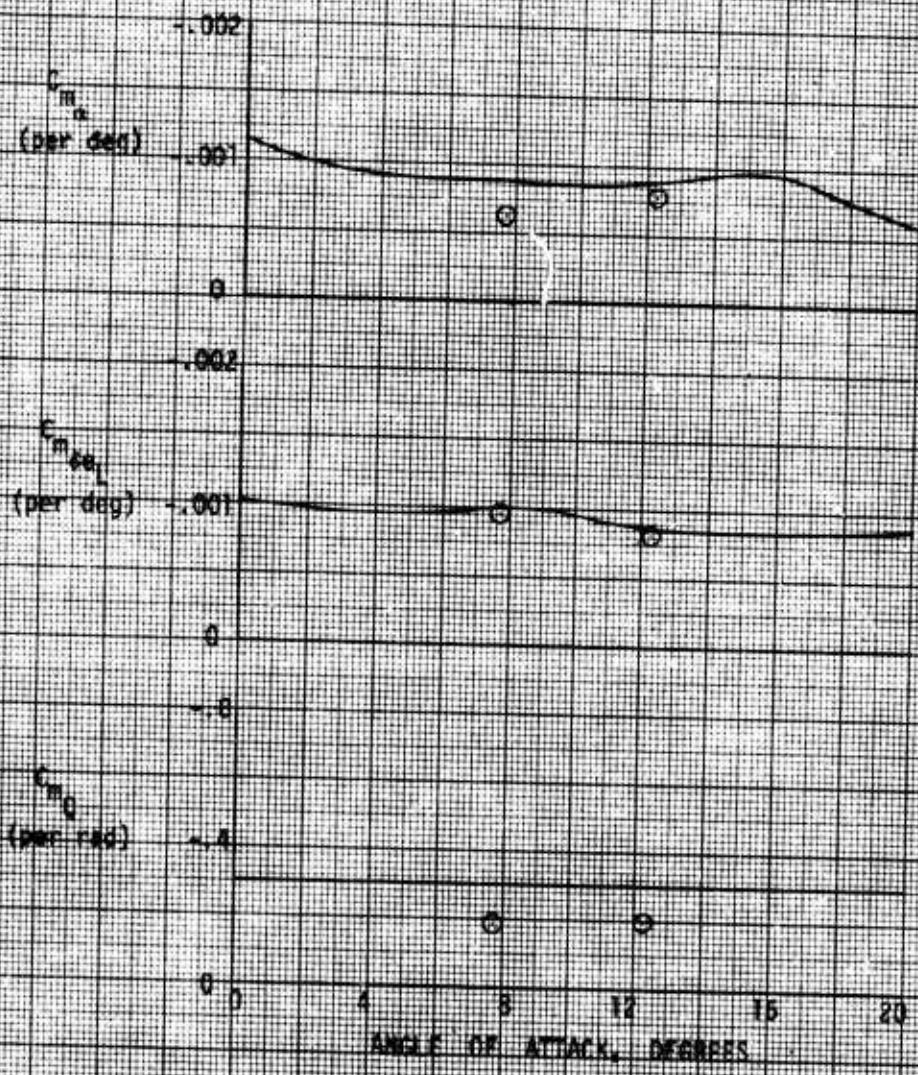


FIGURE A. PITCHING MOMENT DERIVATIVES - W. C. A.



$\delta U_B = -20^\circ$ ,  $\delta R_B = -10^\circ$ ,  $\delta A_B = 7^\circ$ ,  $c_g = 66\%$

SYMBOL

DESCRIPTION

○

MMALE Flight Test Data

□

STABOIV Flight Test Data

—

Wind Tunnel Prediction

Tail

SAS OFF

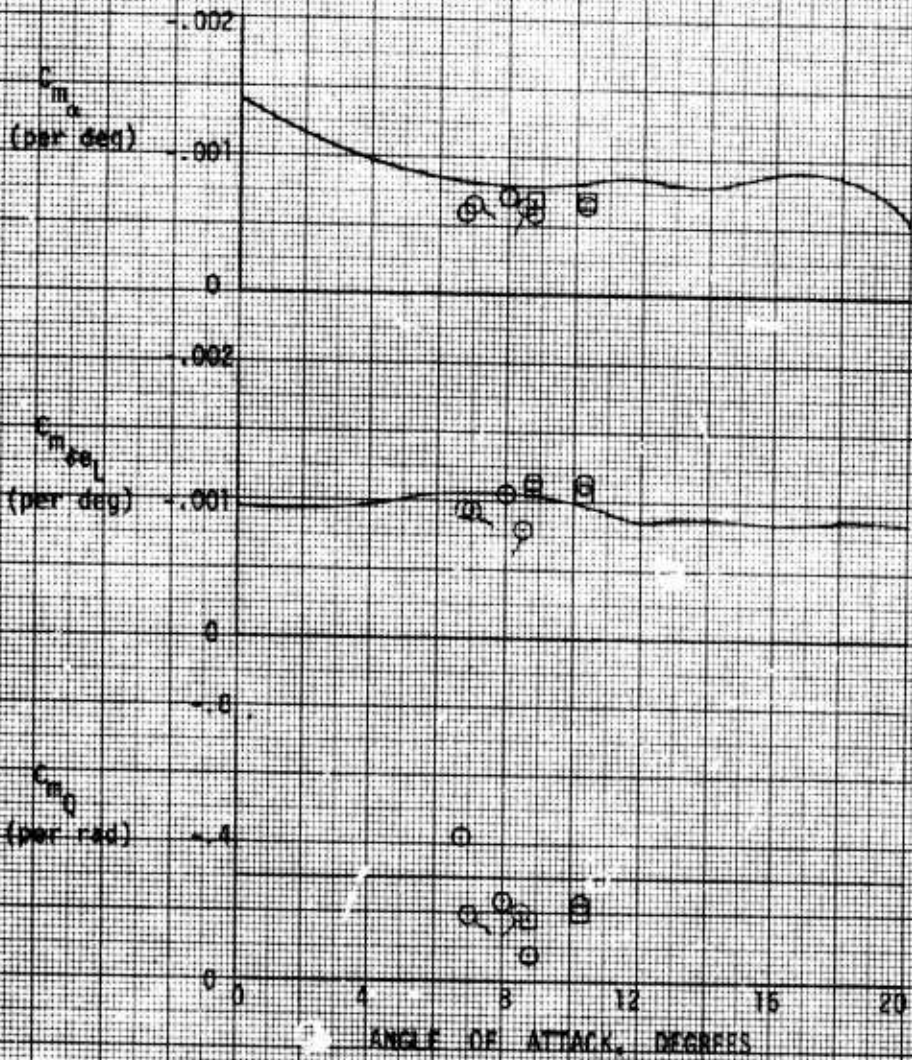


FIGURE A2 PITCHING MOMENT DERIVATIVES - M-Q-6

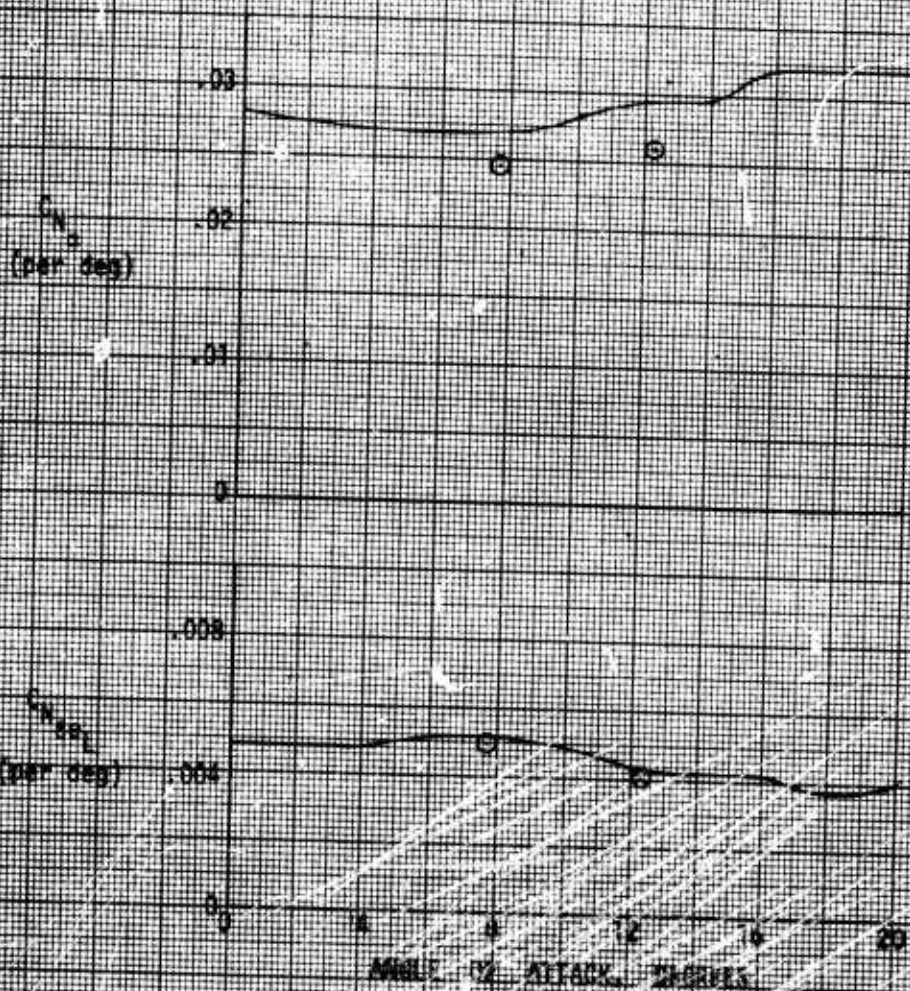
$\delta U_B = -20^\circ$ ,  $\delta R_B = -10^\circ$ ,  $\delta A_B = 7^\circ$ , CG-66%

SYMBOL

DESCRIPTION

○

WALLS Flight Test Data  
Wind Tunnel Prediction



MISSILE (2) ATTACK, THERMIS

FIGURE A1. NORMAL FORCE DERIVATIVES—WALLS



$\delta U_B = 20^\circ$ ,  $\delta R_B = -10^\circ$ ,  $\delta A_B = 7^\circ$ ,  $c_g = 55\%$

SYMBOL	DESCRIPTION
○	MMLB Flight Test Data
□	STARDIV Flight Test Data
—	Wind Tunnel Prediction
Tail	SAS def

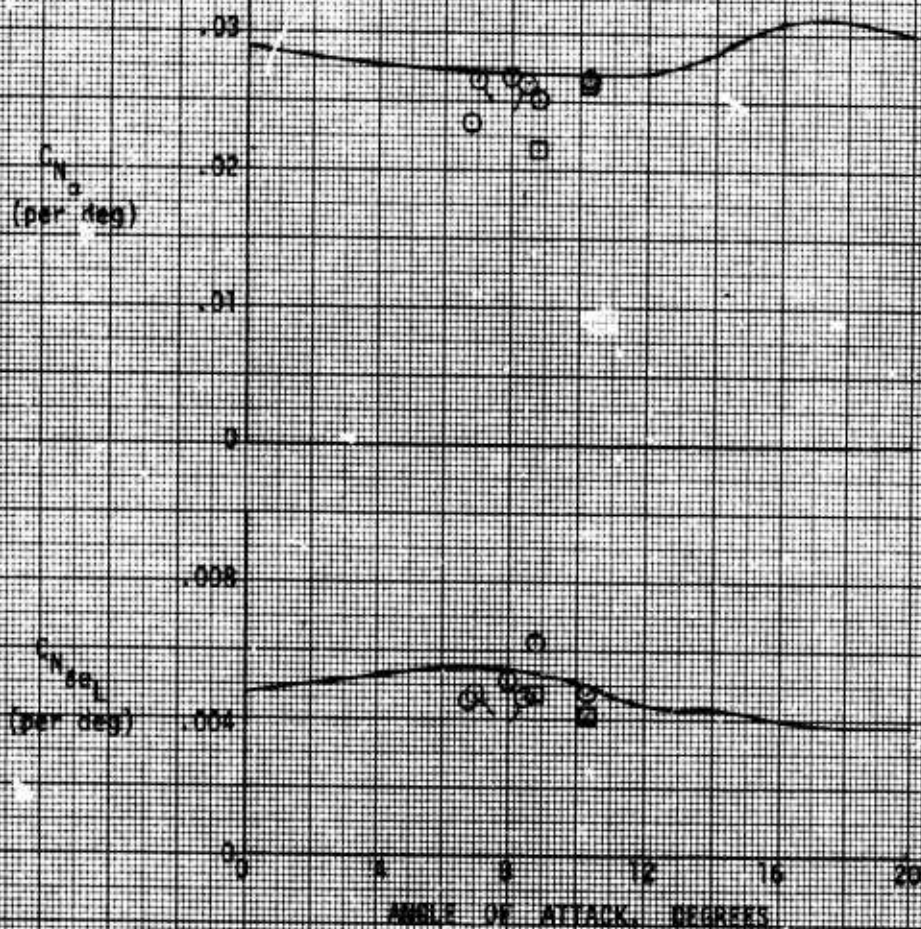


FIGURE A1. NORMAL FORCE DERIVATIVES—M=0.6

$\delta U_g = -40^\circ$ ,  $\delta \alpha_g = 0^\circ$ ,  $\delta \beta_g = 7^\circ$ ,  $c_g = 66\%$

SYMBOL	DESCRIPTION
○	ANNAE Flight Test Data
□	STANBY Flight Test Data
Tail	SAS OFF
—	Wind Tunnel Prediction

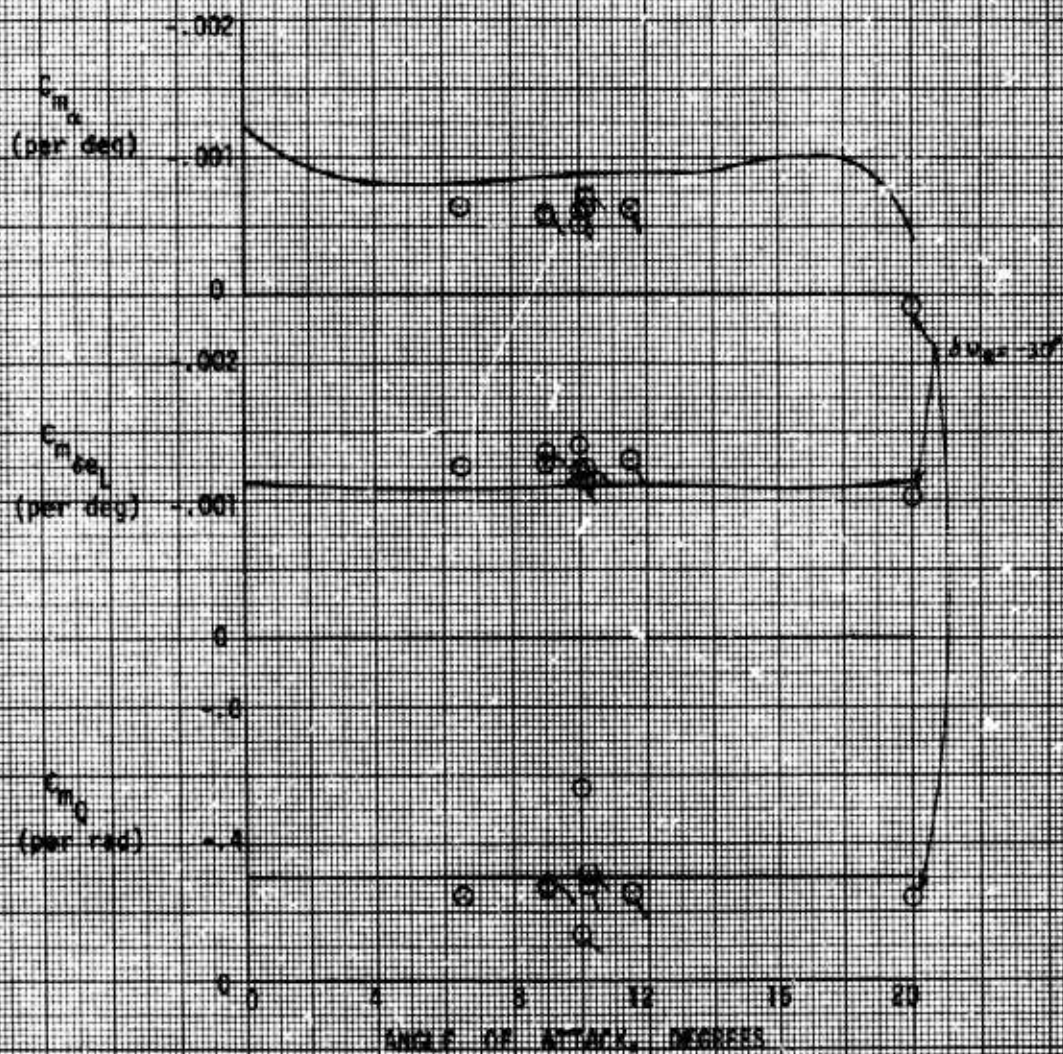


FIGURE A4 PITCHING MOMENT DERIVATIVES - W-C-A



**THIS REPORT HAS BEEN DELIMITED  
AND CLEARED FOR PUBLIC RELEASE  
UNDER DOD DIRECTIVE 5200.20 AND  
NO RESTRICTIONS ARE IMPOSED UPON  
ITS USE AND DISCLOSURE.**

**DISTRIBUTION STATEMENT A**

**APPROVED FOR PUBLIC RELEASE;  
DISTRIBUTION UNLIMITED.**

$\alpha_{B_0} = -40^\circ$ ,  $\delta R_B = 0^\circ$ ,  $\delta A_B = 7^\circ$ ,  $c_g = 66\%$

SYMBOL

DESCRIPTION

○

MMLE Flight Test Data  
SAS Off

Tail

Solid

Rocket Engine On  
Wind Tunnel Prediction

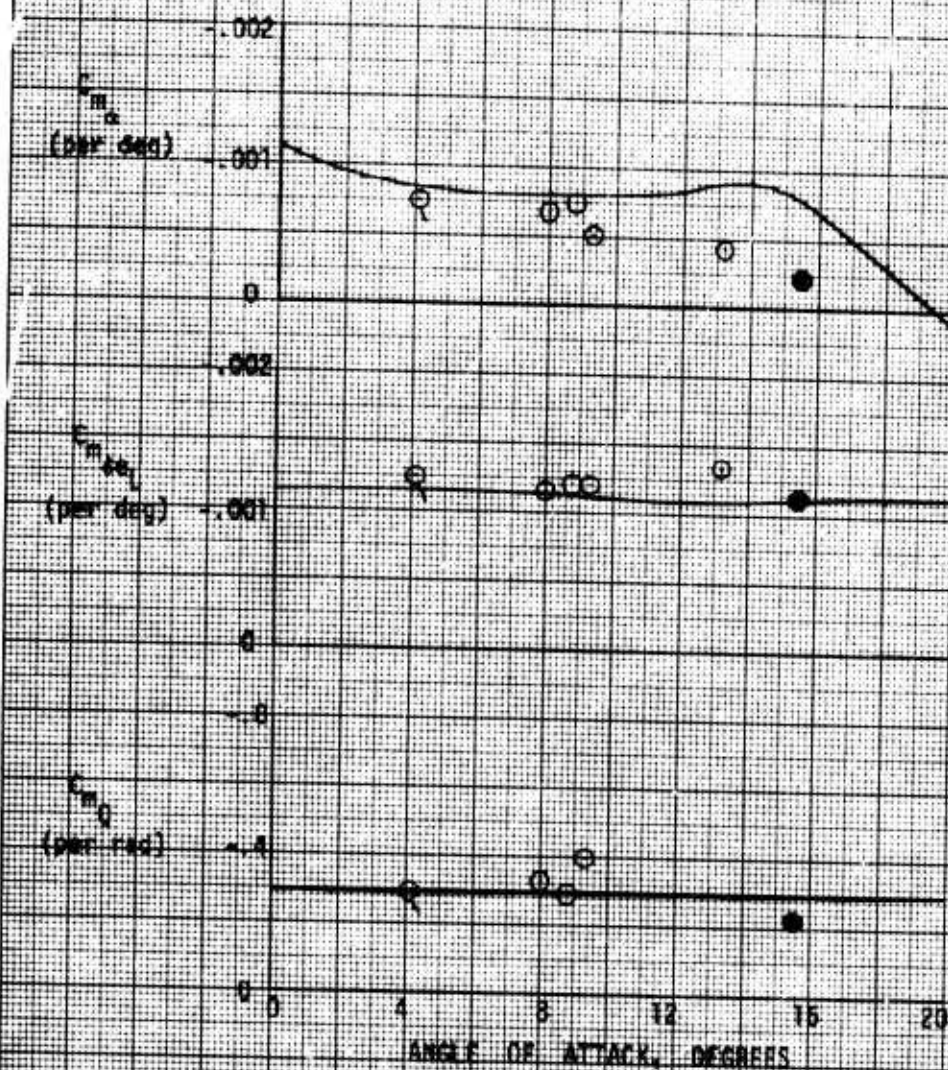


FIGURE A4 PITCHING MOMENT DERIVATIVES  $M = 0.7$

$\delta H_B = -40^\circ$ ,  $\delta R_B = 0^\circ$ ,  $\delta A_B = 7^\circ$ ,  $c_g = 66\%$

SYMBOL	DESCRIPTION
O	MMLE Flight Test Data
Tail	SAS off
Solid	Rocket Engine On
-----	Wind Tunnel Prediction

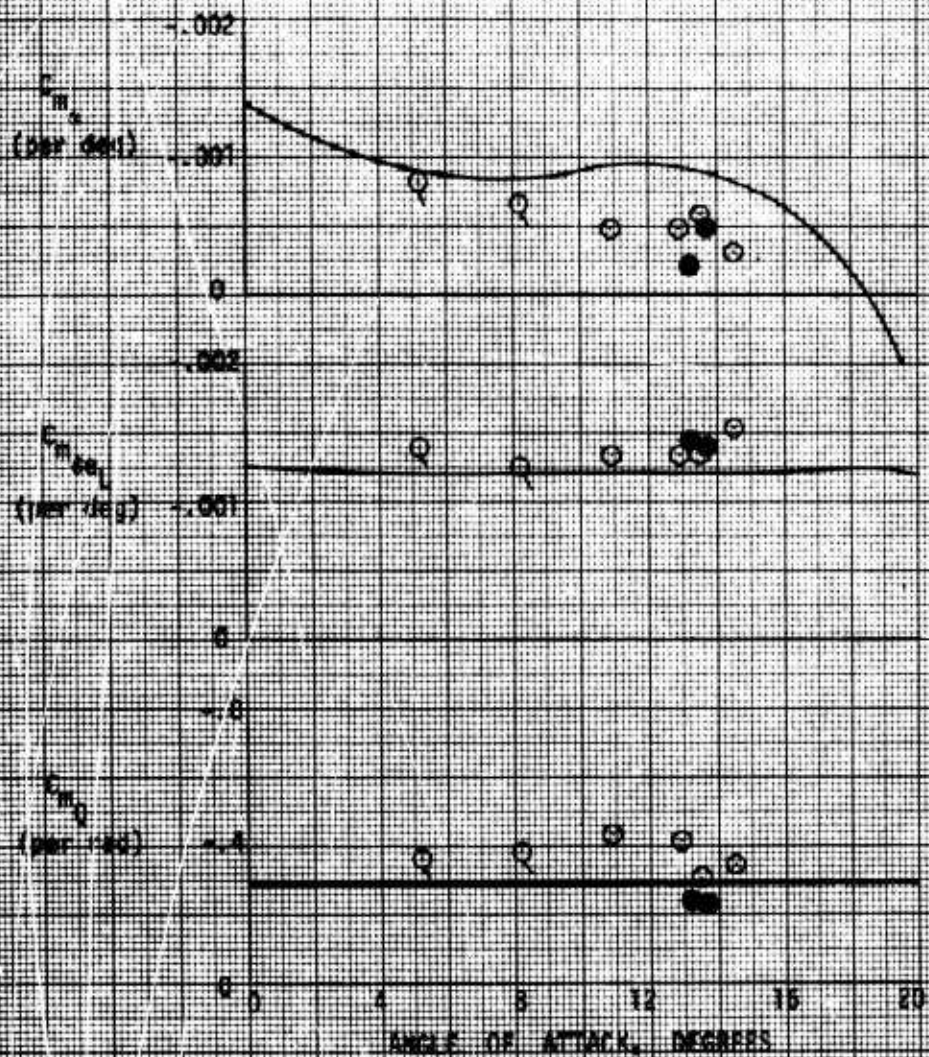


FIGURE A1 PITCHING MOMENT DERIVATIVES - W-0.2



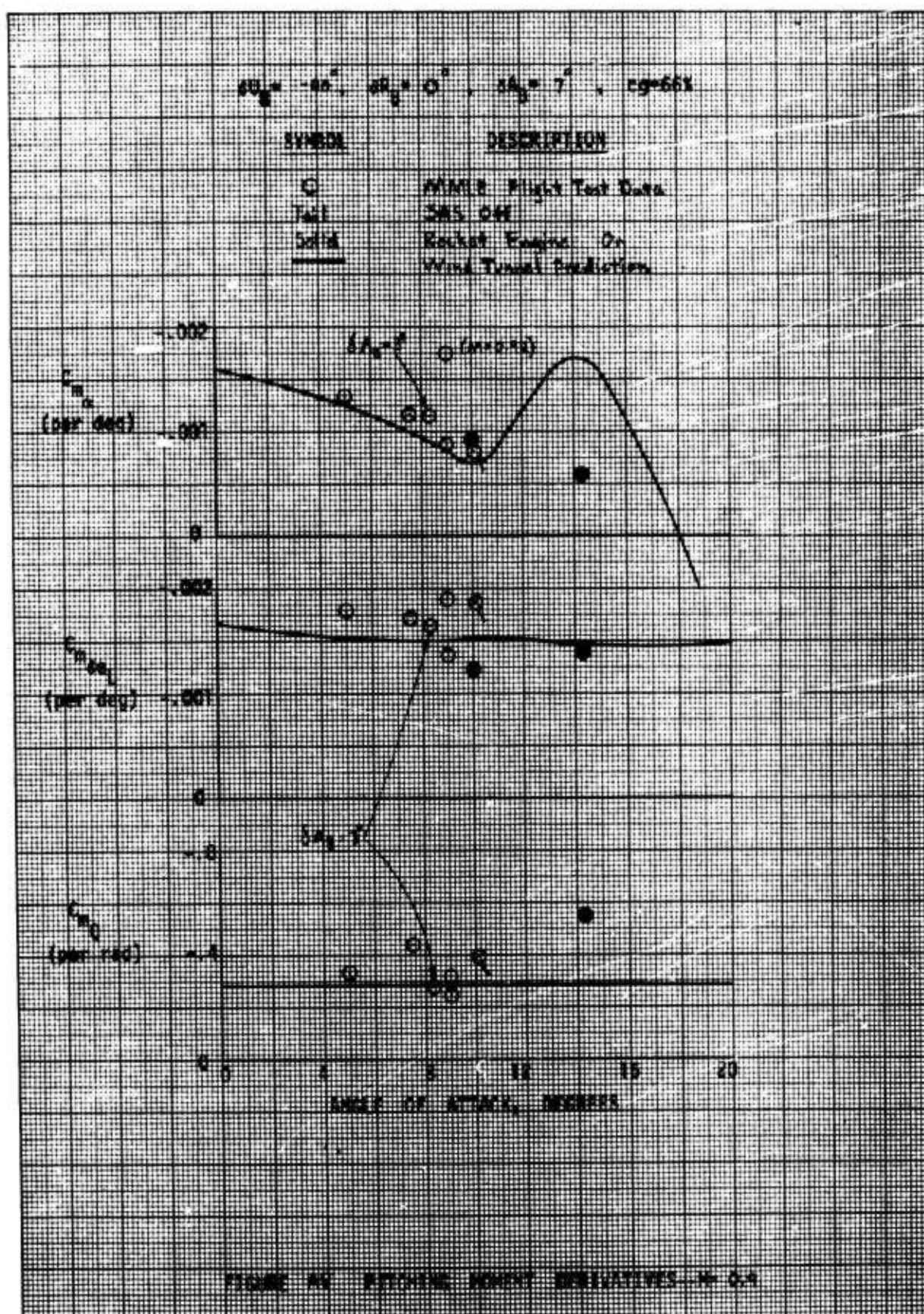


FIGURE A4 PITCHING MOMENT DERIVATIVES  $M = 0.4$



$\delta U_B = -40^\circ$ ,  $\delta R_B = 0^\circ$ ,  $\delta A_B = 7^\circ$ ,  $c_g = 66\%$

SYMBOL

DESCRIPTION

○

MALE Flight Test Data  
Wind Tunnel Prediction

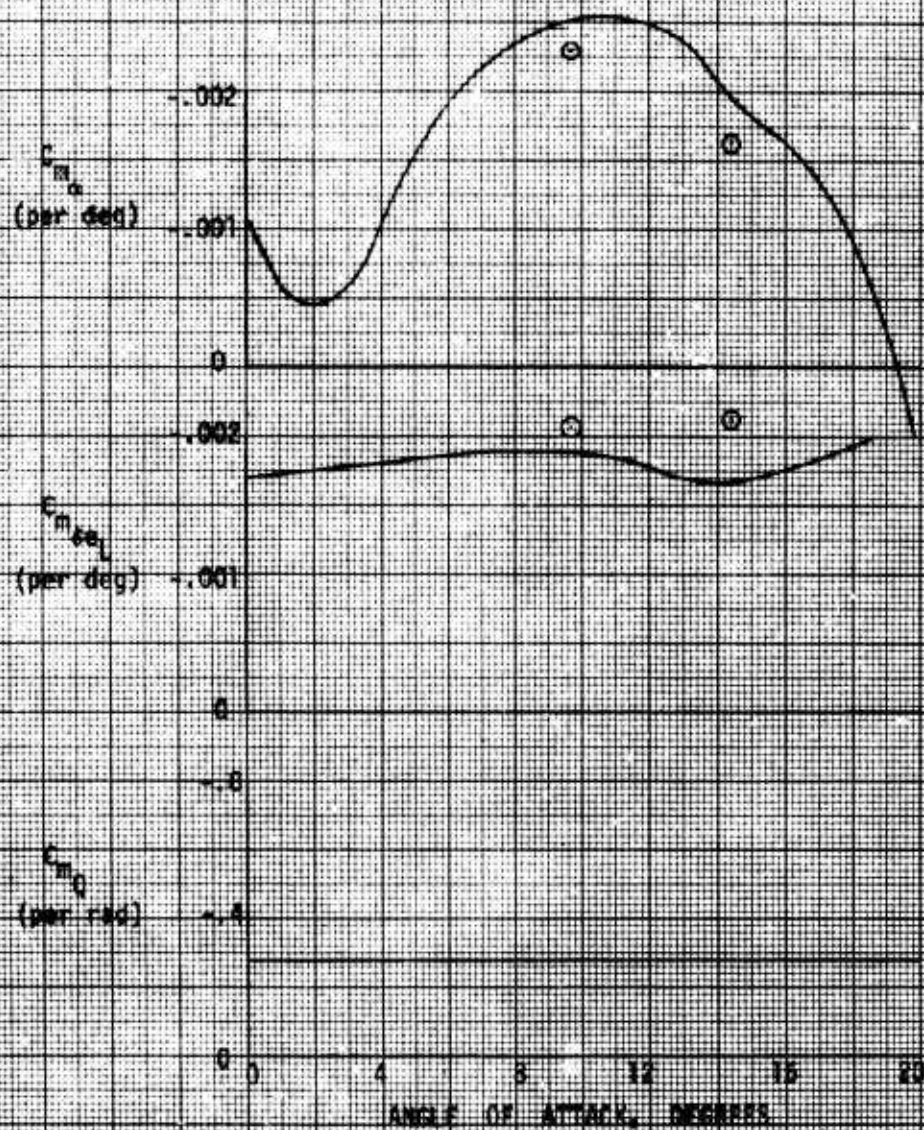


FIGURE A4 PITCHING MOMENT DERIVATIVES  $M = 0.15$





$\delta A_B = -40^\circ$ ,  $\delta R_B = 0^\circ$ ,  $\delta A_B = 7^\circ$ ,  $c_g = 66\%$

SYMBOL

DESCRIPTION

O	MMLE Flight Test Data
□	STABDIV Flight Test Data
Tail	SAS OFF
Solid	Rocket Engine On
---	Wind Tunnel Prediction

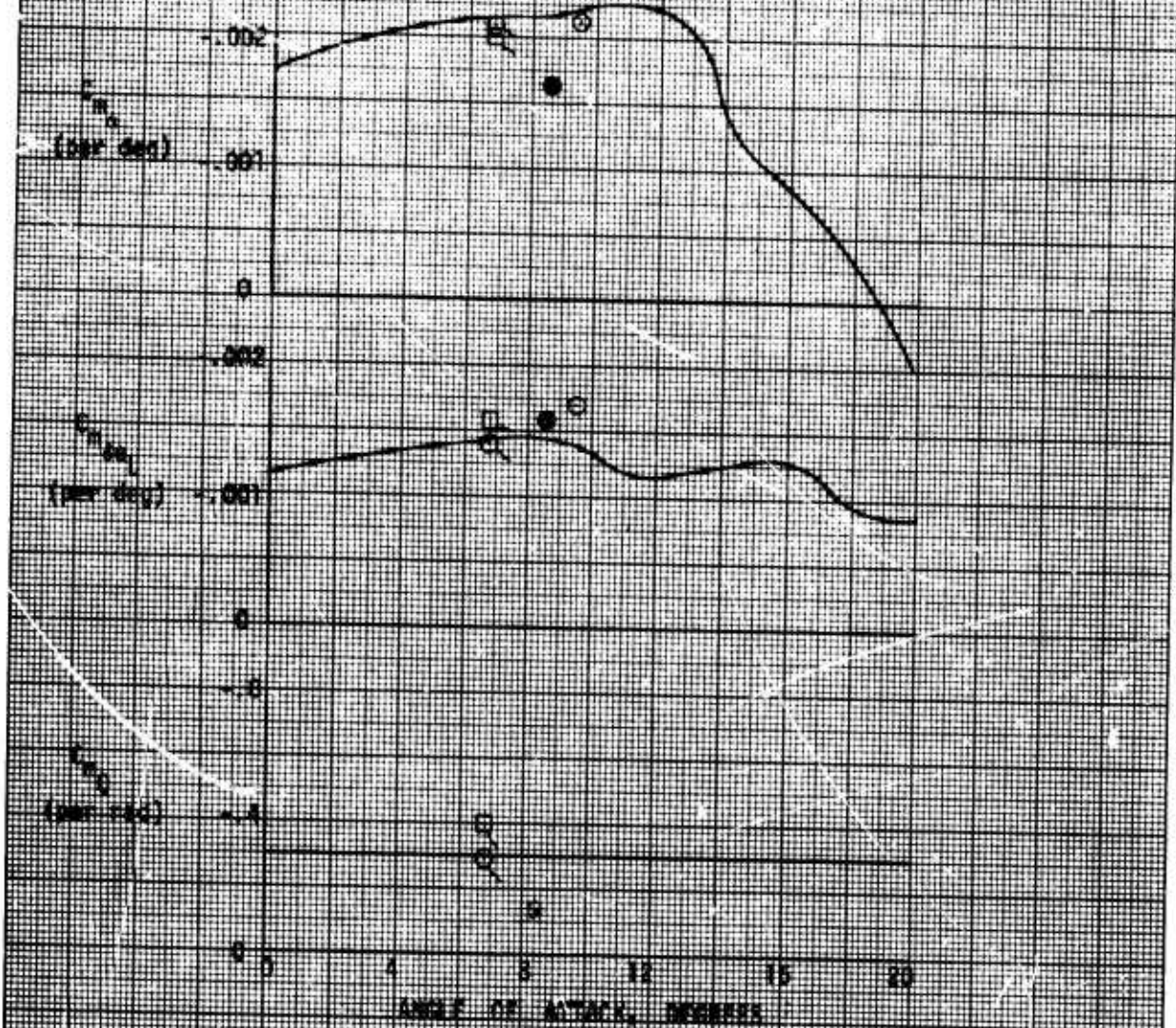


FIGURE A-10 PITCHING MOMENT DERIVATIVES (N. 1)

$\delta U_B = -40^\circ$ ,  $\delta R_B = 0^\circ$ ,  $\delta A_B = 7^\circ$ ,  $cg = 68\%$

SYMBOL

DESCRIPTION

○

AAALE Flight Test Data

Tail

SAS On

Solid

Rocket Engine On  
Wind Tunnel Prediction

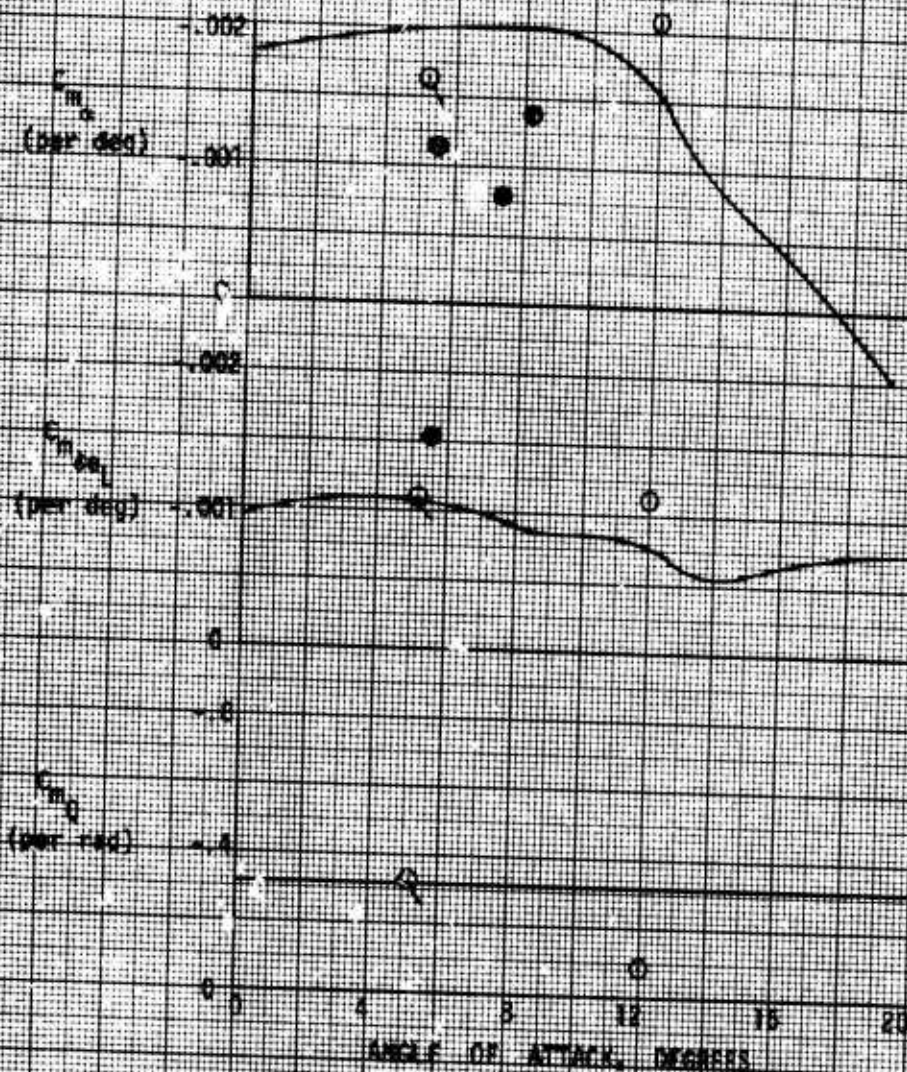


FIGURE A-5 PITCHING MOMENT DERIVATIVES - W-12



$\alpha_{L_0} = -40^\circ$ ,  $\alpha_{L_0} = 0^\circ$ ,  $\alpha_{L_0} = 7^\circ$ ,  $\alpha_{L_0} = 66^\circ$

SYMBOL	DESCRIPTION
$\circ$	WALL Flight Test Data
$\bullet$	SAS 001
$\bullet$	Rocket Engine On
$\bullet$	Wind Tunnel Prediction

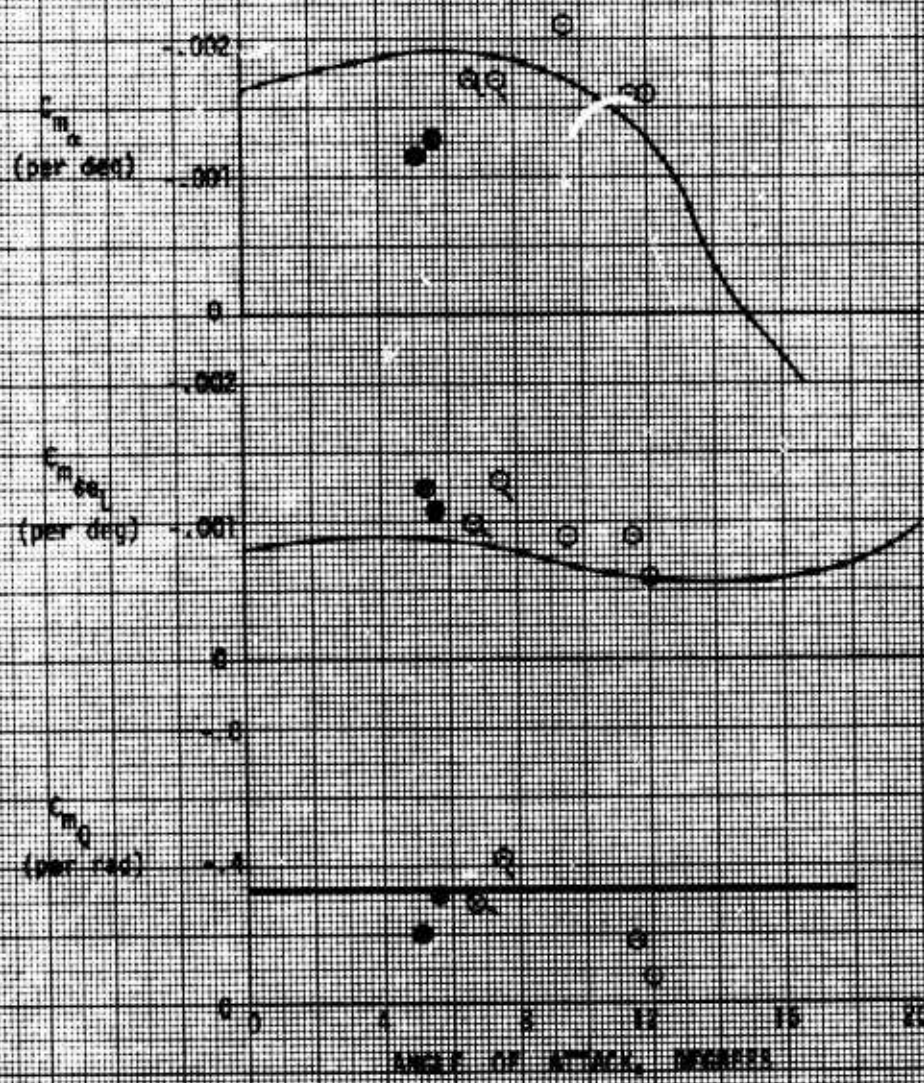
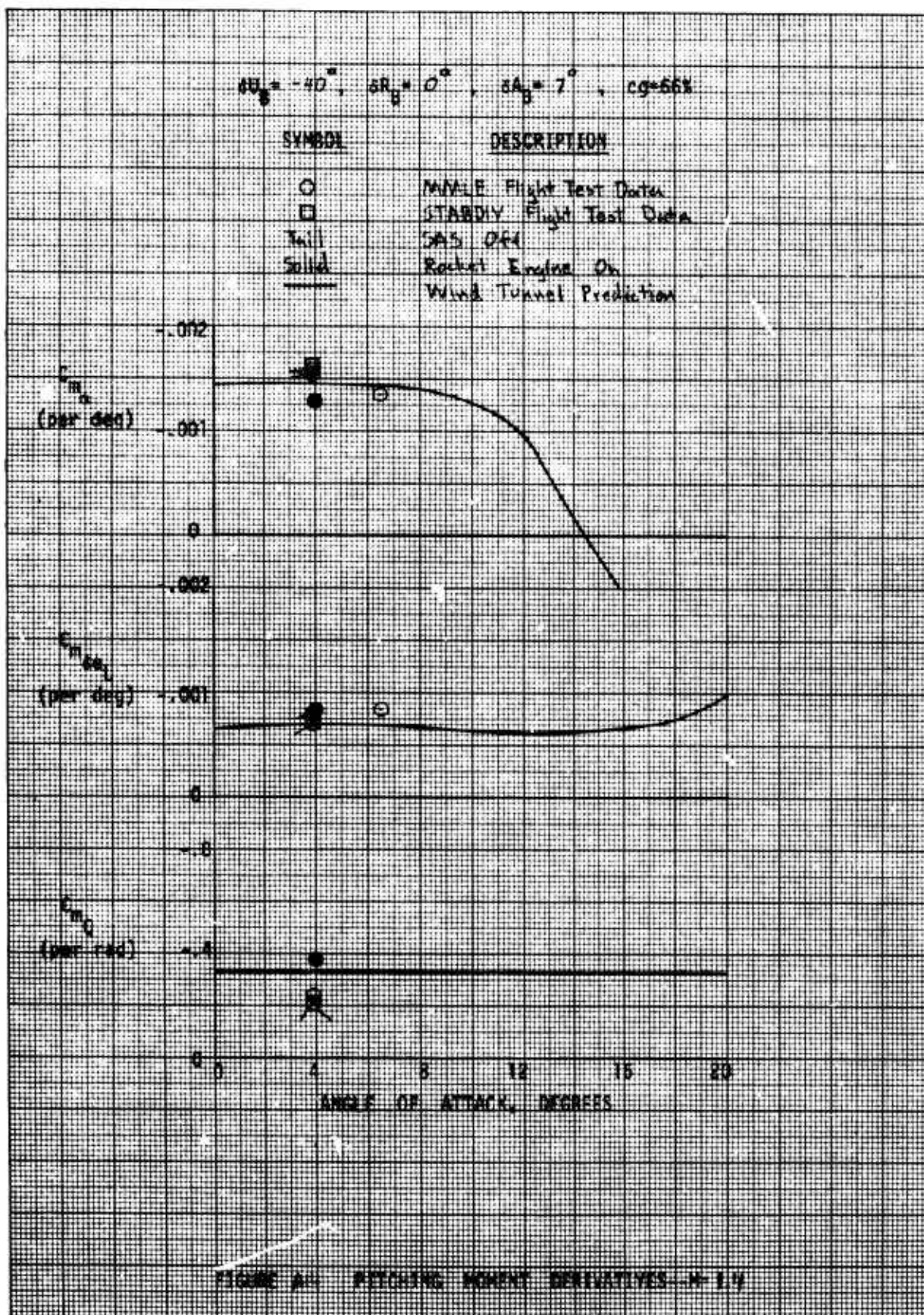


FIGURE A13 PITCHING MOMENT DERIVATIVES, A-13





$\delta V_B = -40^\circ$ ,  $\delta R_B = 0^\circ$ ,  $\delta A_B = 7^\circ$ ,  $c_g = 66\%$

SYMBOL

DESCRIPTION

○  
Tail  
Solid  
Prediction

MMLE Flight Test Data  
SAS 044  
Rack: Engine On  
Wind Tunnel Prediction

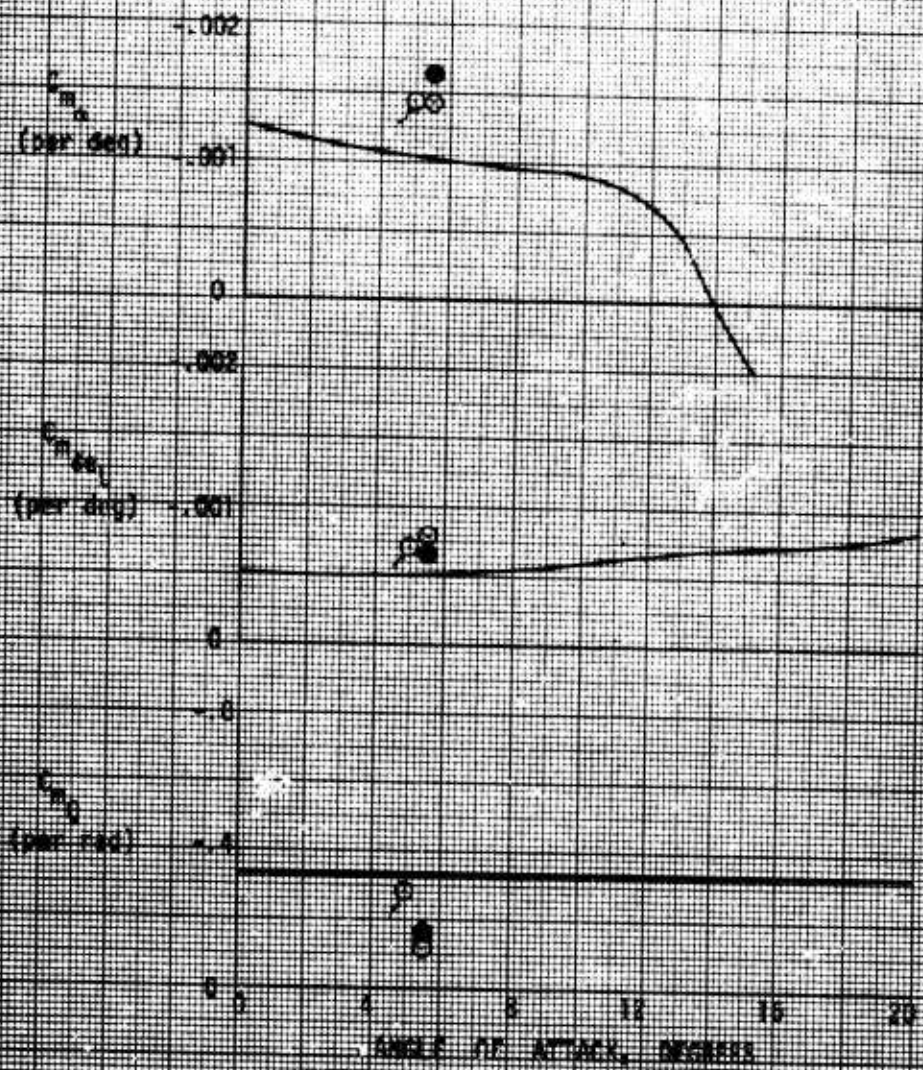
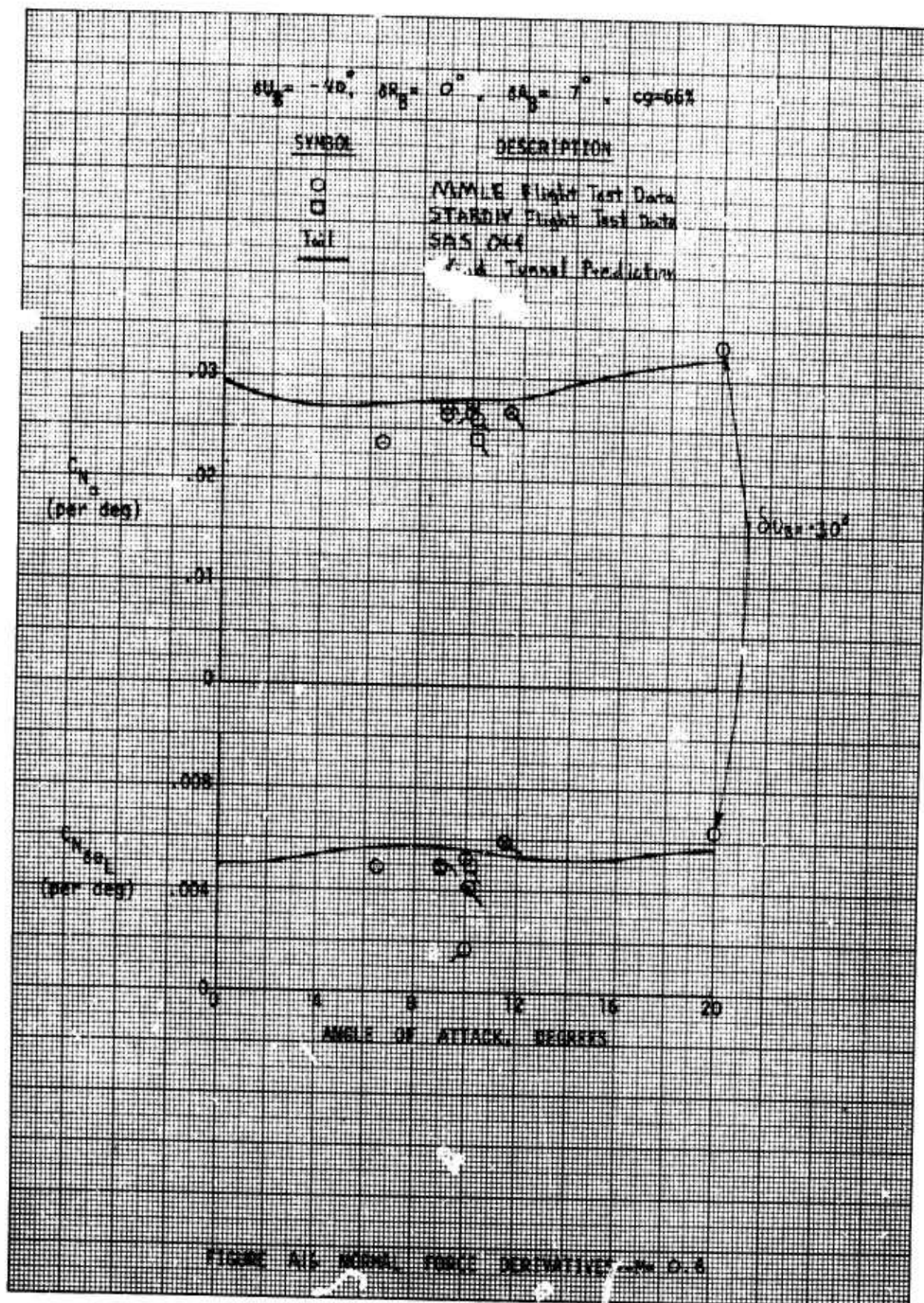


FIGURE A-2 PITCHING MOMENT DERIVATIVES - W-1A





$\delta U_B = -40^\circ$ ,  $\delta R_B = 0^\circ$ ,  $\delta A_B = 7^\circ$ ,  $CG = 65\%$

SYMBOL

DESCRIPTION

O

MMLE Flight Test Data

Tail

SAS OFF

Solid

Rocket Engines On

Wind Tunnel Prediction

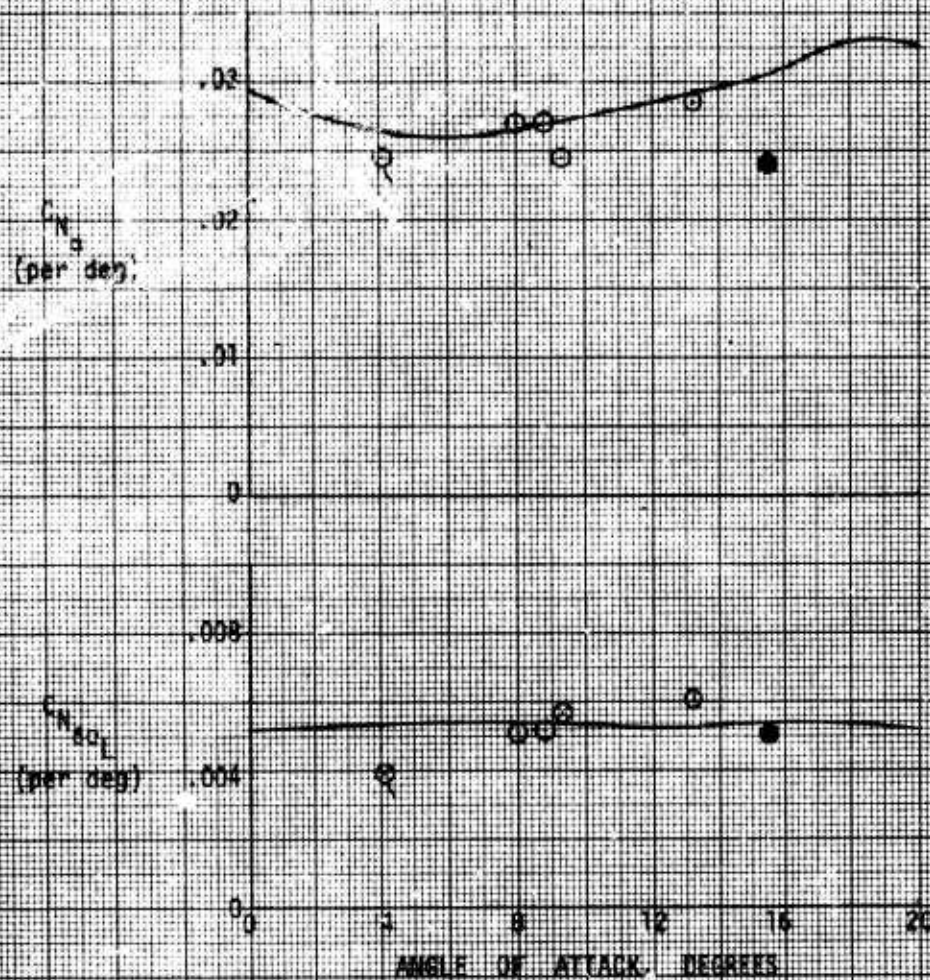


FIGURE A7. NORMAL FORCE DERIVATIVES-- $\gamma = 0.7$

$\delta U_B = -40^\circ$ ,  $\delta R_B = 0^\circ$ ,  $\delta A_B = 7^\circ$ ,  $cg=66\%$

SYMBOL

DESCRIPTION

○

MM&E Flight Test Data

Test

SAS off

Solid

Rocket Engine On

Wind Tunnel Prediction

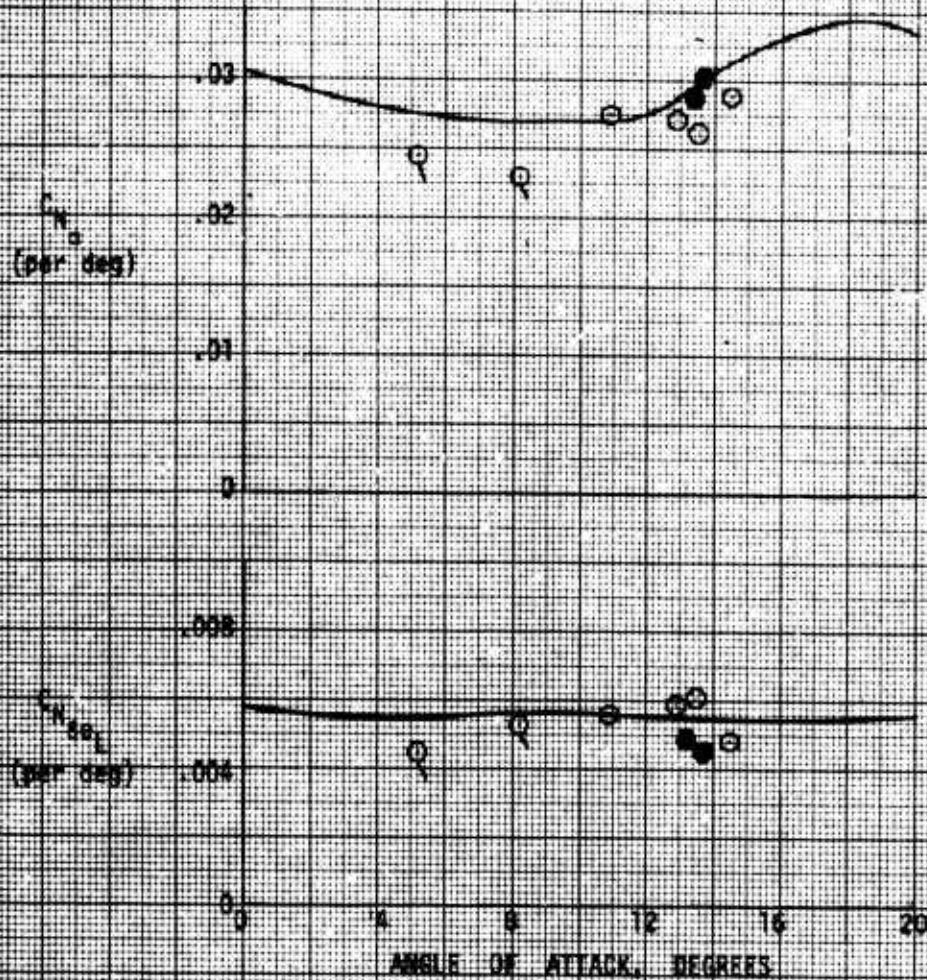


FIGURE A10 NORMAL FORCE DERIVATIVES--P-0-8



$\delta U_B = -40^\circ$ ,  $\delta R_B = 0^\circ$ ,  $\delta A_B = 7^\circ$ ,  $cg = 55\%$

SYMBOL	DESCRIPTION
○	AMLE Flight Test Data
Tail	SAS Off
Solid	Rocket Engine On
	Wind Tunnel Prediction

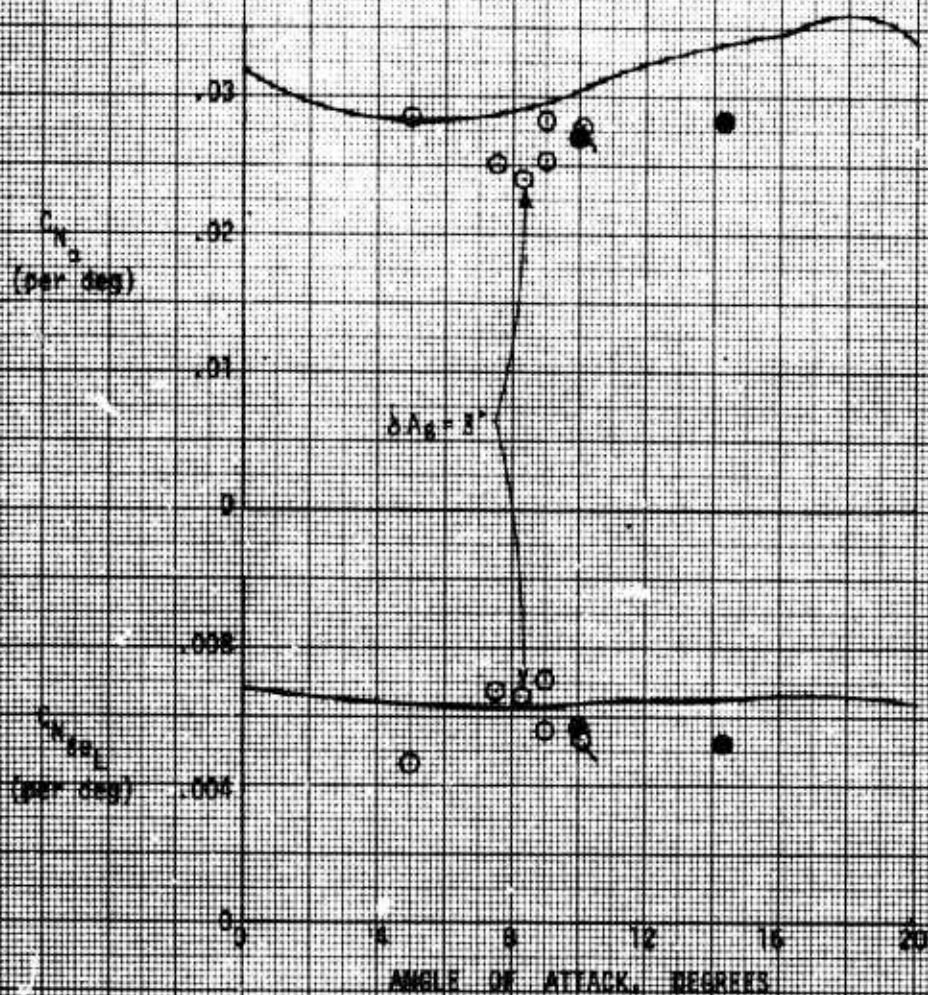


FIGURE A-9 NORMAL FORCE DERIVATIVES-- $M = 0.9$



$\alpha_{S_1} = -10^\circ$ ,  $\alpha_{S_2} = 0^\circ$ ,  $\alpha_{S_3} = 7^\circ$ ,  $C_D = 0.02$

SYMBOL

DESCRIPTION

$\circ$   
—

AWALE Plain Test Data  
Wind Tunnel Prediction

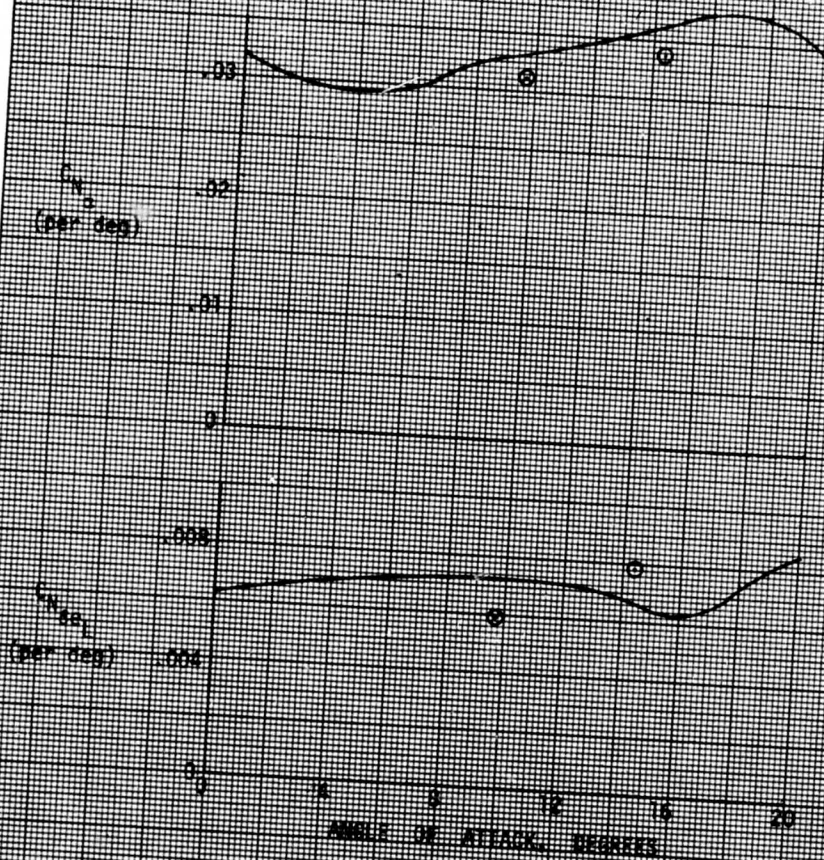


FIGURE A.10 WING FORCE DERIVATIVES -  $M = 0.15$

$\alpha_{1/2} = 40^\circ$ ,  $\alpha_{1/2} = 0^\circ$ ,  $\alpha_{1/2} = 7^\circ$ ,  $C_g = 65\%$

SYMBOL

DESCRIPTION

○	MALE Flight Test Data
Tail	SAS OK
Solid	Rocket Engine On
-----	Wind Tunnel Prediction

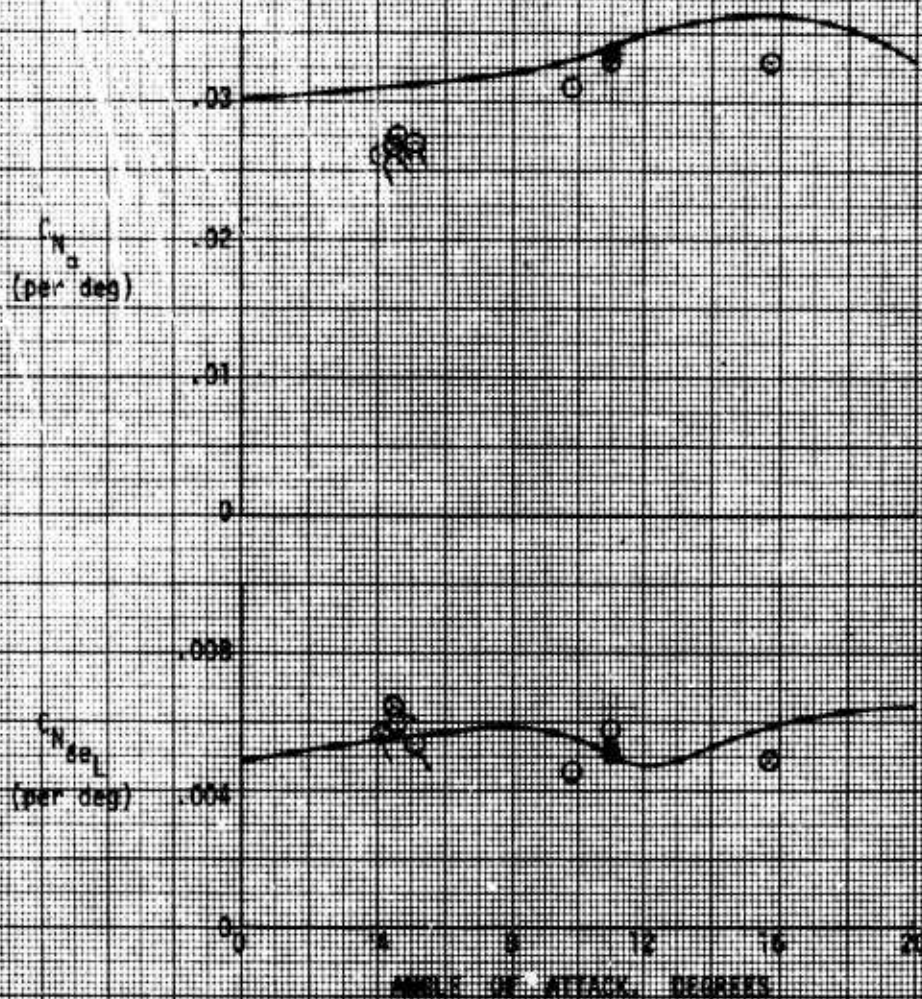


FIGURE A-11 NORMAL FORCE DERIVATIVES—ON L.O.



$\alpha_{y_0} = -40^\circ$   $\alpha_{y_0} = 0^\circ$   $\alpha_{y_0} = 7^\circ$   $C_D = 0.01$

SYMBOL

DESCRIPTION

○

MMLE Flight Test Data

□

STANDV Flight Test Data

Tail

SAS OFF

Solid

Rocket Engine On

Wind Tunnel Prediction

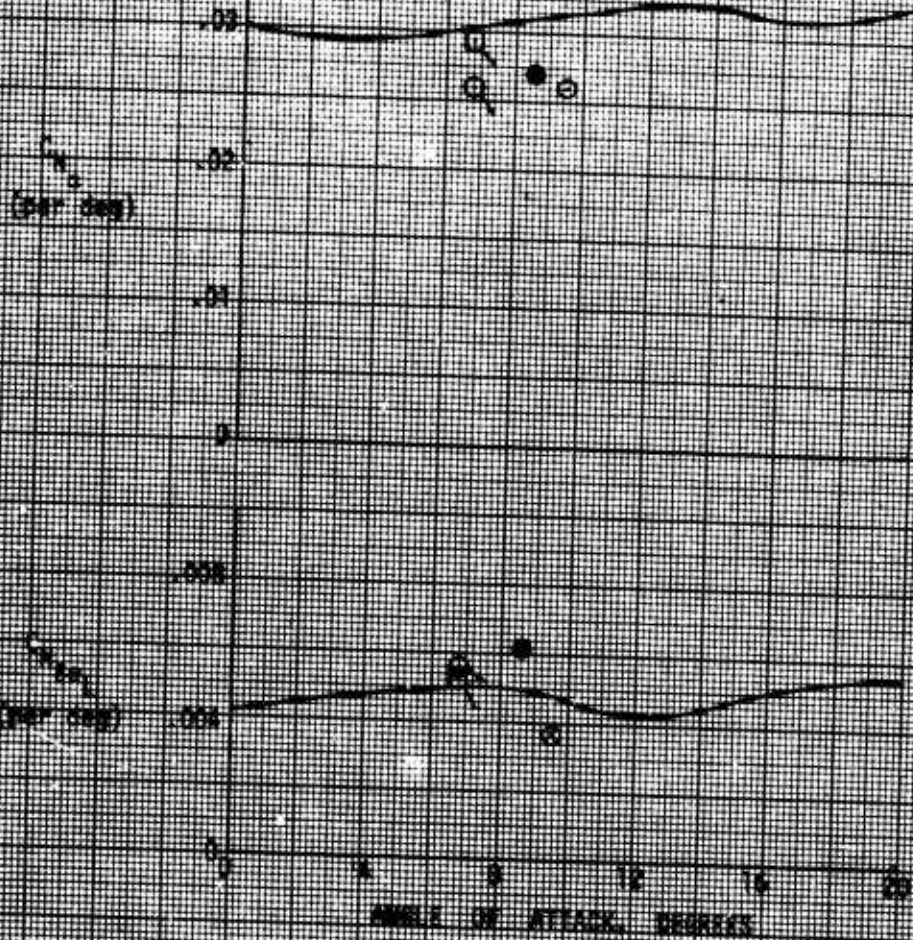


FIGURE 11.1. FORCE DERIVATIVES -  $\alpha_y$



$\delta U_B = -40^\circ$ ,  $\delta R_B = 0^\circ$ ,  $\delta A_B = 7^\circ$ ,  $c_g = 55\%$

SYMBOL	DESCRIPTION
○	MMLE Flight Test Data
Tail	SAS 044
Solid	Rocket Engine On
-----	Wind Tunnel Prediction

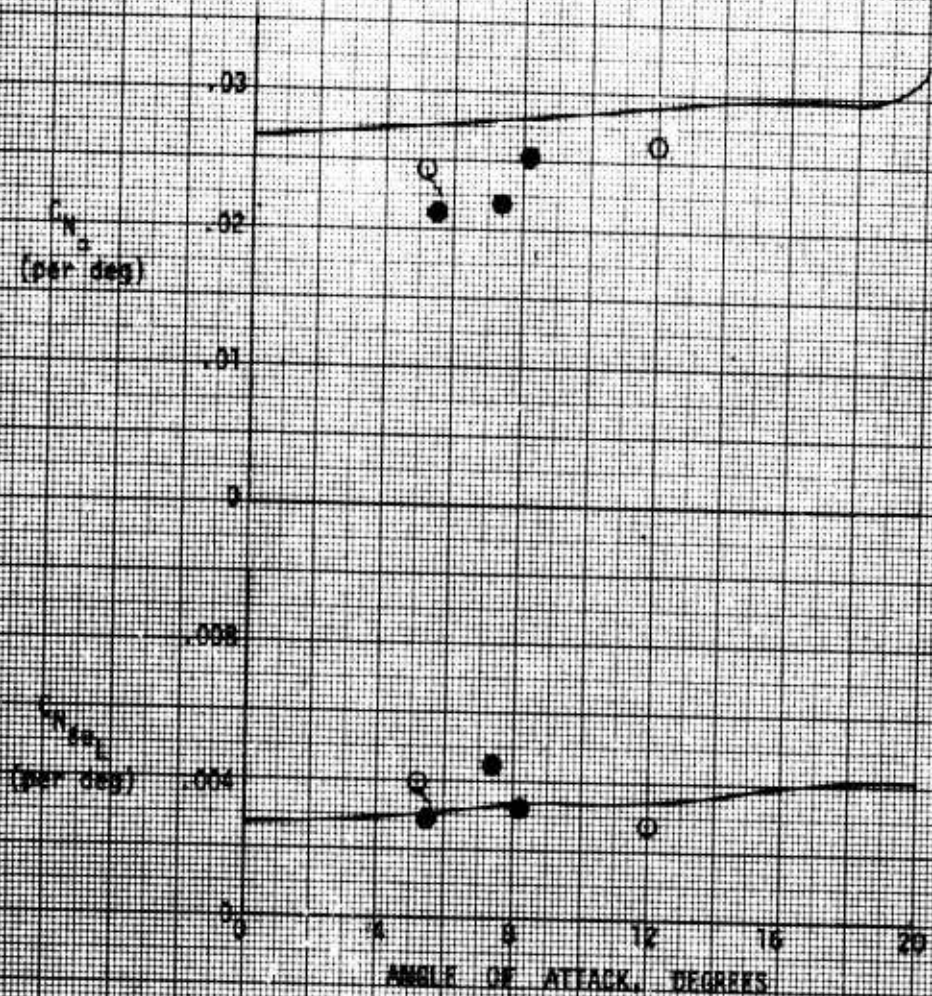


FIGURE A13 NORMAL FORCE DERIVATIVES--PH 1.2

$\delta U_B = -40^\circ$ ,  $\delta R_B = 0^\circ$ ,  $\delta A_B = 7^\circ$ ,  $CG = 65\%$

SYMBOL

DESCRIPTION

O

MALE Flight Test Data

Tail

SAS OFF

Solid

Rocket Engine On  
Wind Tunnel Prediction

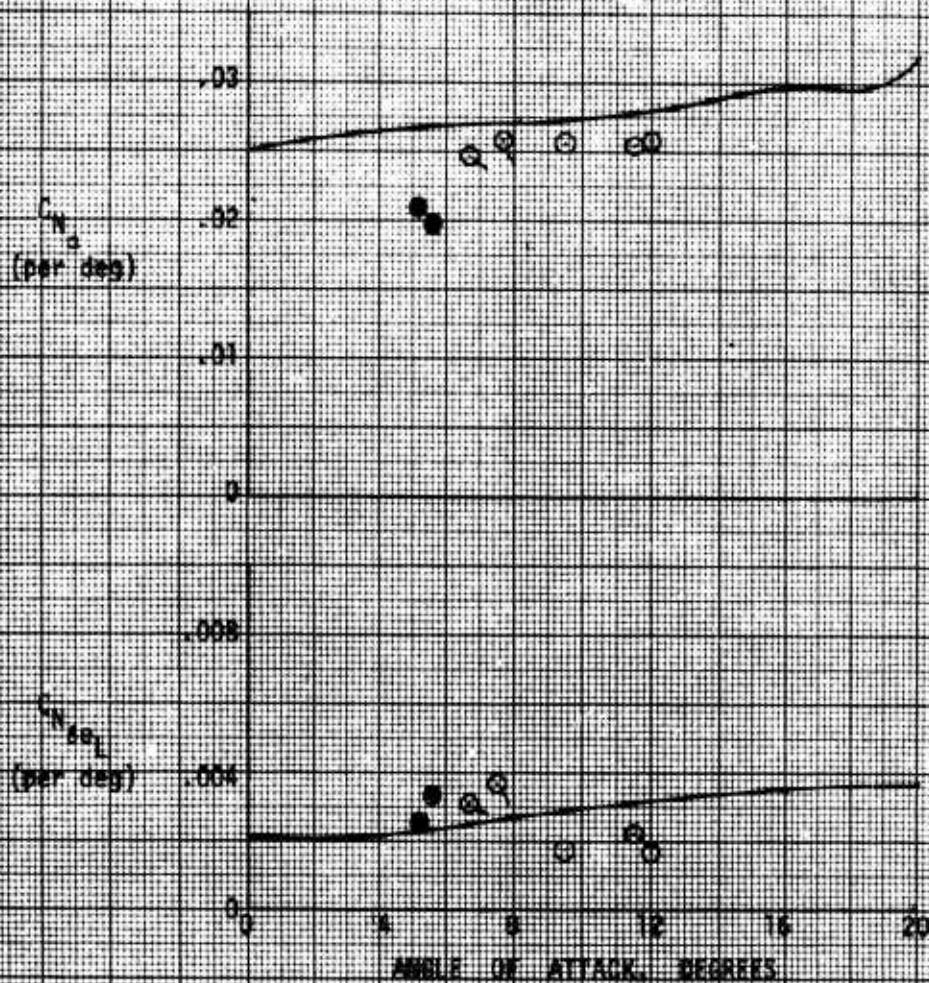


FIGURE A-1. NORMAL FORCE DERIVATIVES—PW-1.3



$\delta U_B = -40^\circ$ ,  $\delta R_B = 0^\circ$ ,  $\delta A_B = 7^\circ$ ,  $C_g = 66\%$

SYMBOL

DESCRIPTION

○

MMME Flight Test Data

□

STABDIV Flight Test Data

||||

SAS OFF

Solid

Rocket Engine On

-----

Wind Tunnel Prediction

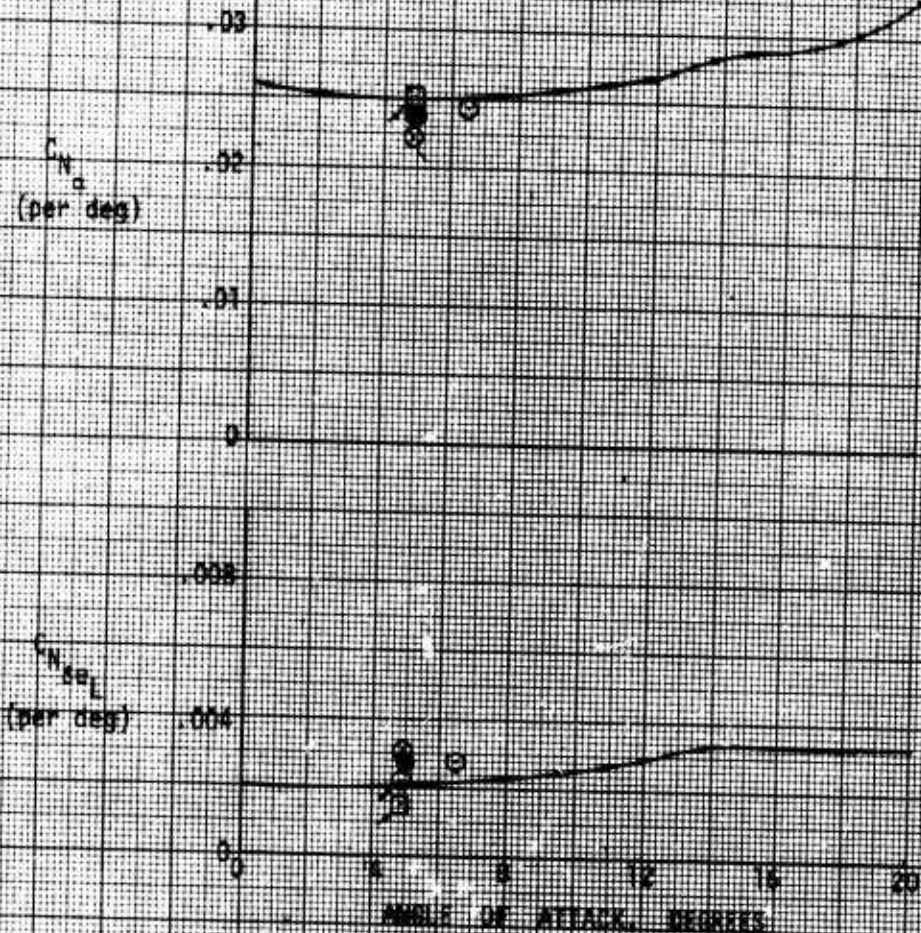


FIGURE A13 NORMAL FORCE DERIVATIVES-ON L3



$\delta A_B = -40^\circ$ ,  $\delta R_B = 0^\circ$ ,  $\delta A_B = 7^\circ$ ,  $c_g = 66\%$

SYMBOL	DESCRIPTION
$\circ$	MALE Flight Test Data
Tail	SAS 044
Solid	Rocket Engine On
-----	Wind Tunnel Prediction

$C_{N_\alpha}$   
(per deg)

$C_{N_{\dot{\alpha}}}$   
(per deg)

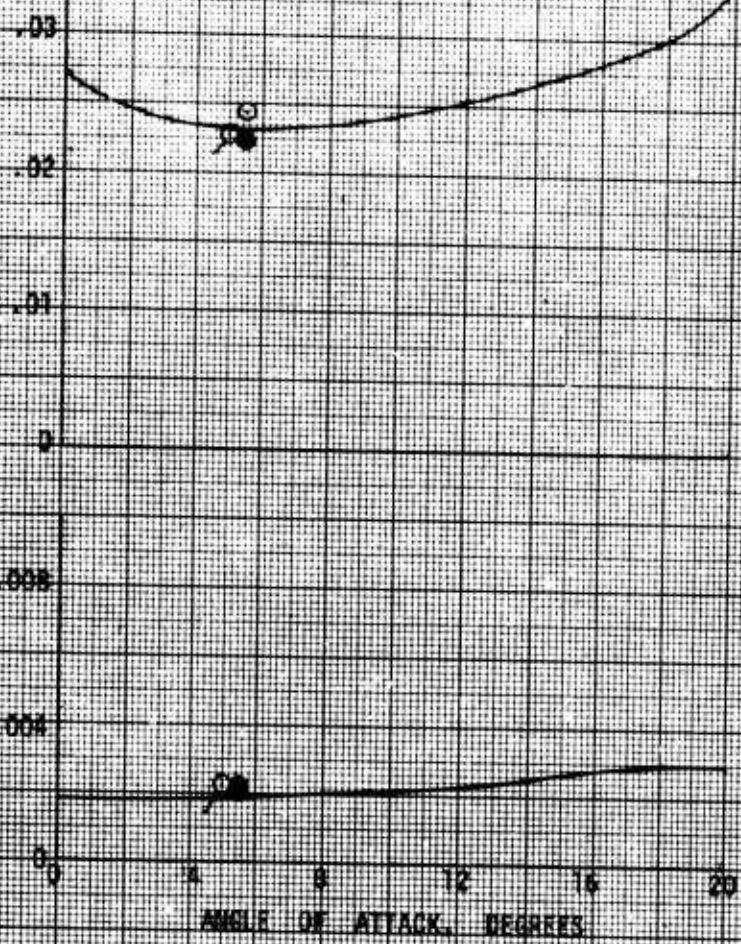


FIGURE 10. NORMAL FORCE DERIVATIVES—MALE

$\delta U_B = -20^\circ$ ,  $\delta R_B = -10^\circ$ ,  $\delta A_B = 7^\circ$ , C11-652

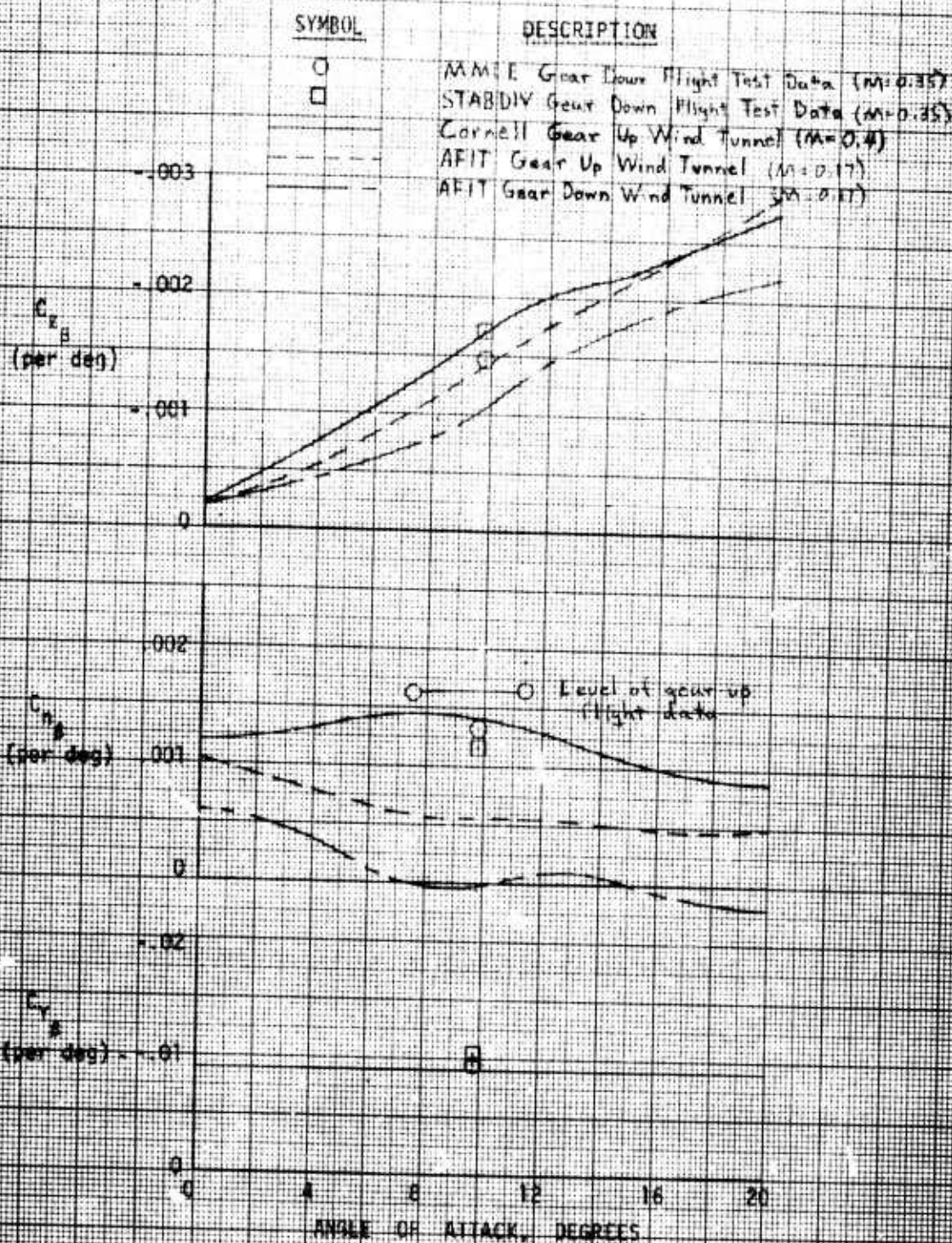
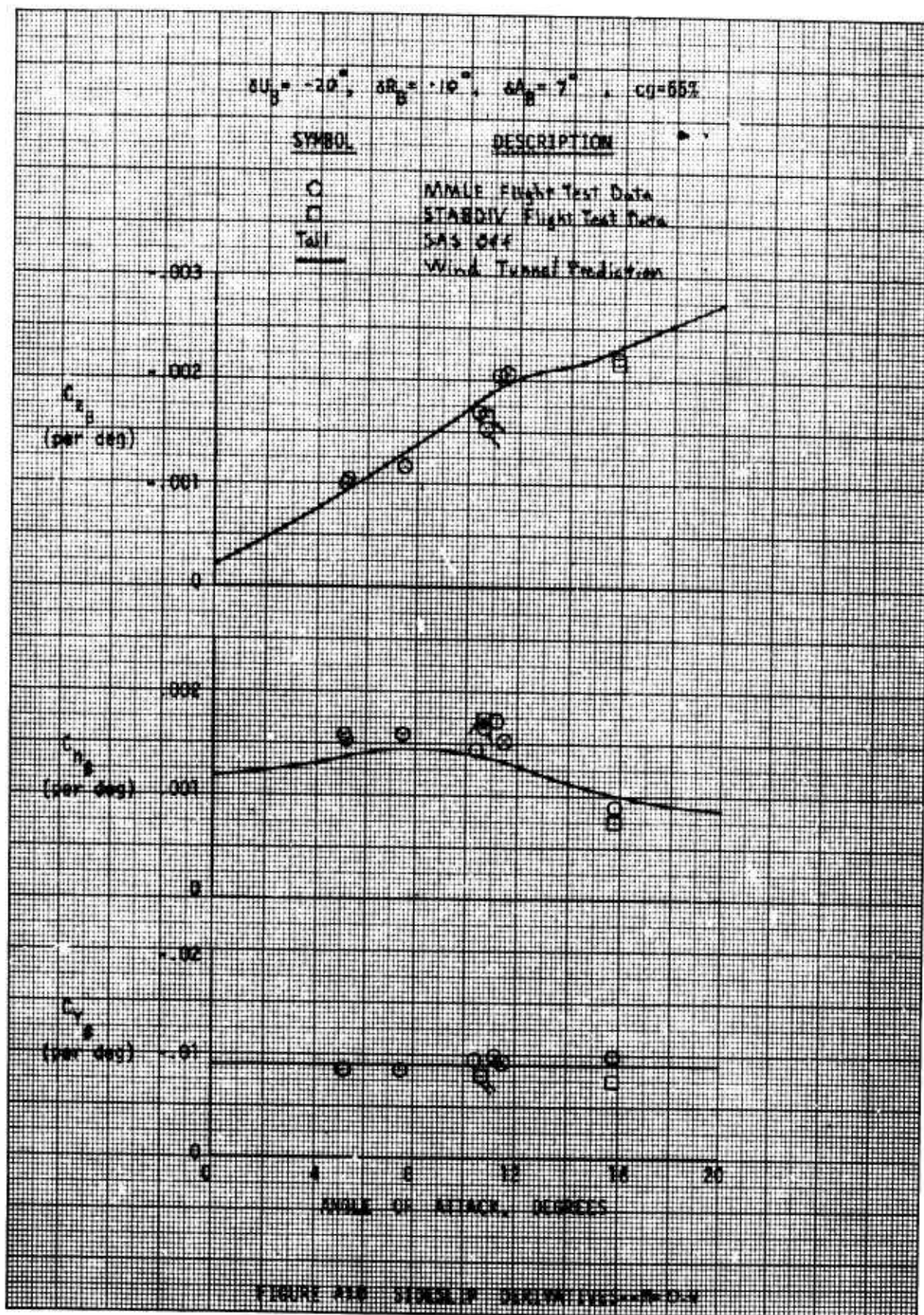


FIGURE A17 SIDESLIP DERIVATIVES  $M=0.35$







$\delta U_B = -20^\circ$ ,  $\delta R_B = -10^\circ$ ,  $\delta A_B = 7^\circ$ ,  $c_{D0} = 65\%$

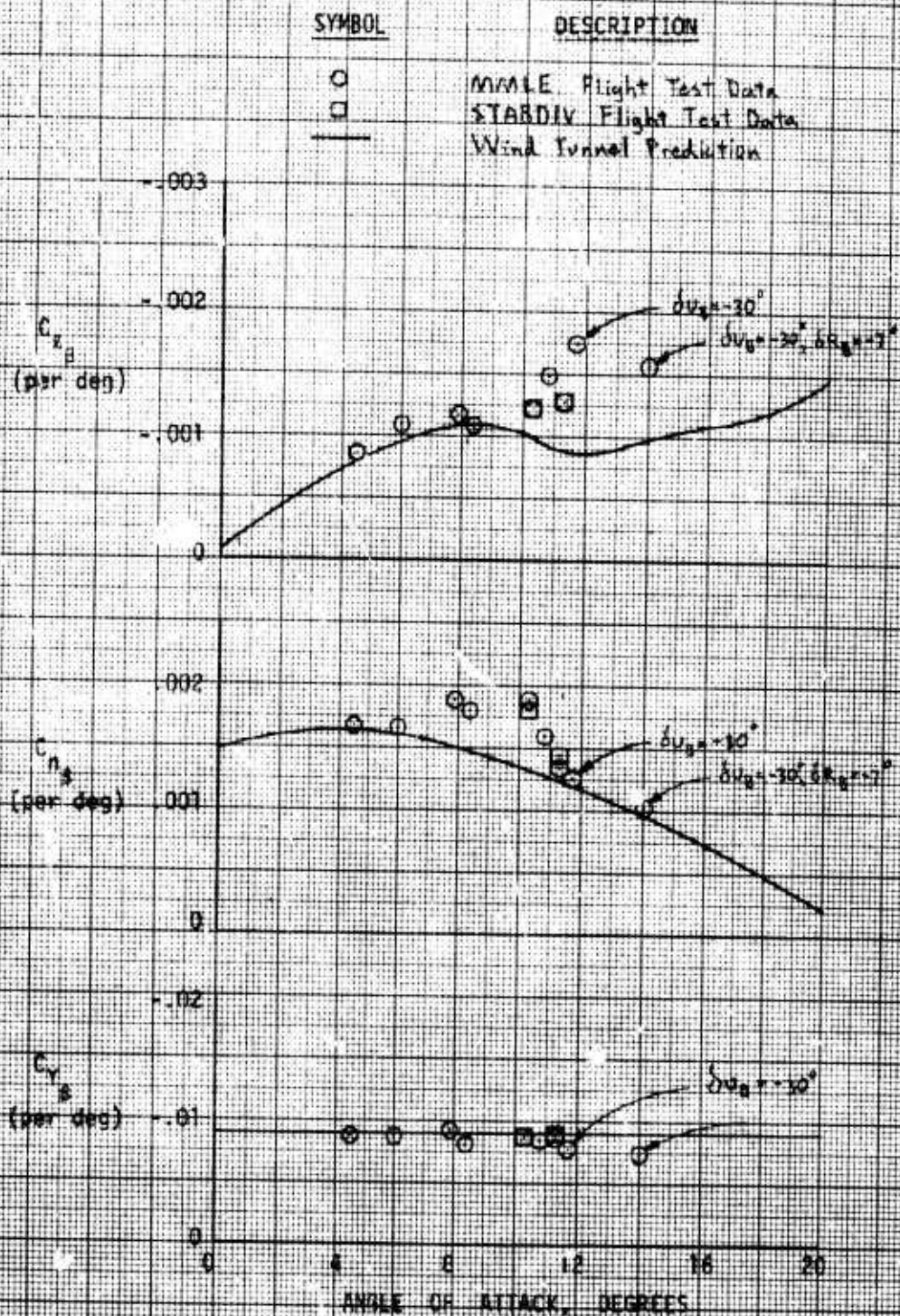


FIGURE AON SIDESLIP DERIVATIVES-- $\alpha = 0.6$

$\delta U_B = -20^\circ$ ,  $\delta R_B = -10^\circ$ ,  $\delta A_B = 0^\circ$ ,  $c_g = 66\%$

SYMBOL	DESCRIPTION
○	MMLE Flight Test Data
□	STABDIV Flight Test Data
Tail	SAS OFF
—	Wind Tunnel Prediction

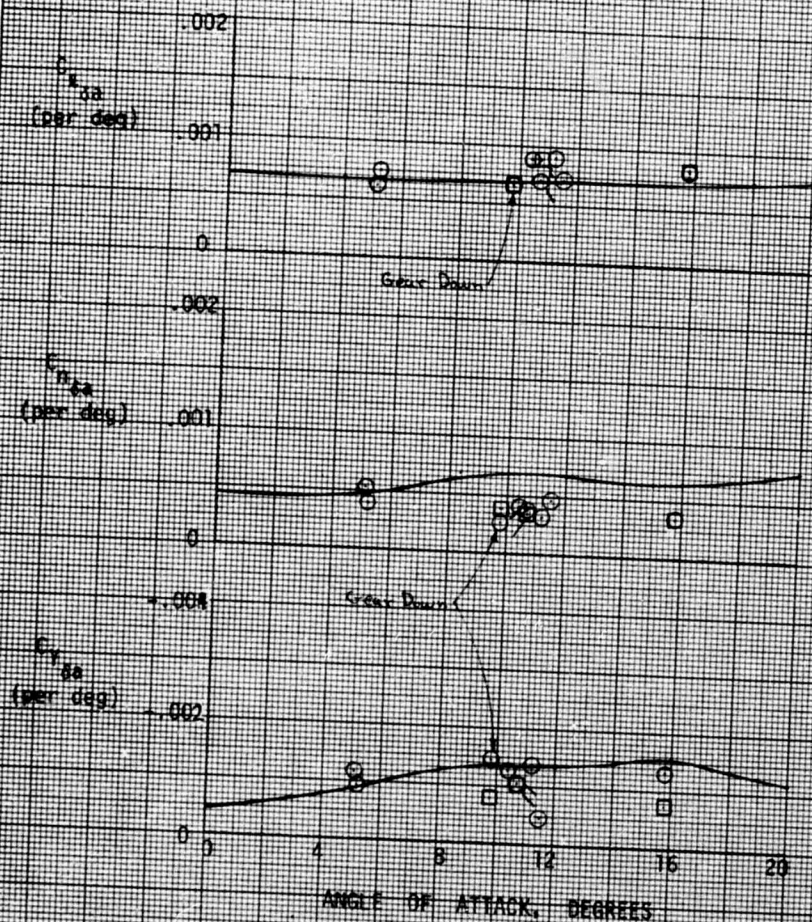


FIGURE A30 ALLERON DERIVATIVES - N O 4



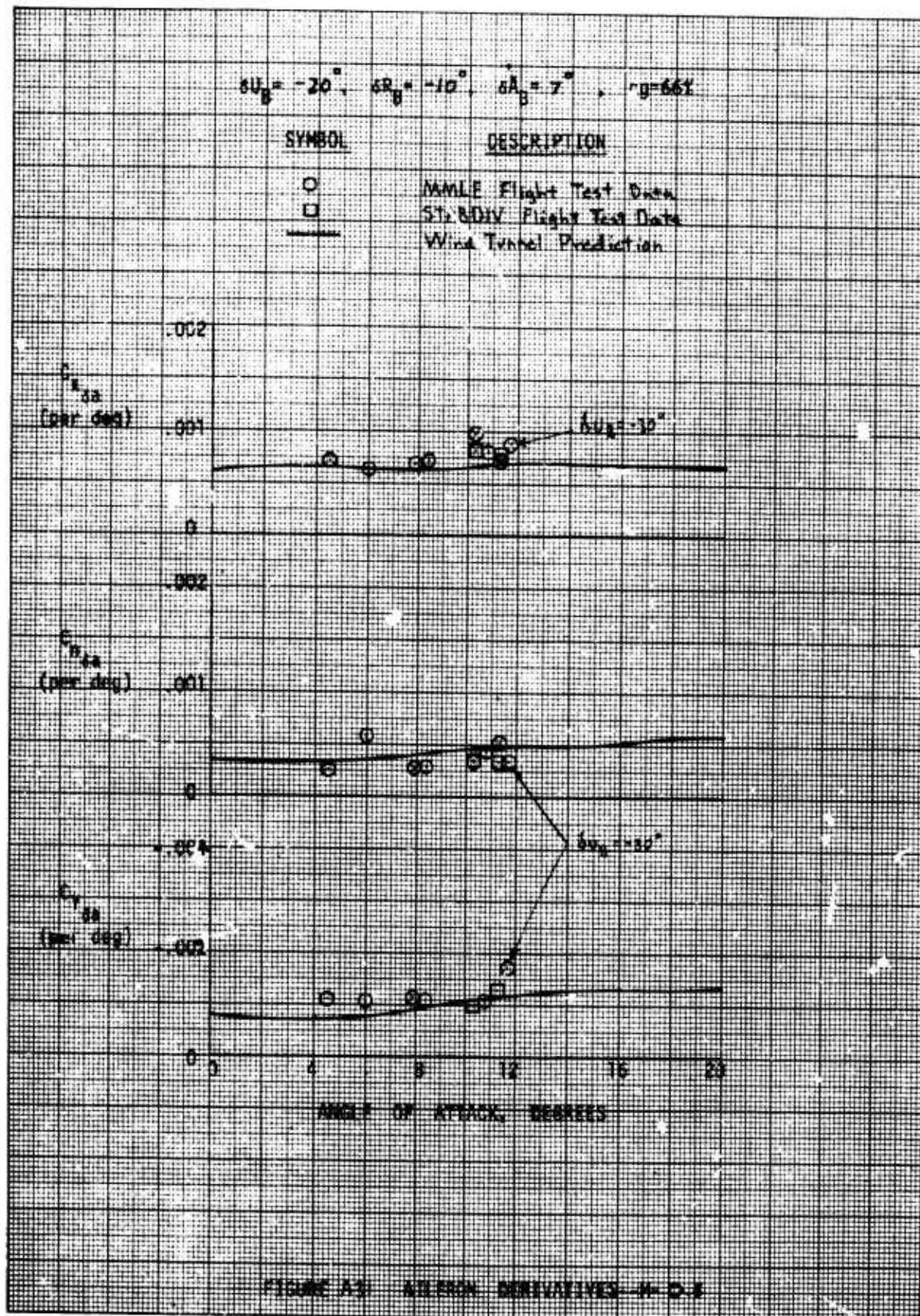
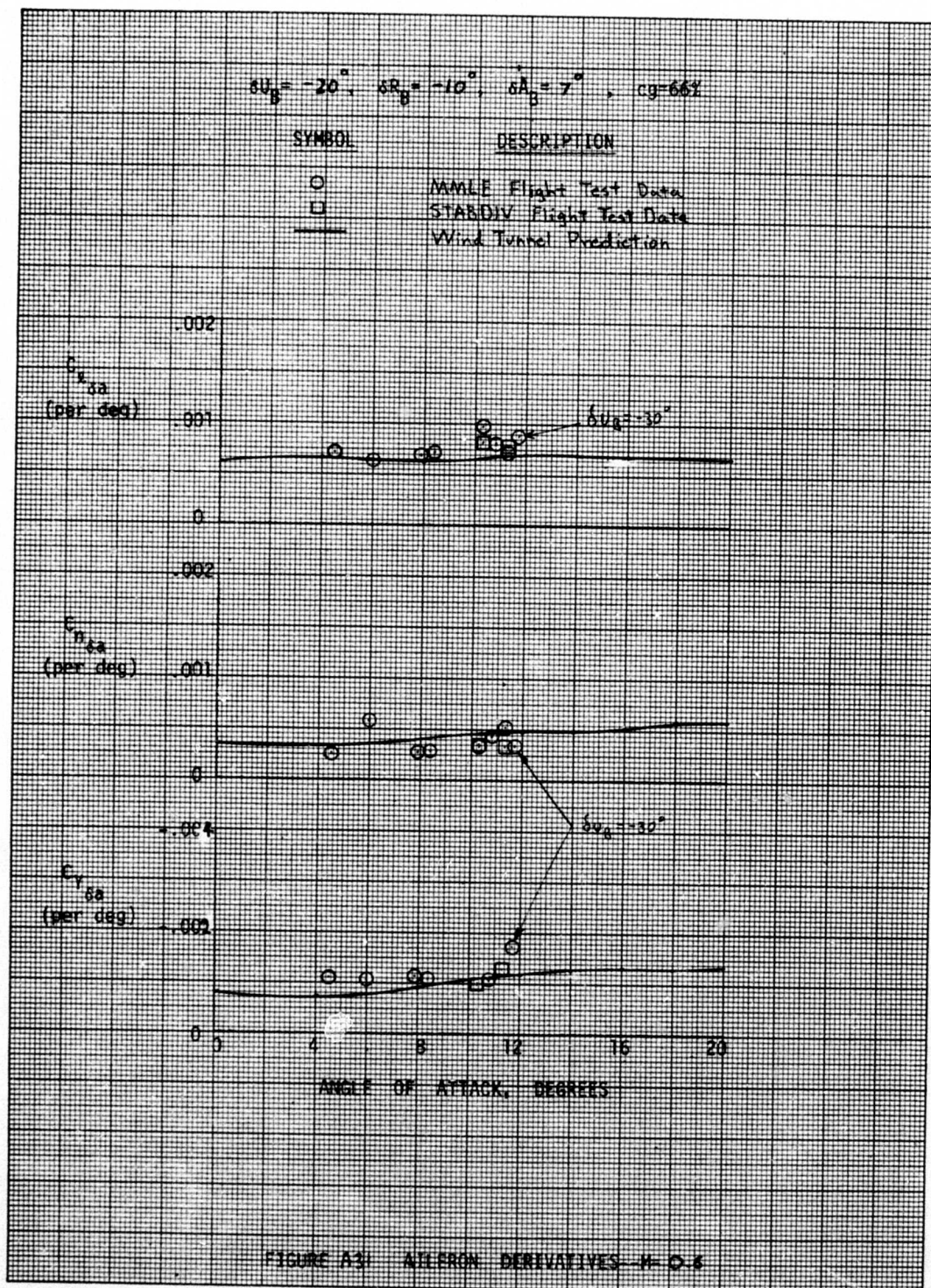


FIGURE A3: ALLERON DERIVATIVES—M-D-2





$\alpha_{L_0} = -20^\circ$ ,  $\alpha_{R_0} = -10^\circ$ ,  $\alpha_{D_0} = 7^\circ$ ,  $CG = 56\%$

SYMBOL	DESCRIPTION
$\circ$	MANUE Flight Test Data
$\square$	STANDIV Flight Test Data
—	SAS OCE
—	Wind Tunnel Prediction

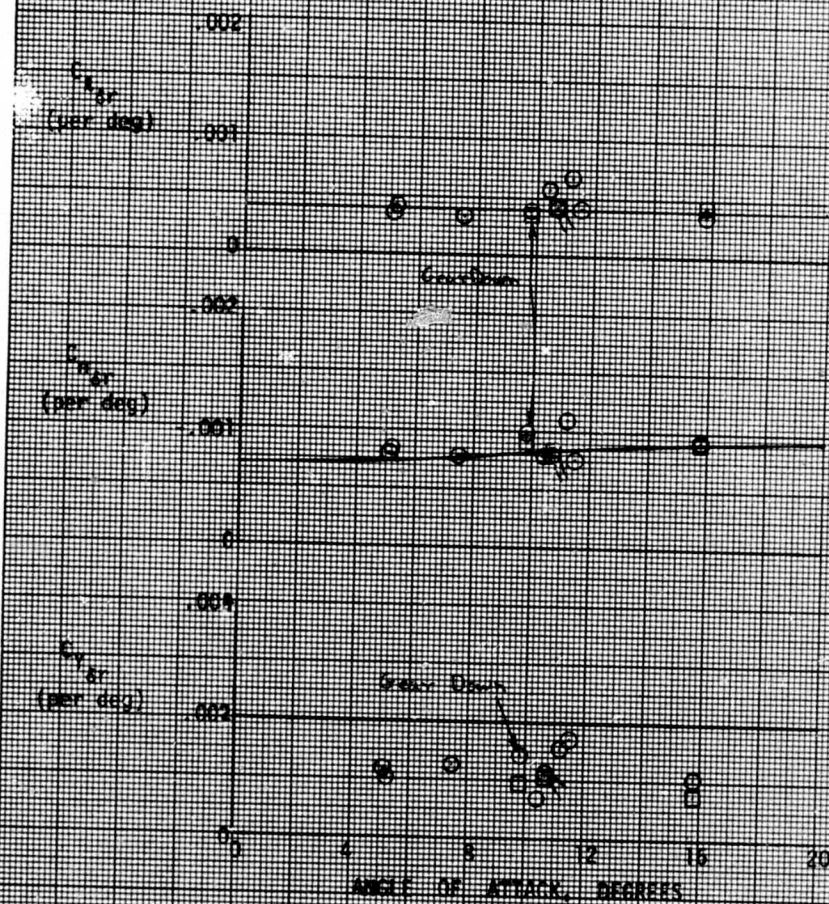
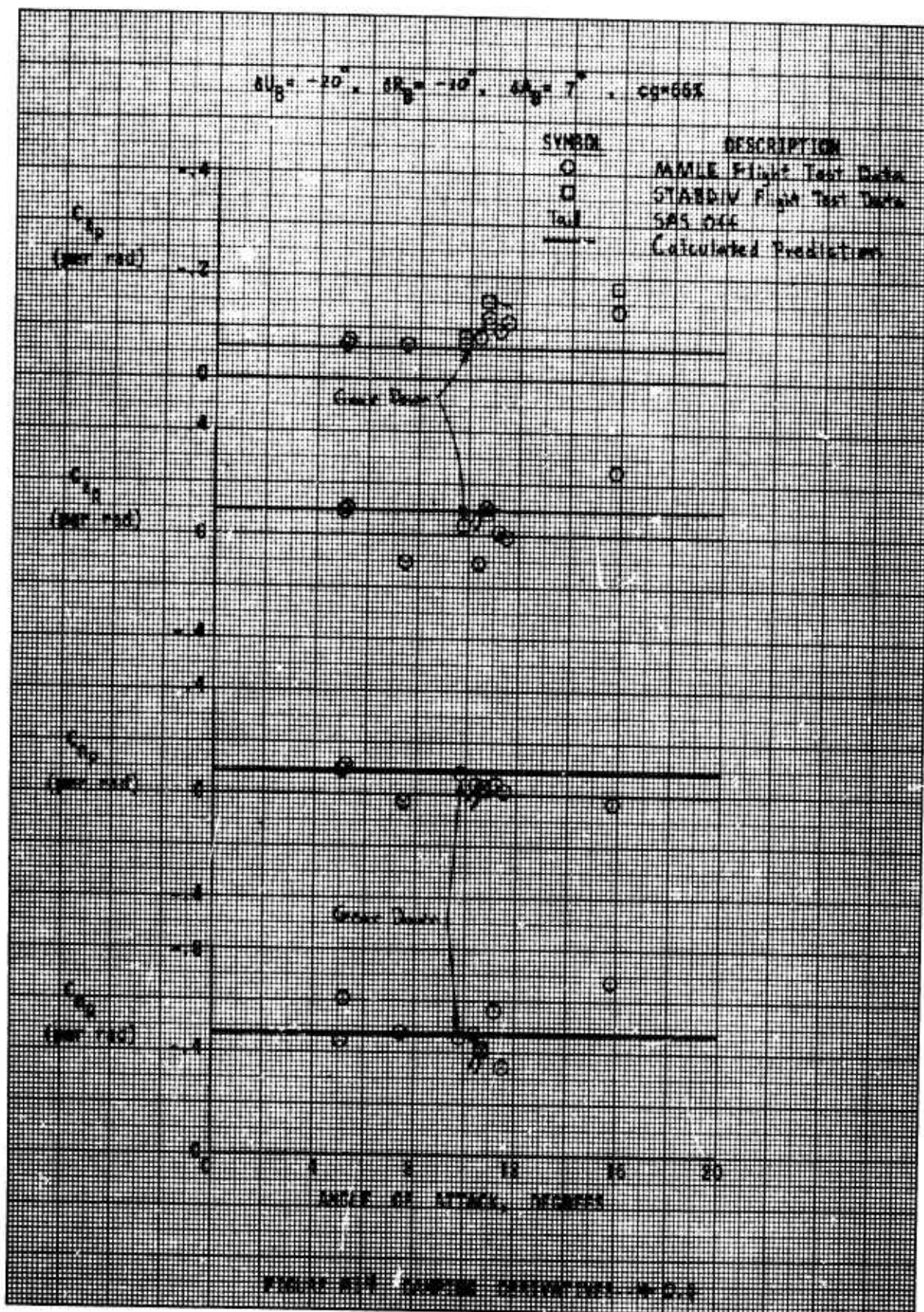
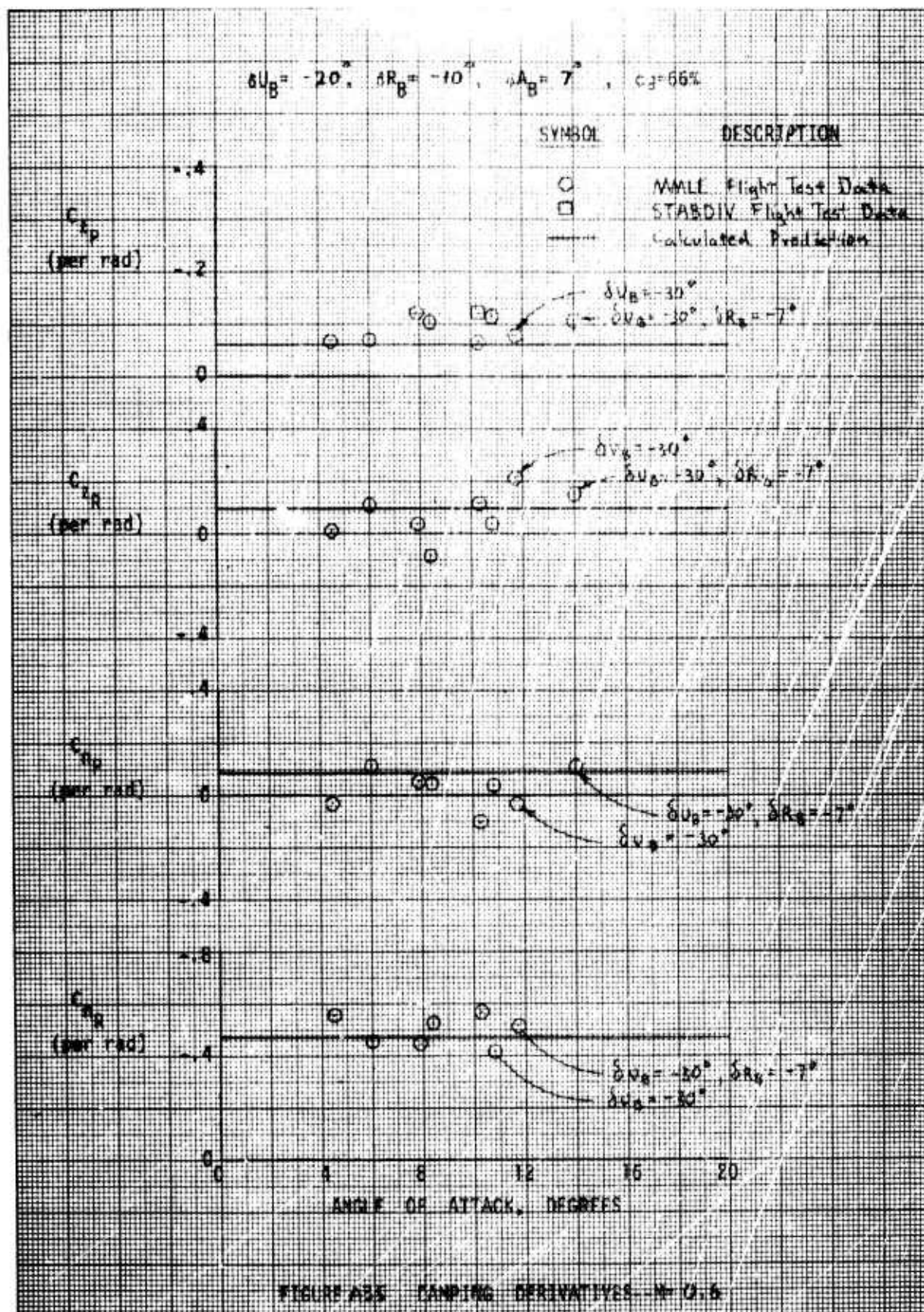


FIGURE 121. WING DERIVATIVES - P-C.4









$\delta J_B = -40^\circ$ ,  $\delta \alpha_B = 0^\circ$ ,  $\delta A_B = 7^\circ$ ,  $c_D = 55\%$

SYMBOL

DESCRIPTION

○

MMLE Flight Test Data

□

STARDIV Flight Test Data

—

Wind Tunnel Prediction

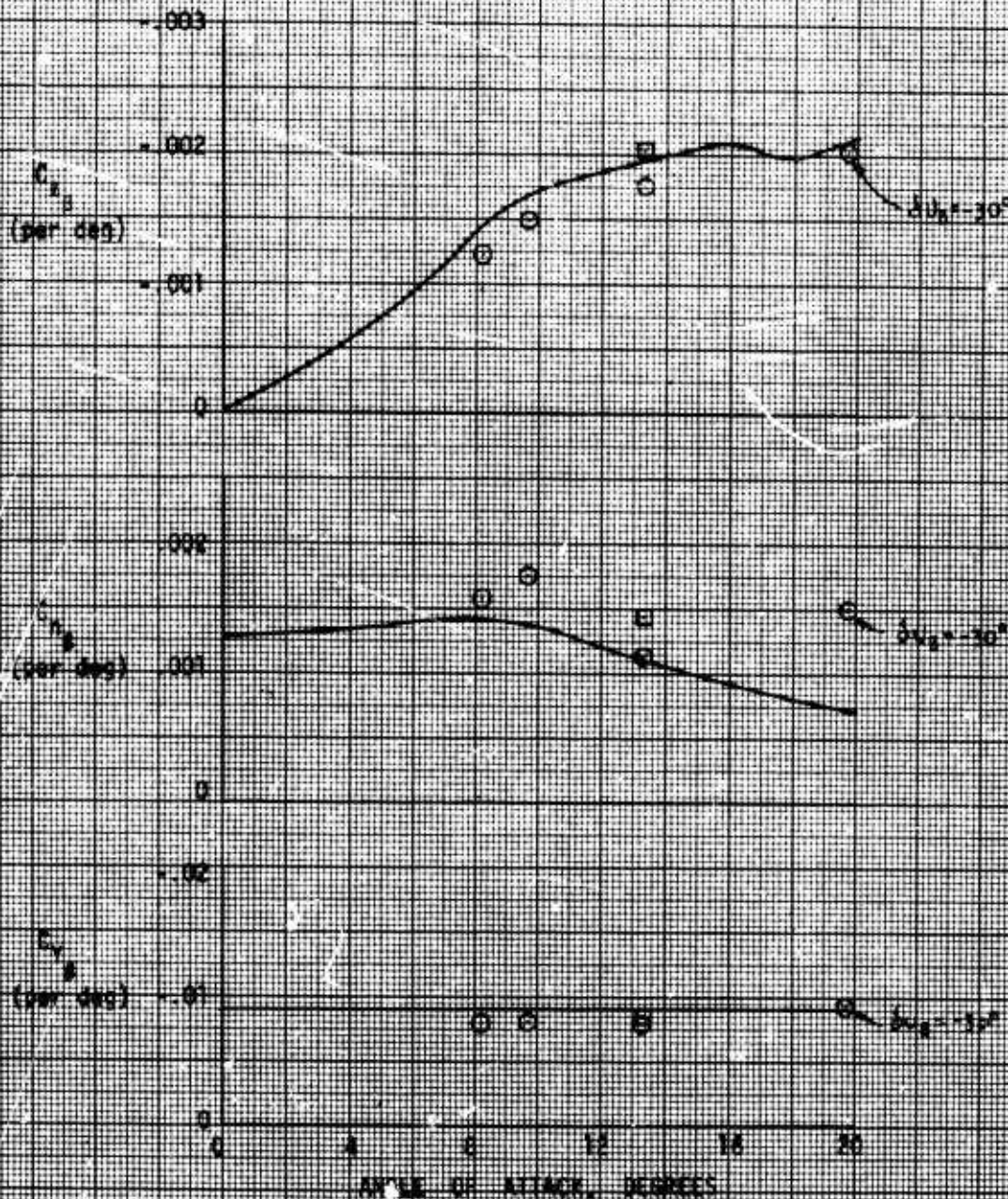
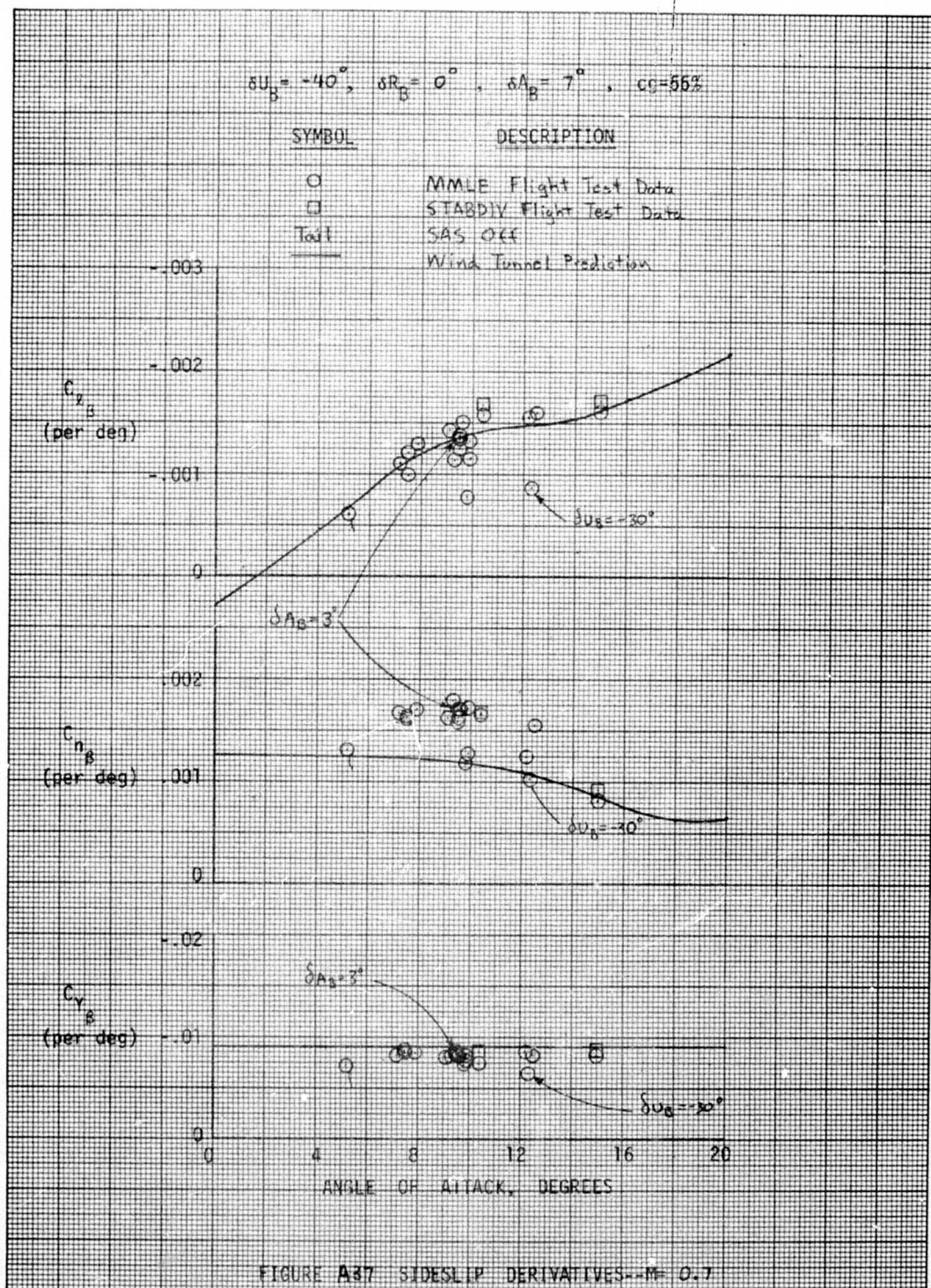
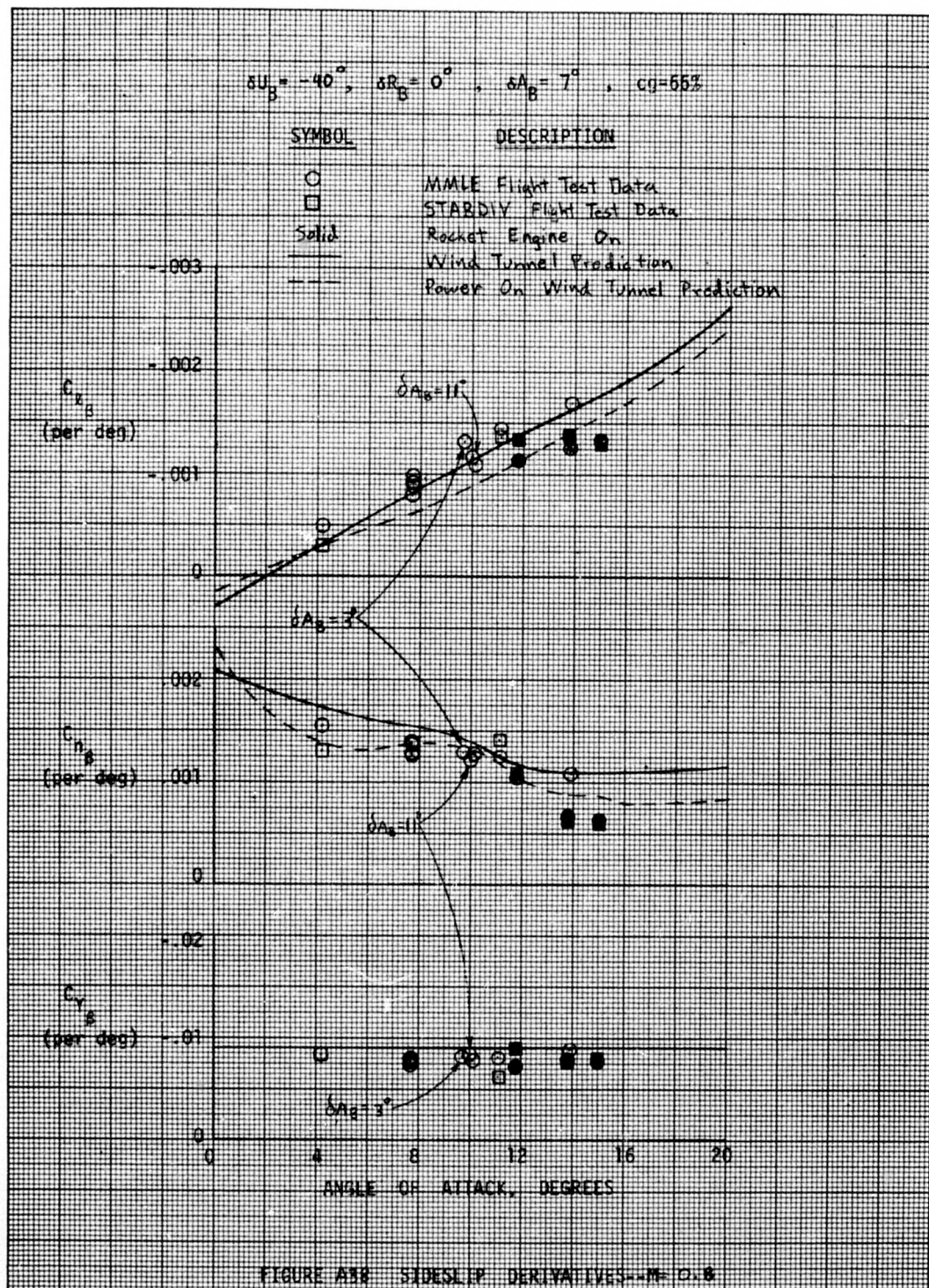


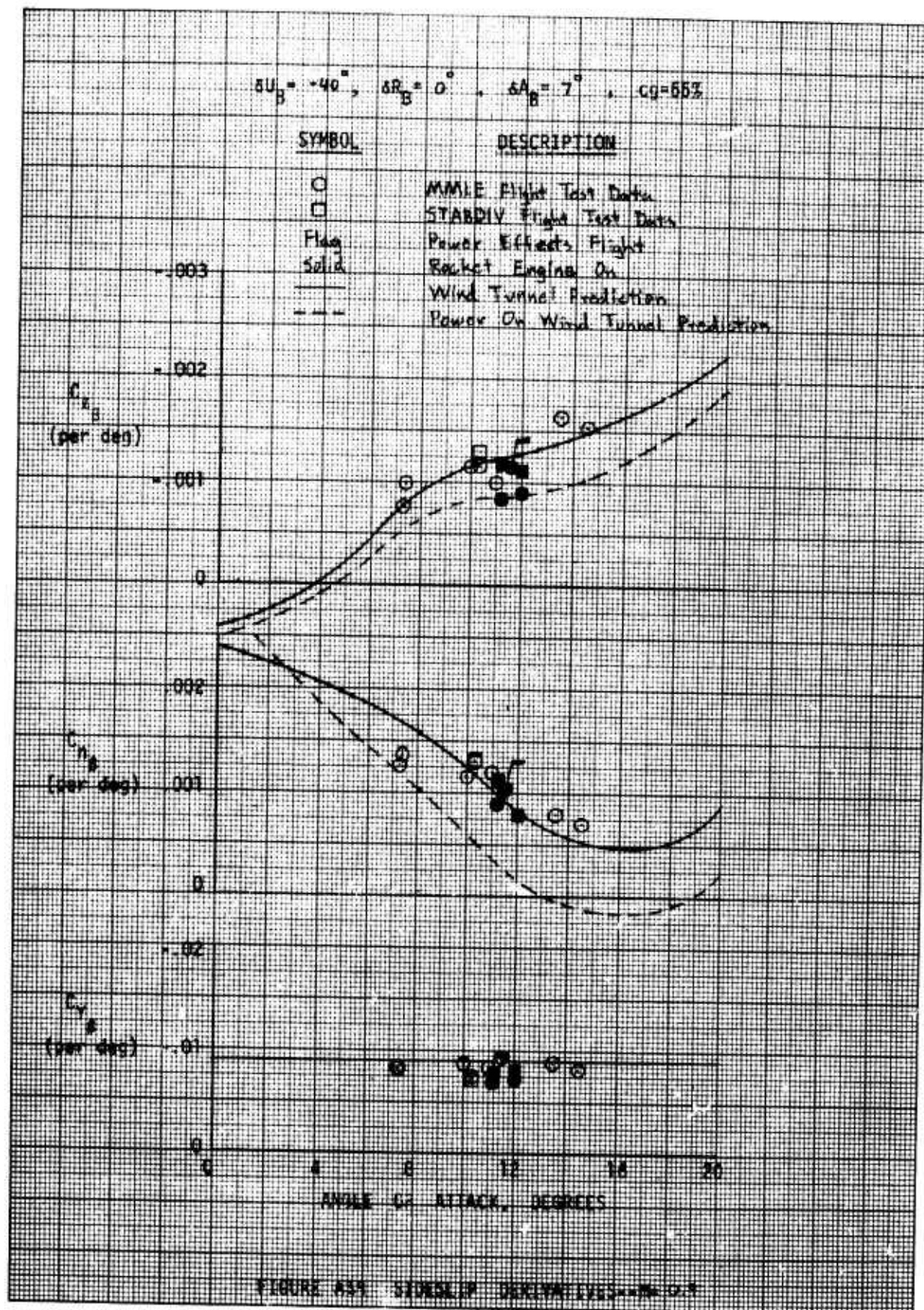
FIGURE 10. SINGLE DERIVATIVES - MMLE



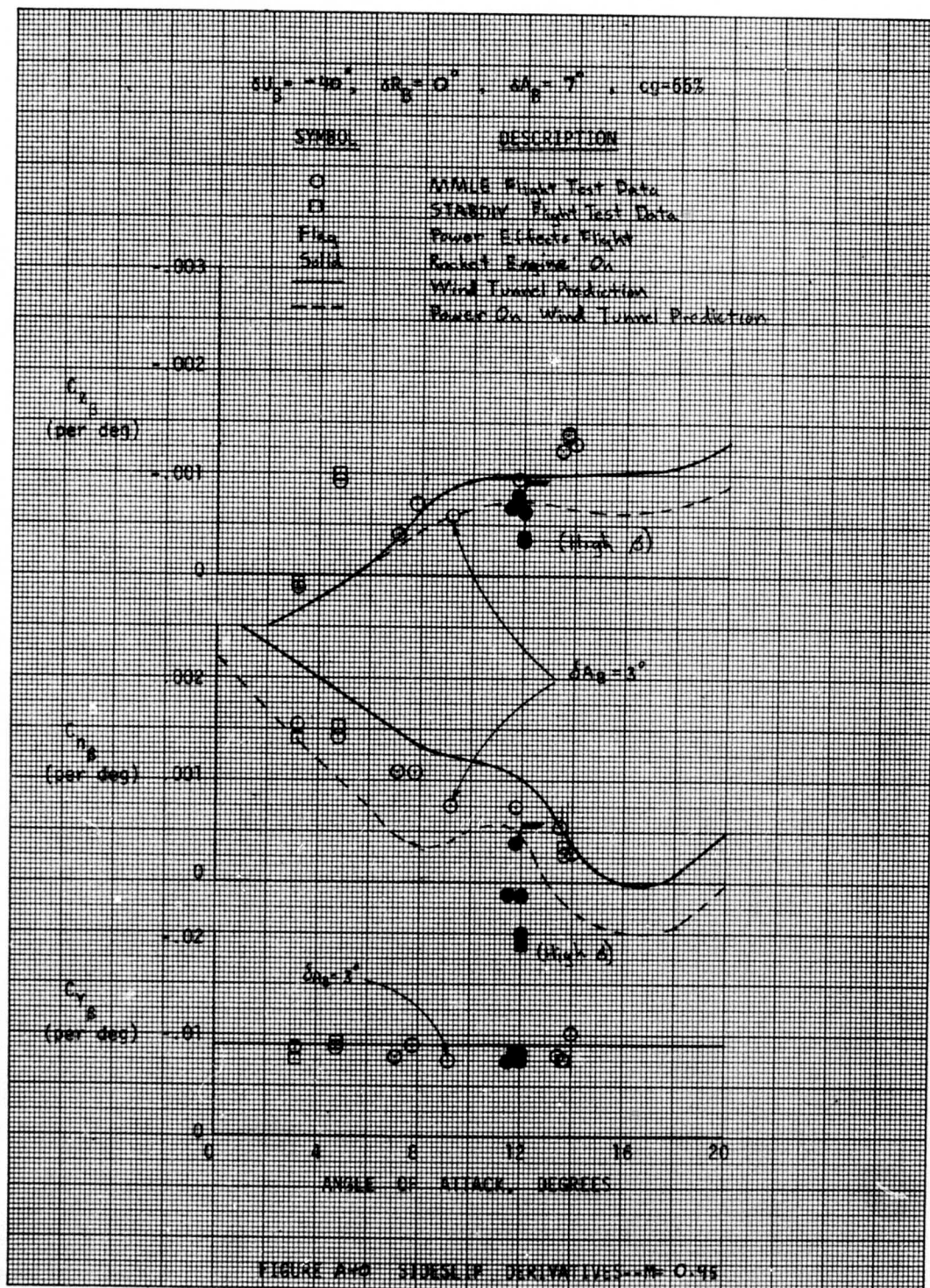














$\delta U_B = -40^\circ$ ,  $\delta R_B = 0^\circ$ ,  $\delta A_B = 7^\circ$ ,  $c_D = 55\%$

SYMBOL

DESCRIPTION

O

MMALE Flight Test Data

Solid

Rocket Engine On

Wind Tunnel Prediction

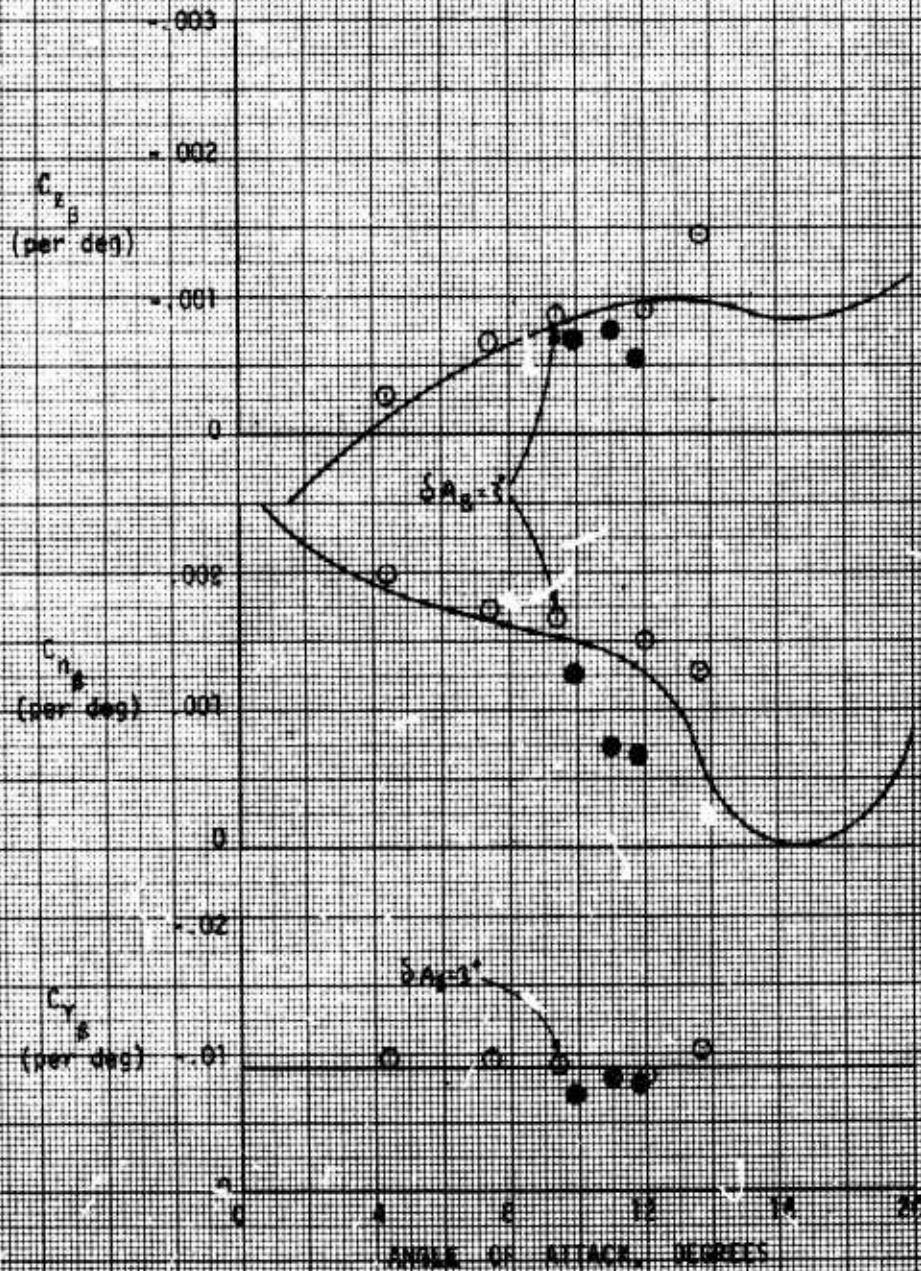
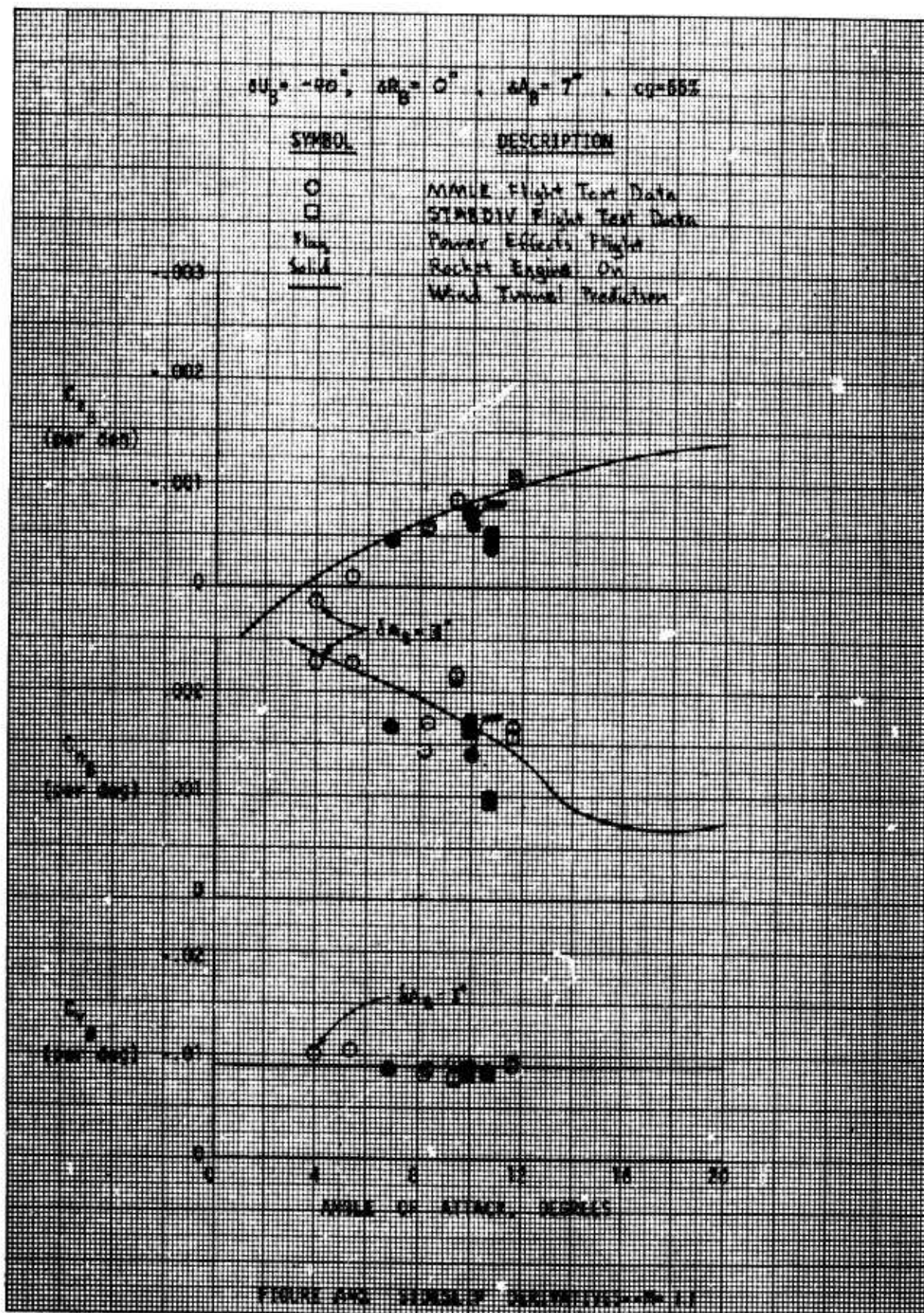
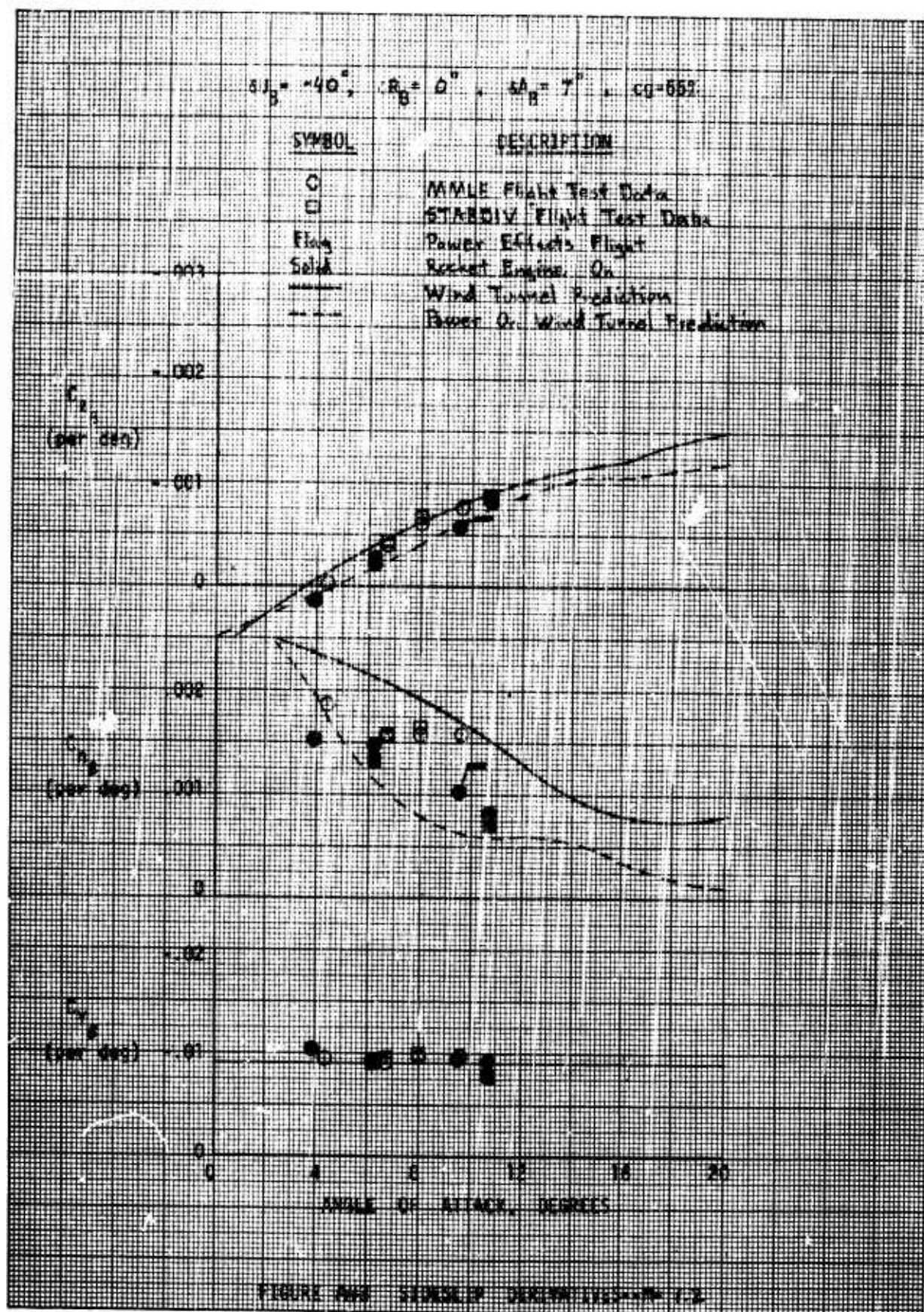


FIGURE A-10. STABILITY DERIVATIVES -  $\alpha = 1.0$









$\Delta A_B = -40^\circ$ ,  $\Delta R_B = 0^\circ$ ,  $\Delta A_B = 7^\circ$ ,  $c_D = 55\%$

SYMBOL

DESCRIPTION

○

AWALE Flight Test Data

□

STABDIV Flight Test Data

—

Power Effects Flight

—

Rocket Engines On

—

Wind Tunnel Prediction

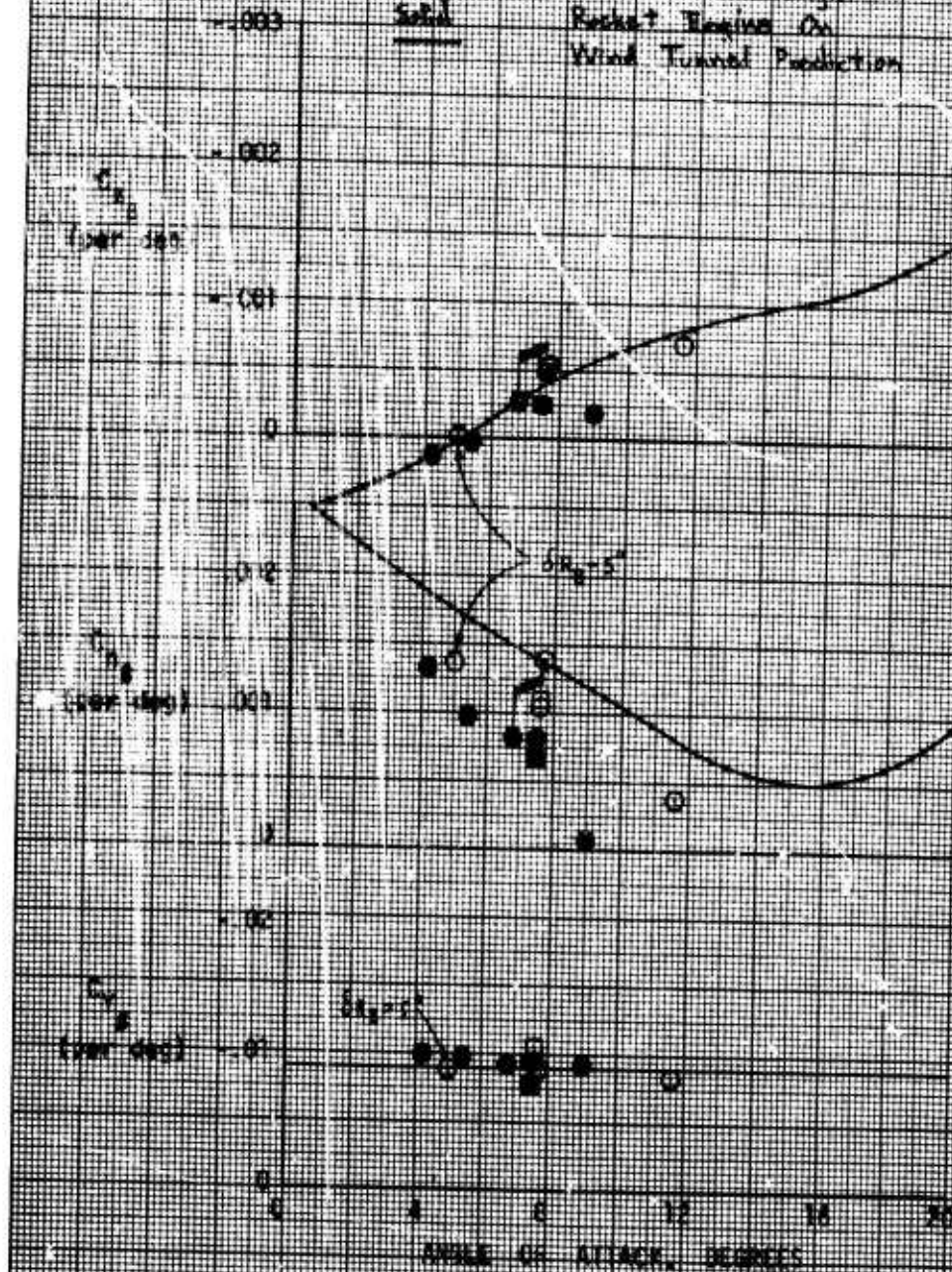
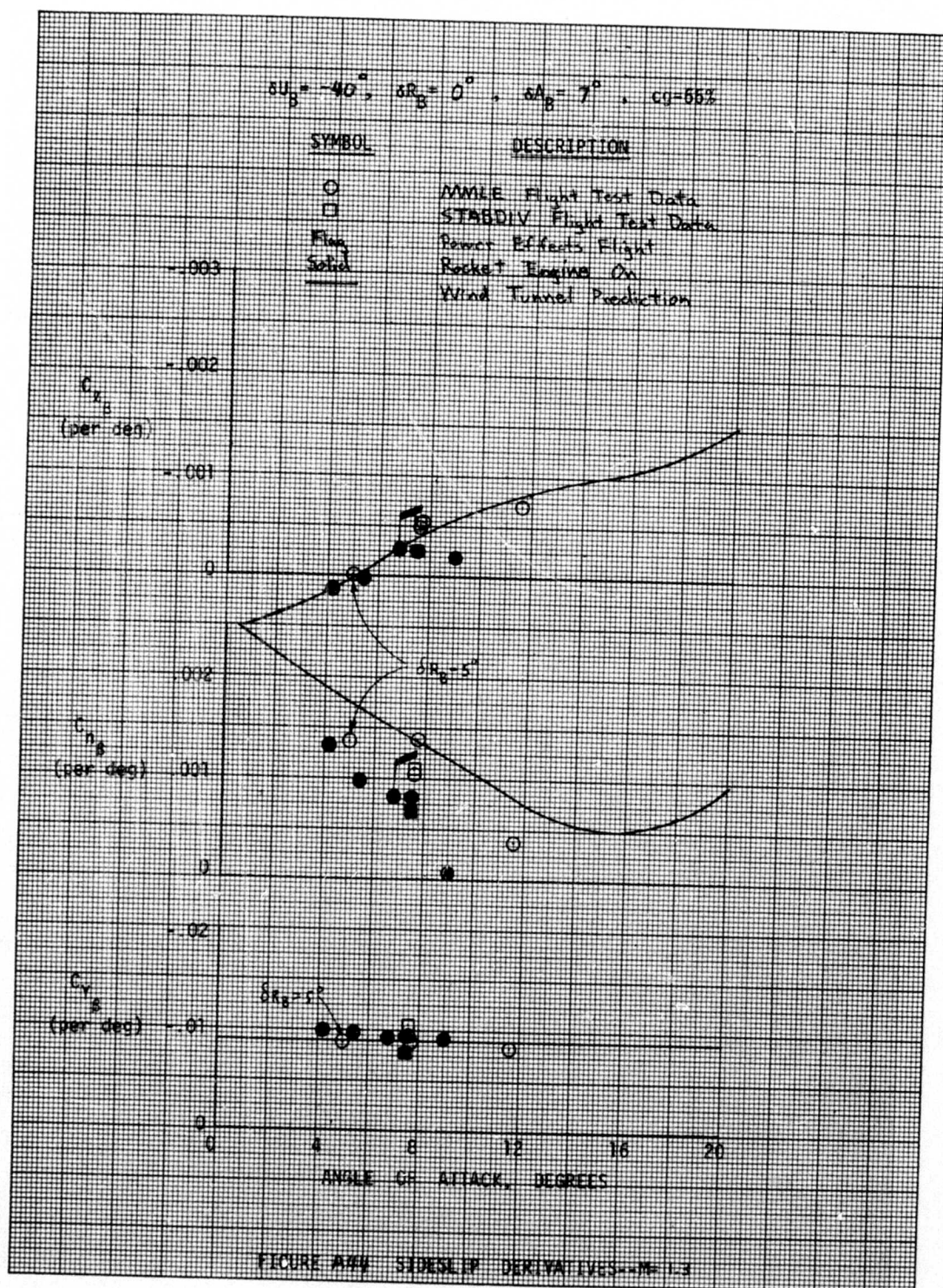


FIGURE 10. STABDIV DERIVATIVE DATA





$\alpha_B = 40^\circ$ ,  $\alpha_B = 0^\circ$ ,  $\alpha_B = 7^\circ$ ,  $C_L = 55\%$

SYMBOL	DESCRIPTION
O	MALE Flight Test Data
□	STANDIV Flight Test Data
Solid	Rocket Engine On
-----	Wind Tunnel Prediction

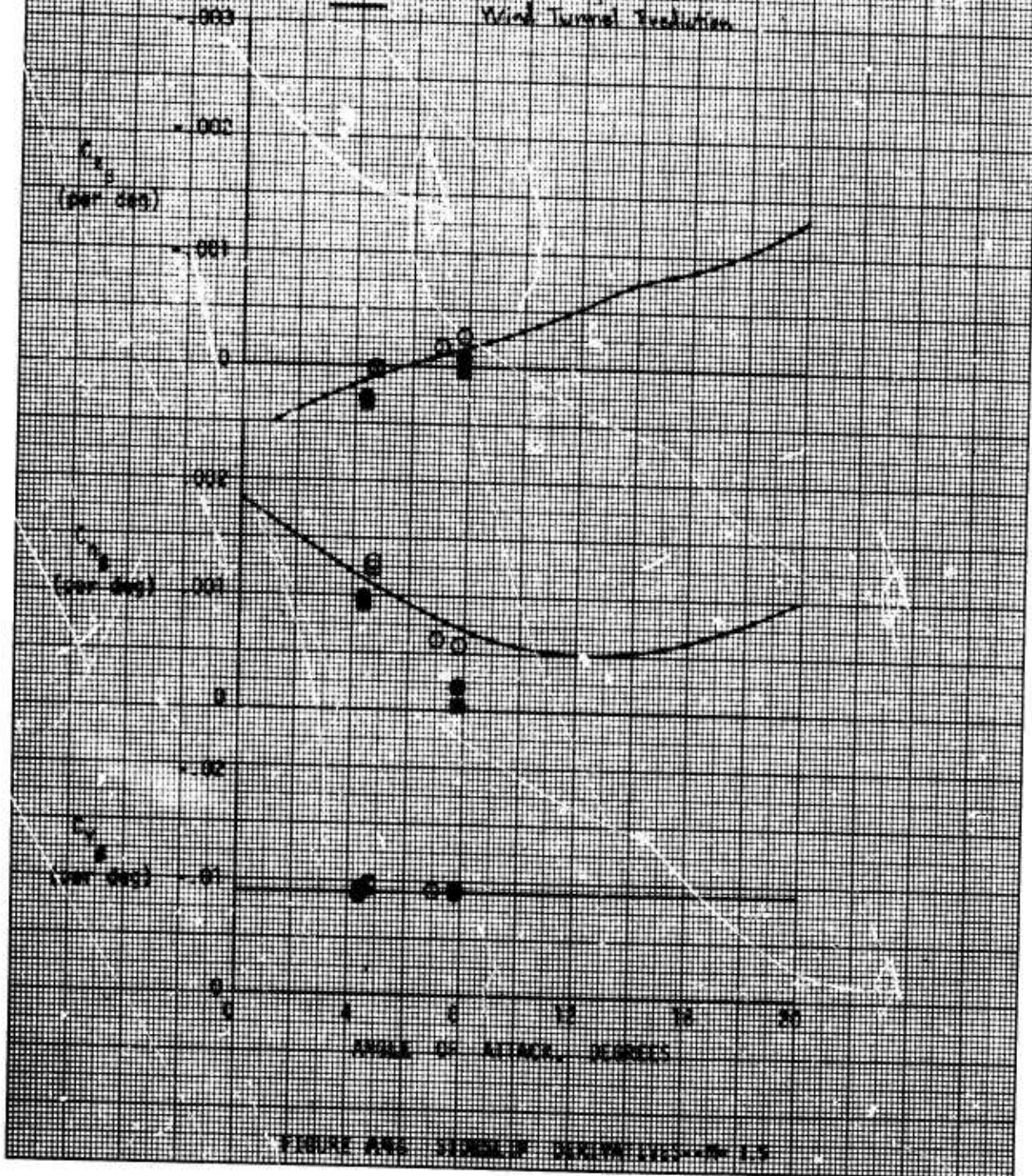
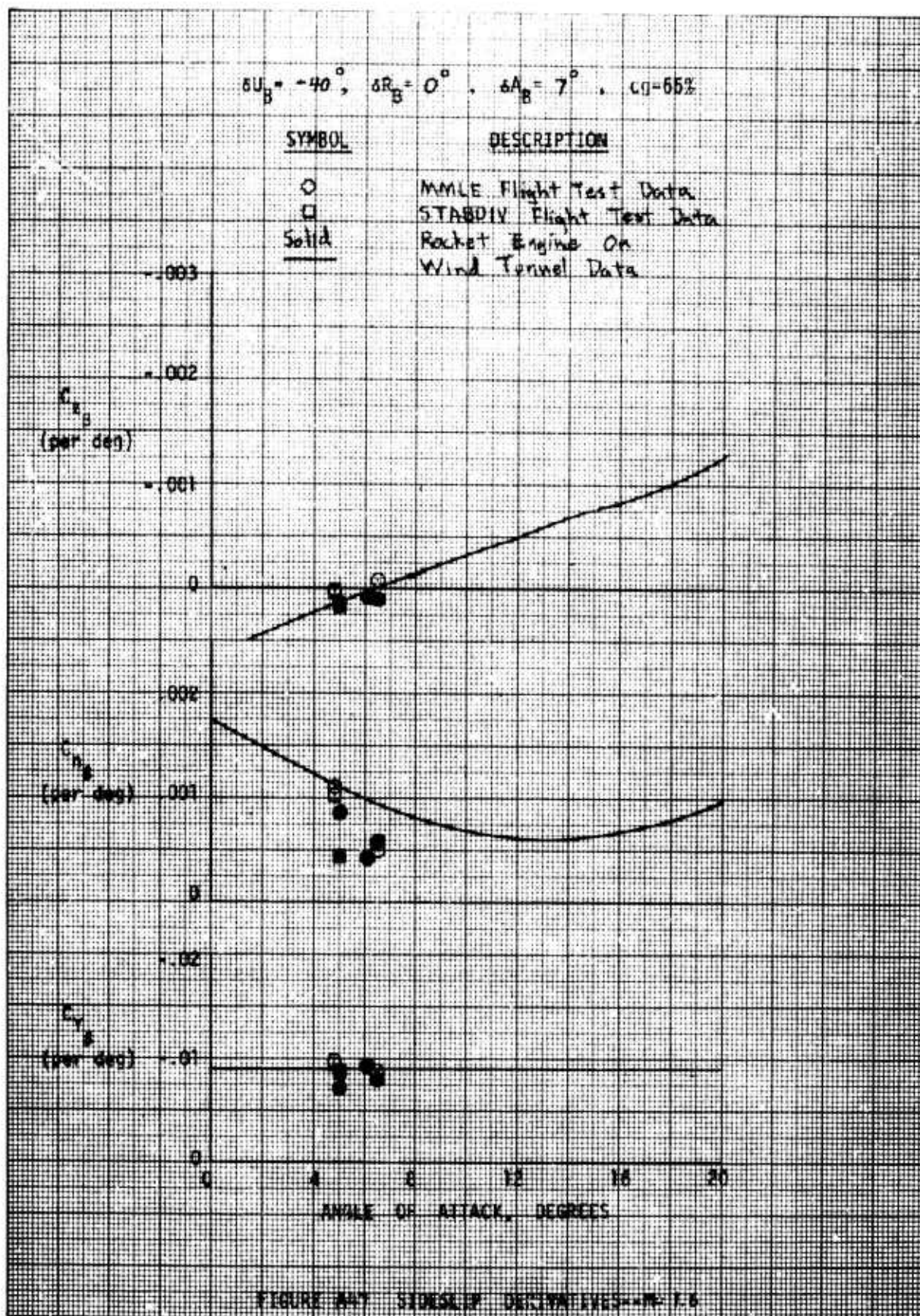
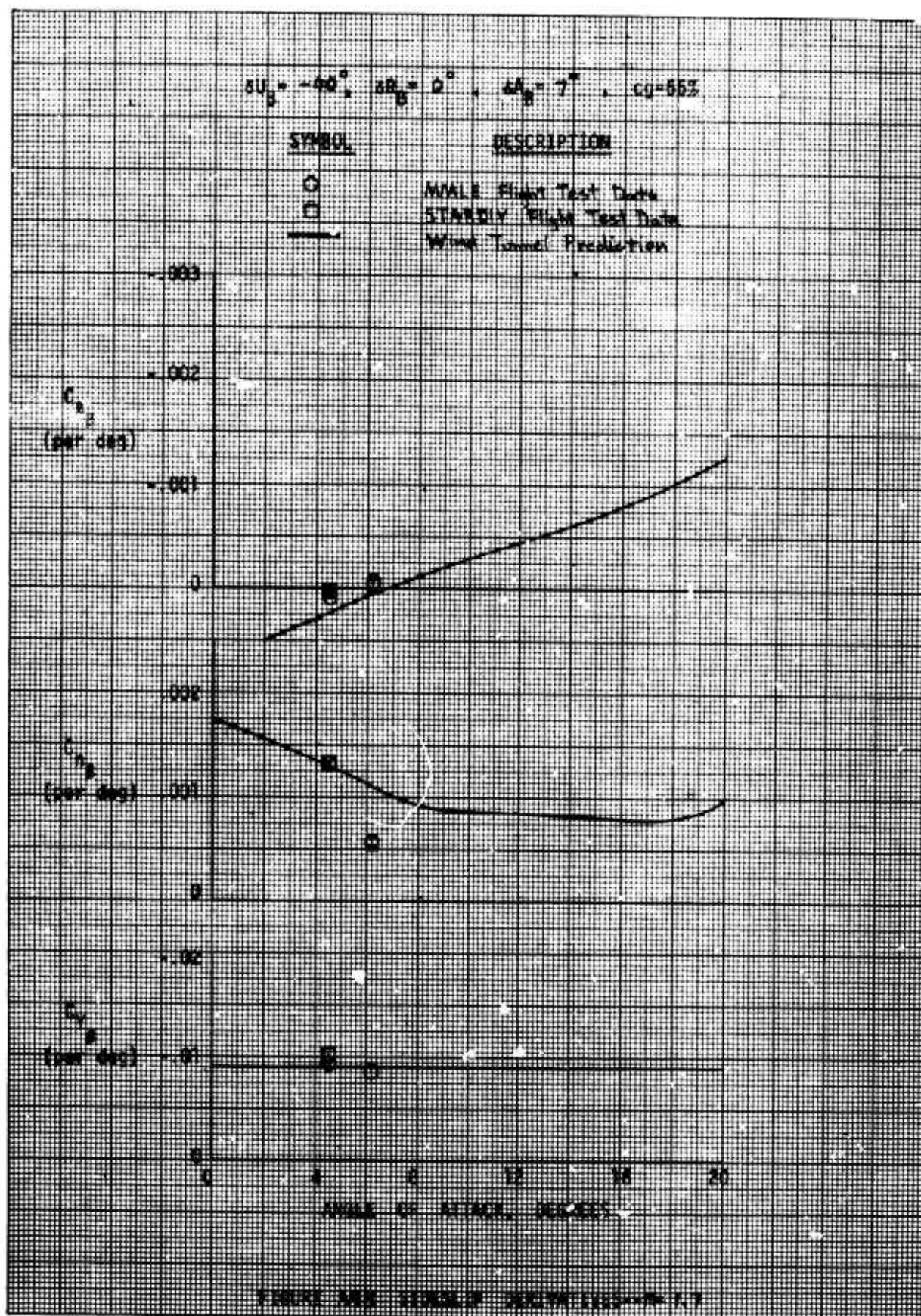


FIGURE ANG. SIMULIN. DERIVATIVES - W-15









$\delta U_B = -40^\circ$   $\delta R_B = 0^\circ$   $\delta A_B = 7^\circ$   $C_D = 0.651$

SYMBOL	DESCRIPTION
○	MMLE Flight Test Data
□	STARDIV Flight Test Data
—	Wind Tunnel Prediction

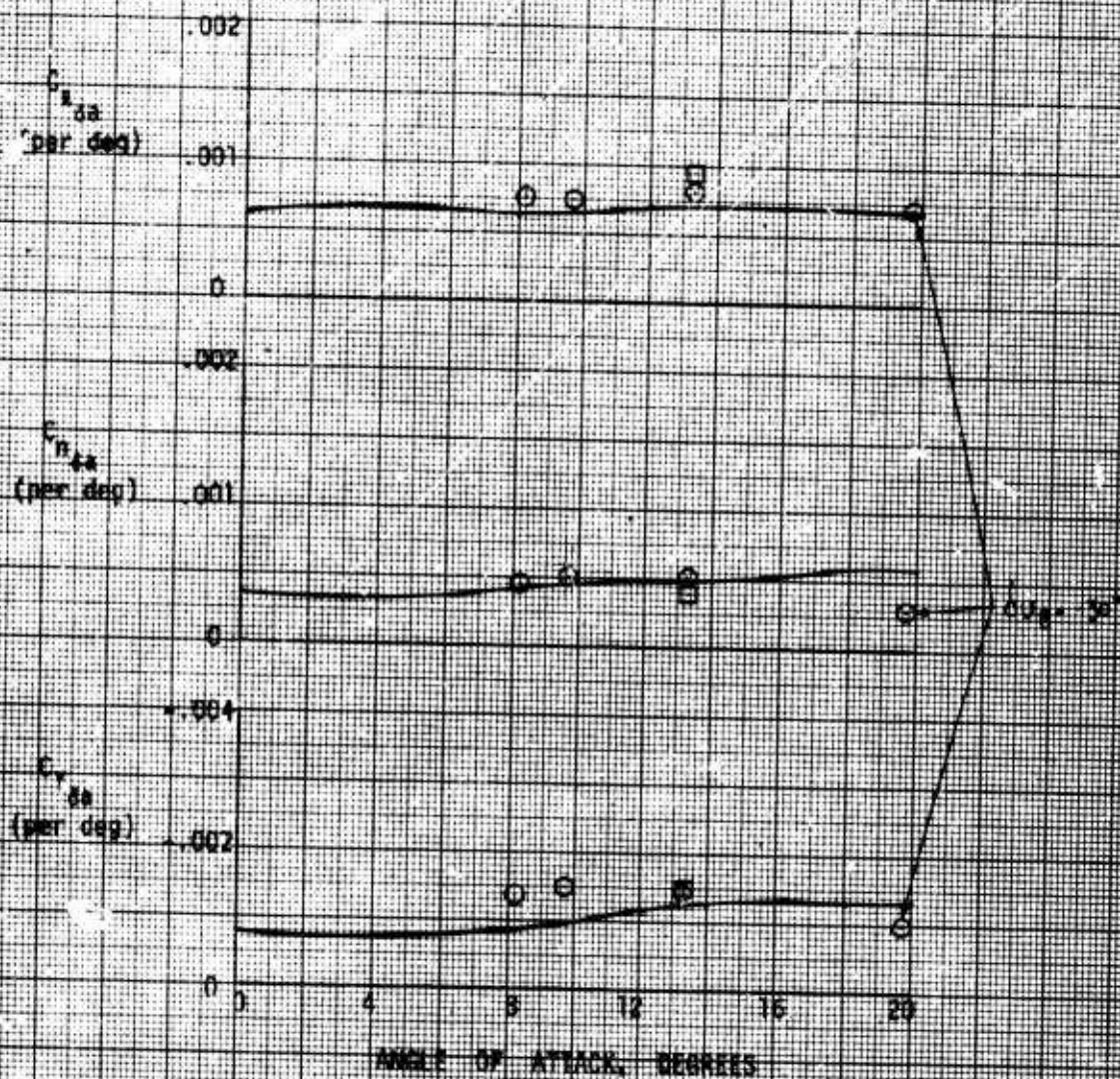


FIGURE A-10. AIRCRAFT DERIVATIVES - W. O. 1



$\delta U_B = -40^\circ$ ,  $\delta R_B = 0^\circ$ ,  $\delta A_B = 7^\circ$ ,  $c_D = 0.61$

SYMBOL	DESCRIPTION
○	MMAR Flight Test Data
□	STABDIV Flight Test Data
△	SAS OFF
—	Wind Tunnel Prediction

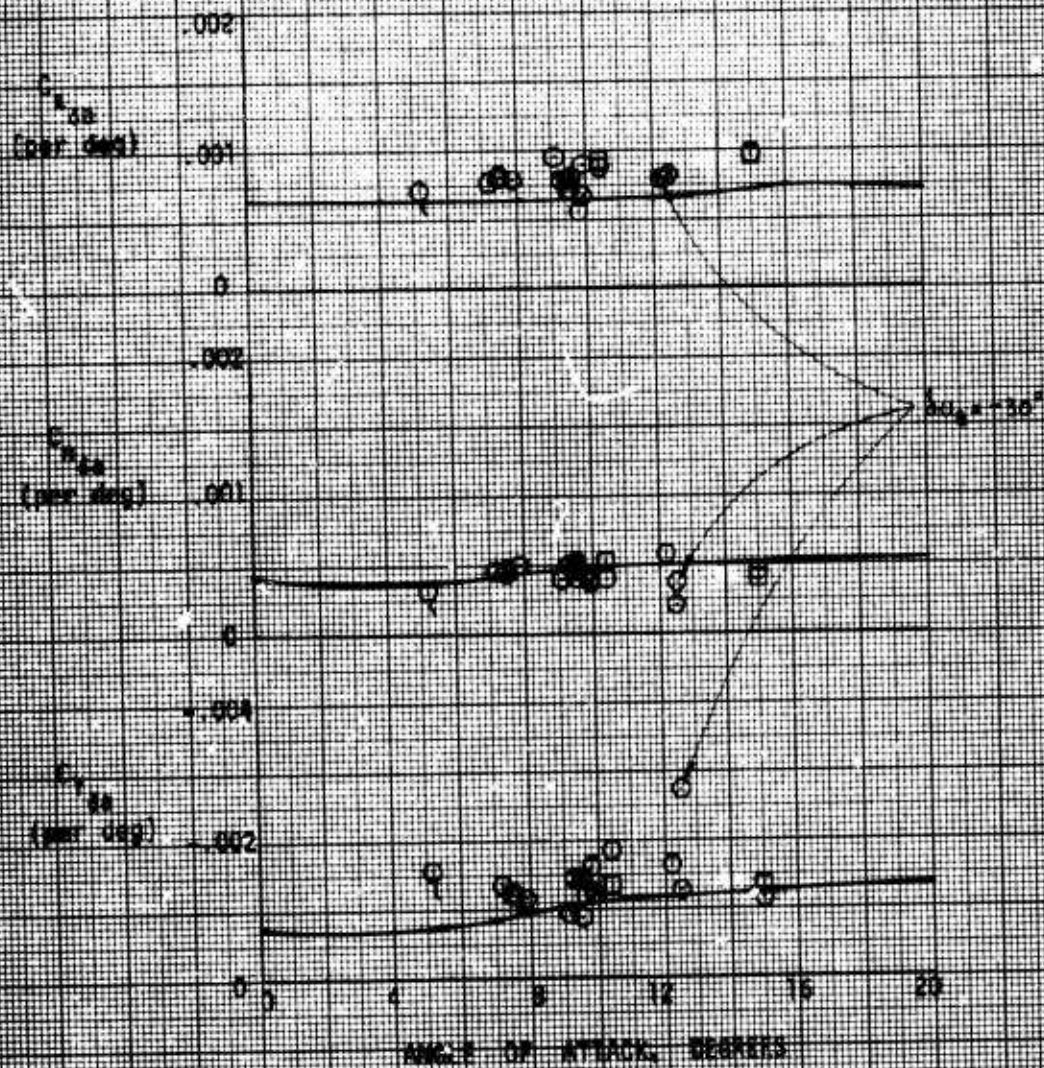
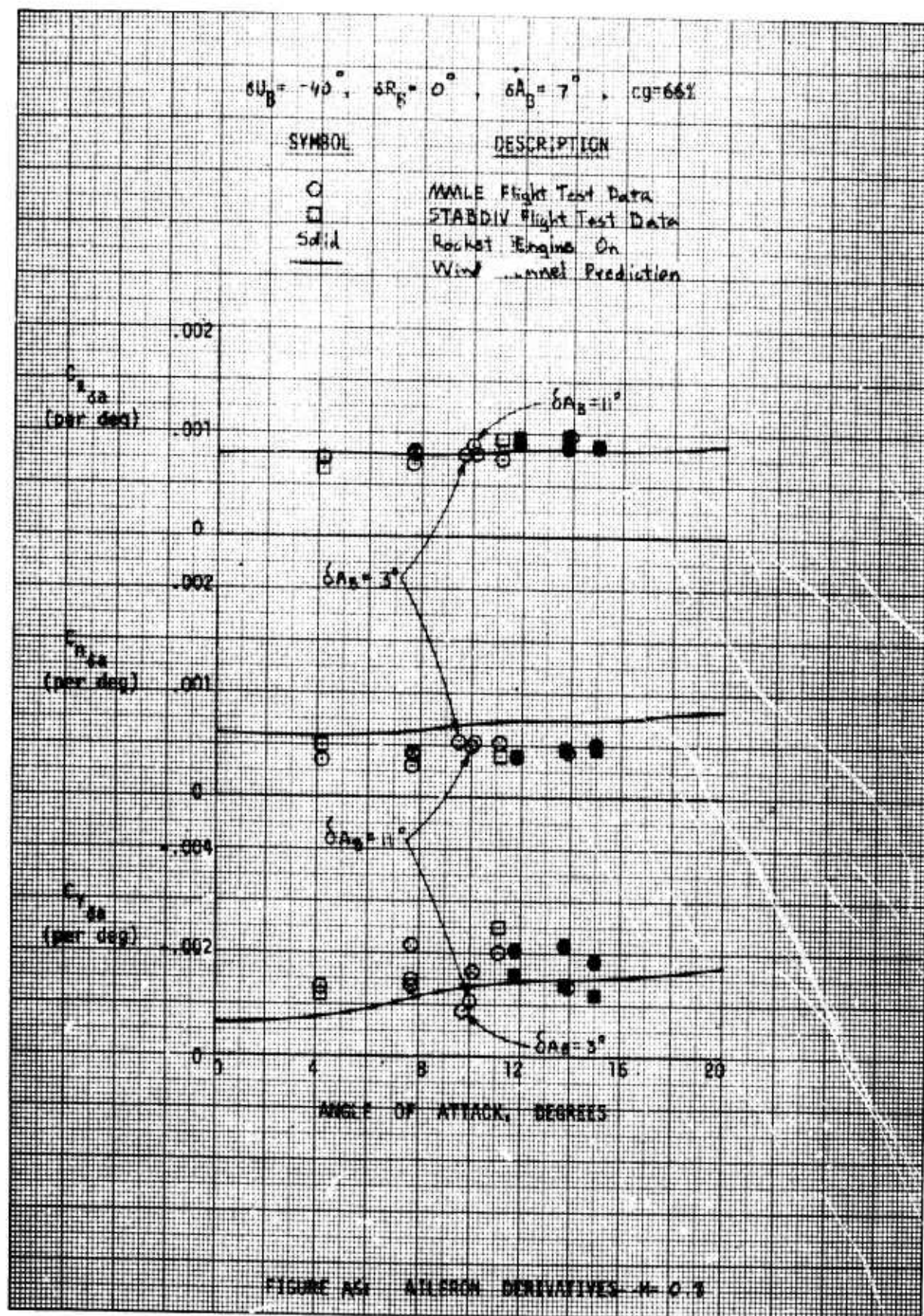
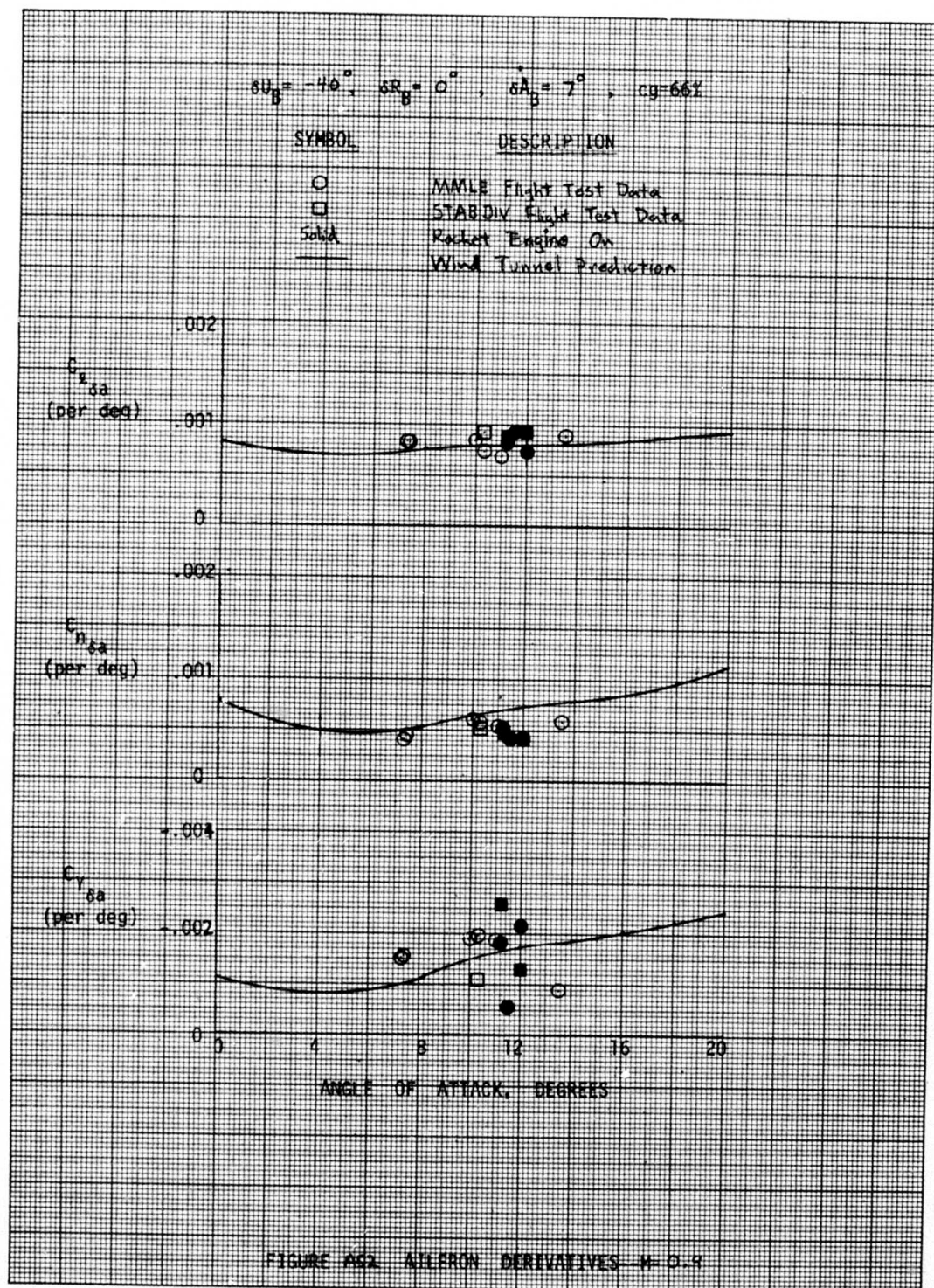


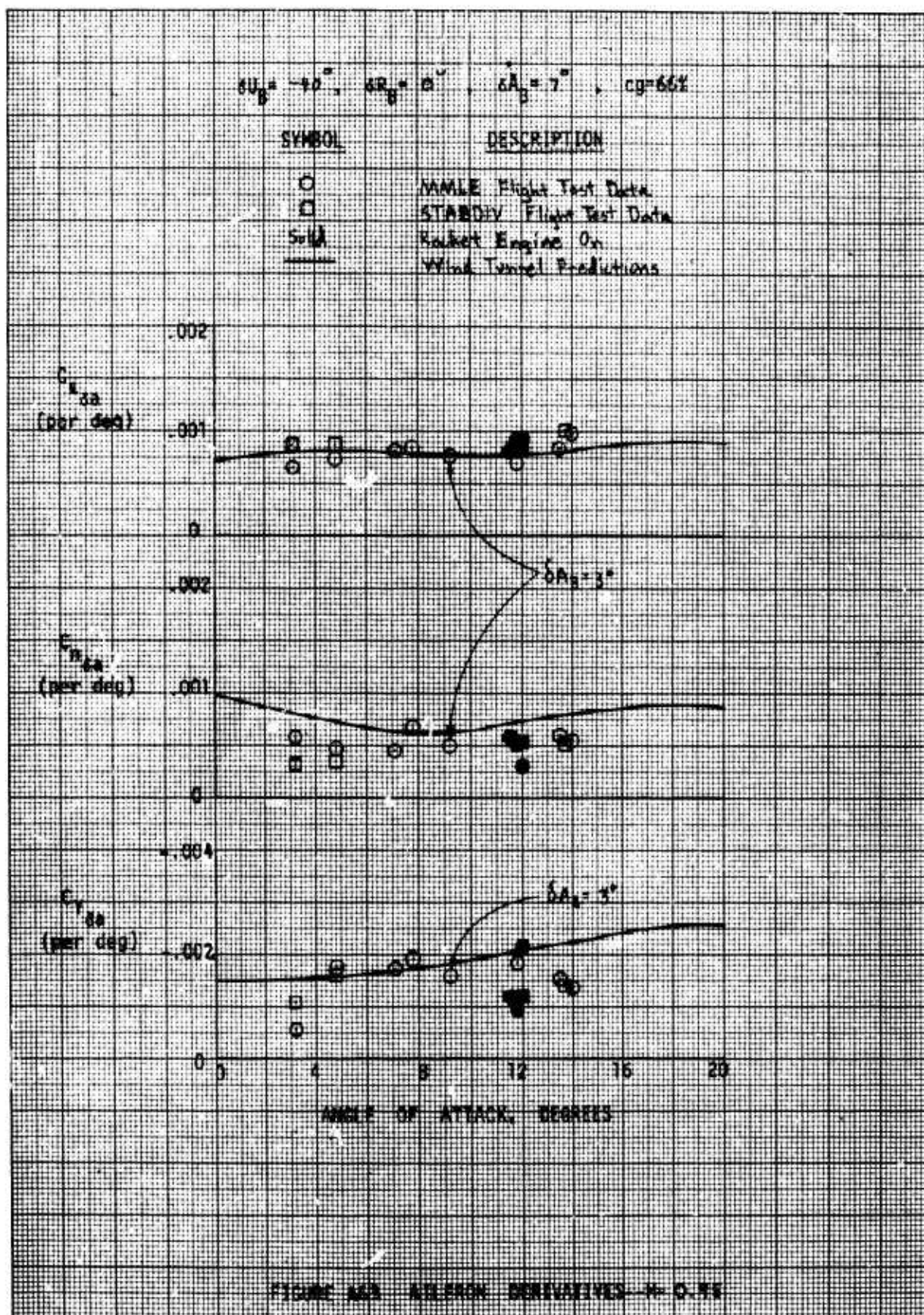
FIGURE A50 AIRCRAFT DERIVATIVES - A-1

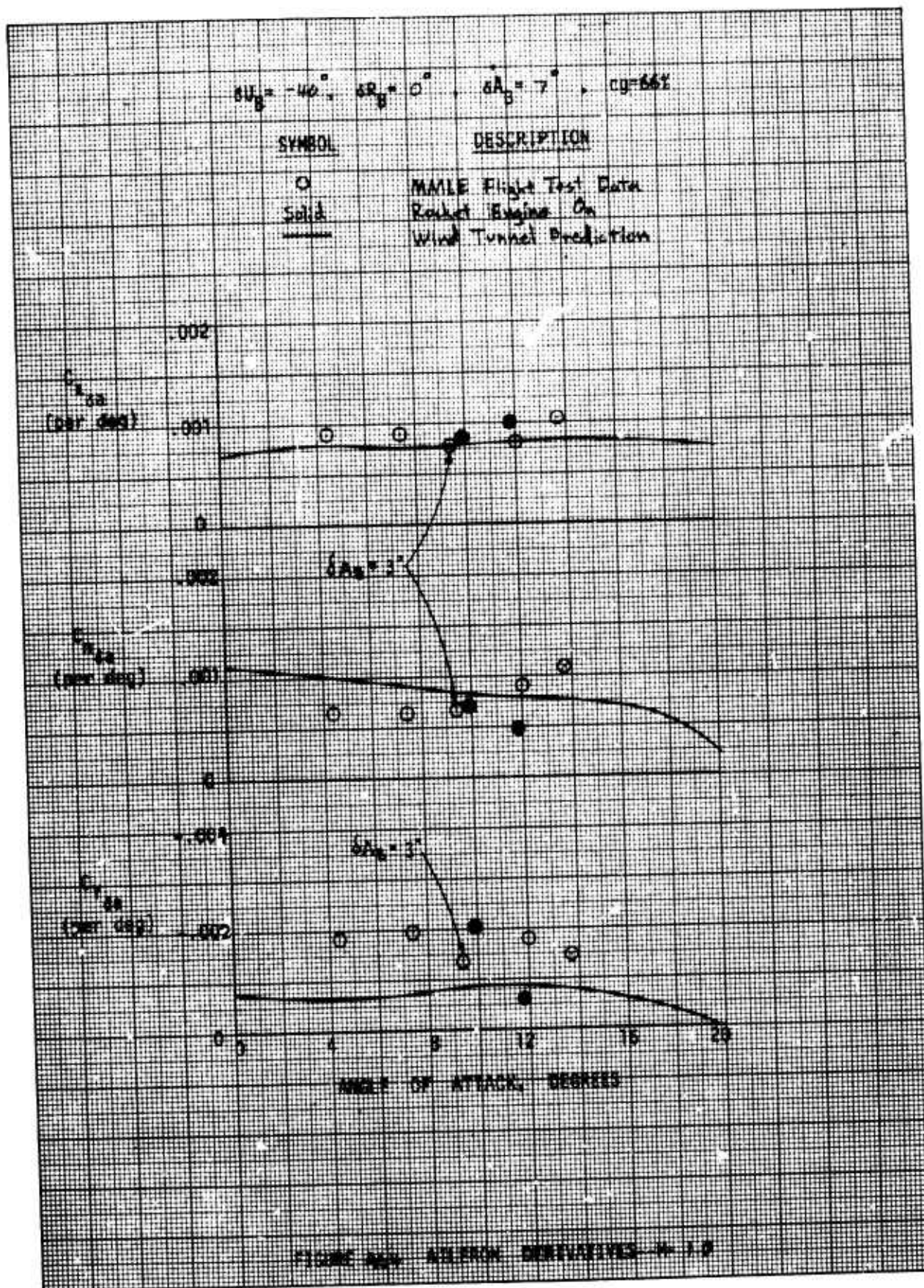




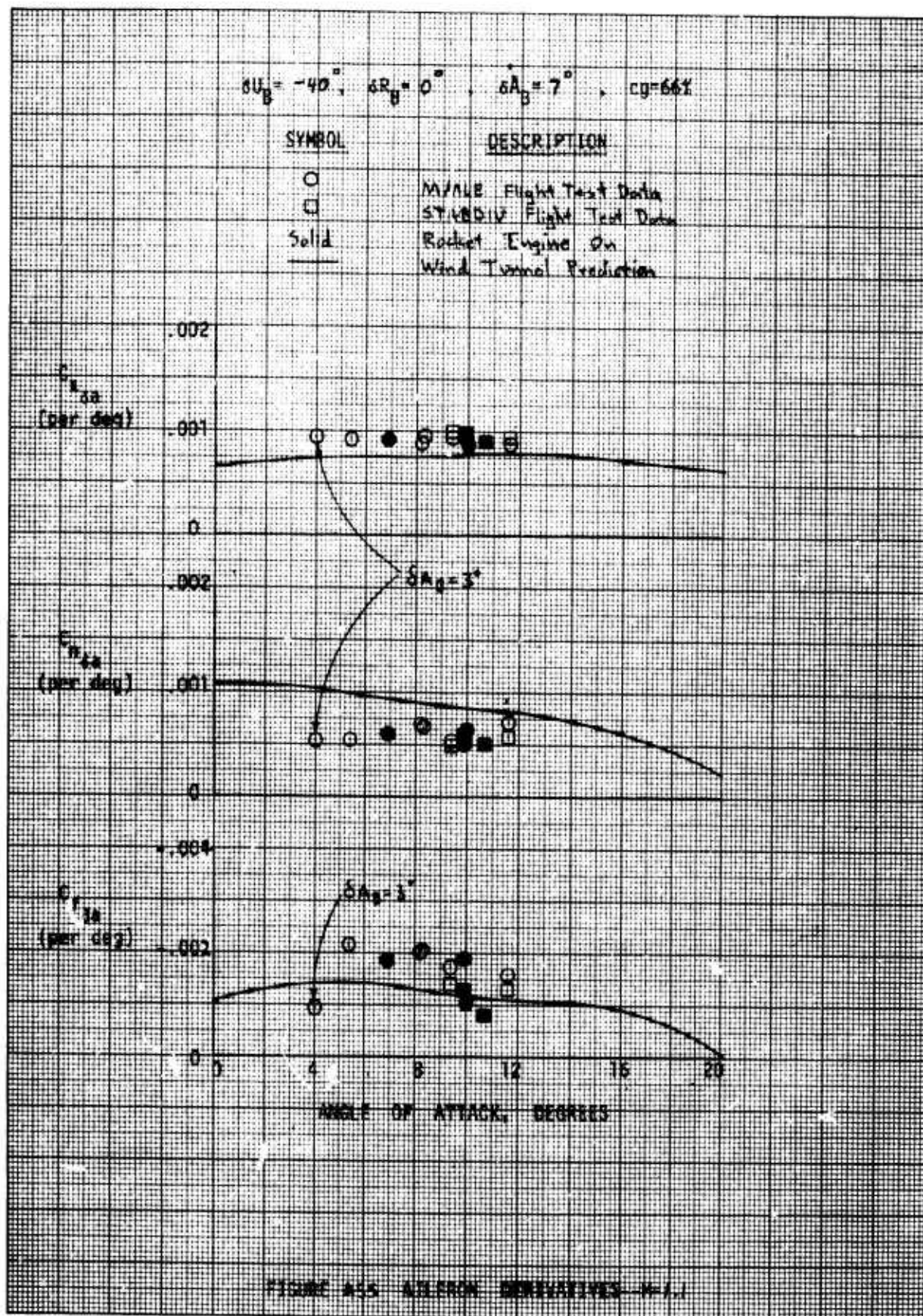














$\alpha_{L_0} = -40^\circ$ ,  $\alpha_{R_0} = 0^\circ$ ,  $\delta A_0 = 7^\circ$ ,  $c_g = 661$

SYMBOL	DESCRIPTION
O	ANGLE Flight Test Data
□	STABILITY Flight Test Data
Solid	Engine On
—	Wind Tunnel Prediction

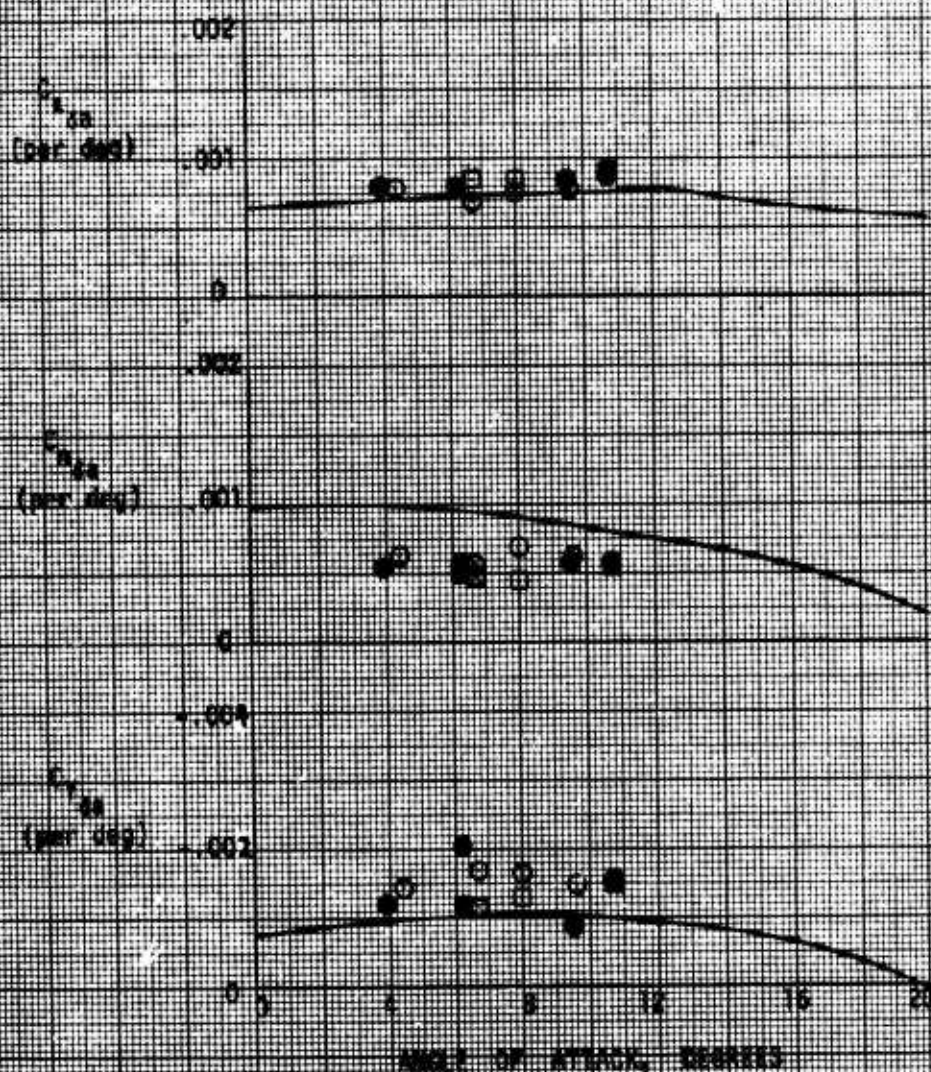


FIGURE 10.1. STABILITY DERIVATIVES - 1.2

$\delta U_0 = -40^\circ$   $\delta \alpha_0 = 0^\circ$   $\delta A_0 = 7^\circ$   $cg=661$

SYMBOL	DESCRIPTION
$\circ$	AMES Flight Test Data
$\square$	STARDY Flight Test Data
Solid	Rocket Engine On
-----	Wind Tunnel Prediction

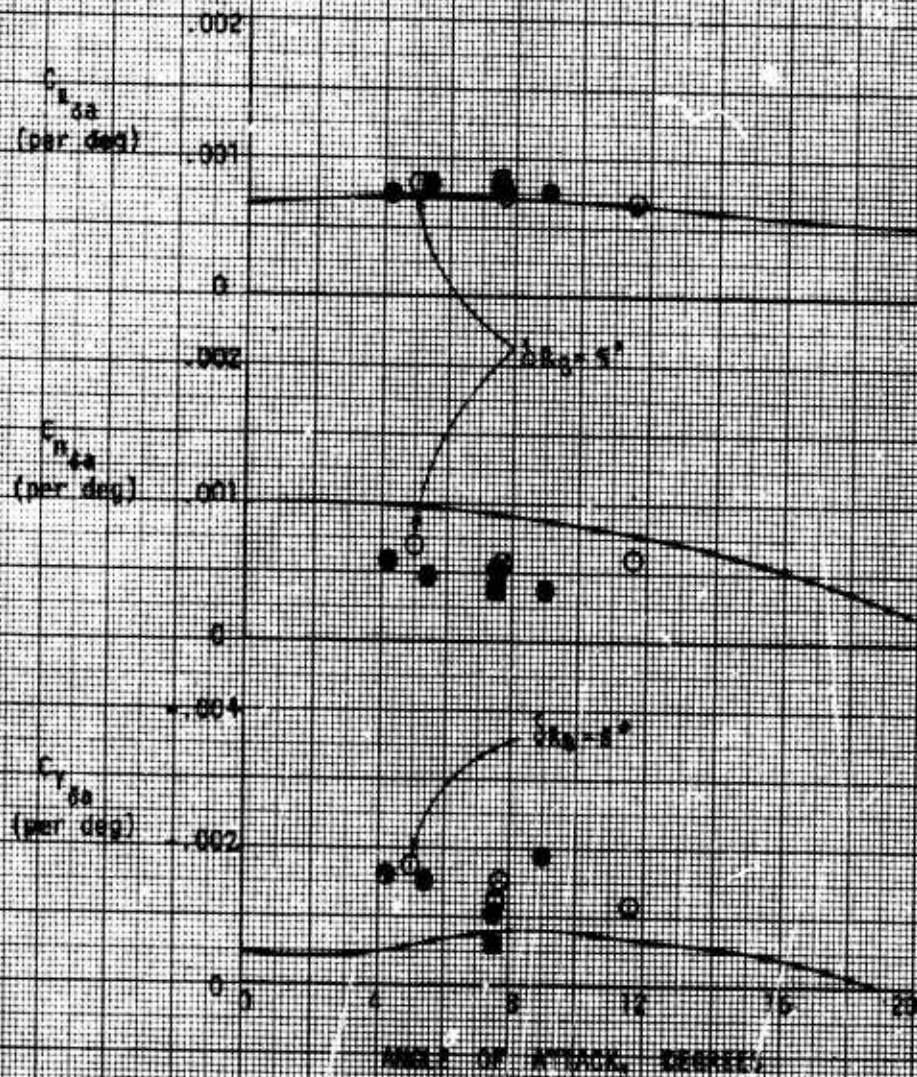


FIGURE 10. SENSITIVITY - 1.3



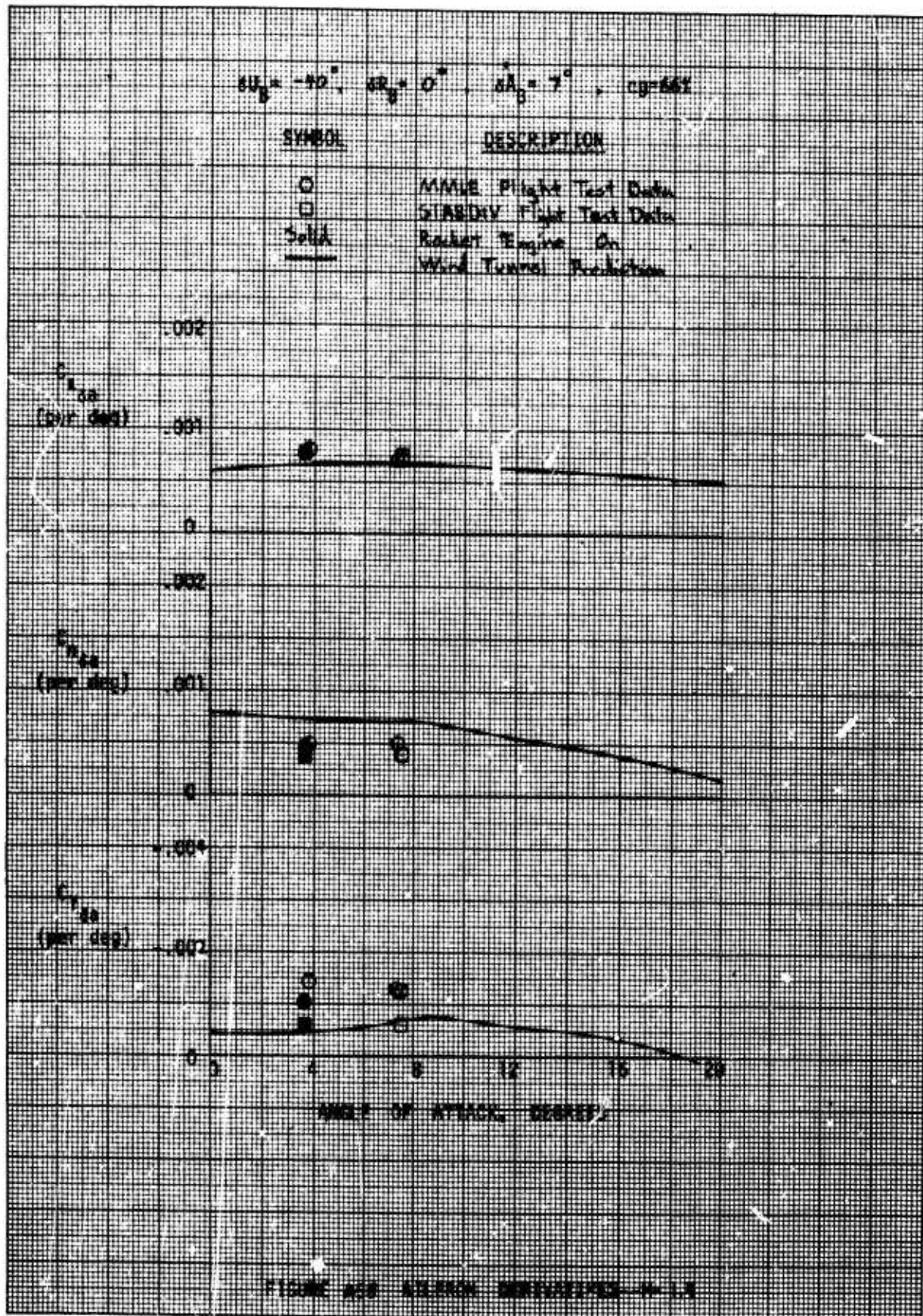


FIGURE 200 AIRCRAFT DERIVATIVES - 1.5



$\delta U_B = -40^\circ$  ,  $\delta R_B = 0^\circ$  ,  $\delta A_B = 7^\circ$  ,  $CG = 66\%$

SYMBOL

DESCRIPTION

○

MMLE Flight Test Data

□

STABDIV Flight Test Data

Solid

Rocket Engine On

Wind Tunnel Prediction

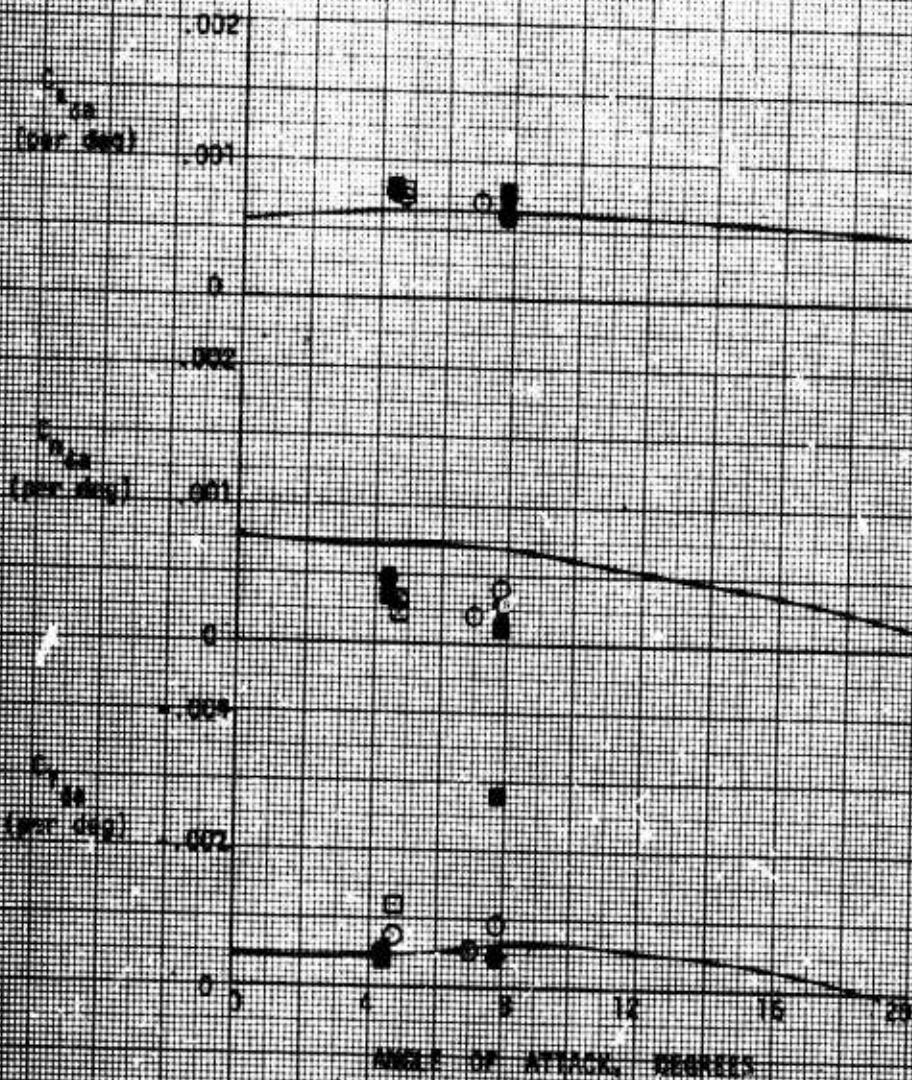


FIGURE A54 AIRCRAFT DERIVATIVES - 1.5

$\alpha_0 = -40^\circ$ ,  $\alpha_{R_0} = 0^\circ$ ,  $\delta A_0 = 7^\circ$ ,  $cg = 66\%$

SYMBOL

DESCRIPTION

○	MMLR Flight Test Data
□	STARDIV Flight Test Data
Solid	Rocket Engine On
-----	Wind Tunnel Prediction

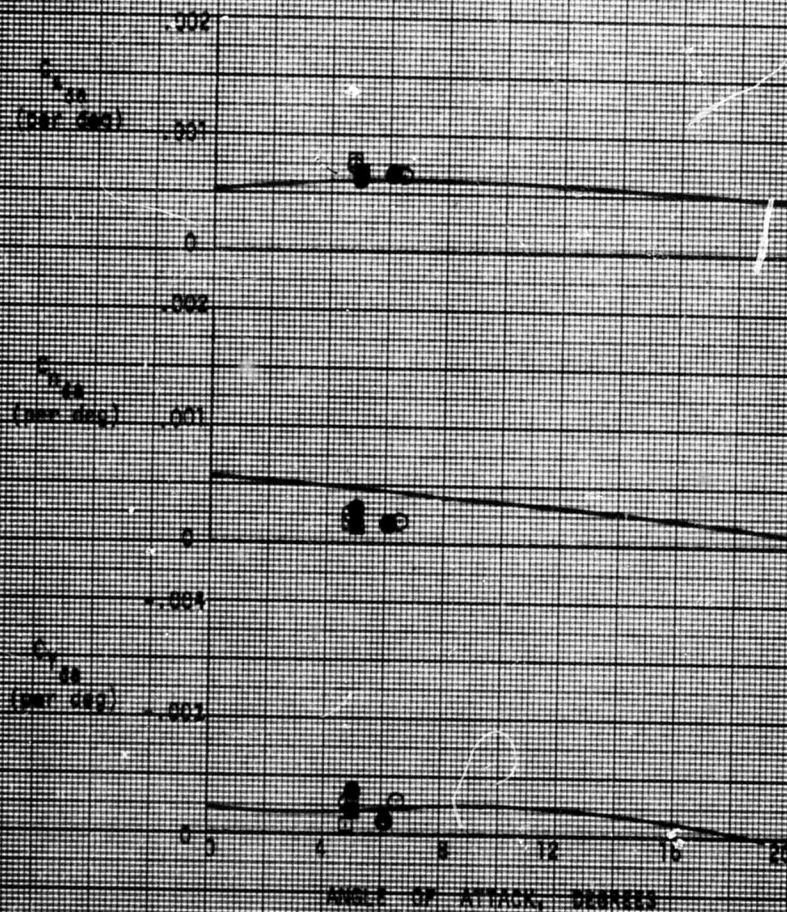


FIGURE 6-10 AIRCRAFT DERIVATIVES - M = 1.0



$\delta U_B = -40^\circ$ ,  $\delta R_B = 0^\circ$ ,  $\delta A_B = 7^\circ$ ,  $\rho = 0.001$

SYMBOL	DESCRIPTION
○	ANNAE Flight Test Data
□	STANDIV Flight Test Data
—	Wind Tunnel Prediction

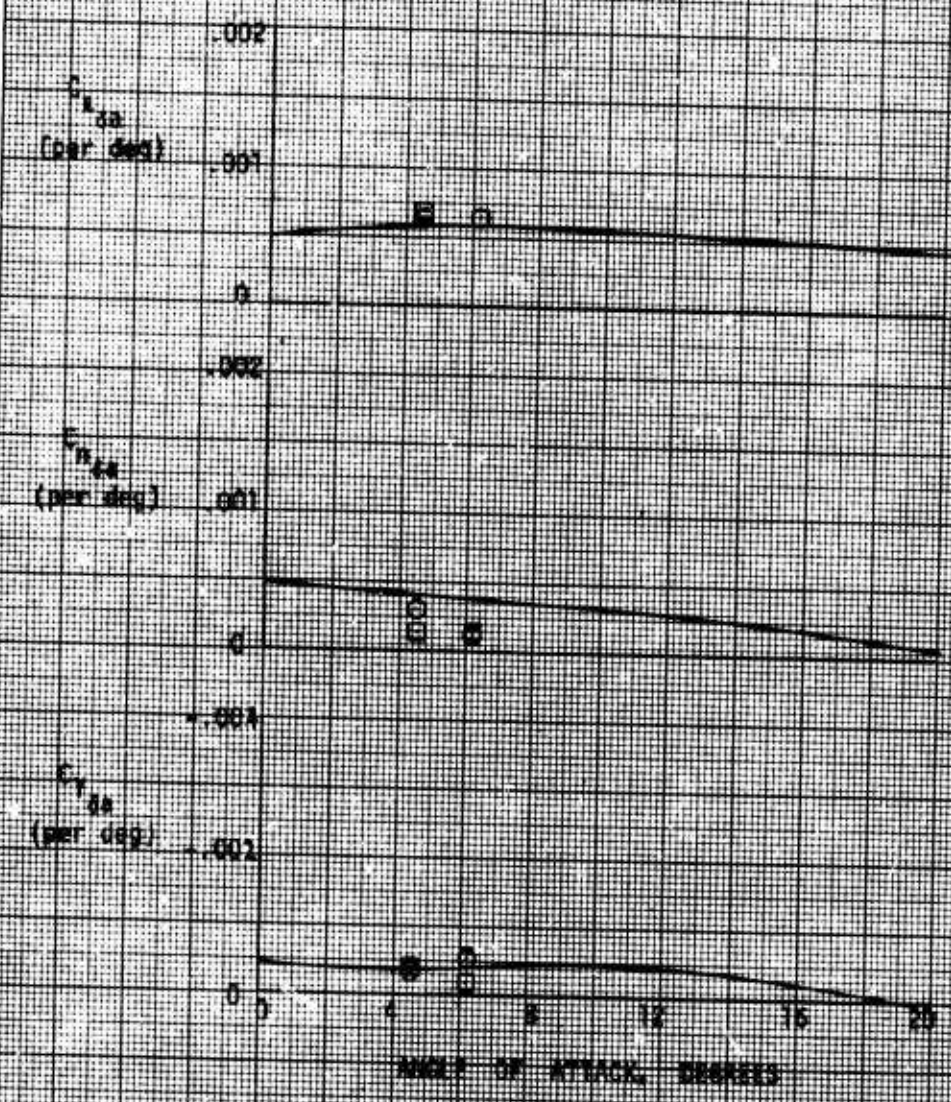


FIGURE 4-1. DERIVATIVES OF LIFT, DRAG, AND SIDE FORCE COEFFICIENTS



$\delta U_B = -40^\circ$ ,  $\delta R_B = 0^\circ$ ,  $\delta A_B = 7^\circ$ ,  $c_g = 66\%$

SYMBOL

DESCRIPTION

○

MMLE Flight Test Data

□

STABDV Flight Test Data

Wind Tunnel Prediction

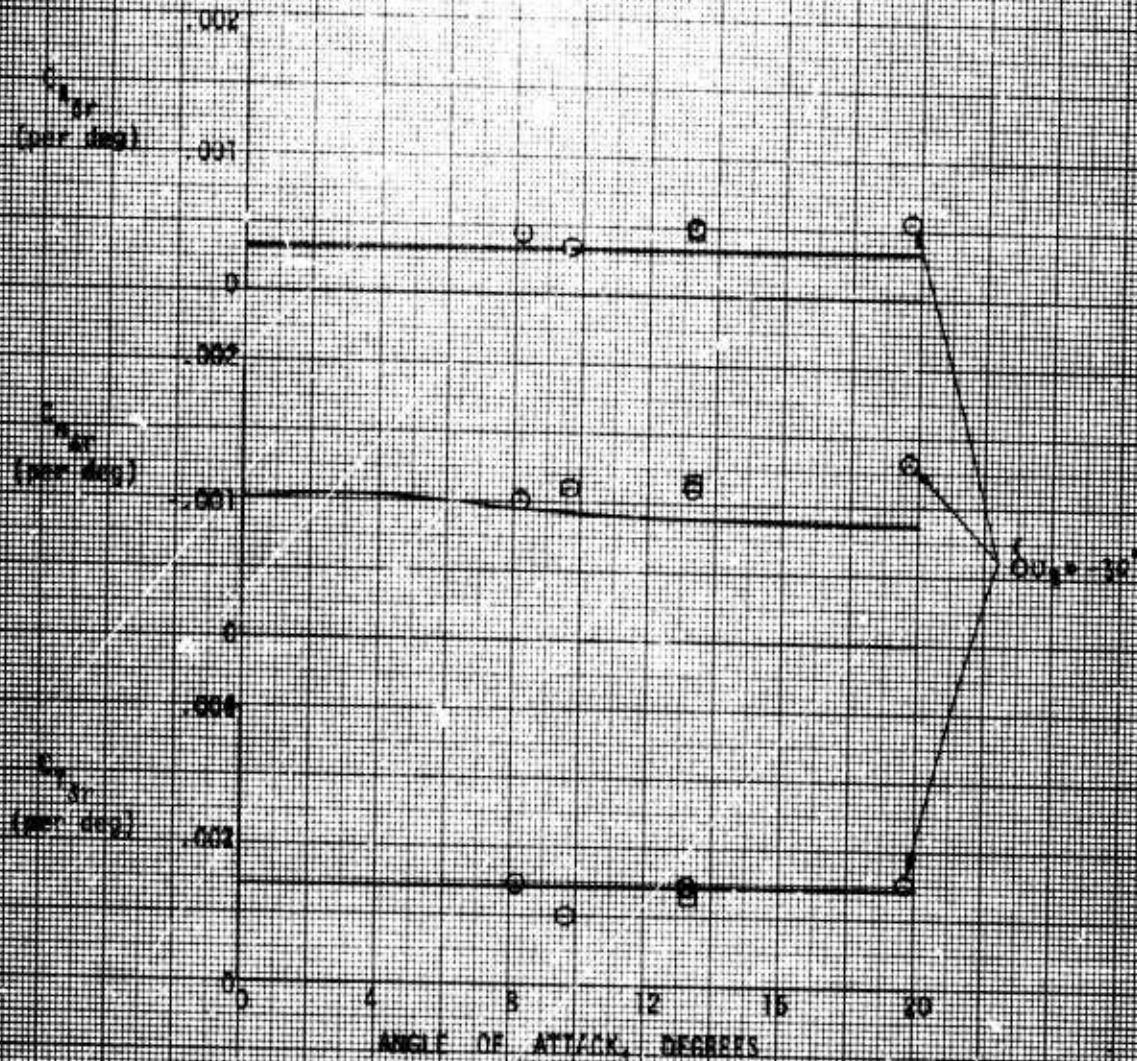


FIGURE A6.1 DERIVATIVE DATA

$\delta U_B = -40^\circ$ ,  $\delta X_B = 0^\circ$ ,  $\delta A_B = 7^\circ$ ,  $c_g = 66\%$

SYMBOL	DESCRIPTION
O	MALE Flight Test Data
□	STABIN Flight Test Data
Tail	SAS OFF
—	Wind Tunnel Prediction

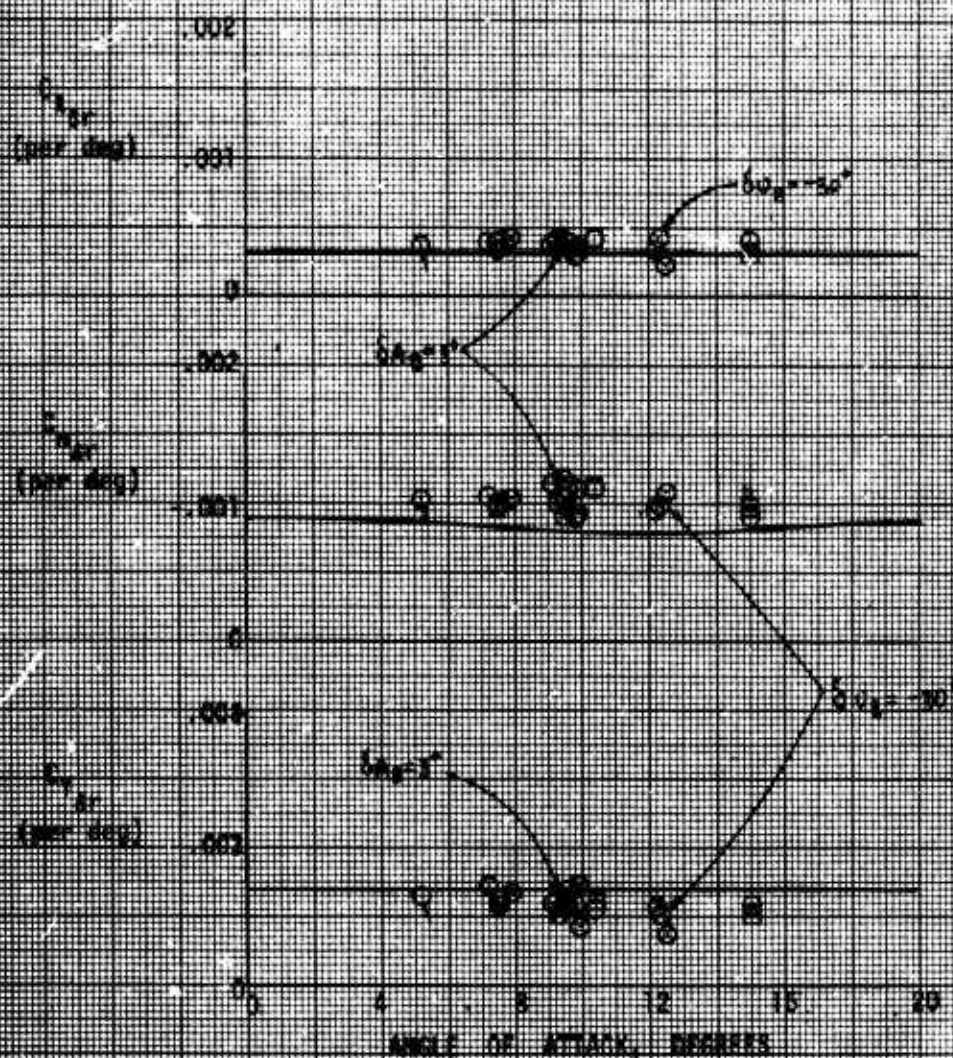


FIGURE A13 - WIND TUNNEL DATA - N-0.7



$\alpha_{L_0} = -40^\circ$ ,  $\alpha_{L_0} = 0^\circ$ ,  $\alpha_{L_0} = 7^\circ$ ,  $c_g = 66\%$

SYMBOL	DESCRIPTION
O	AMIE Flight Test Data
□	STARDIV Flight Test Data
Solid	Rocket Engine On
—	Wind Tunnel Prediction

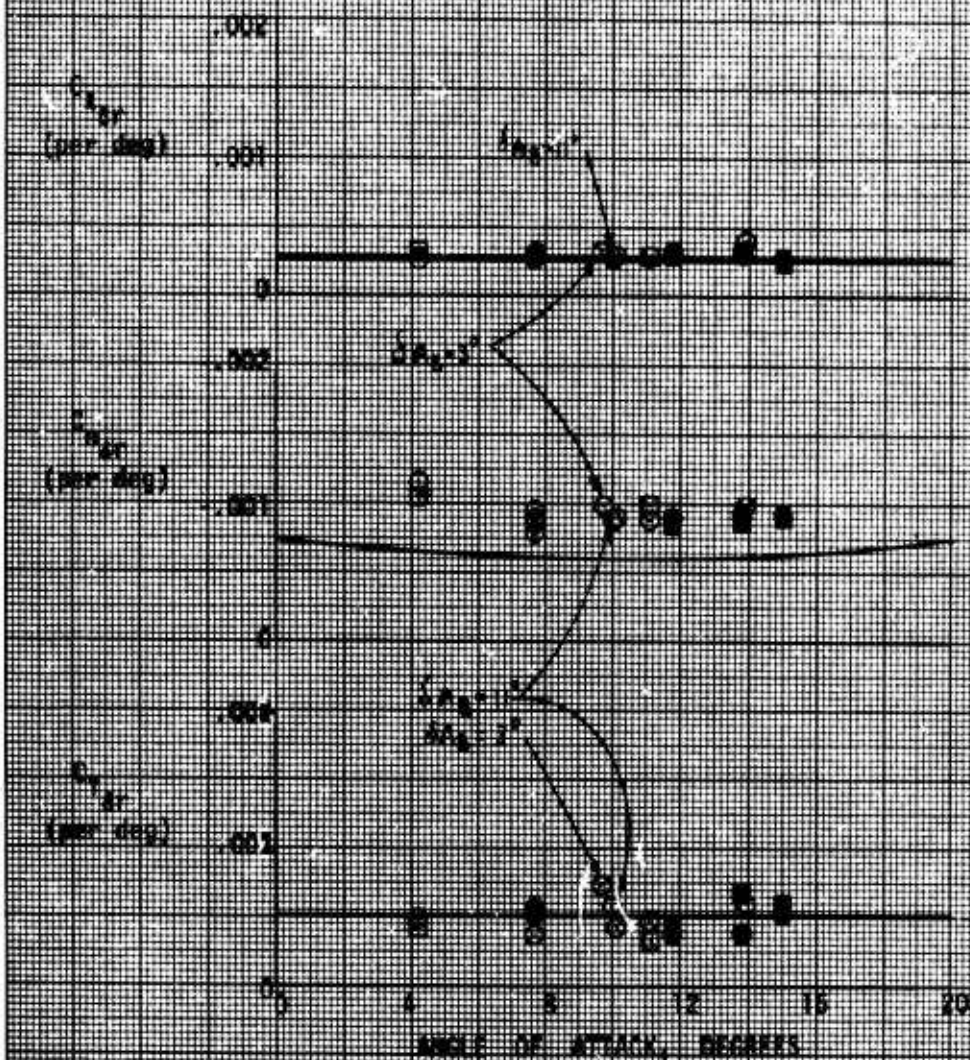
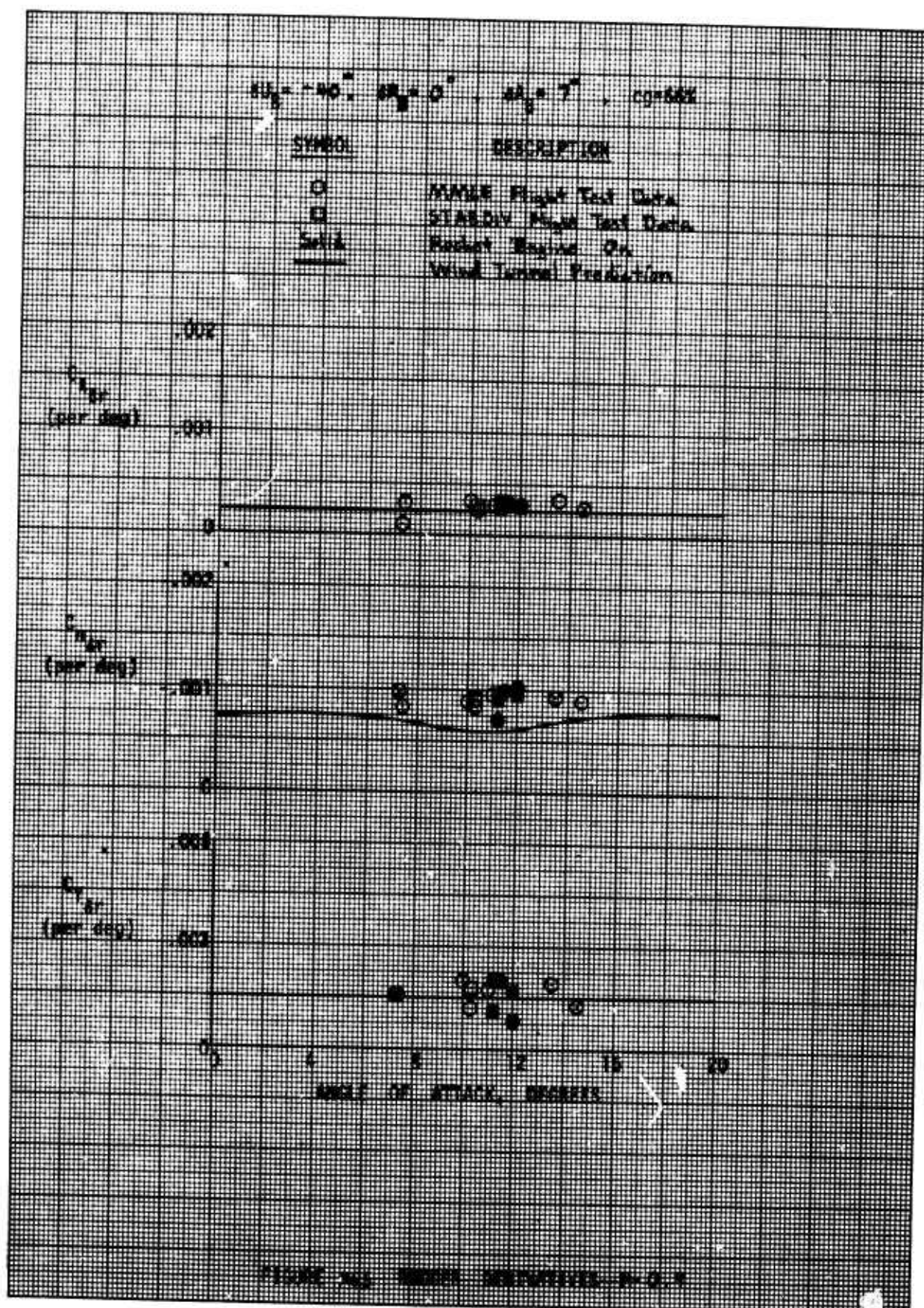


FIGURE 4-3. LIFT COEFFICIENTS— $M = 0.2$





$\alpha_{10} = -40^\circ$ ,  $\alpha_{10} = 0^\circ$ ,  $\alpha_{10} = 7^\circ$ ,  $c_g = 66\%$

SYMBOL	DESCRIPTION
○	MMLE Flight Test Data
□	STANDIV Flight Test Data
Solid	Rocket Engine On
—	Wind Tunnel Prediction

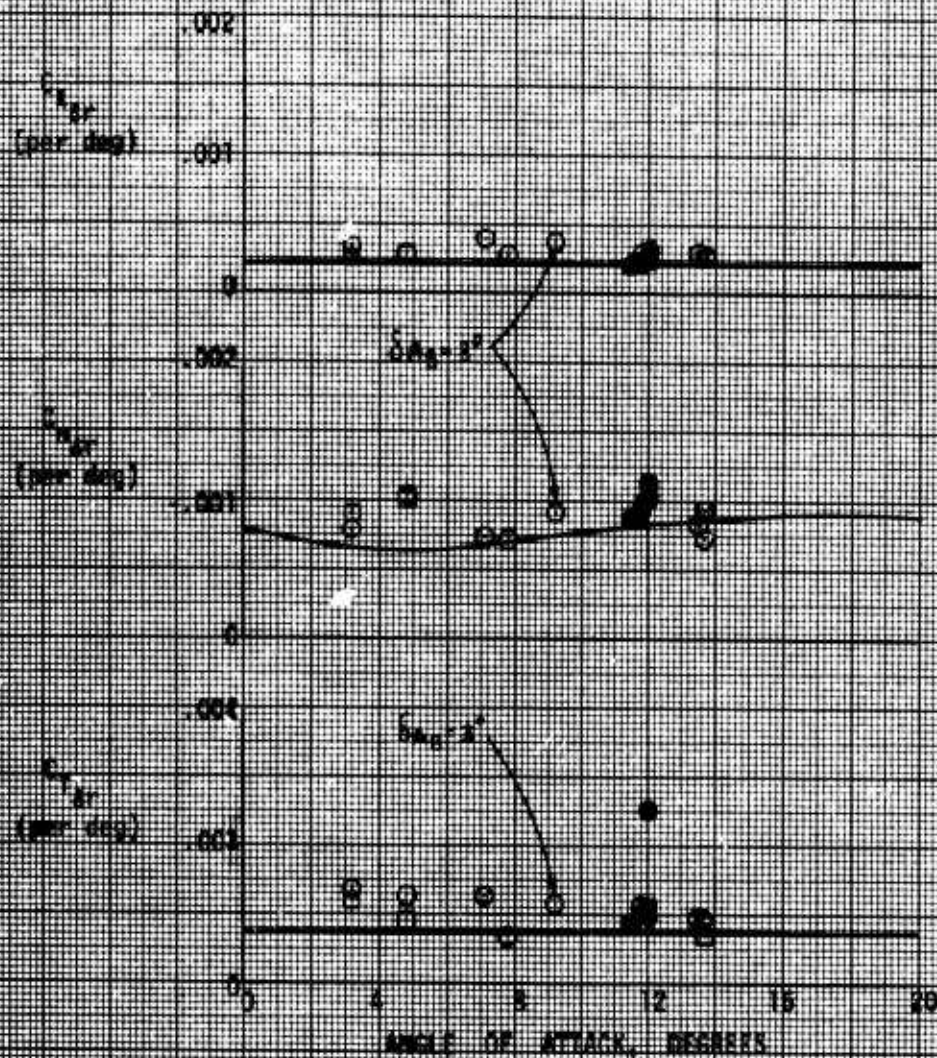


FIGURE A-11 DERIVATIVES - P-O-75



$\delta U_B = -40^\circ$ ,  $\delta \alpha_B = 0^\circ$ ,  $\delta \alpha_B = 7^\circ$ ,  $c_g = 86\%$

SYMBOL

DESCRIPTION

O

MMME Flight Test Data

Solid

Rocket Engine On

Wind Tunnel Prediction

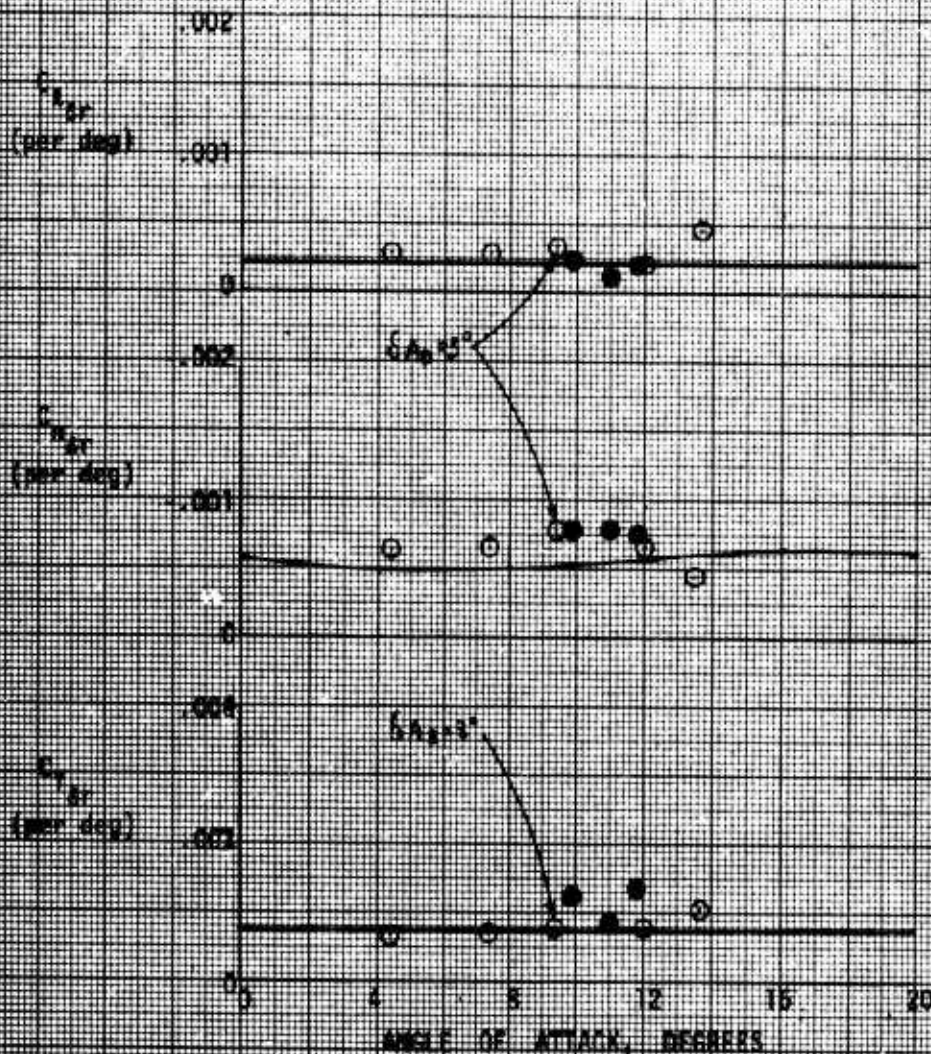


FIGURE 101 ROCKET DERIVATIVES - M=10



$\alpha_{L_0} = -40^\circ$ ,  $\alpha_{R_0} = 0^\circ$ ,  $\alpha_{D_0} = 7^\circ$ ,  $CG = 66\%$

SYMBOL

DESCRIPTION

○

AVALE Flight Test Data

□

STANDIV Flight Test Data

Solid

Rocket Engine On

-----

Wind Tunnel Prediction

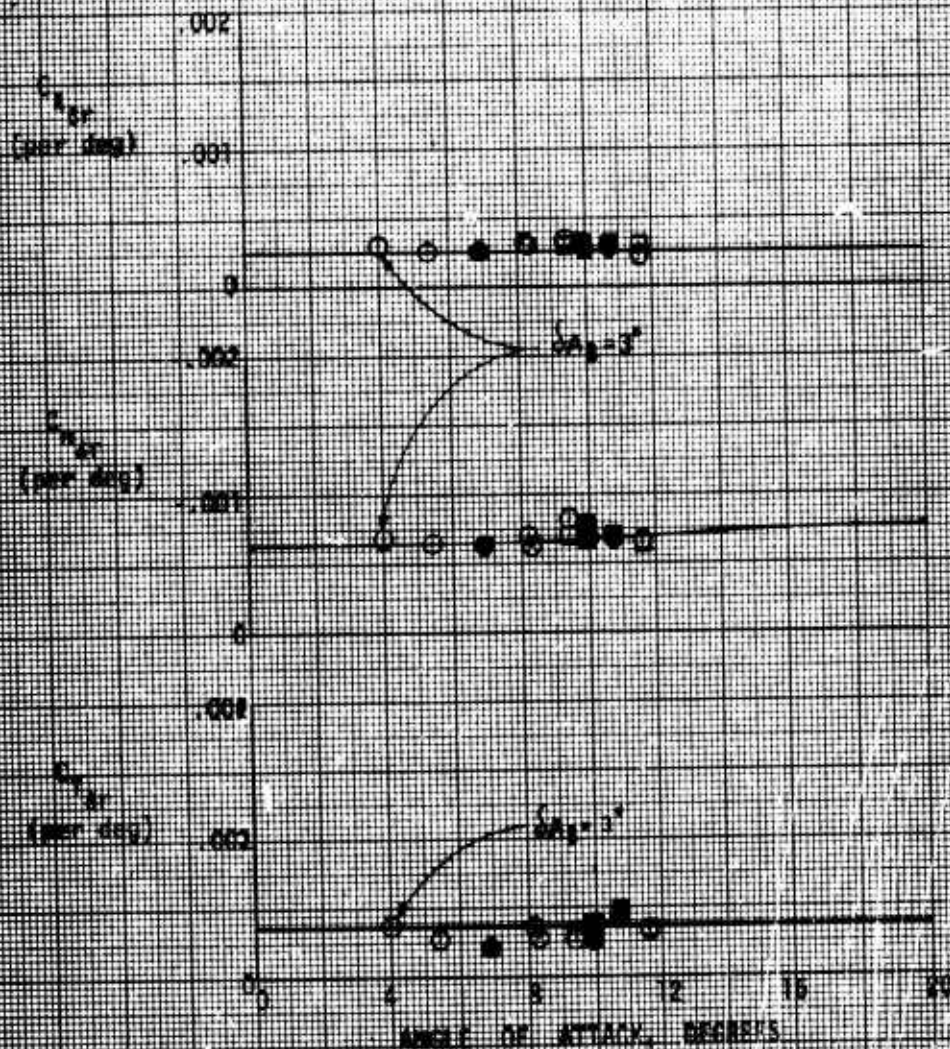


FIGURE A-6. ROCKET DERIVATIVES - R-11

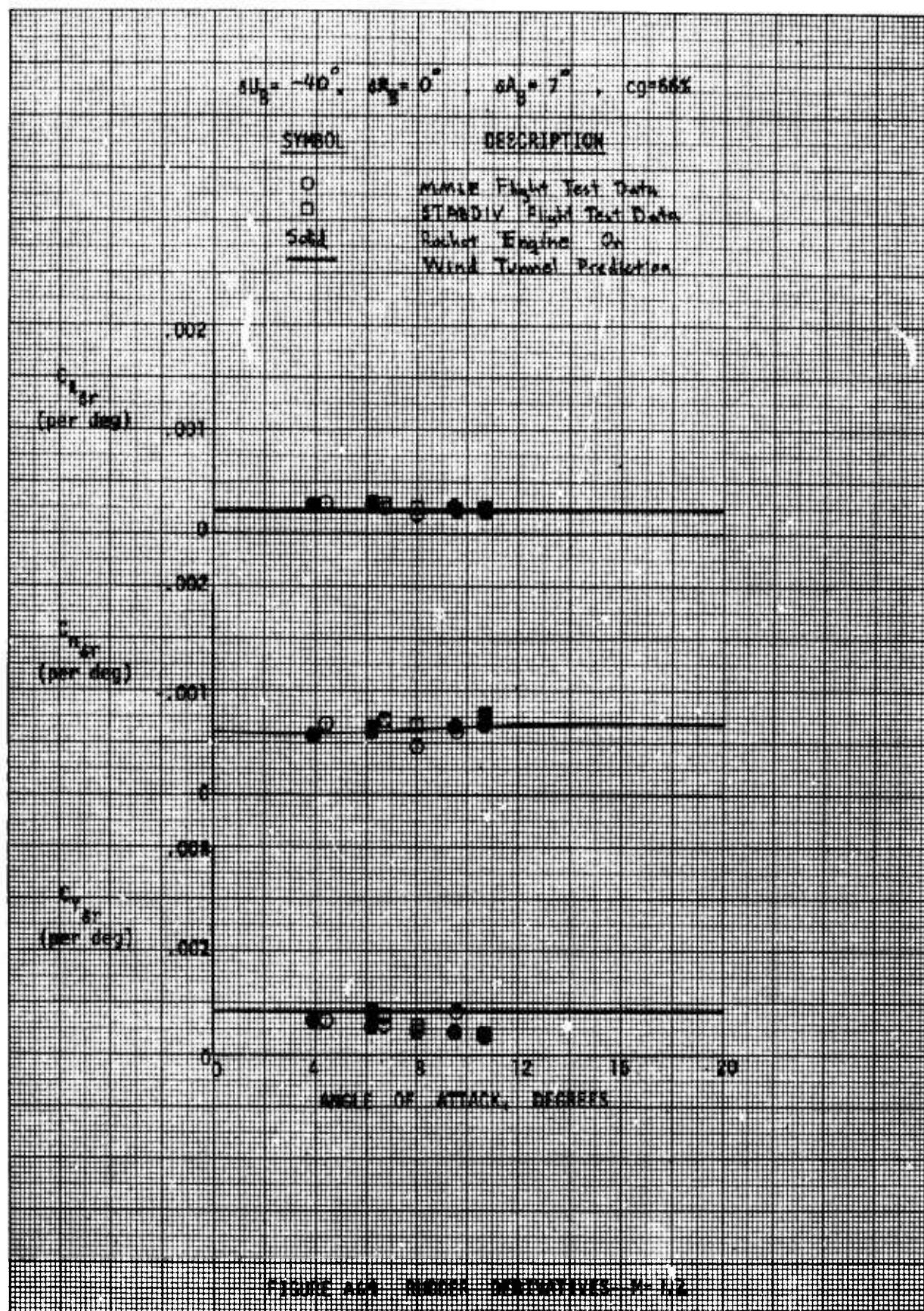


FIGURE A-4. ROCKET MANEUVERING - 1/2



$\alpha_{B_0} = -40^\circ$ ,  $\delta R_B = 0^\circ$ ,  $\delta A_B = 7^\circ$ ,  $c_D = 56\%$

SYMBOL	DESCRIPTION
O	MMLE Flight Test Data
E	STABDIV Flight Test Data
Solid	Rocket Engine On
—	Wind Tunnel Prediction

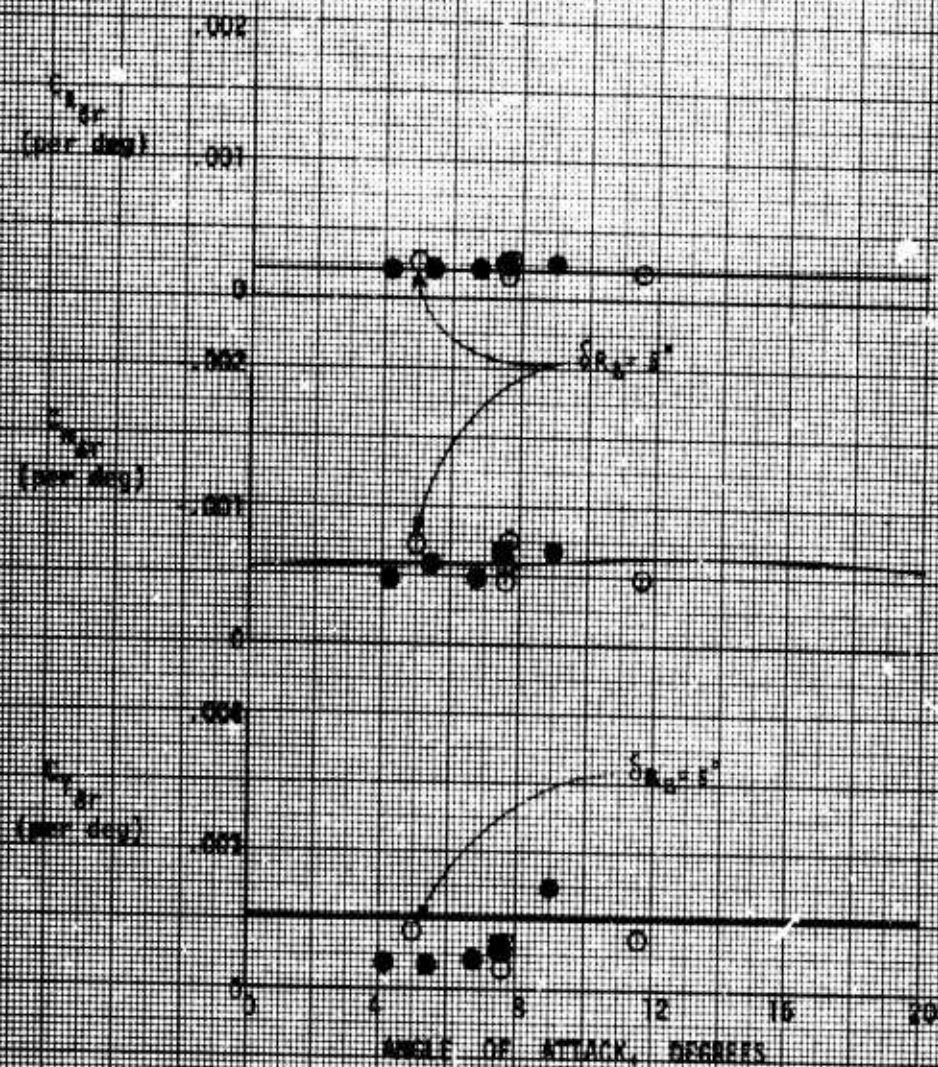


FIGURE A10 RIGID DERIVATIVES R-1.3



$\delta U_B = -40^\circ$ ,  $\delta R_B = 0^\circ$ ,  $\delta A_B = 7^\circ$ ,  $CG = 66\%$

SYMBOL

DESCRIPTION

○

WVLE Flight Test Data

□

STBDIV Flight Test Data

Solid

Rocket Engine On

Wind Tunnel Prediction

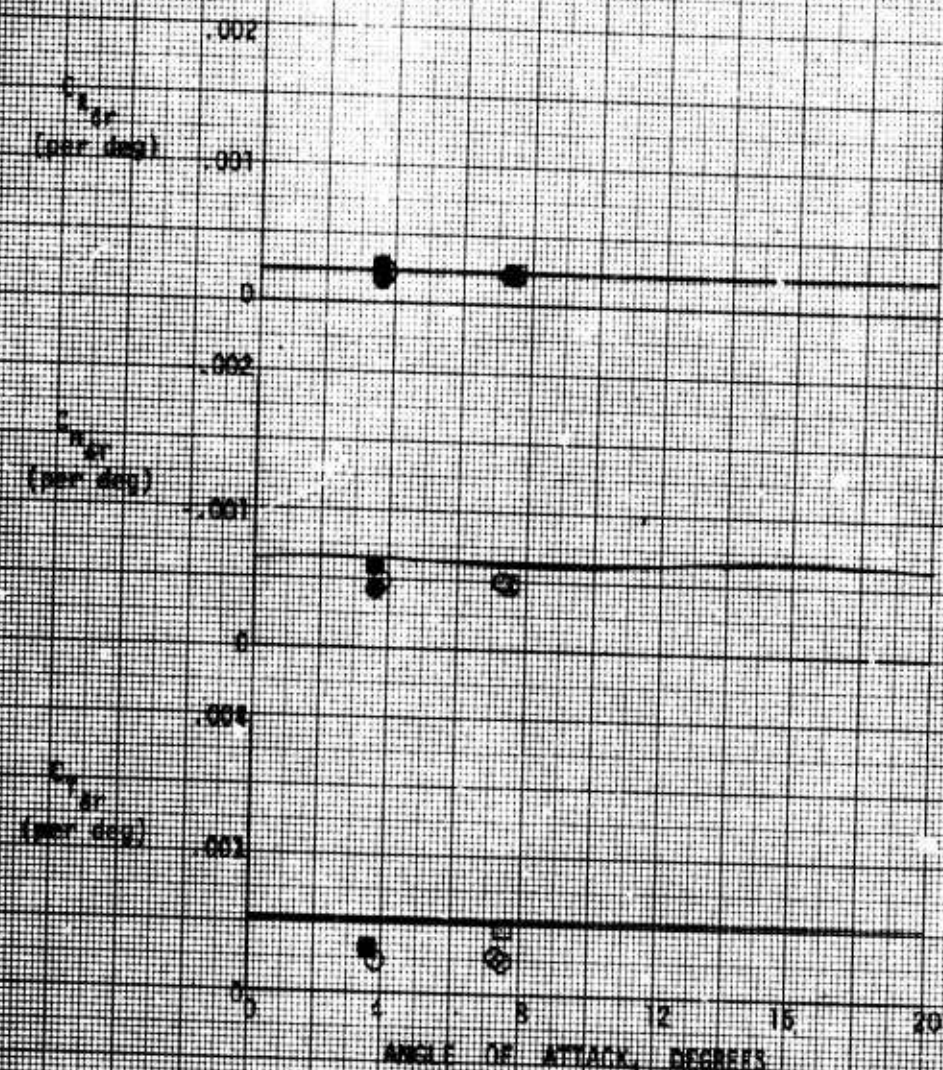


FIGURE A71. BUDGET DERIVATIVES - P-1.1

$\delta U_B = -40^\circ$ ,  $\delta R_B = 0^\circ$ ,  $\delta A_B = 7^\circ$ ,  $CG = 66\%$

SYMBOL	DESCRIPTION
○	AWALE Flight Test Data
□	STADIV Flight Test Data
Solid	Rocket Engine On Wind Tunnel Prediction

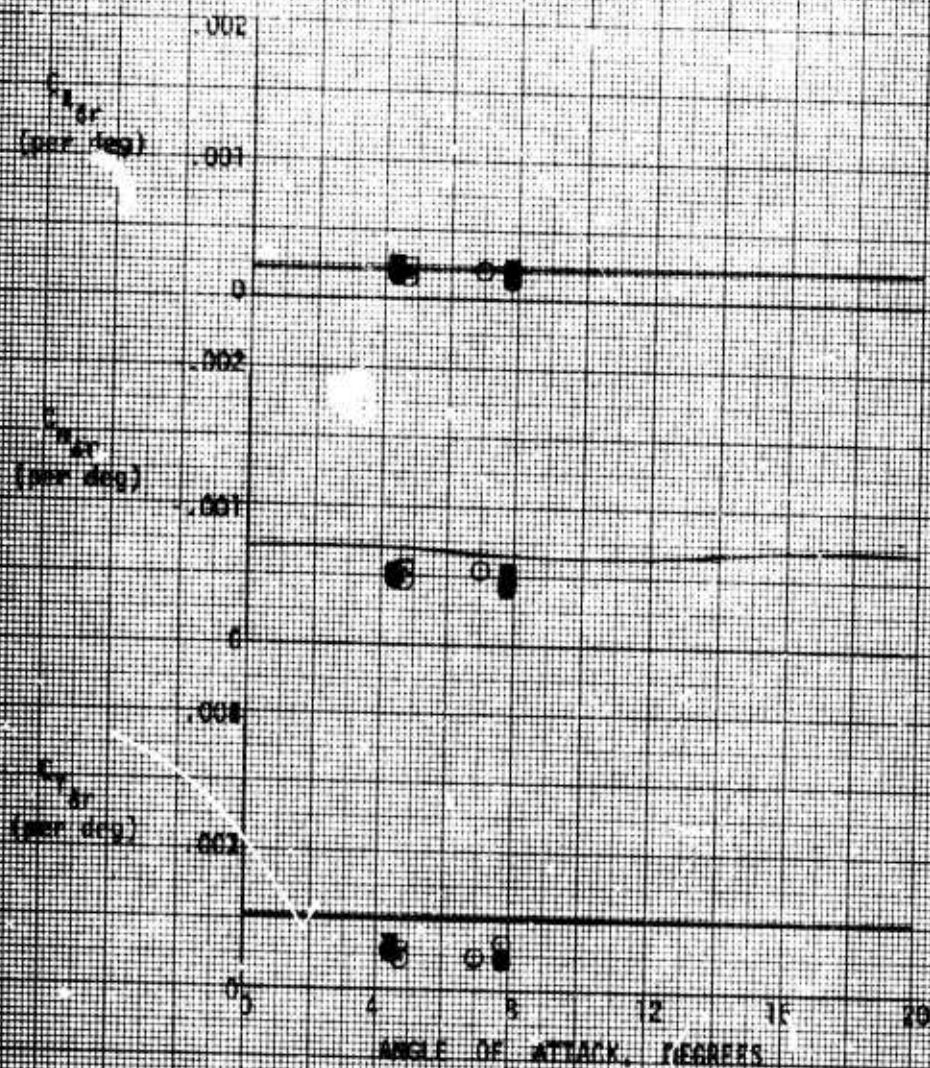


FIGURE A12 - DERIVATIVES - M-1.3



$\alpha_{D_0} = -10^\circ$ ,  $\alpha_{D_0} = 0^\circ$ ,  $\alpha_{D_0} = 7^\circ$ ,  $C_D = 66\%$

SYMBOL

DESCRIPTION

○

AMIE Flight Test Data

□

STARDIV Flight Test Data

Solid

Rocket Engine On

—

Wind Tunnel Prediction

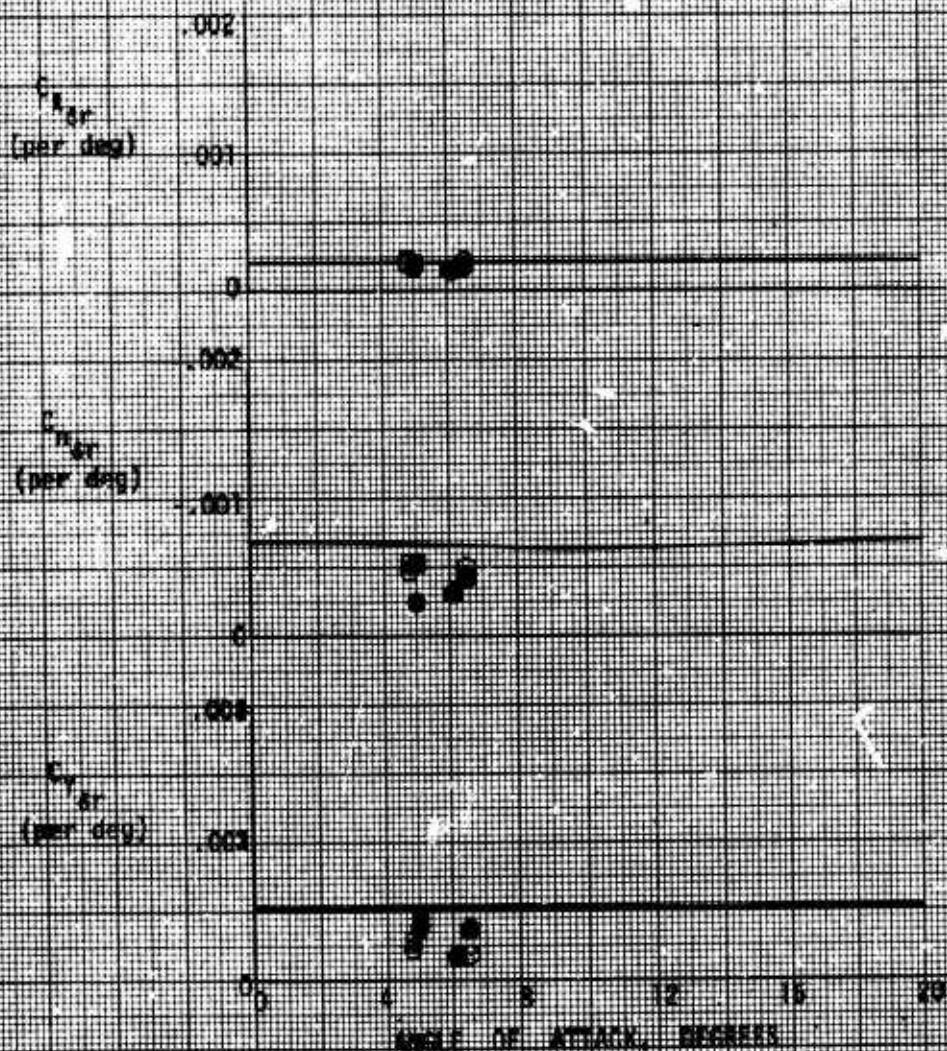
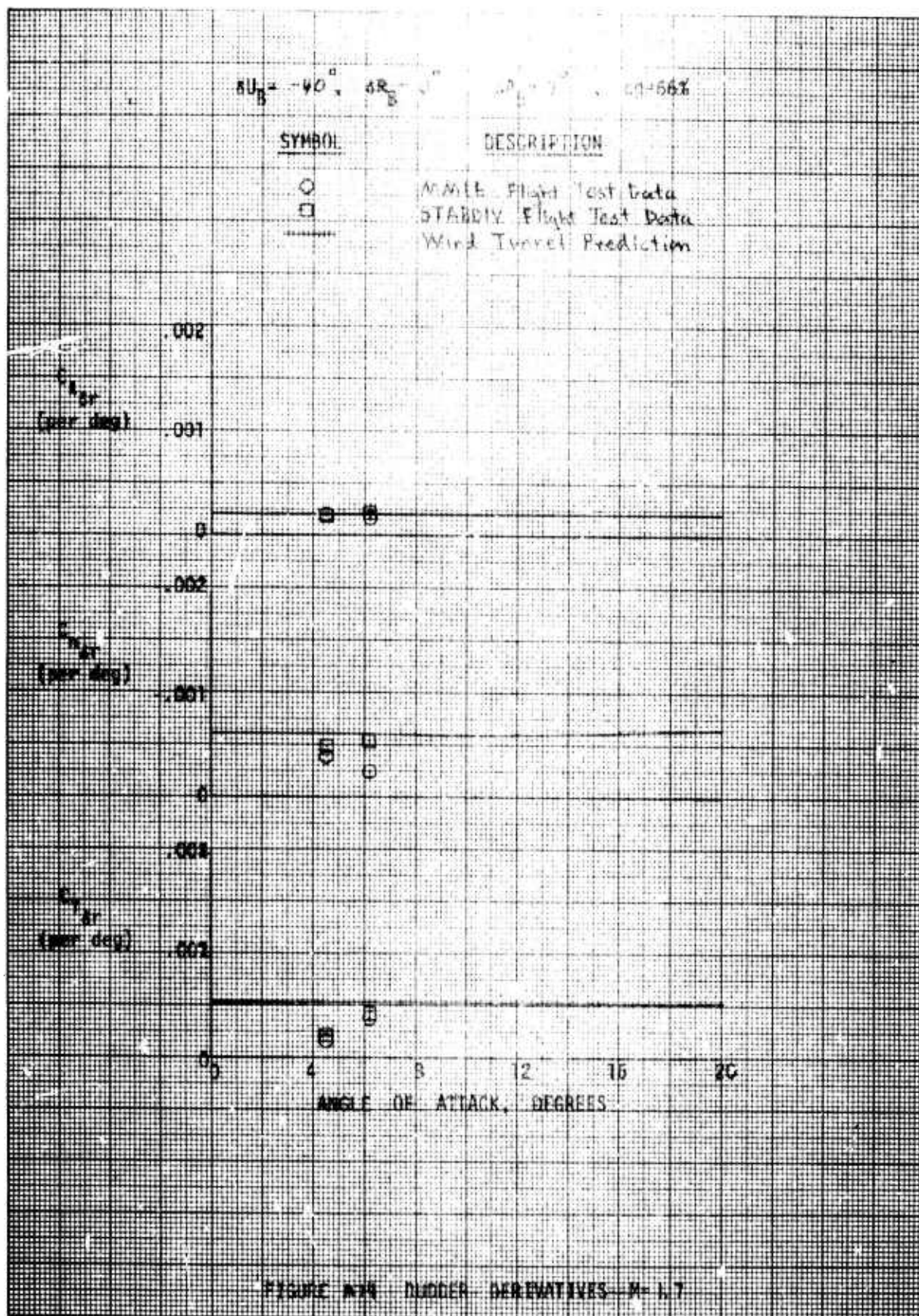


FIGURE 4-3. AERODYNAMIC COEFFICIENTS - 4-1.2





$\delta U_B = -40^\circ$  ,  $\delta R_B = 0^\circ$  ,  $\delta A_B = 7^\circ$  ,  $c_g = 0.55X$

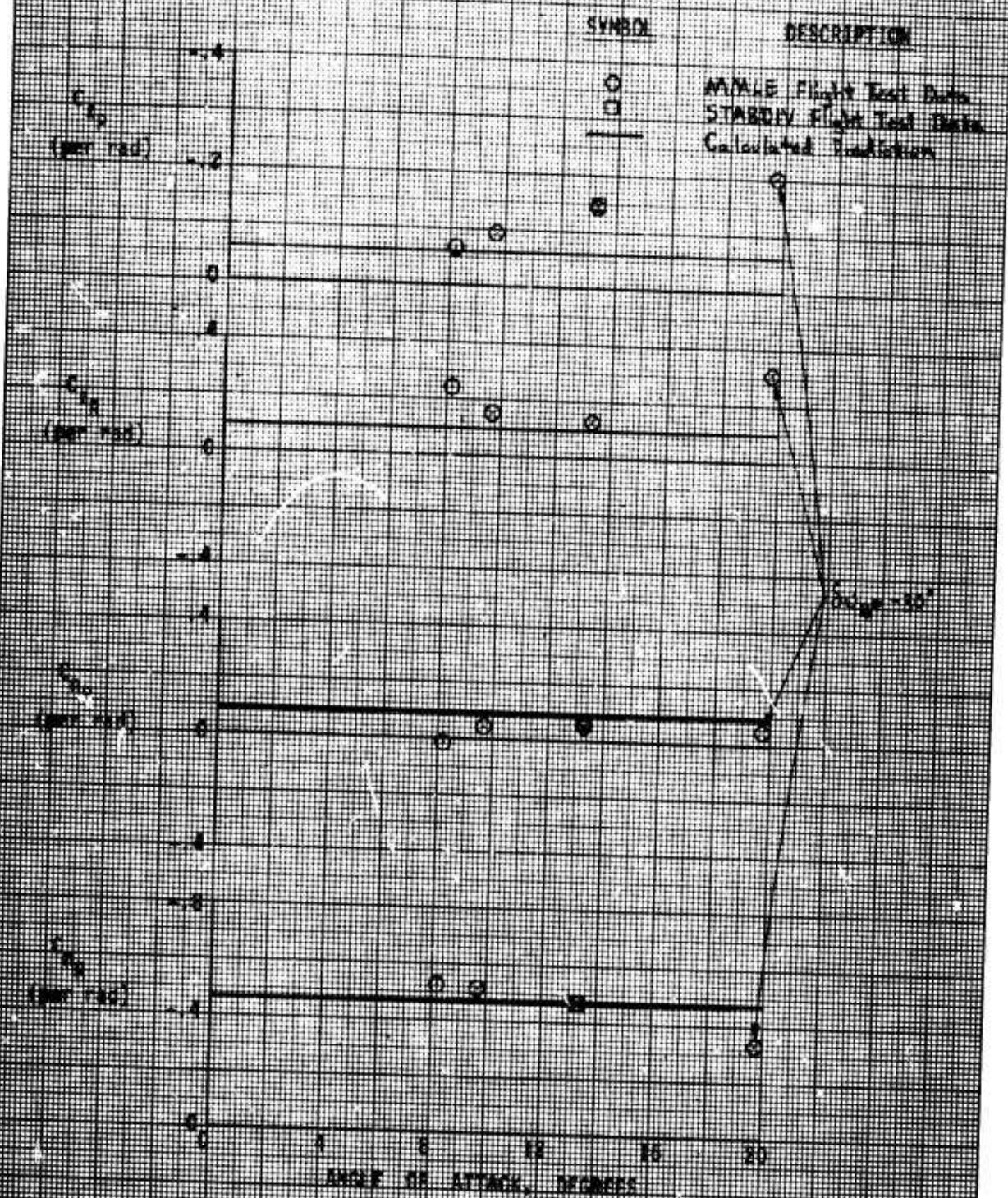
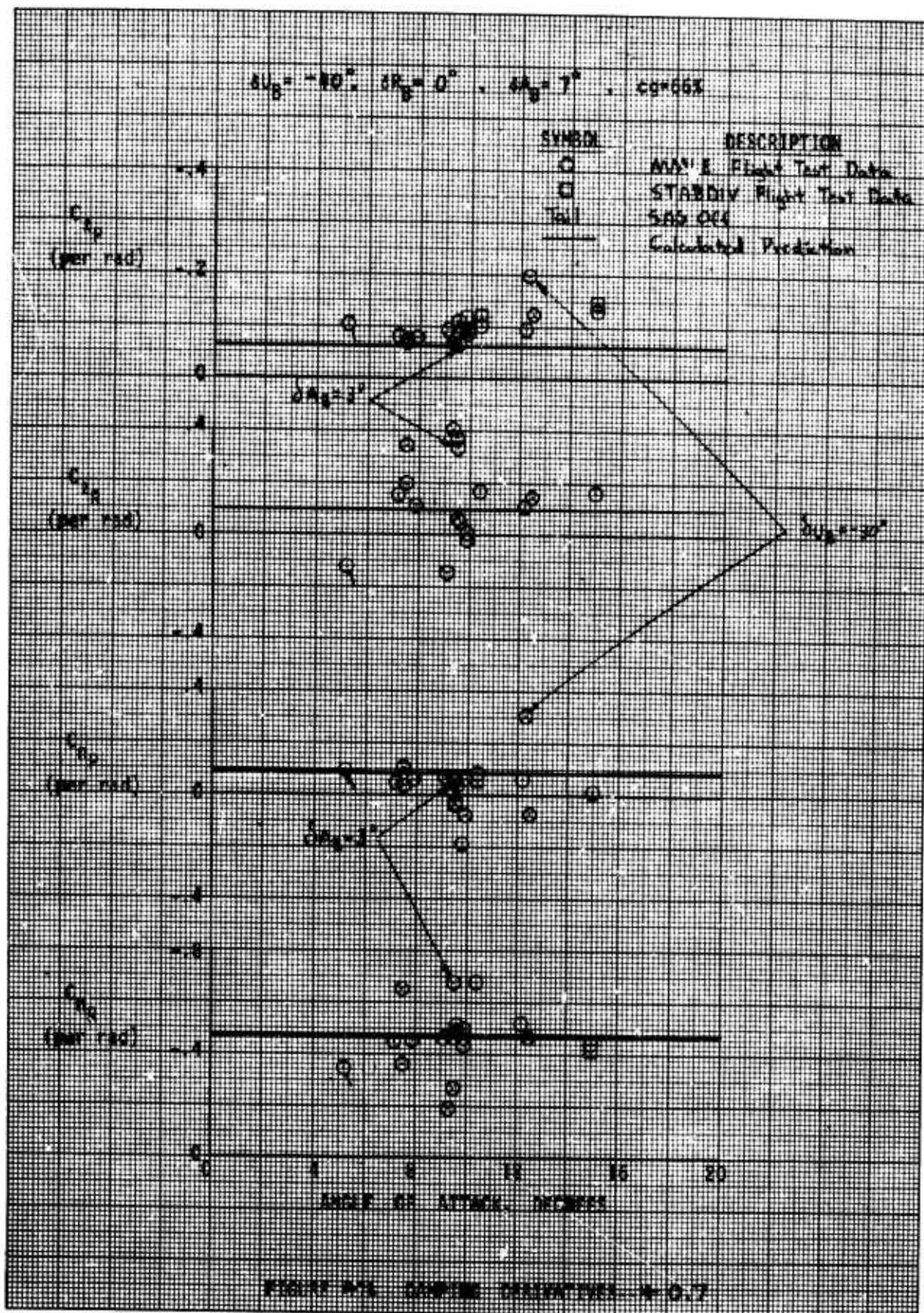
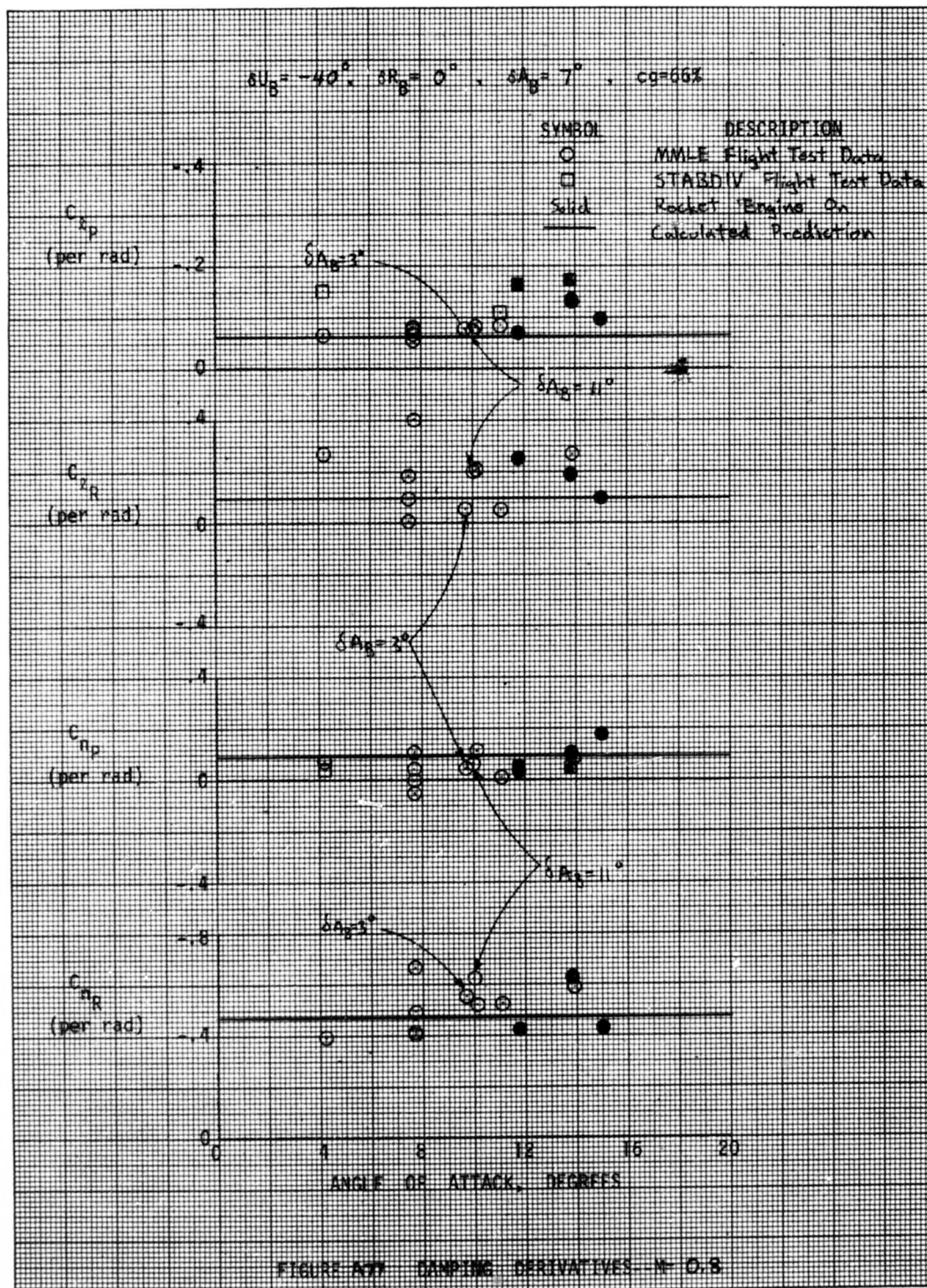


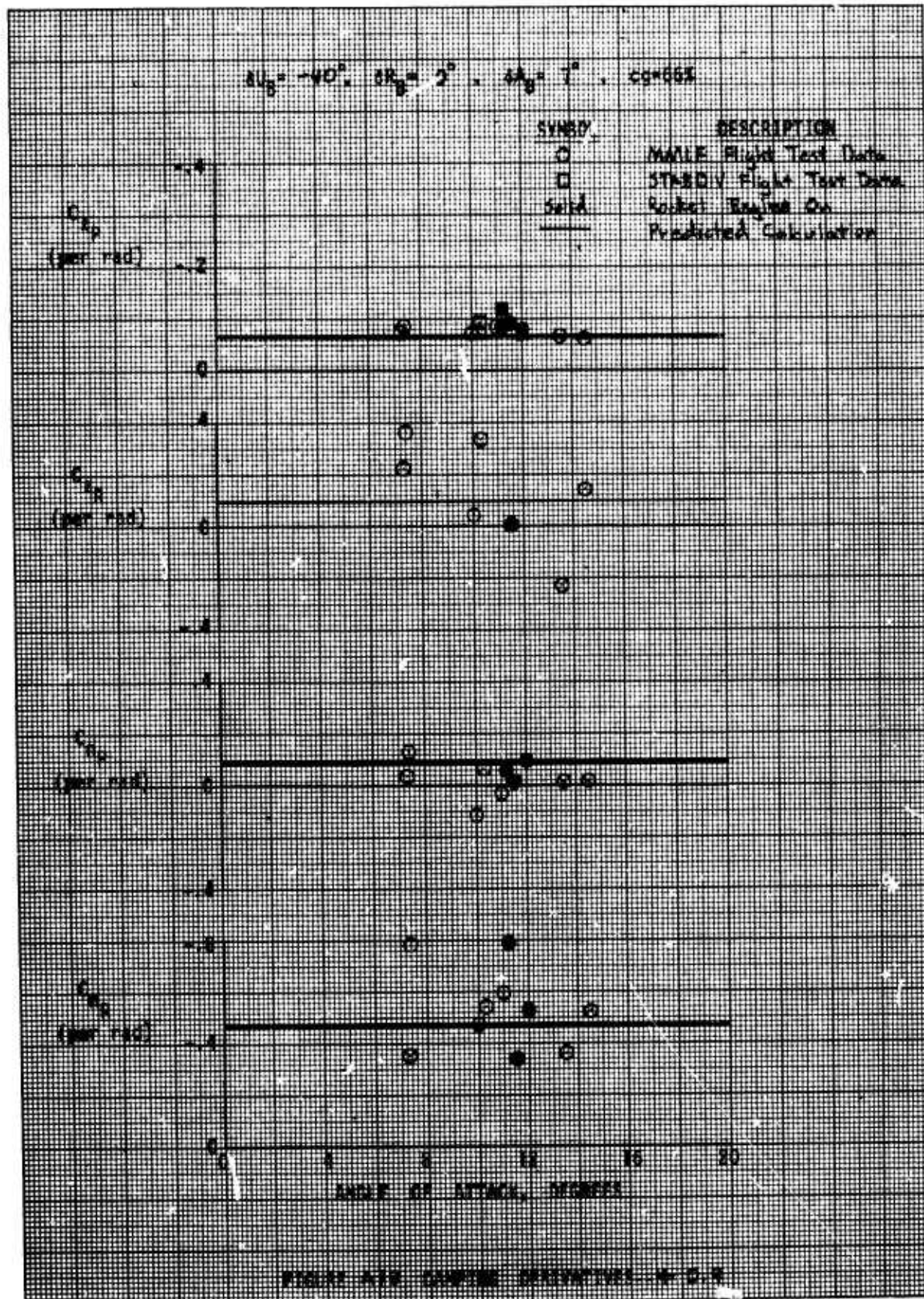
FIGURE 10. COEFFICIENT DERIVATIVES -  $\delta = 0.6$



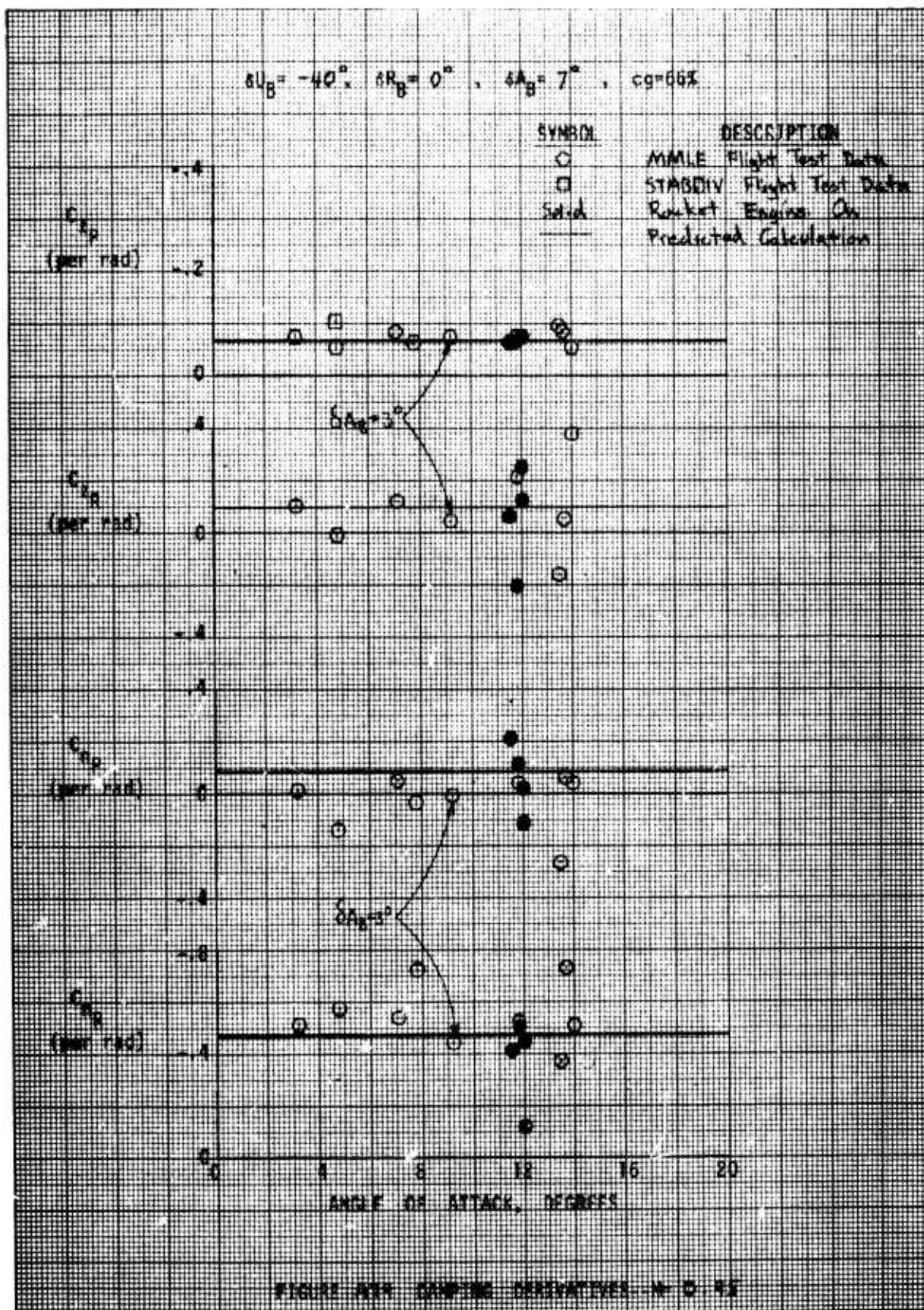




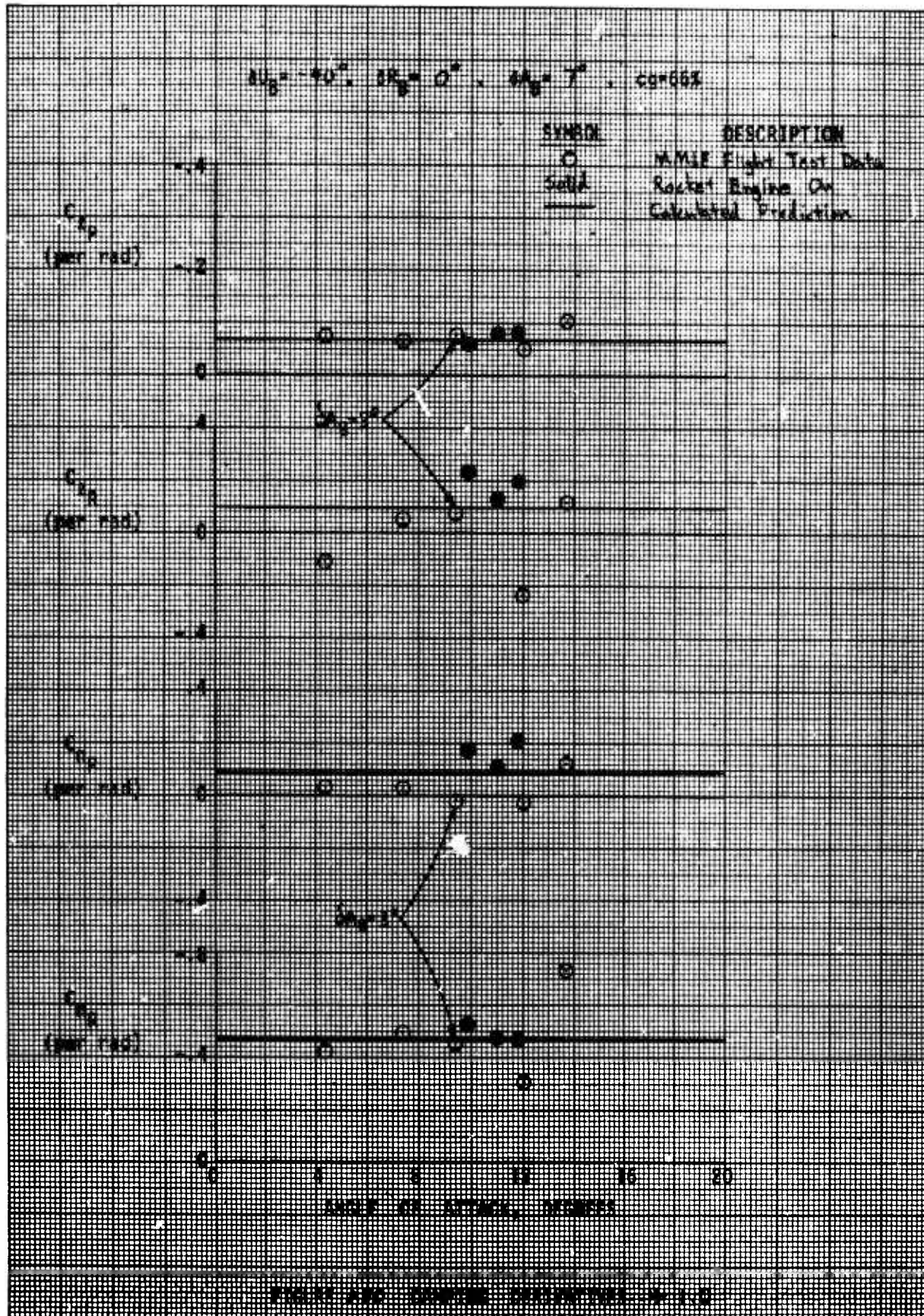


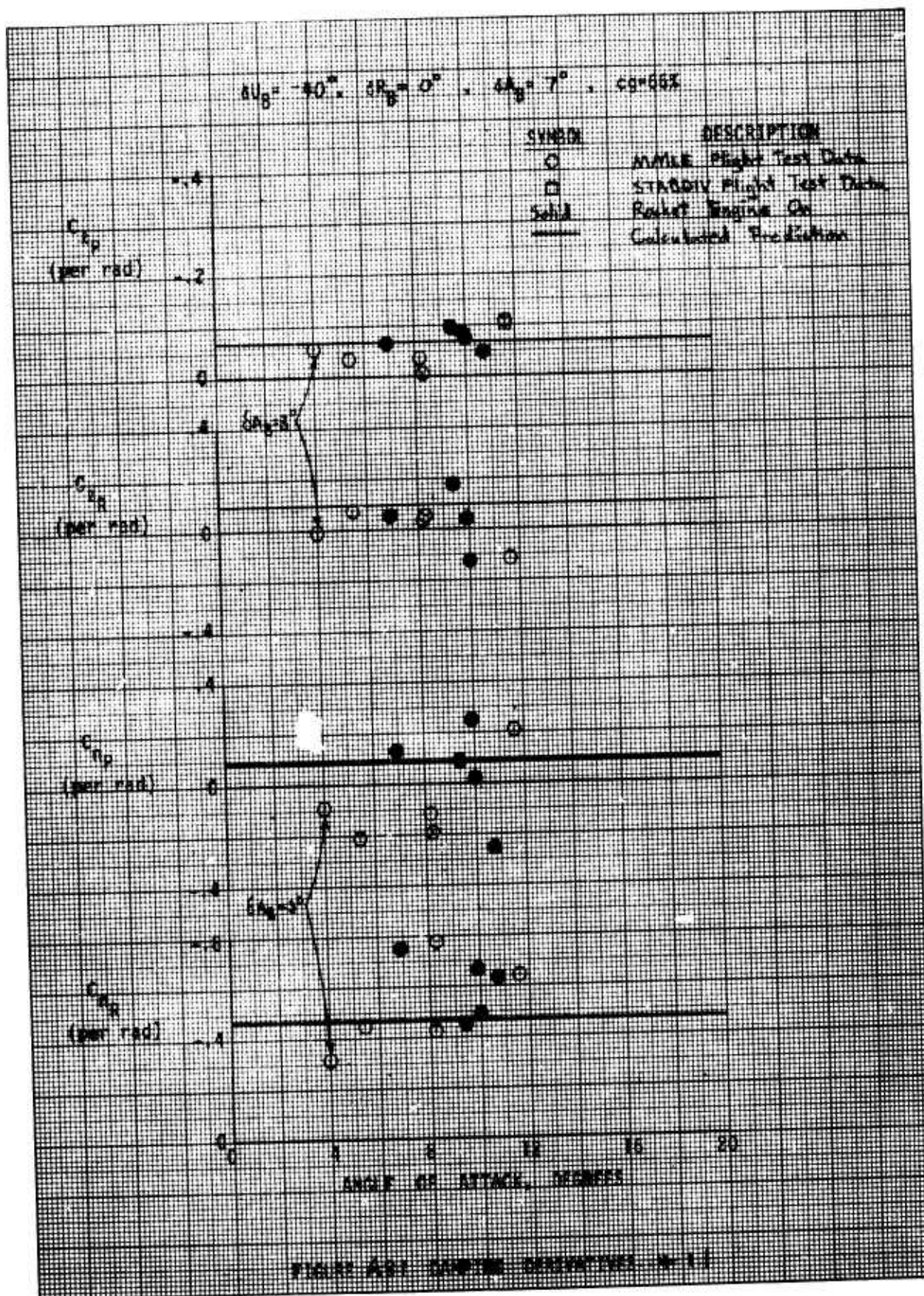




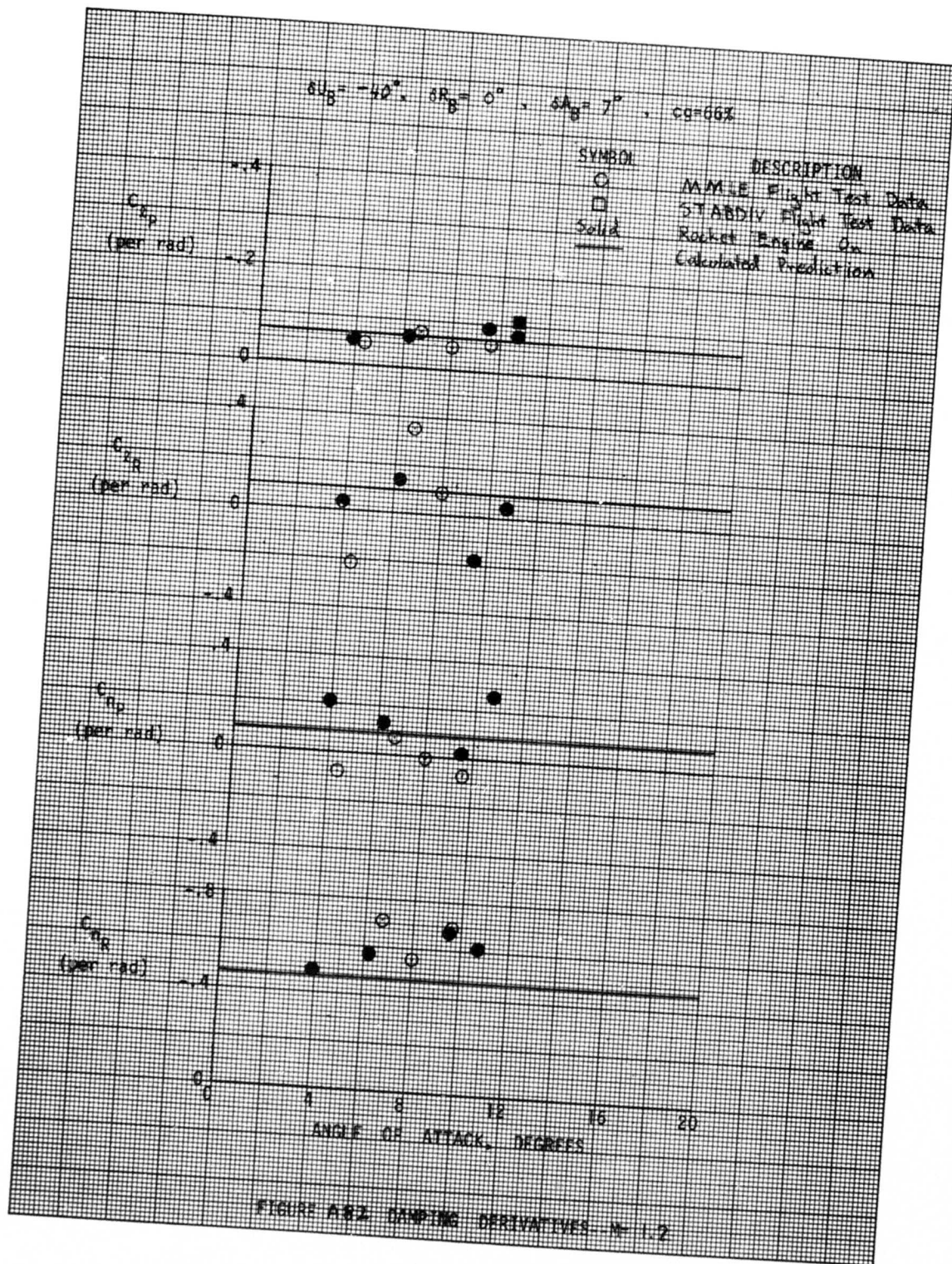




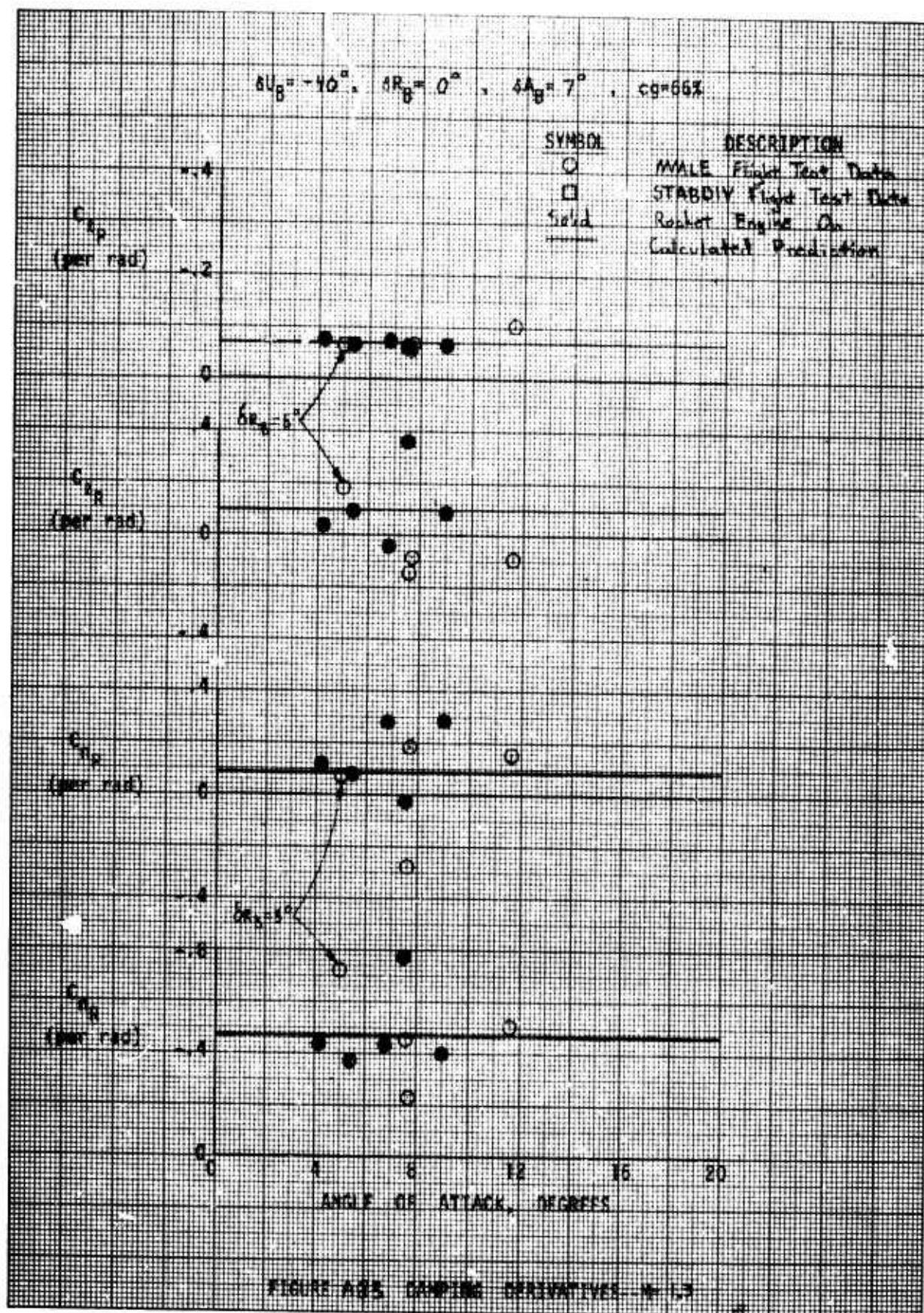


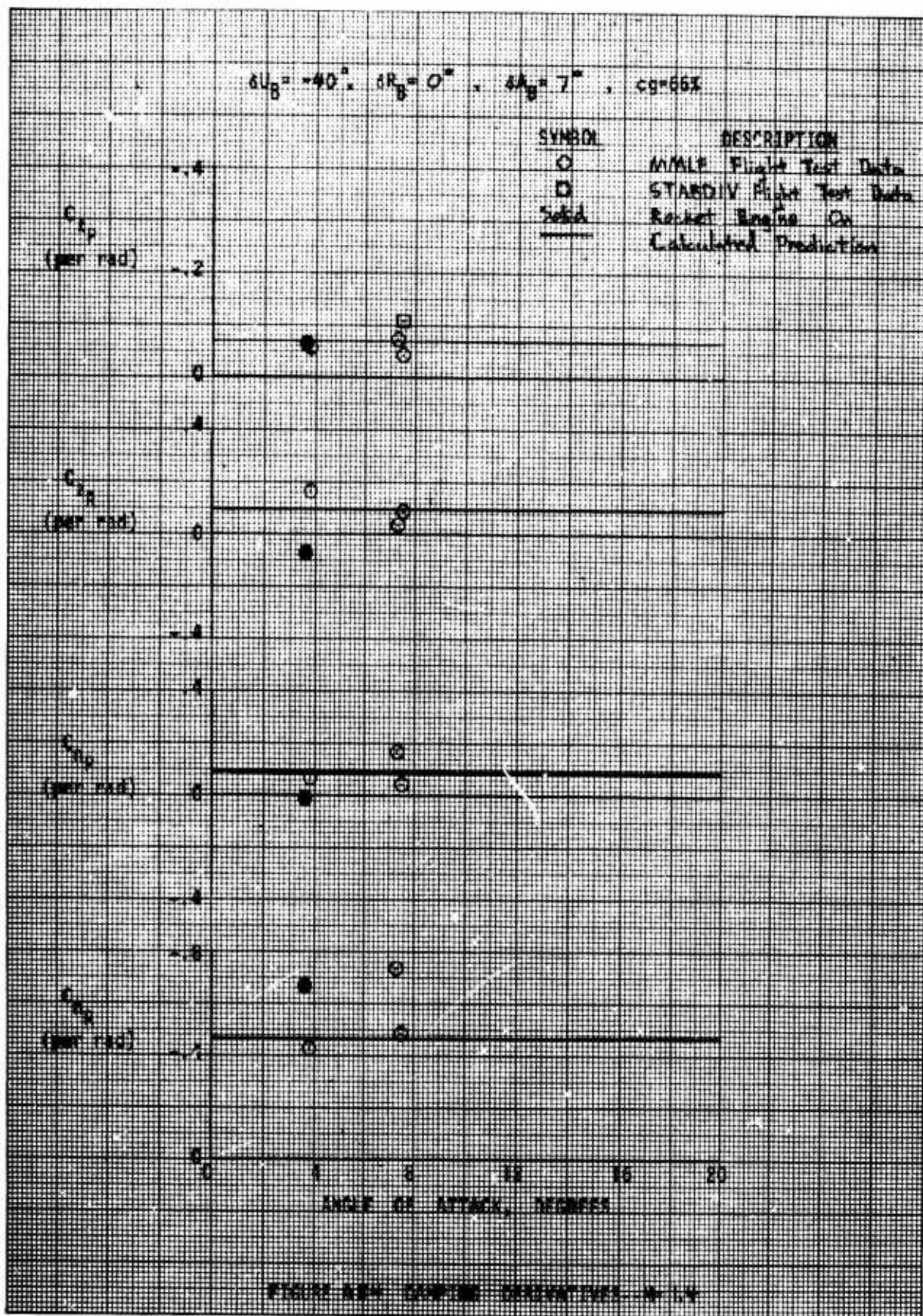




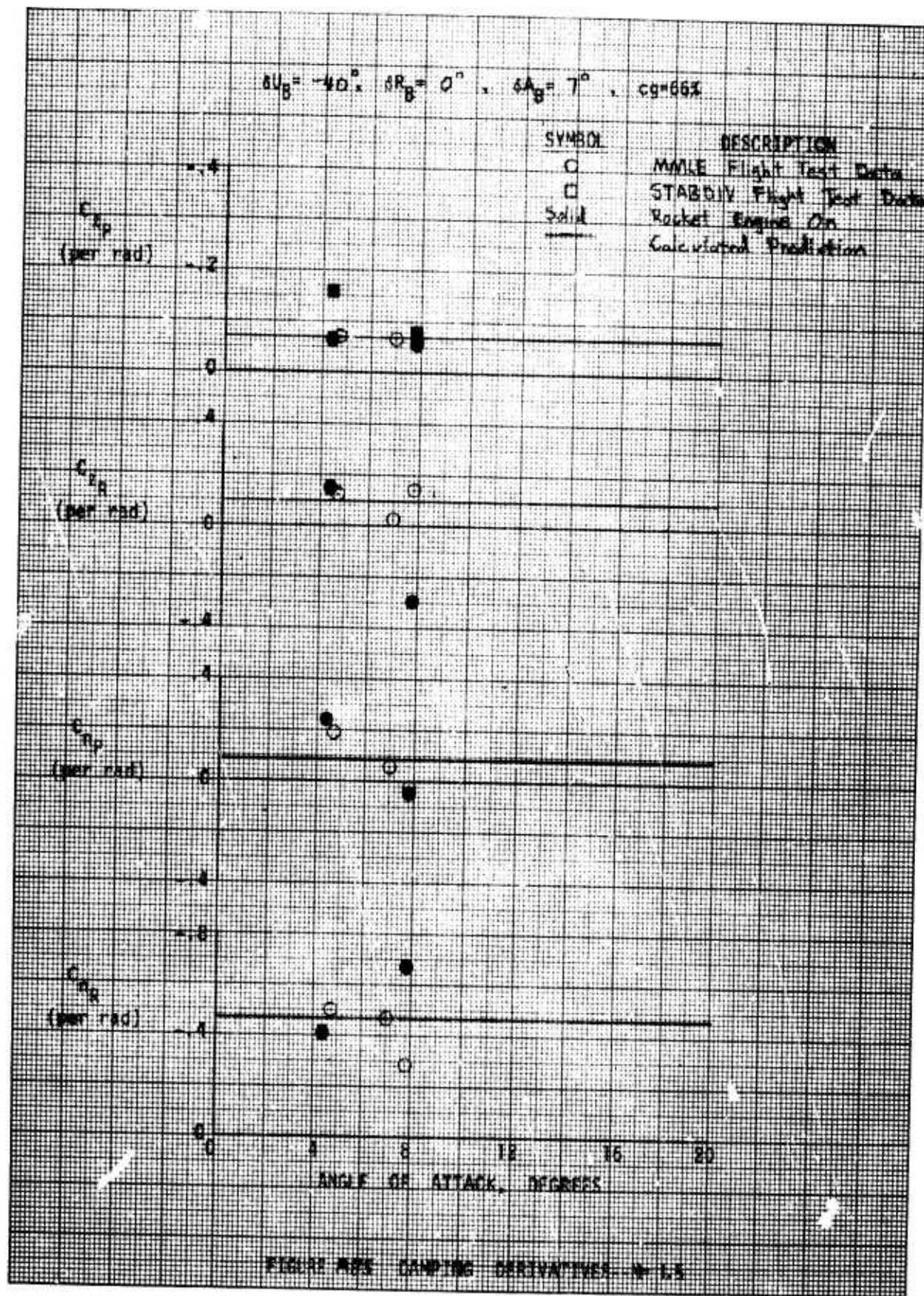




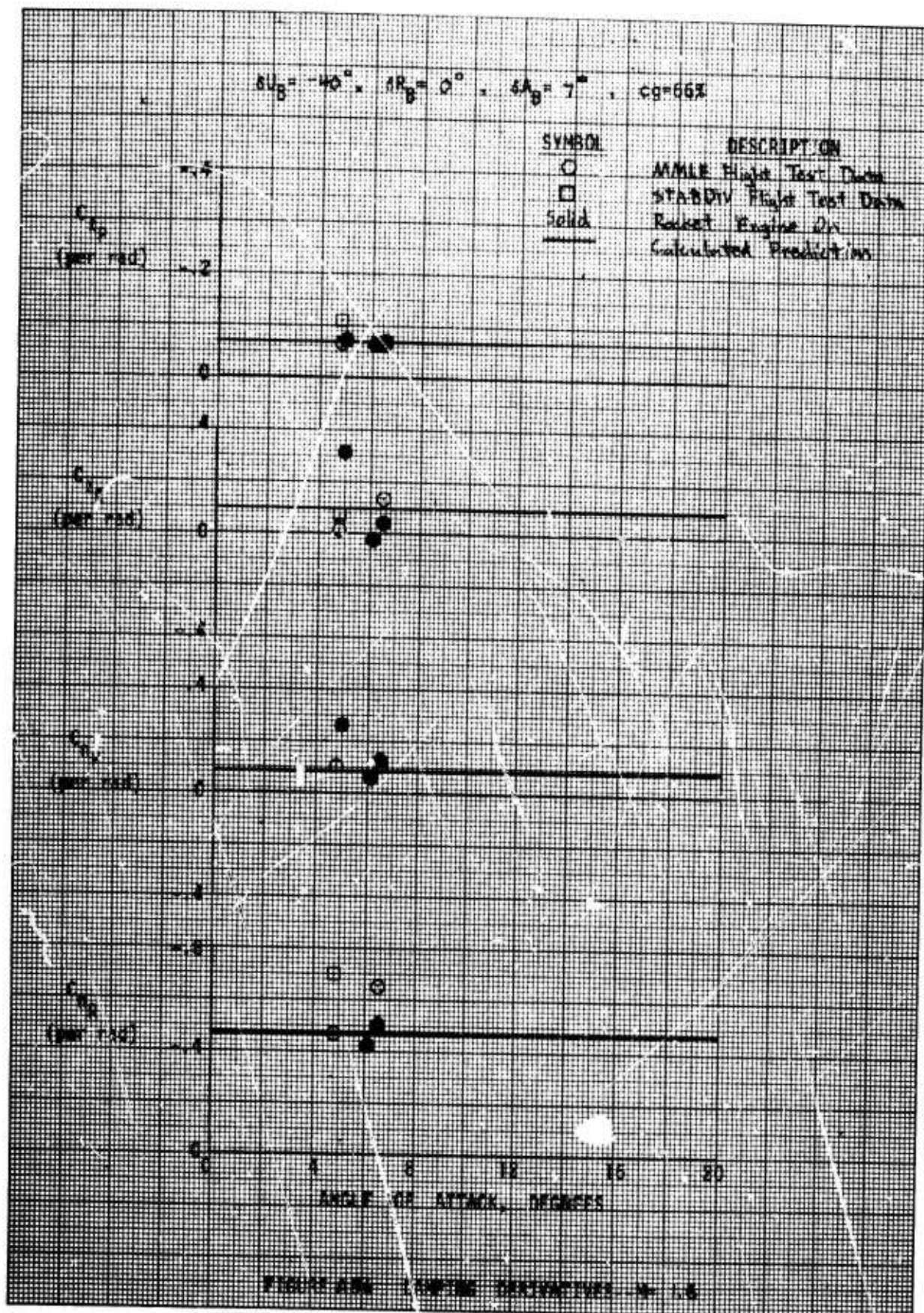


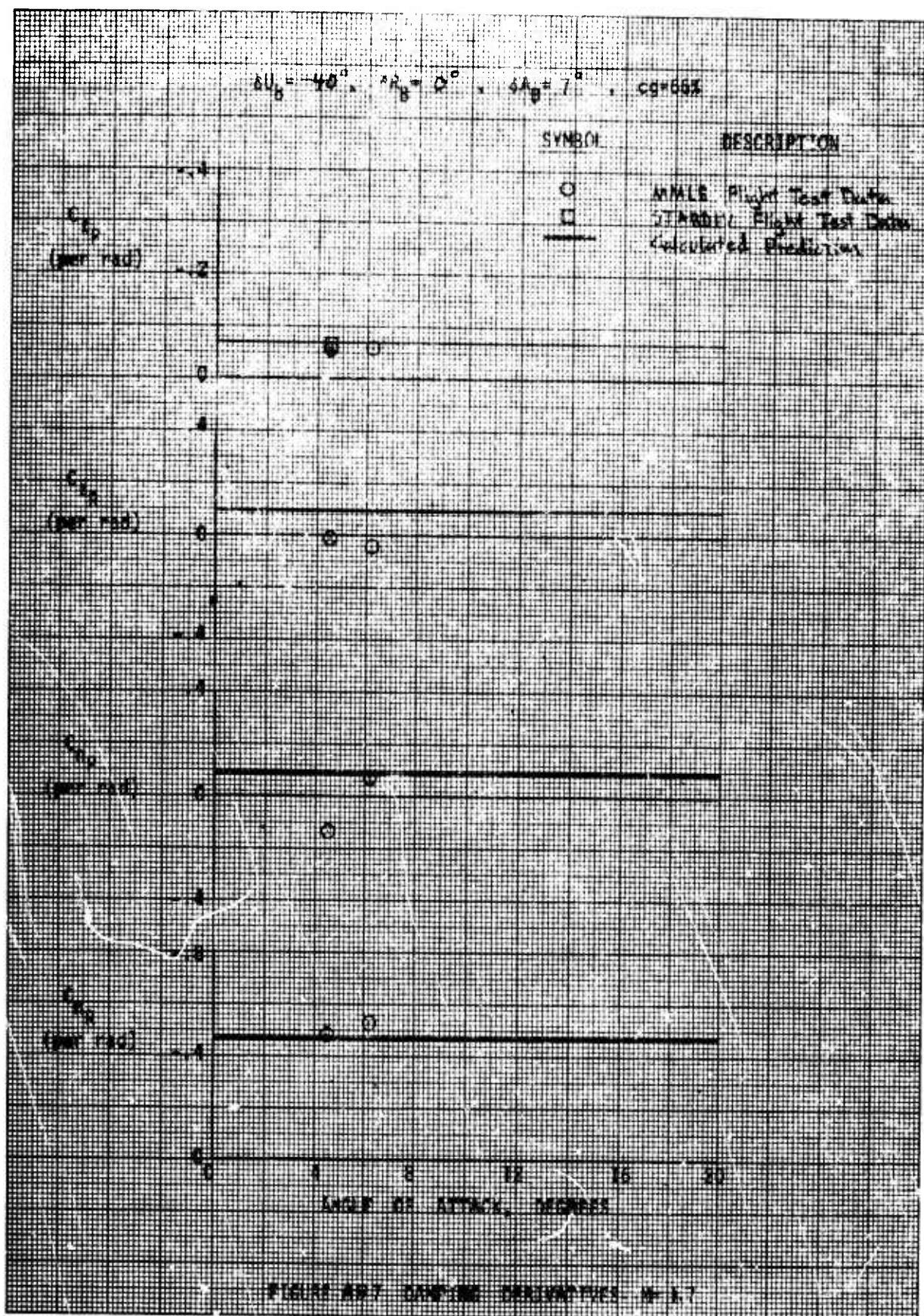




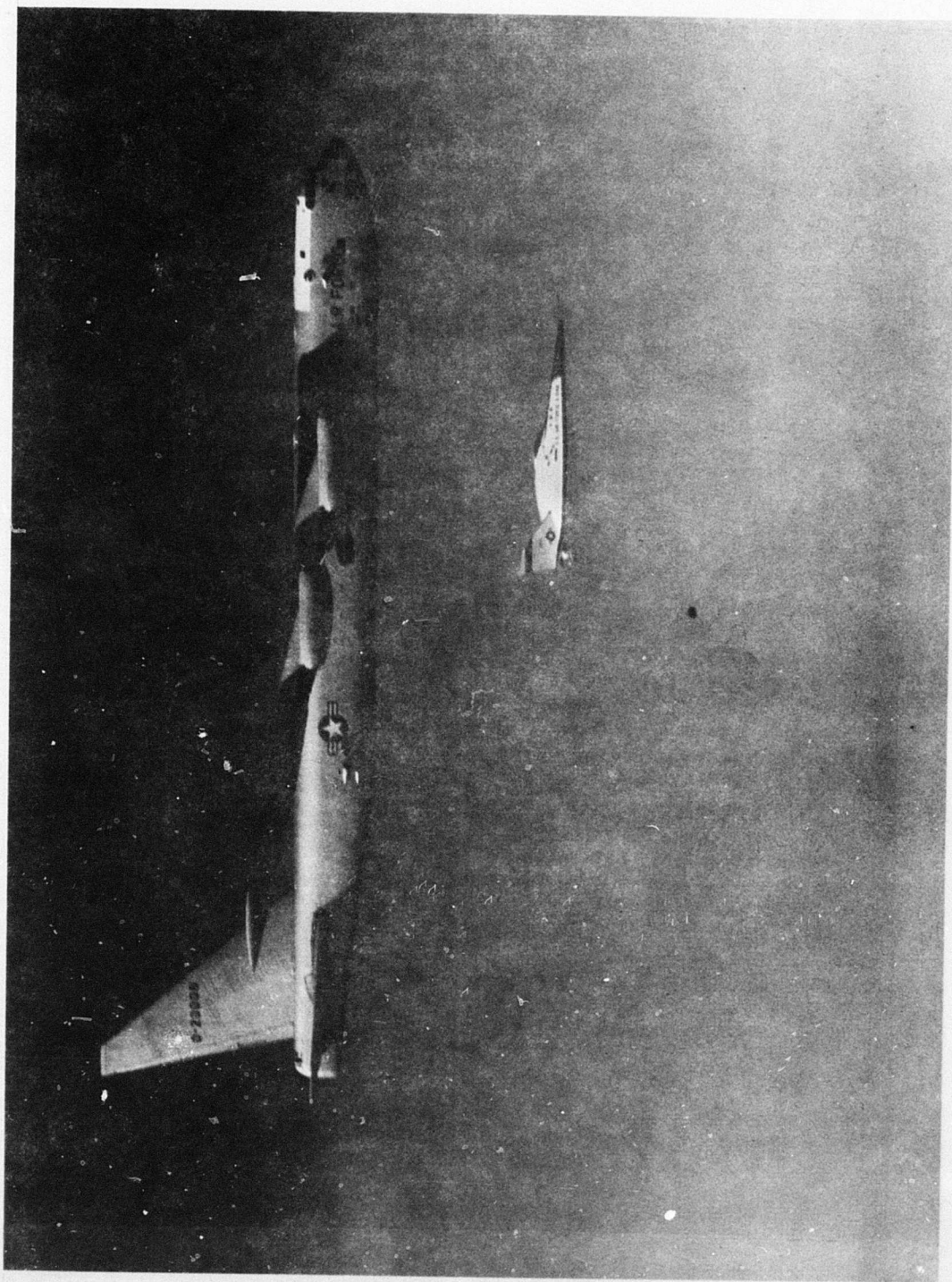










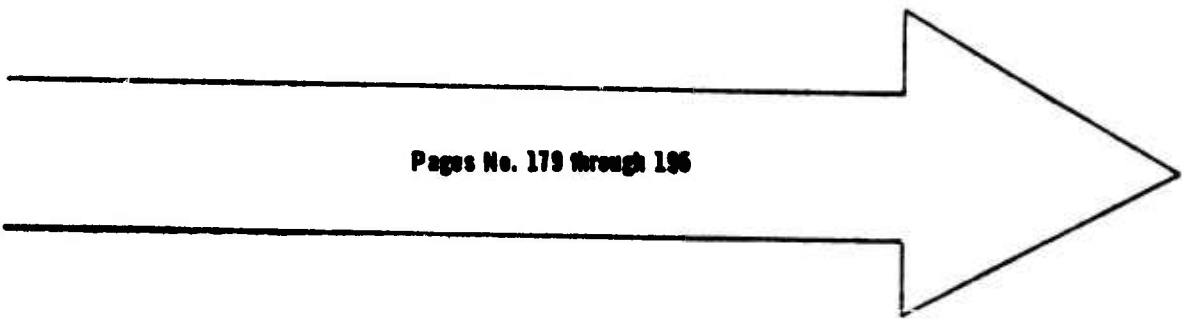




## **APPENDIX B**

# **APPENDIX B**

## **LONGITUDINAL TRIM CURVES**



**Pages No. 179 through 196**

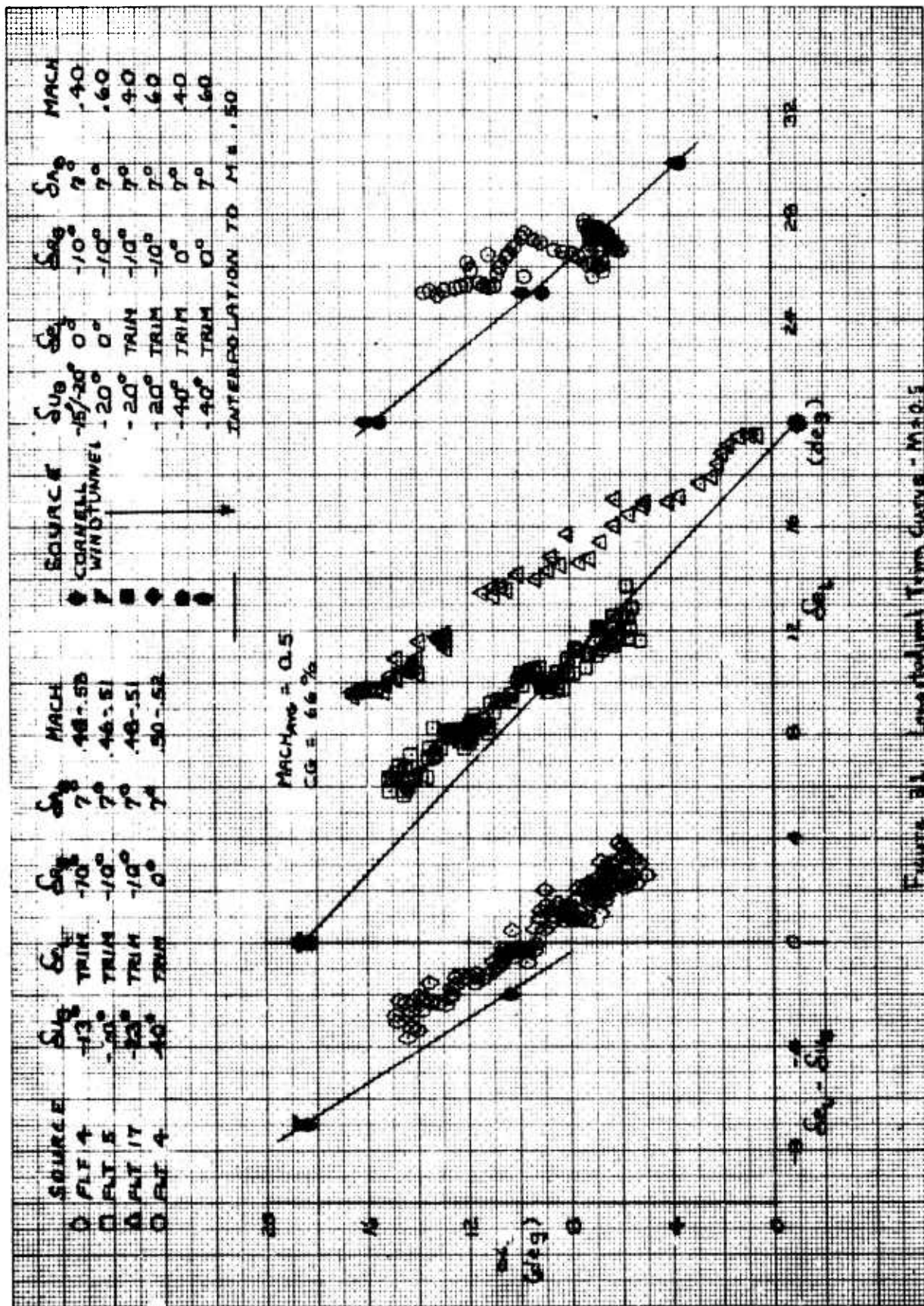


Figure 31. Longitudinal Trim Curves - M=0.5



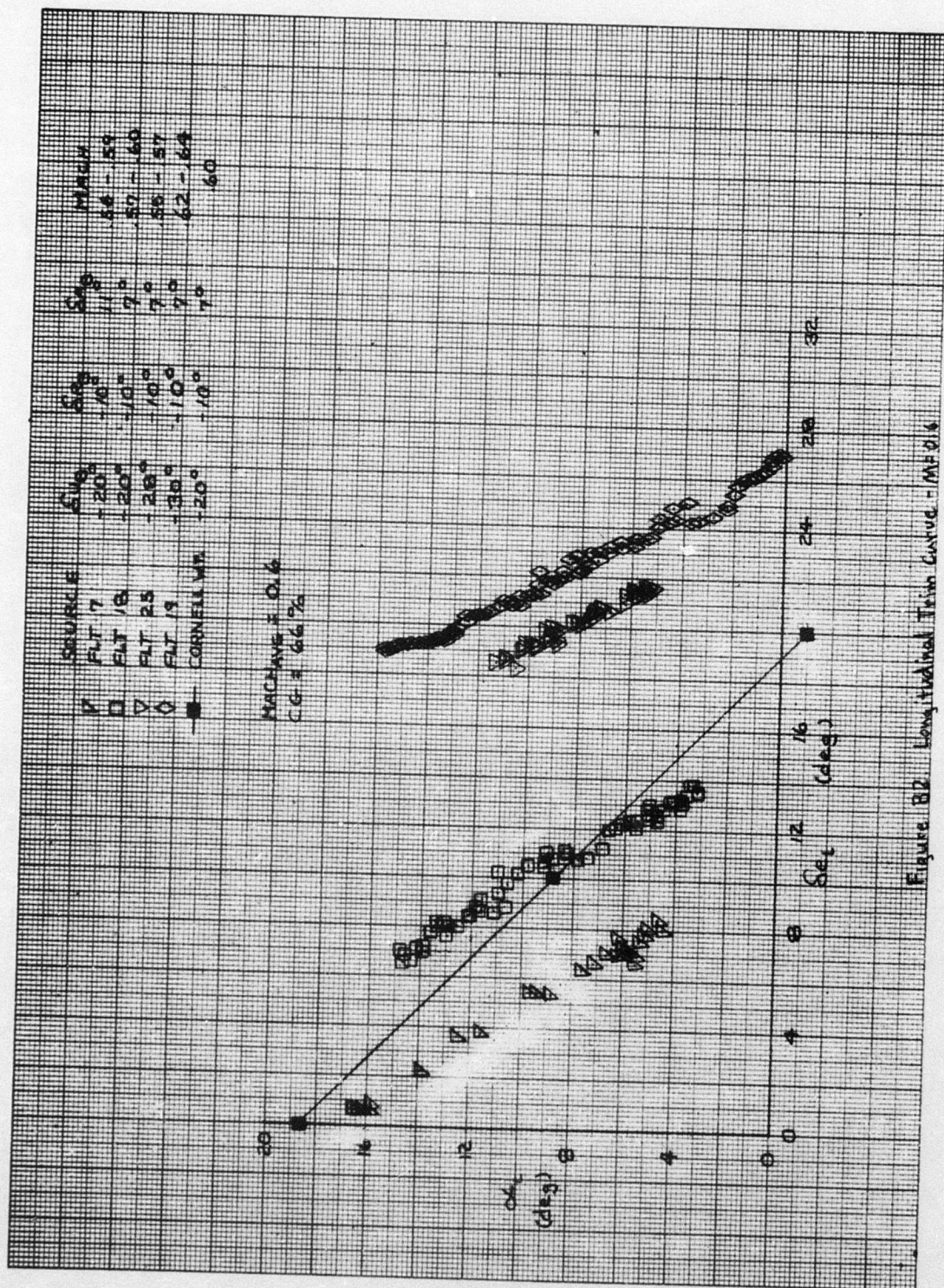


Figure B2. Longitudinal Trim Curve -  $M=0.6$

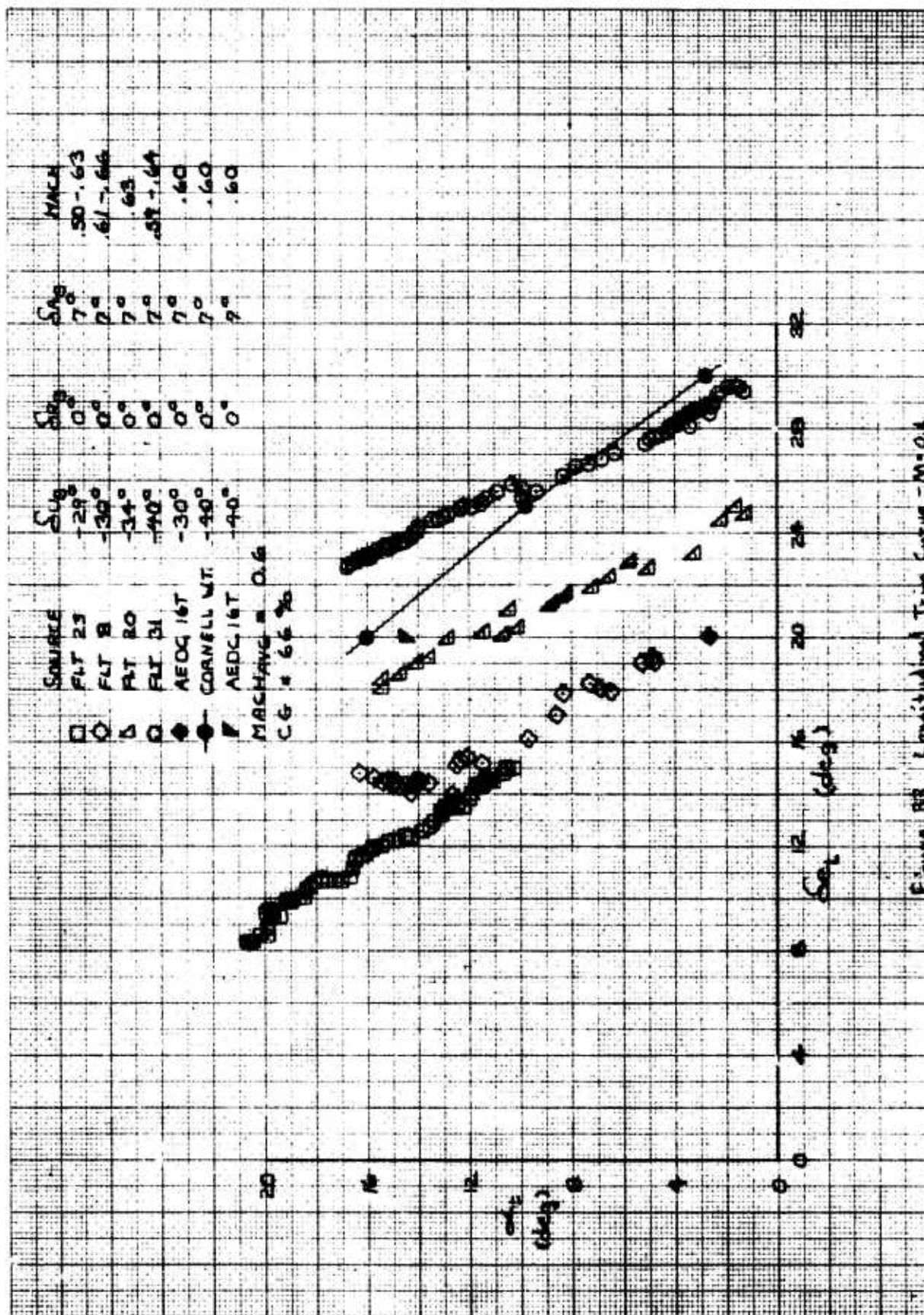


Figure 88. Longitudinal Trim Curves - M=0.6



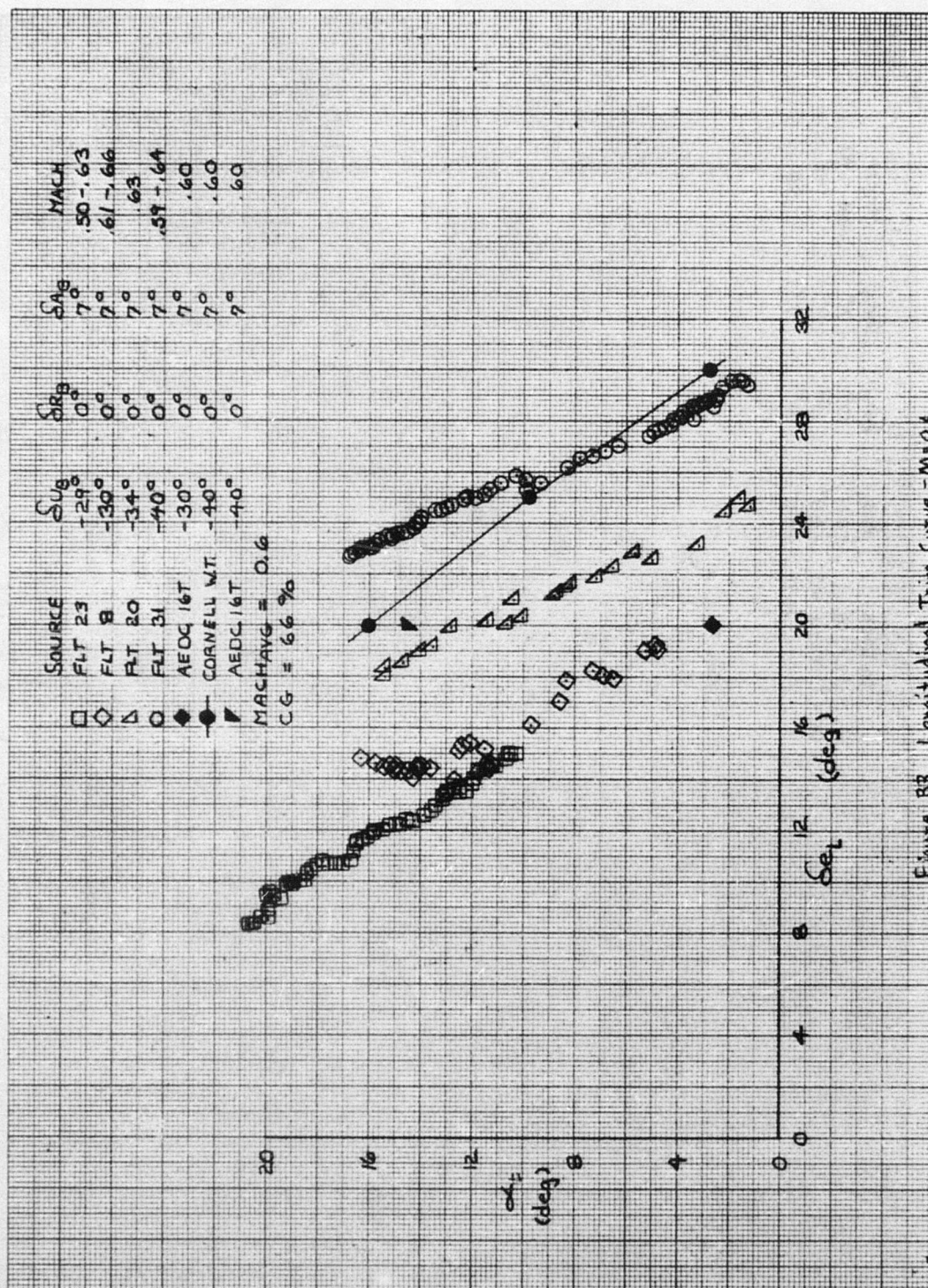
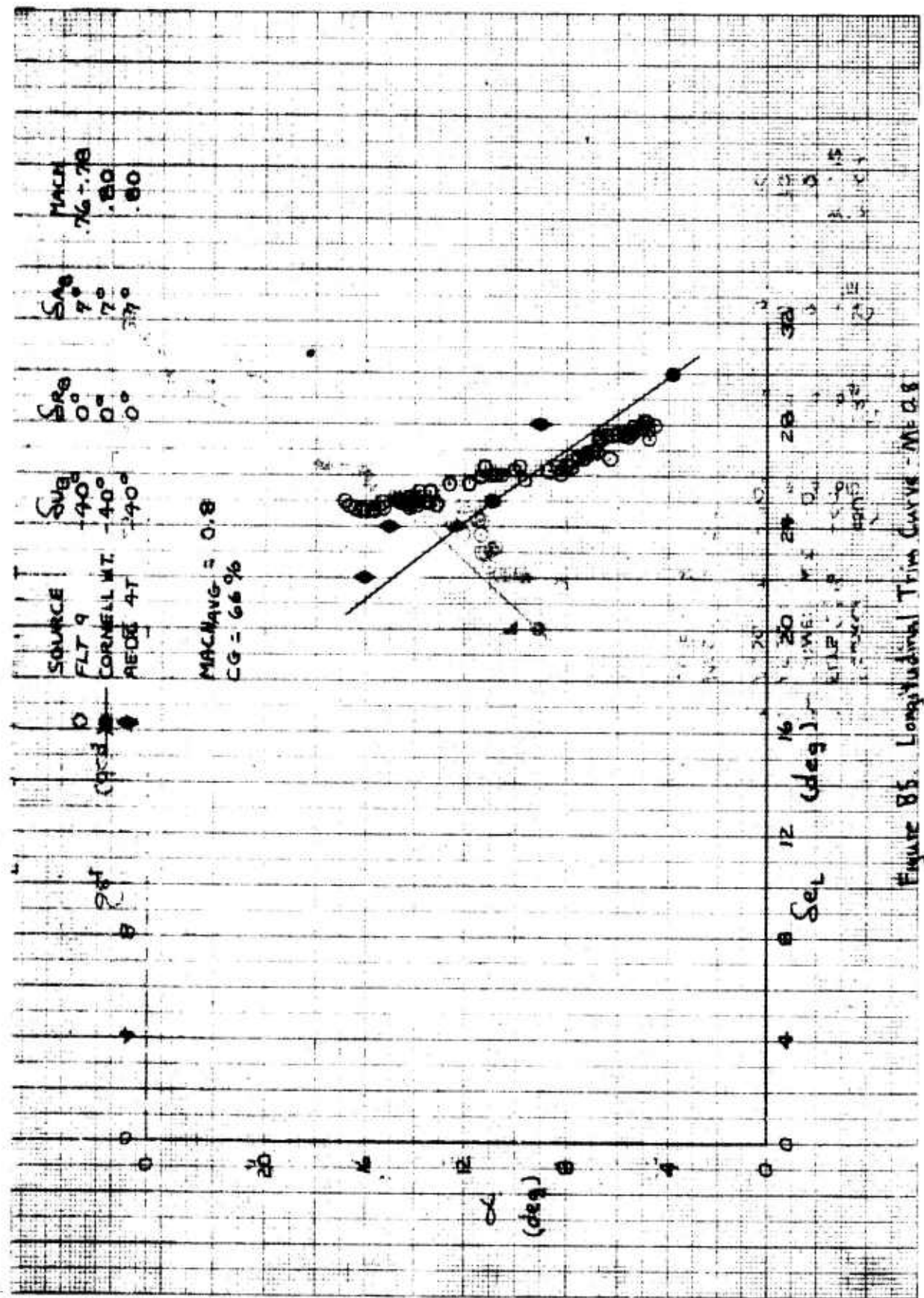


Figure 83. Longitudinal Trim Curve - M=0.6





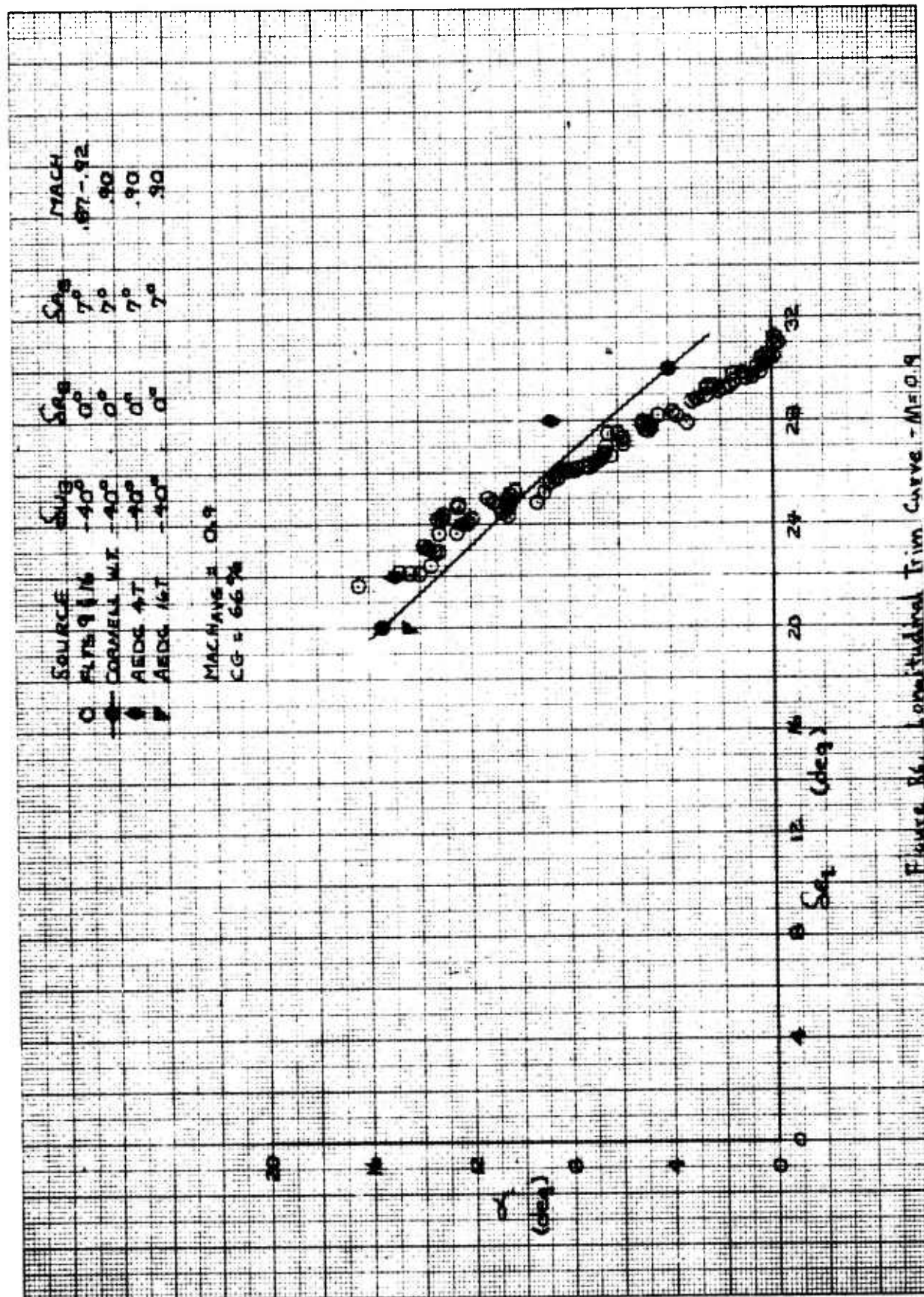


Figure 86. Longitudinal Trim Curve -  $M=0.9$

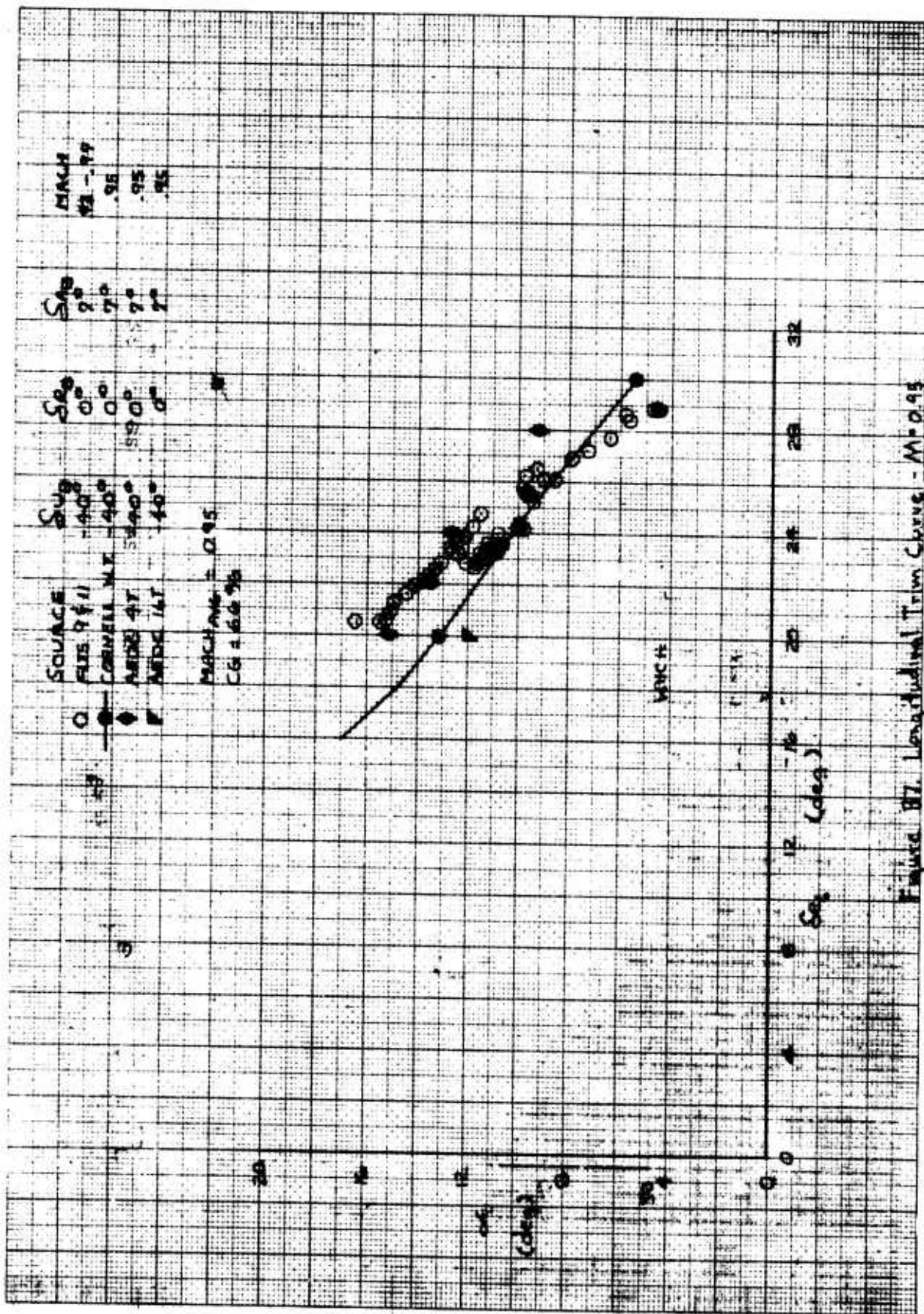


Figure 87. Longitudinal Trim Curve -  $M = 0.95$



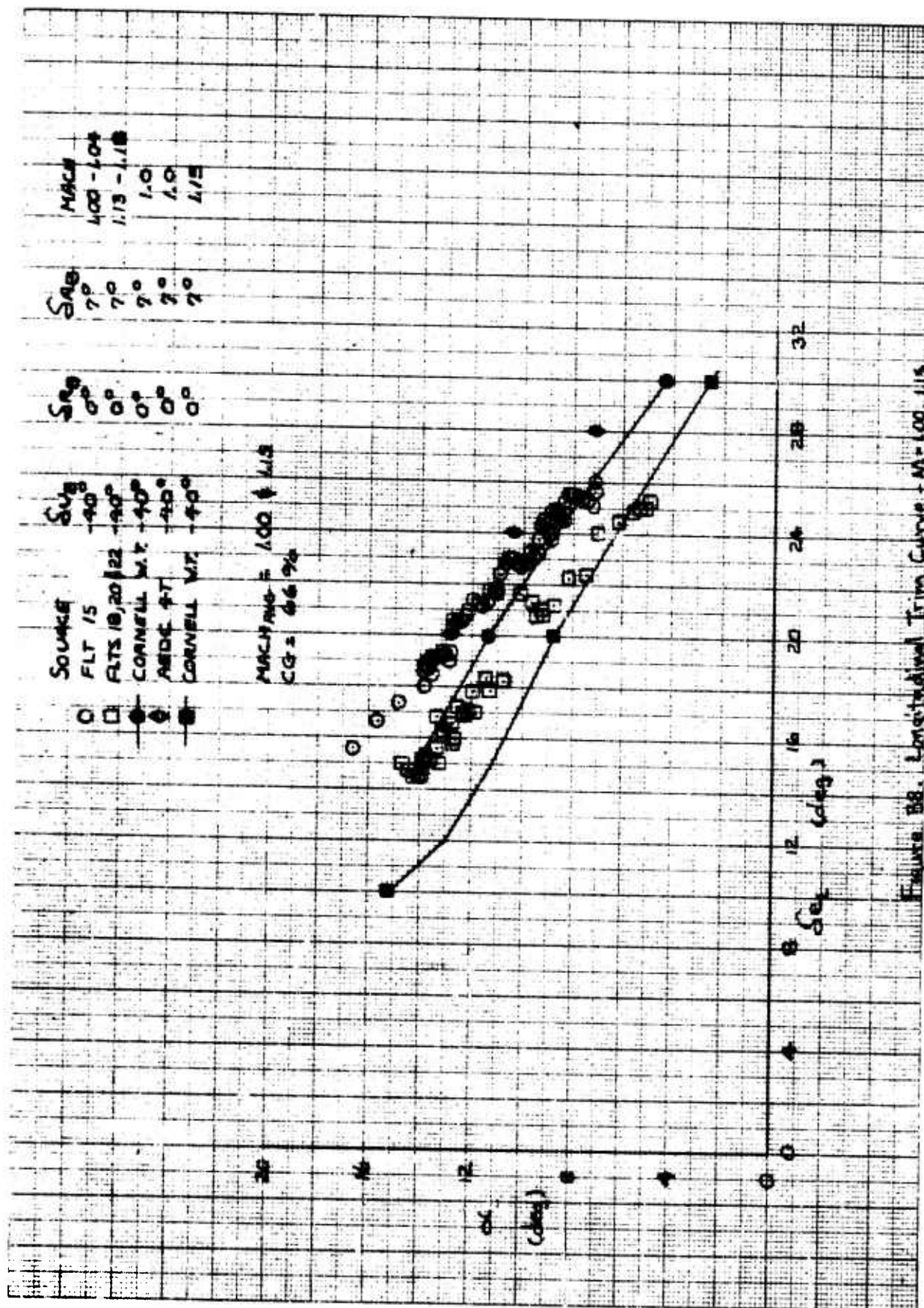


Figure 28. Longitudinal Trim Curve - M=1.00, 1.15

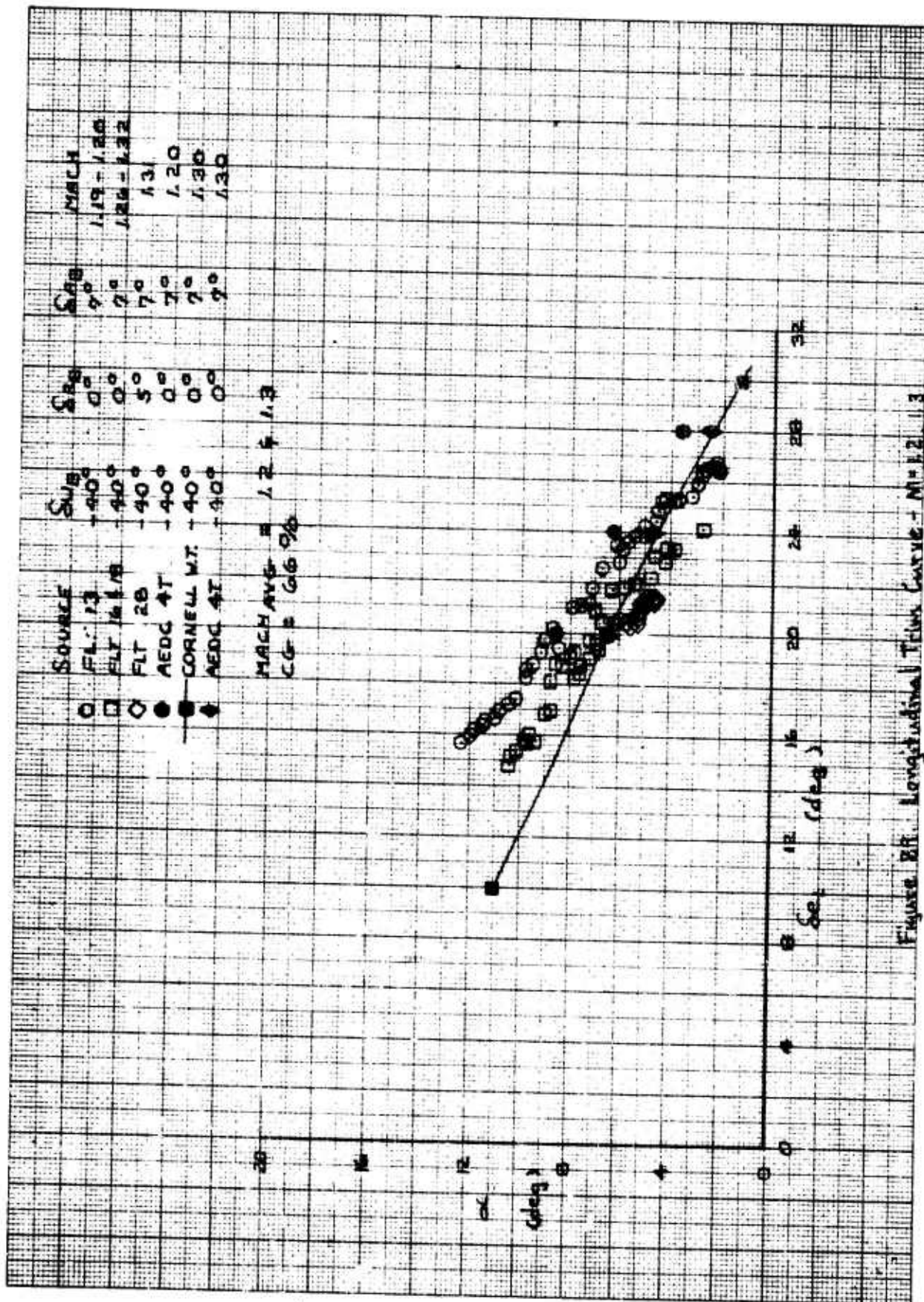


Figure 24. Longitudinal Tilt Curve - M=1.2, 1.3

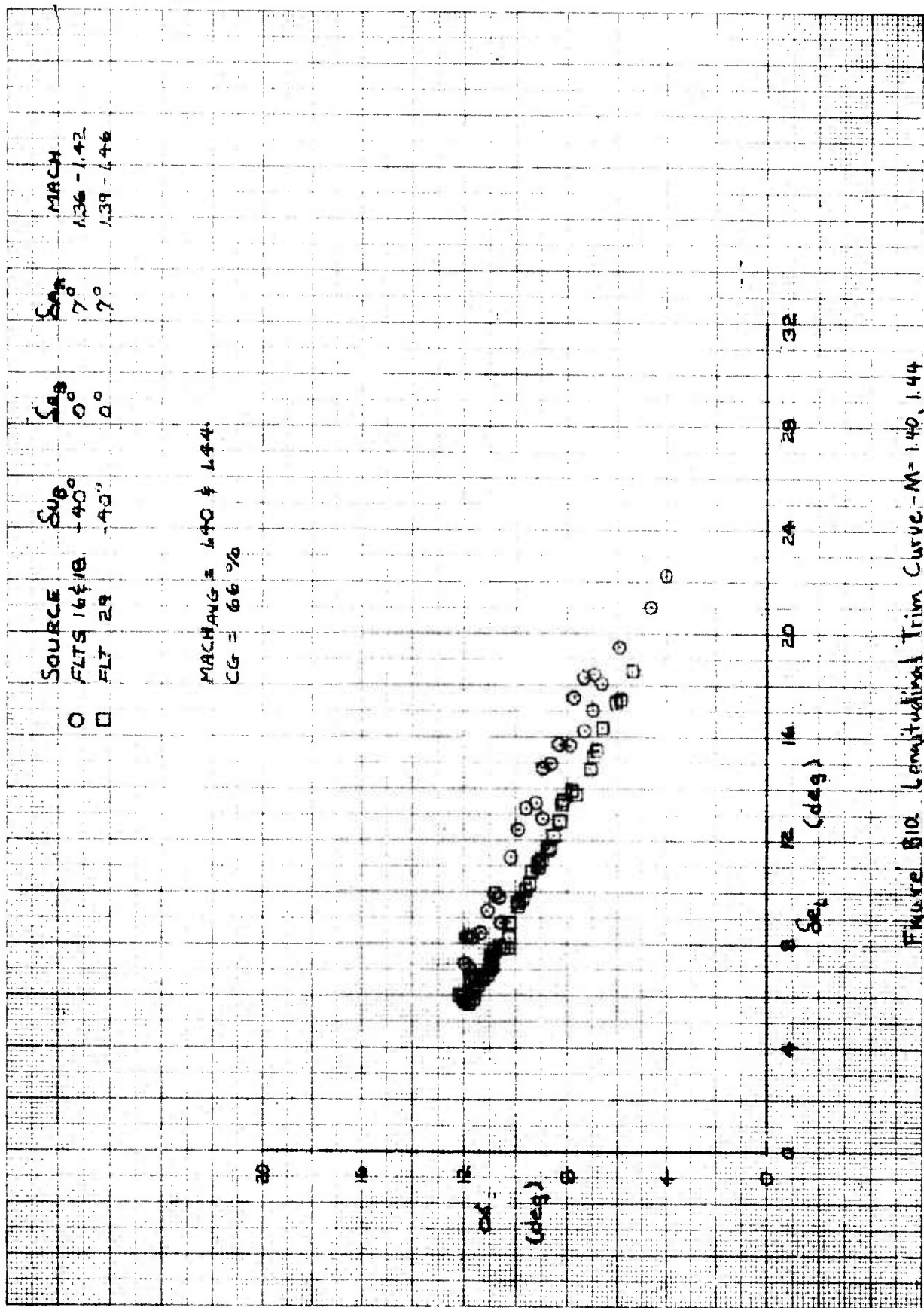


Figure 810. Longitudinal Trim Curve - M=1.40, 1.44



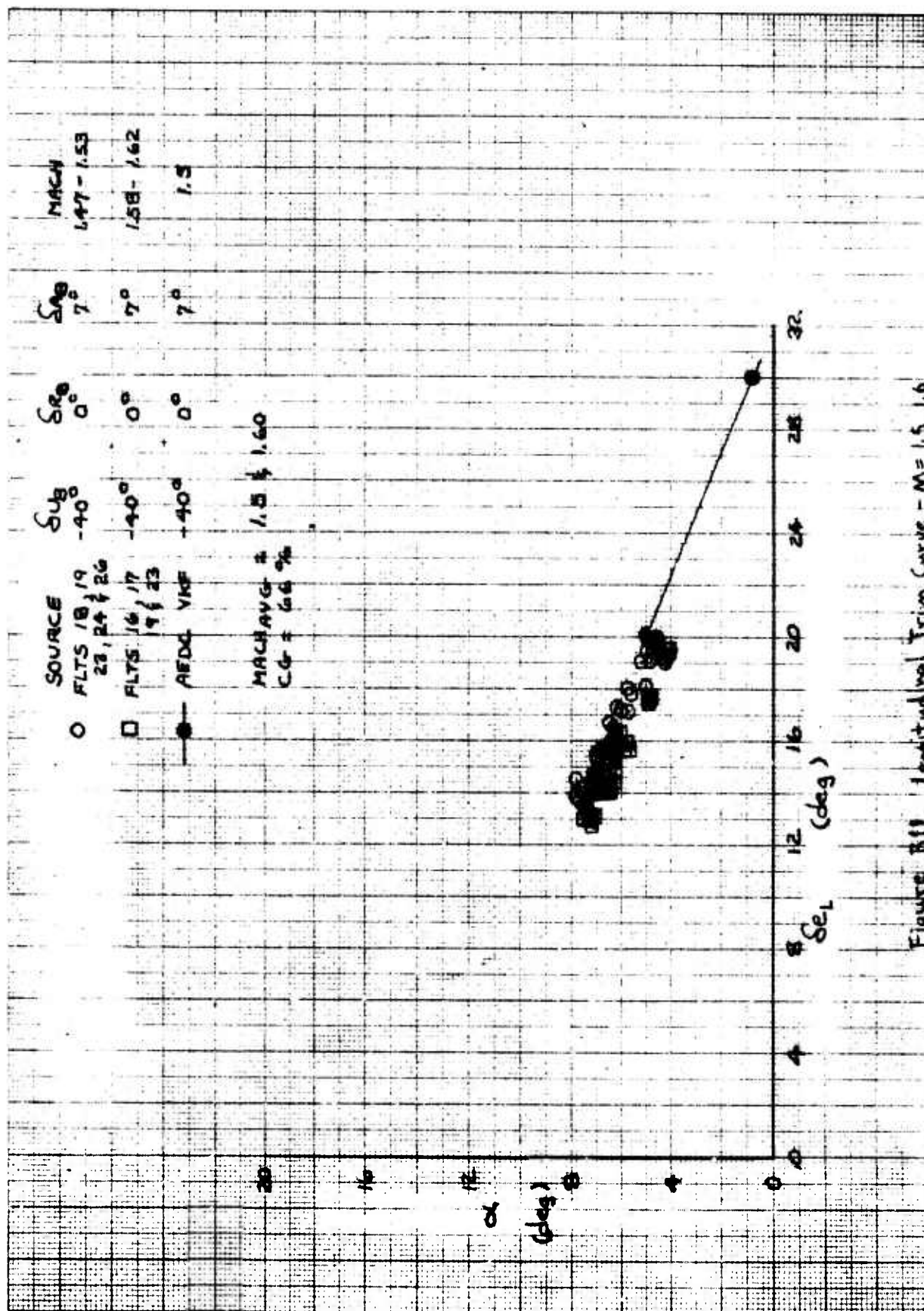


Figure B11. Longitudinal Trim Curve -  $M=1.5, 1.6$

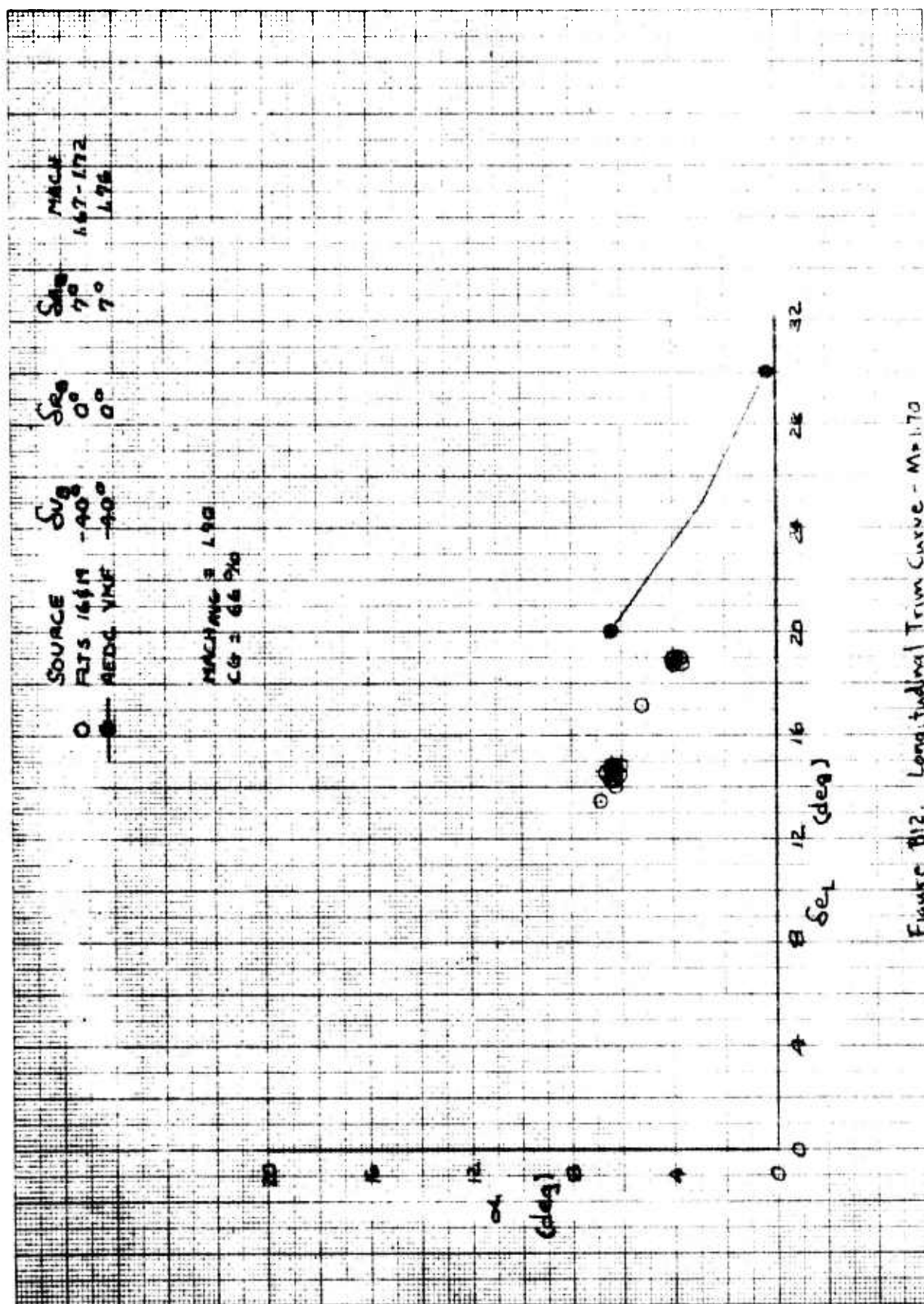


Figure B12. Longitudinal Trim Curve -  $M=1.70$

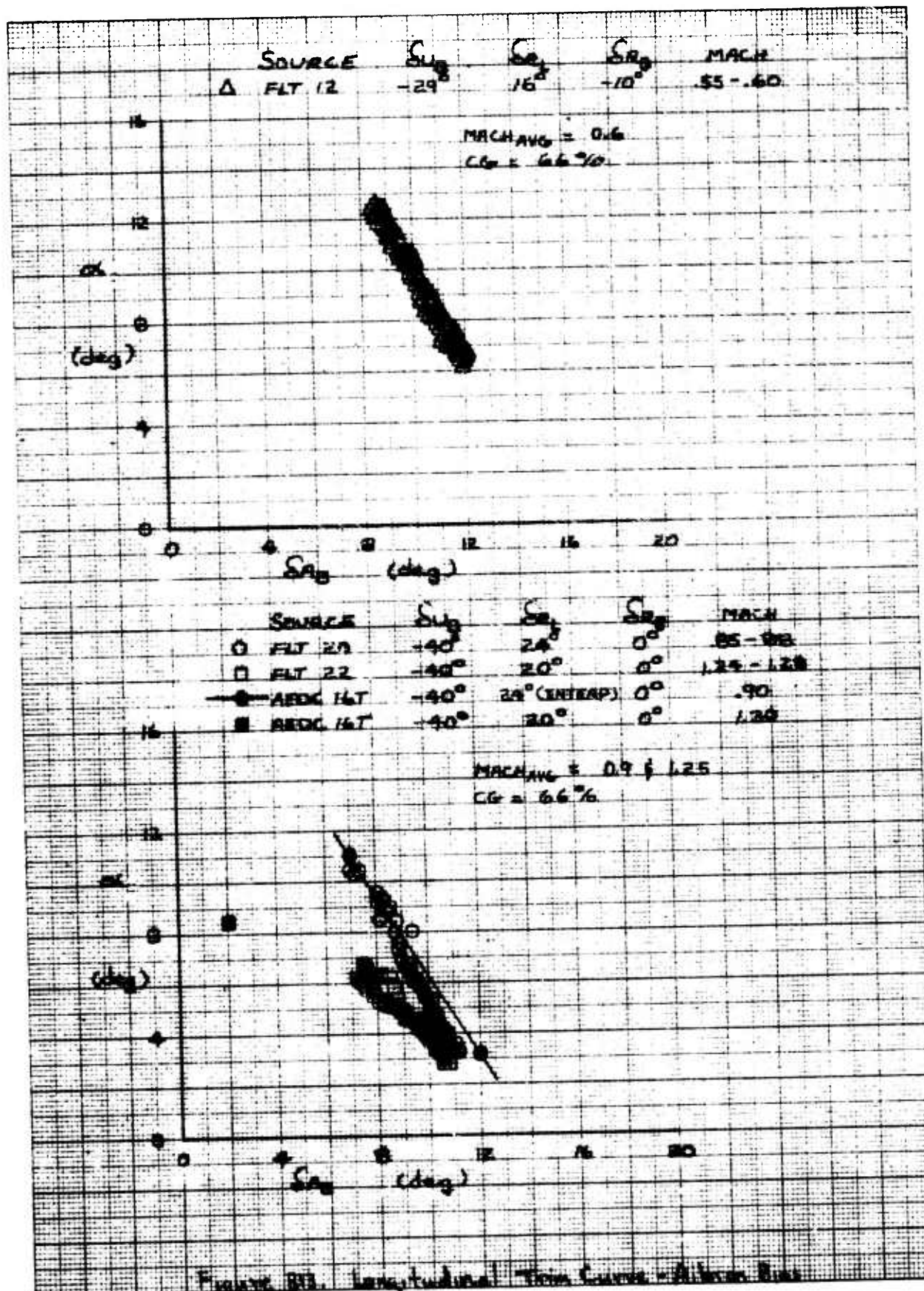


Figure B13. Longitudinal Trim Curves - Allison B13



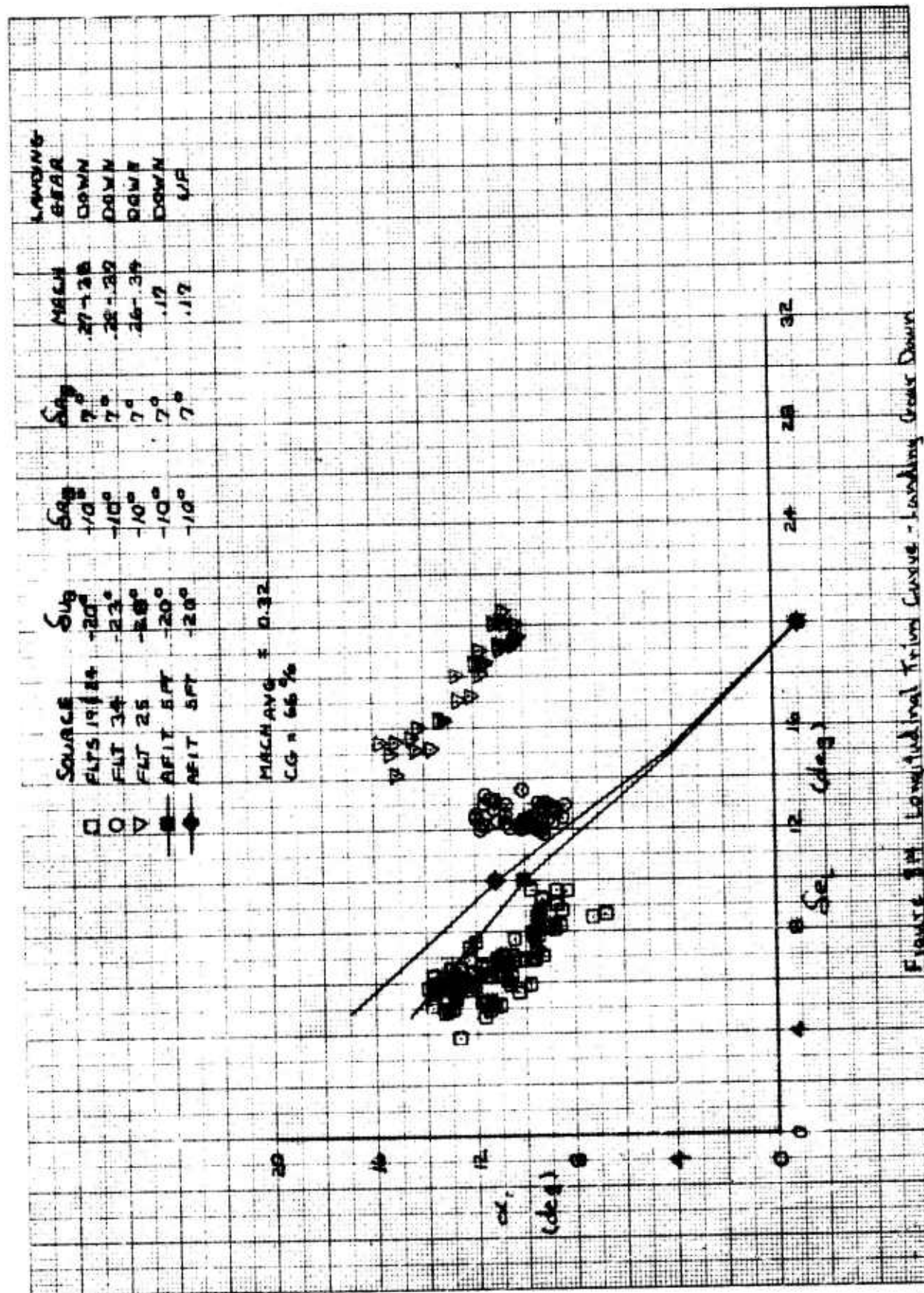


Figure 34 Longitudinal Trim Curves - Landing Gear Down

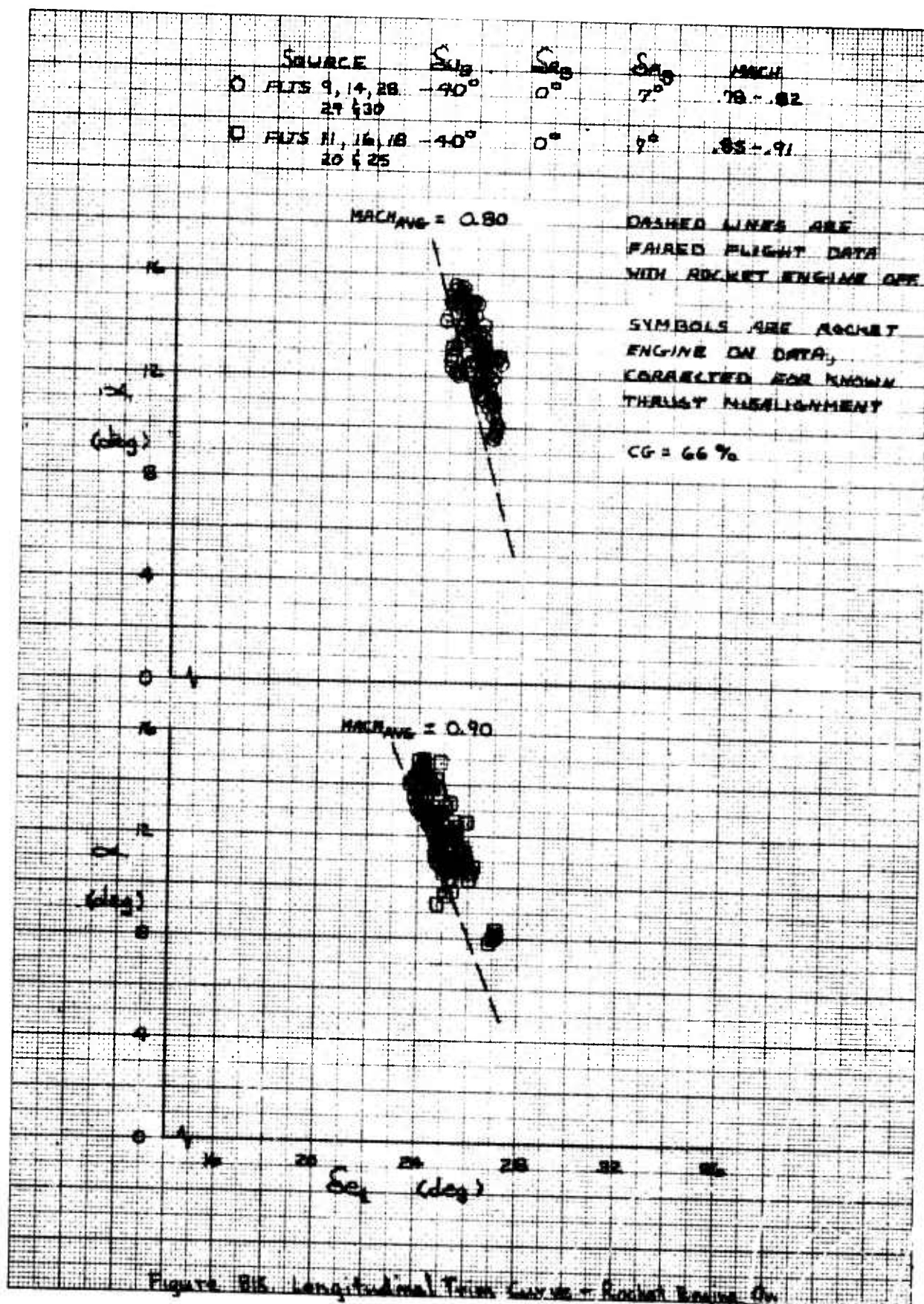
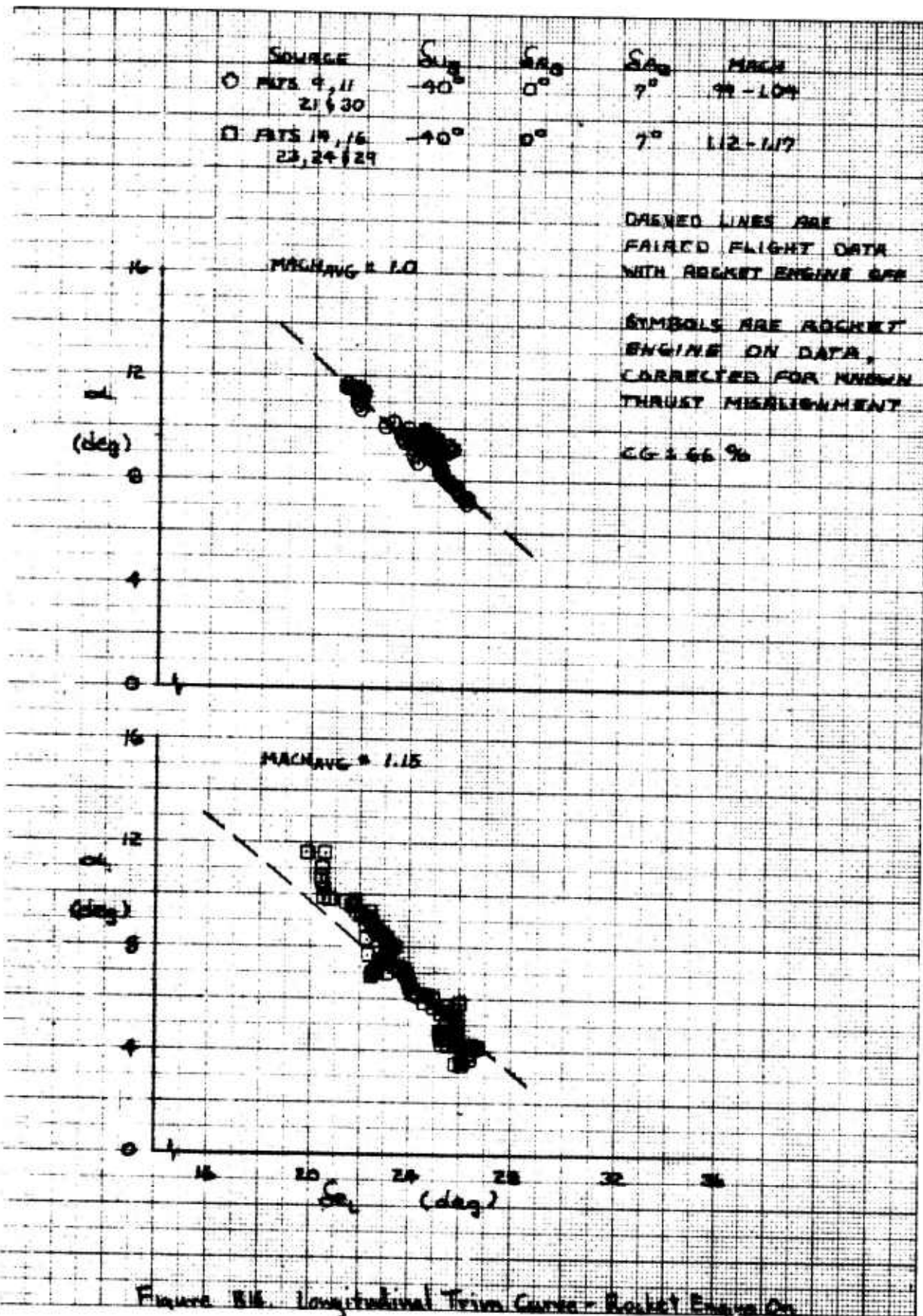
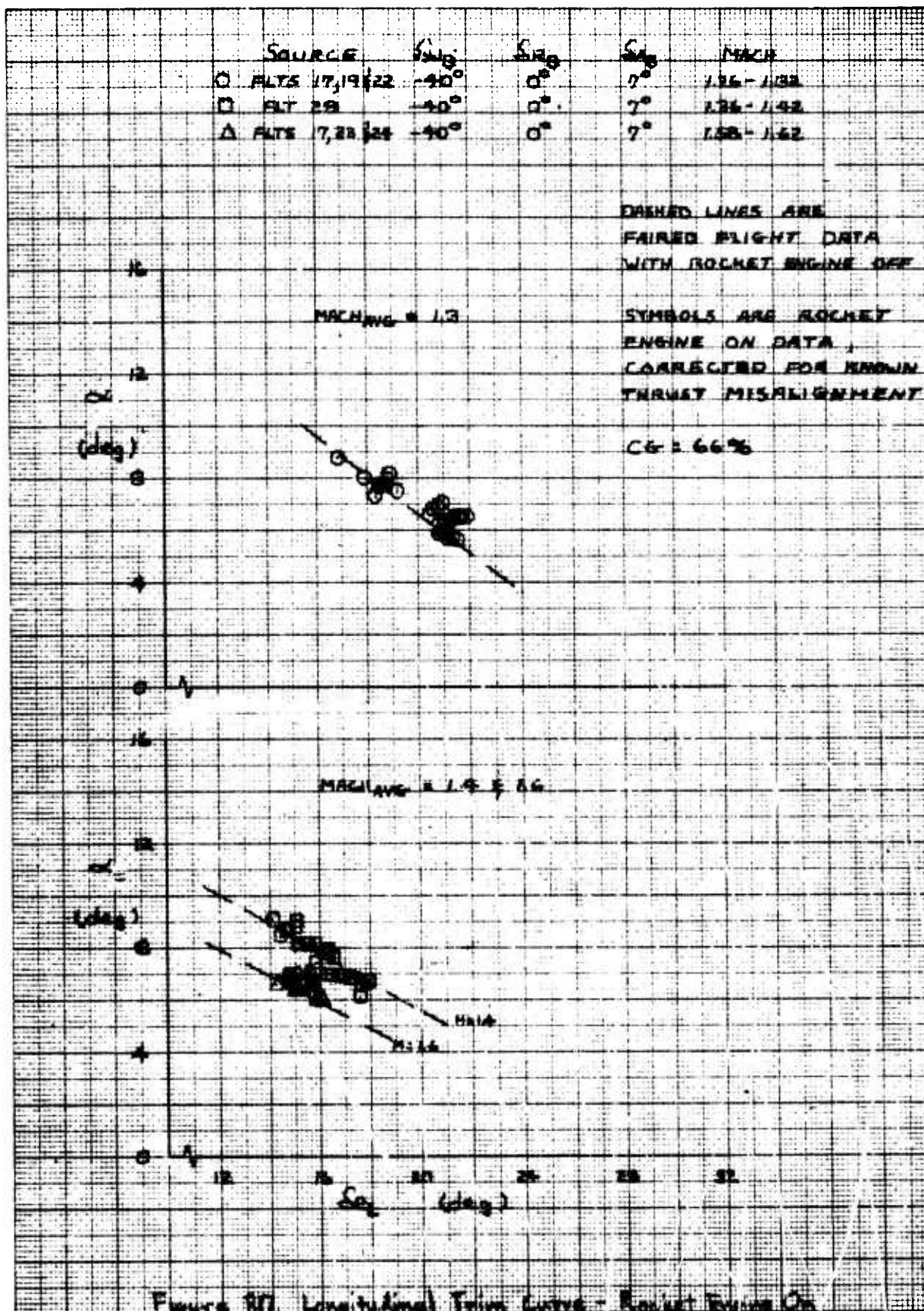
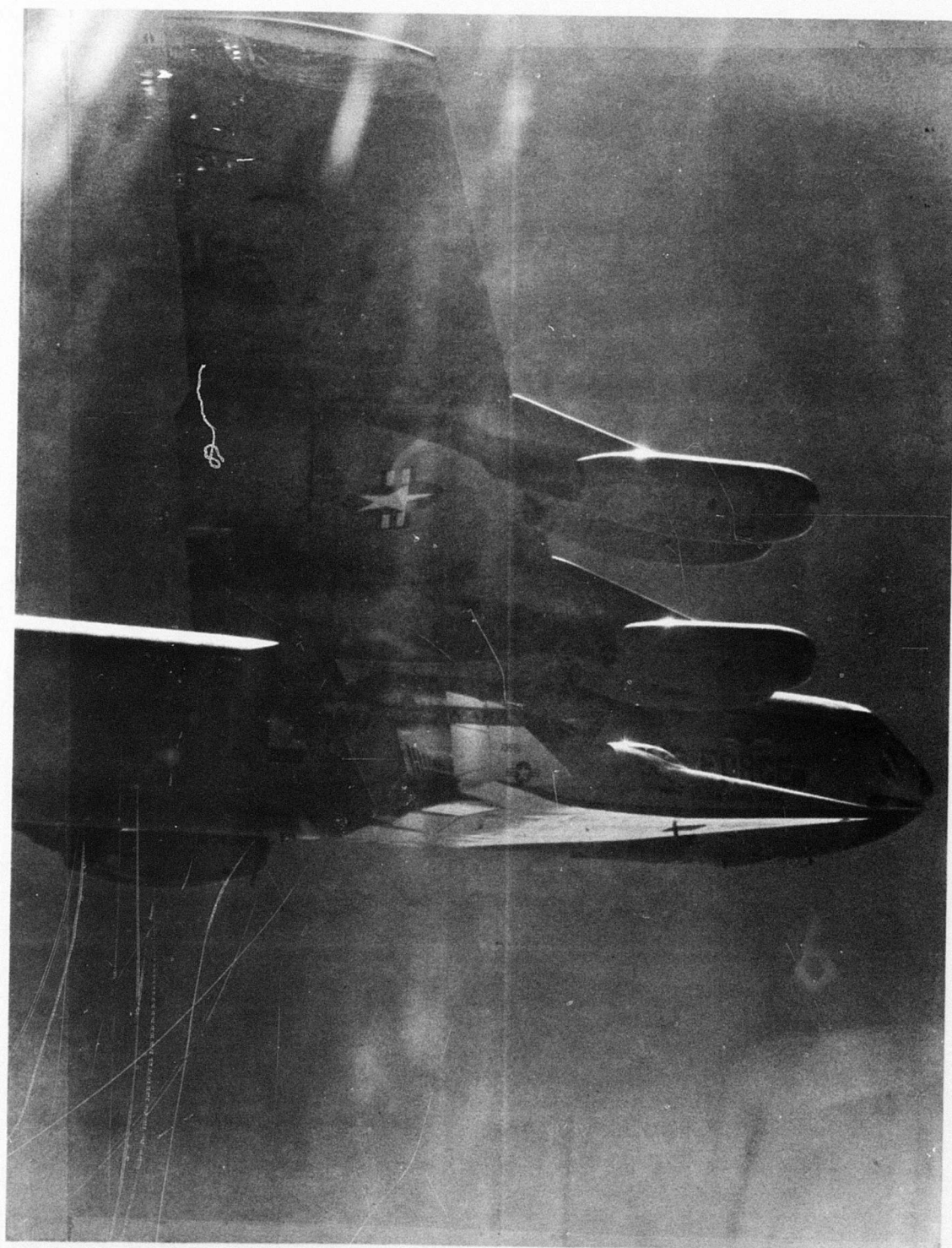


Figure B15. Longitudinal Trim Curves - Rocket Engine On









## **APPENDIX C**



## APPENDIX C WIND SHEAR TECHNIQUES

During the powered boost phase of several X-24B missions, pilots commented on uncommanded lateral-directional disturbances. Following flight 7, the pilot described these disturbances by saying: "They manifest themselves as just a little Dutch-Roll ..... a rather sharp input and then it goes away". One suggested explanation for these sideslip excursions was that the vehicle encountered abrupt wind changes with altitude which induced the sideslip disturbance. This appendix summarizes the results of an investigation to relate the sideslip excursions to wind changes.

The method used was to compute sideslip angle as a function of time using the sideforce equation of motion and to compare this computed value with the vane measured sideslip angle. The difference between the two values was defined as the sideslip disturbance since it represented sideslip excursions which were not accounted for by the equations of motion. This time history of sideslip excursions was then used to determine a theoretical profile of sidewind component vs altitude by computing the magnitude of sidewind required to account for the observed disturbance. This computation was performed over very short time intervals producing increments of sidewind which were then summed to compute the profile of wind magnitude starting from zero velocity at some arbitrary altitude. The thinking behind this approach can be visualized by imagining the vehicle entering a step change in sidewind. This change initially manifests itself as a sideslip unaccounted for by the equations of motion. After the initial input was made, however, the vehicle would respond dynamically in a lateral-directional mode as described by the equations of motion until eventually it returned to a steady-state, zero-sideslip condition at which time it would be translating laterally relative to an earth fixed reference frame at the velocity of the sidewind disturbance. The computation of the sidewind profiles was made during the powered boost and unpowered descent portion of the X-24B missions, when the vehicle was undergoing rapid changes in altitude.

Now that the general approach has been reviewed, the details of the method will be presented. The sideforce equation of motion used in the computation was as follows:

$$\dot{\beta} = P \sin \alpha - R \cos \alpha + (1/\cos \beta) \frac{g}{V_t} \cos \theta \sin \phi - \sin \theta \sin \beta \\ + \left( \frac{\bar{q} S}{V_t m \cos \beta} \right) C_{Y\beta} \cdot \beta + C_{Y\delta a} \cdot \delta a + C_{Y\delta r} \cdot \delta r$$

This equation was numerically integrated using a second order Runge-Kutta algorithm to obtain the computed sideslip angle ( $\beta$ ) as a function of time. The parameters required for this computation were obtained from the on-board instrumentation system. The required stability derivatives were input as fixed values although they were known to vary with flight condition. A sensitivity study was done which indicated that wide variations in the values of these derivatives had little effect on the computed wind profiles. The integration algorithm

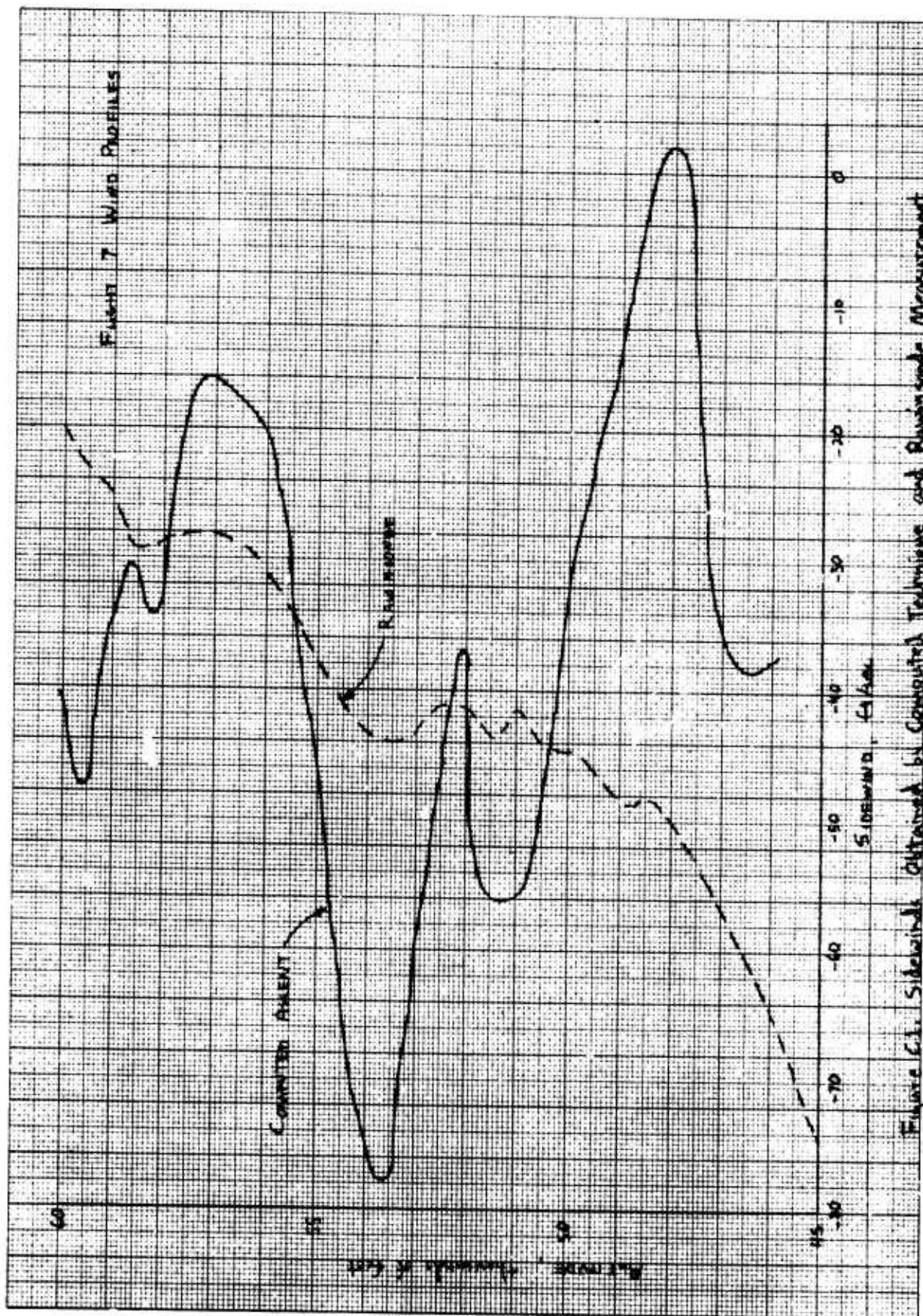


Figure 6.1. Sidewind obtained by Computed Technique and RAVINSOPE Measurement

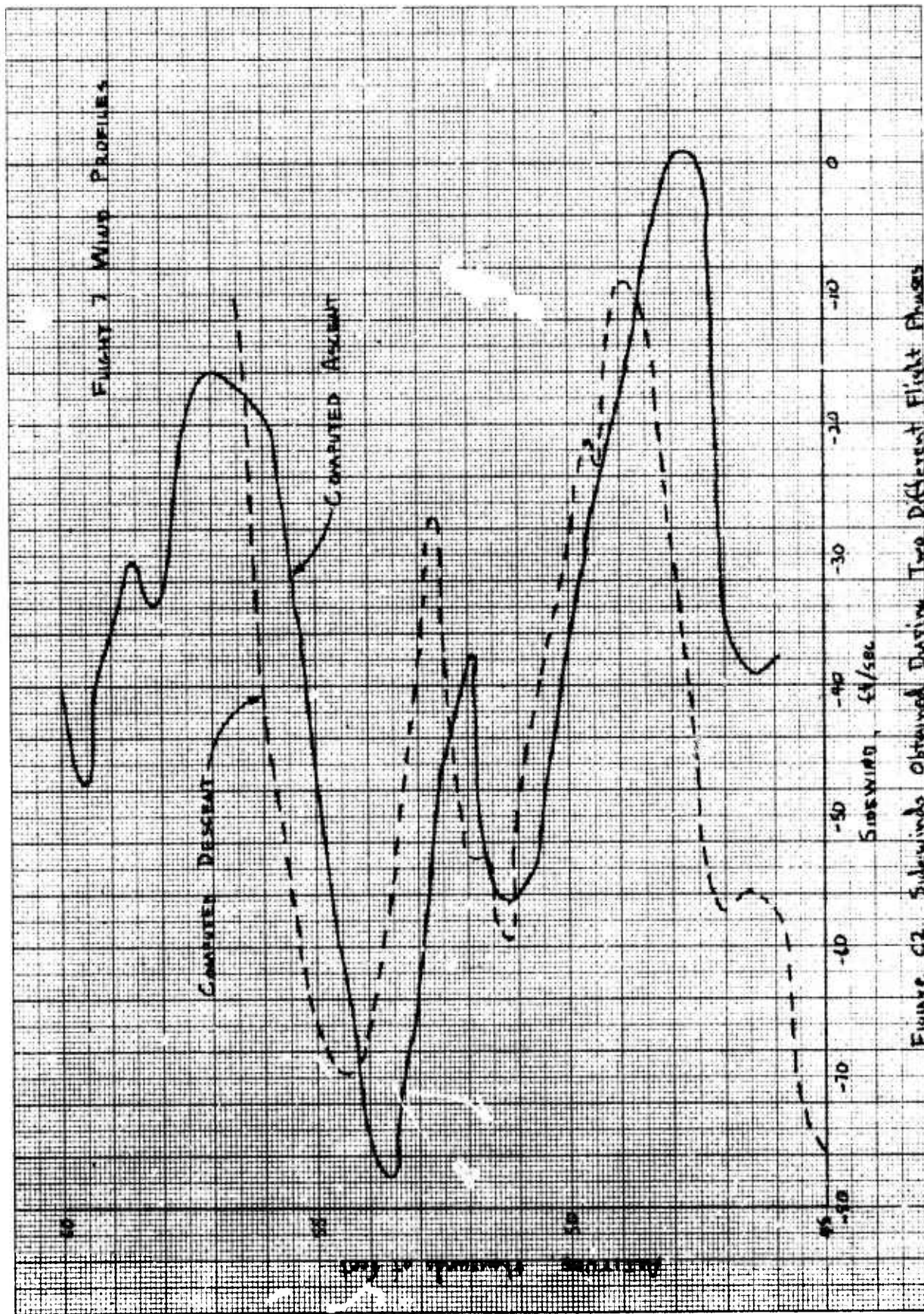


Figure C2. Sideswinds Obtained During Two Different Flight Phases



used was:

$$\beta_{n+1} = \beta_n + \frac{h}{2} \dot{\beta}(\bar{X}_n, \beta_n) + \dot{\beta}(\bar{X}_{n+1}, \beta_n) + h \dot{\beta}(\bar{X}_n, \beta_n)$$

where  $\bar{X} = (P, R, V_t, \alpha, \theta, \phi, \bar{q})$

$h$  = integration interval size

and the subscript "n" denotes values at the start of the integration interval and "n + 1", the values at the end. After each integration interval, the computed value of sideslip ( $\beta_c$ ) was compared with the vane measured value ( $\beta_m$ ) and the difference used to compute a sidewind velocity component using the relationship:

$$\Delta V = V_t (\sin \beta_m - \sin \beta_c)$$

The computed value of sideslip at the end of the interval was then set equal to the measured value and the process was repeated for the next interval.

The sidewind velocity component was computed in the vehicle's body-axis system along the y-axis with the convention that a positive sideslip disturbance is produced by a positive wind increment. Since the vehicle was flying wings-level on a constant heading during the portions of the missions studied, the vehicle y body-axis is aligned with an axis in an earth-fixed reference frame which lies in a horizontal plane and is oriented 90° to the aircraft's heading. The earth-axis system used has the x and y-axes in a horizontal plane with the x-axis along the vehicle's heading and the y-axis orthogonal to it with its positive direction aligned out the vehicle's left wing (opposite to the convention used in the body-axis system). The z-axis was vertical with the positive direction up. The computed sidewind components were summed and the resulting magnitude plotted as a function of pressure altitude in the earth-axis system. The result then was a computed sidewind profile with altitude which accounted for all "sideslip disturbances" during the portion of the mission analyzed. The problem then became one of verifying, by some independent means, whether this computed profile could be correlated with actual wind conditions.

Figure C1 shows the computed sidewind profile for the powered boost portion of flight 7, the first mission analyzed, together with the profile obtained from a Rawinsonde balloon. The computed profile is a faired curve through the computed data points since there was a large amount of data scatter, as might be expected. The Rawinsonde weather balloon was launched during each mission as a normal part of X-24B flight operations in order to obtain current upper atmosphere data. As can be seen, correlation between the two wind profiles is poor with the Rawinsonde data showing none of the abrupt wind shifts and steep gradients seen in the theoretical profile. When a wind profile was computed from descent data through the same altitude range for this mission, however, good agreement with the ascent profile was obtained as shown in figure C2. The vertical offset between the two curves was attributed to pneumatic lag in the static pressure measurement caused by the rapid rates of climb and descent and resulting in pressure

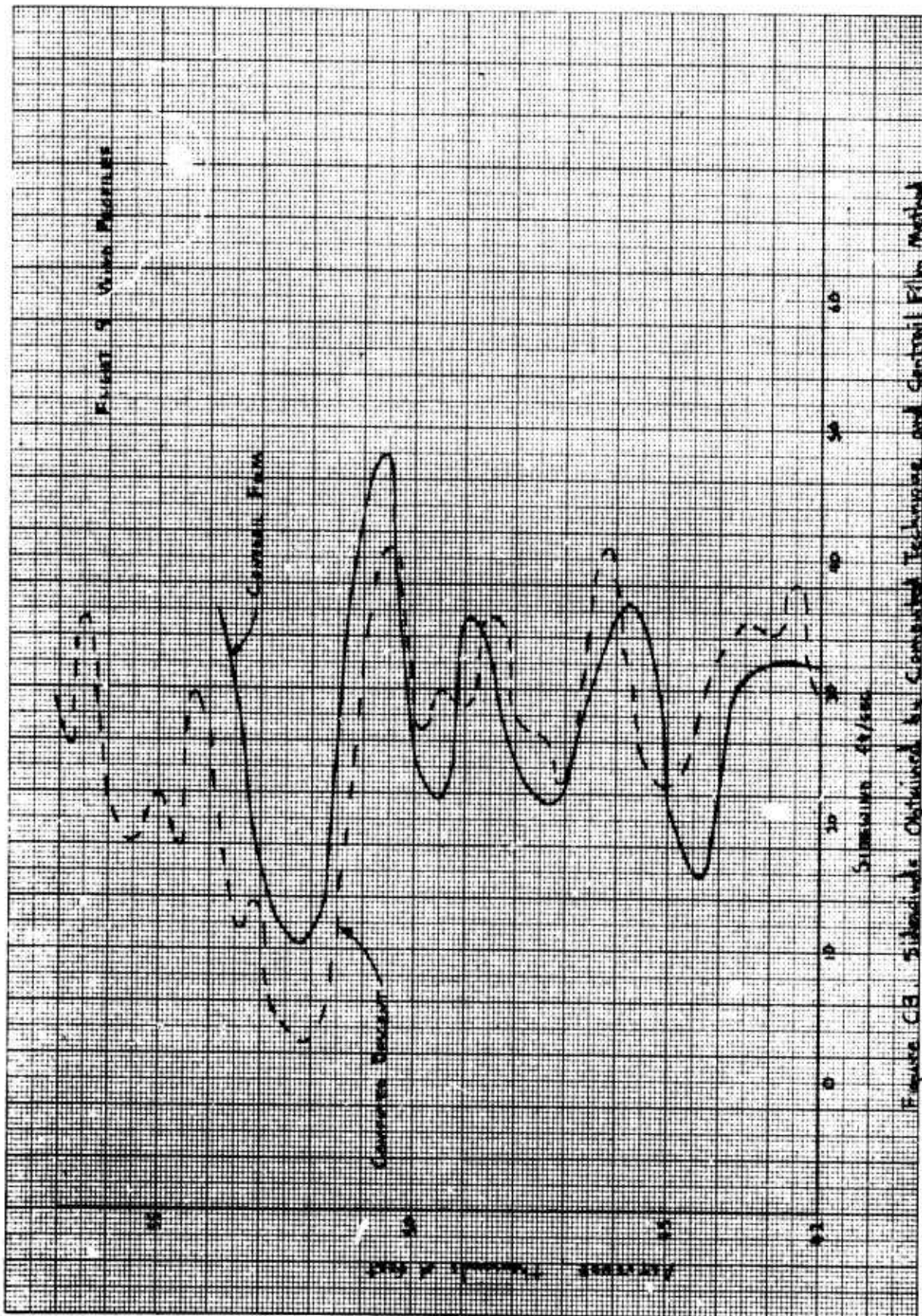


Figure 5. Video Profiles Obtained by Computer Technique and Control Film Method

altitude errors. This type of analysis was repeated using data from flight 6 and again good correlation was obtained between the computed ascent and descent profiles while correlation to Rawinsonde wind data was poor. These results were taken as an indication that the computed profiles could be presenting a better picture of the upper atmosphere wind conditions than that obtained from the Rawinsonde data.

Other independent methods of obtaining wind profiles were explored in an attempt to substantiate the computed wind profiles. Beginning with flight 9 a fixed ground-based camera was used to film the contrail left by the X-24B during the powered boost portion of the mission. A crude wind profile was computed from this film by measuring the lateral movements of the contrail with time. This analysis indicated that there were sharp wind changes with altitude and a profile was obtained with agreed very well with the computed sidewind disturbance profiles (figure C3). Once again, the agreement with the Rawinsonde data was poor.

On flight 10, a wind profile was obtained using a Jimsphere balloon tracked by FPS-16 radar. This is a more accurate and responsive technique for measuring winds aloft and has a published capability of determining the mean wind value in an altitude increment of 25-150 meters to within  $\pm 1.5$  kts.<sup>18</sup> The sidewind profile computed from the Jimsphere wind data showed the same type of abrupt wind changes with altitude seen in the computed sideslip disturbance profiles. Comparison between the Jimsphere data and the winds computed during the descent portion of this mission was good while the Rawinsonde wind data showed almost none of the steep gradients and abrupt shifts seen in the other data (figure C4).

Jimsphere balloon data were obtained for flights 11 and 13 and, once again, comparison with the computed profiles for these missions was very good. This agreement was taken as verification that the steep gradients and abrupt wind shifts indicated by the computed wind profiles were, in fact, present in the upper atmosphere. Based on this, it was concluded that the lateral-directional disturbances noted during the powered boost portion of several X-24B missions were caused by abrupt wind changes with altitude combined with the rapid ascent rate. Similar "disturbances" were often observed during the powered climb portion of flights in the X-24A, M2-F3 and HL-10, although each vehicle responded somewhat differently to the disturbance.<sup>19</sup> It was also noted that the Rawinsonde wind data provides average wind values over relatively large altitude increments and does not, therefore, reflect higher frequency wind shifts such as those seen in the data from the radar-tracked Jimsphere balloon.

<sup>18</sup>Reference 14: Anon., Reliability of Meteorological Data, Meteorological Working Group, Inter-Range Instrumentation Group, Document 110-71, Secretariat, Range Commanders Council, White Sands Missile Range, New Mexico, March 1971.

<sup>19</sup>Reference 15: Hoey, Robert G., Flight Test Handling Qualities of the X-24A Lifting Body, AFFTC-TD-71-11, Air Force Flight Test Center, Edwards AFB, California, February 1973.



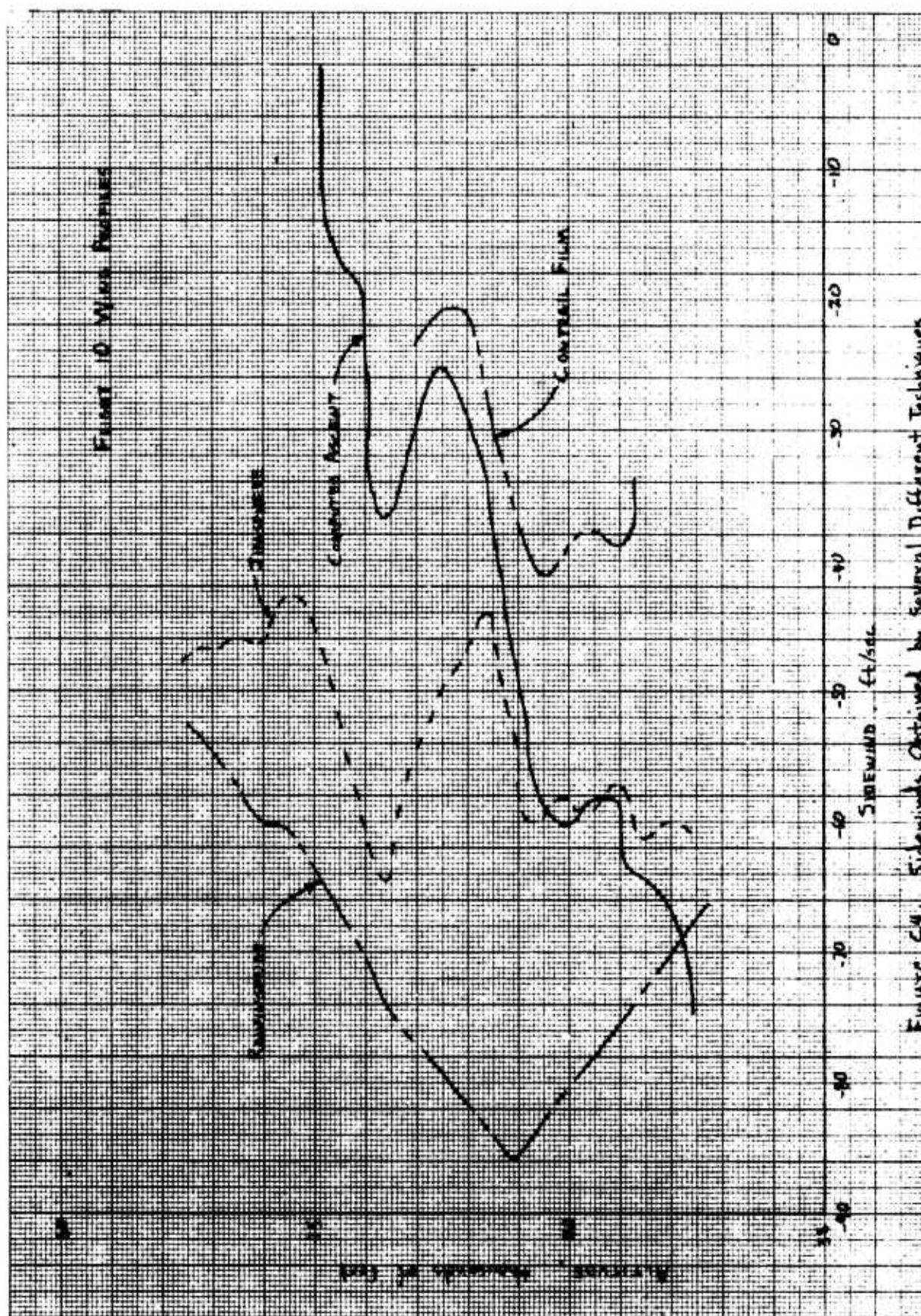
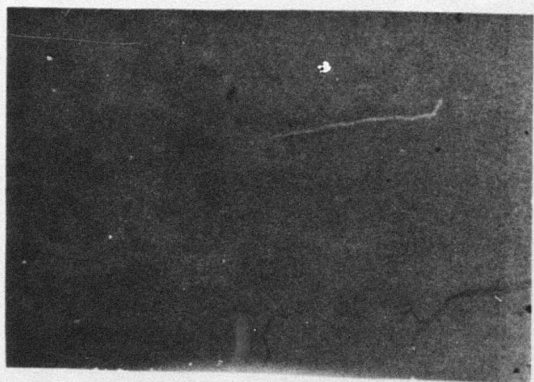


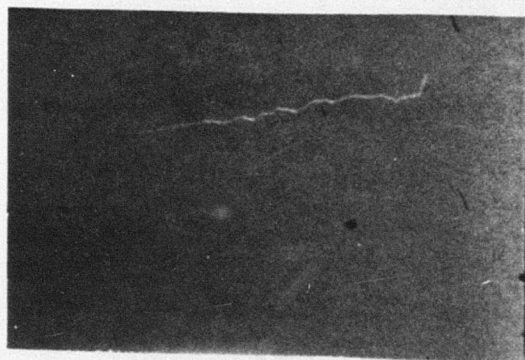
Figure C4. Sidewinds Obtained by Several Different Techniques

In addition to the above, one further item was noted. During the course of this program several lateral-directional data maneuvers produced poor results when extraction of stability derivatives was attempted. One possible cause for this is the wind-induced sideslip disturbances were encountered during the data maneuver resulting in values for measured sideslip angle which could not be made to agree with sideslip computed from the equations of motion with only the stability derivatives as variables.

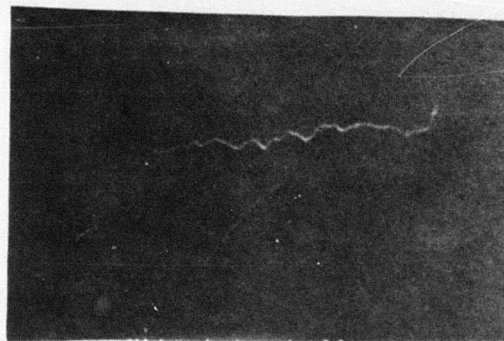
In summary, this investigation was conducted in an attempt to determine if lateral-directional disturbances noted during the boost phase of several X-24B missions could be related to wind disturbances. The approach taken was to compute the wind profile required to account for differences between the measured sideslip angle and sideslip computed from the equations of motion (the differences being, by definition, uncommanded sideslip disturbances). These computed profiles were then related to actual wind conditions by correlation with wind profiles by observation of the movements in the contrail left during the powered boost and by radar-tracked Jimsphere balloons. In addition, the computed profiles for the ascent and descent of the same mission generally agreed quite well with each other. Based on this it was concluded that the type of upper atmosphere wind behavior indicated by the computed wind profiles could exist and that the reported lateral-directional disturbances were attributable to wind disturbances.



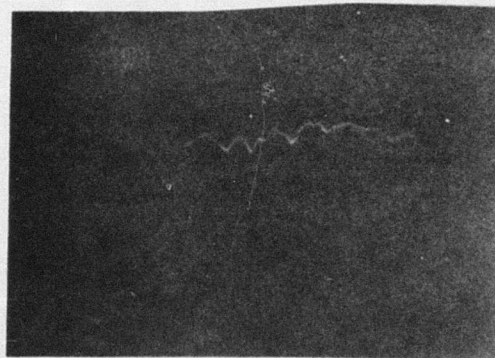
Elapsed time = 0 seconds



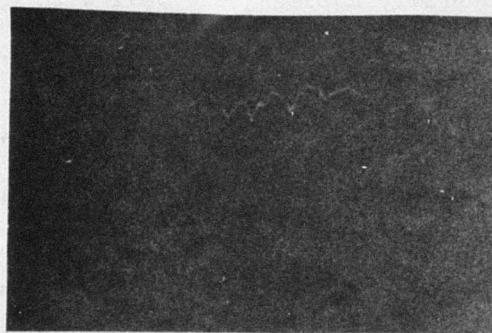
Elapsed time = 20 seconds



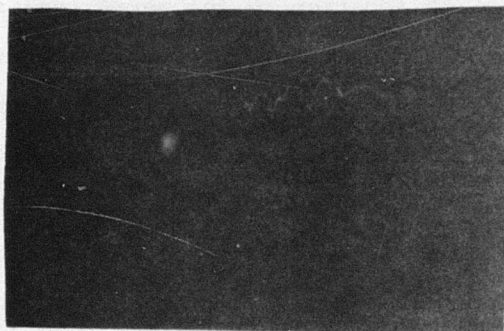
Elapsed time = 40 seconds



Elapsed time = 60 seconds



Elapsed time = 80 seconds



Elapsed time = 100 seconds



## **APPENDIX D**

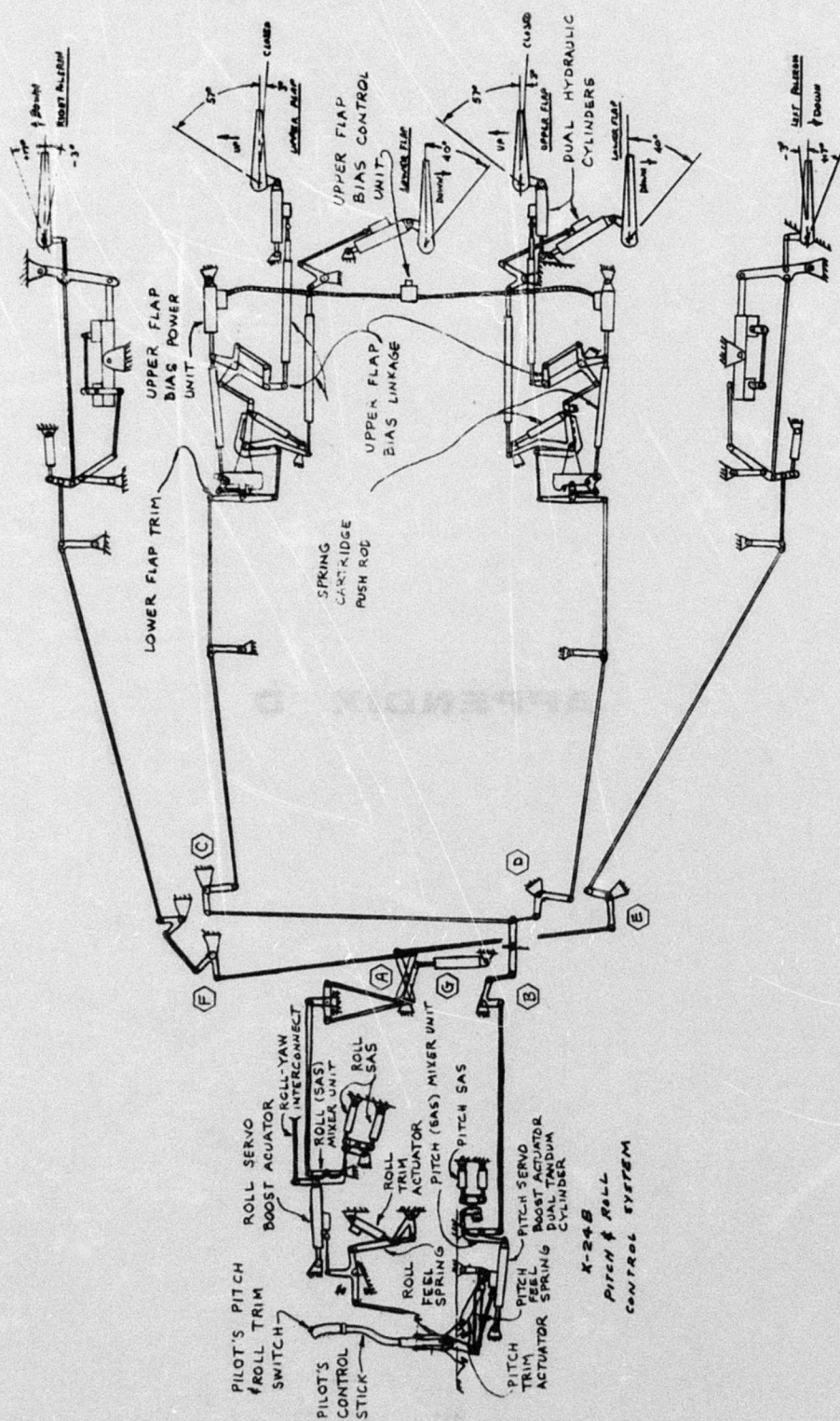


Figure D1. Flight Control System Schematic (Pitch and Roll)

## APPENDIX D

### FLIGHT CONTROL SYSTEM

The X-24B flight control system was basically an X-24A flight control system with strake ailerons added for roll control in lieu of roll control on the lower flaps (elevons). The X-24A flight control system was described in detail in Measured Characteristics of the X-24A Lifting Body Flight Control System,<sup>20</sup> and a detailed description will therefore not be repeated in this report. Only a cursory analysis of the system, and the data describing the system, will be presented.

#### System Description

Schematic linkage diagrams for the X-24B flight control system are shown in figures D1 and D2. A control system block diagram is given in figure D3. The X-24B flight control system was fully powered and irreversible. Stick commands in pitch and roll were transmitted to a hydraulic power boost actuator. The boost actuator prevented force and motion feedback to the pilot's stick. Outputs of the boost actuator were summed with stability augmentation system (SAS) inputs, mechanically mixed, and then transmitted to the hydraulic servo valve driving each of the control surface actuators. Rudder pedal deflections were mechanically mixed with SAS and aileron-to-rudder interconnect (KRA) inputs and mechanically transmitted to the hydraulic servo valve of the rudder surface actuators. An artificial feel system gave a sense of control force to the pilot under all flight conditions. These control stick and rudder pedal forces were produced by spring bungees. Trim was provided in all three axis through electric actuators which biased the zero force position of the stick and rudder pedals.

Relatively simple mechanical changes were made to the X-24A to convert it from a system which used lower flaps as elevons (pitch and roll control), to the X-24B which used the lower flaps for pitch control only and added outboard strake ailerons for roll control. Referring to figure D1, the scissor linkage marked "A" was a pitch/roll mixer which sent both pitch and roll commands to the lower flaps through rods which connected the outputs of linkage "A" to bellcranks "C" and "D". Pitch commands were transmitted to linkage "A" through a rod which connected bellcrank "B" to the input of linkage "A" (replacing preload spring "G"). Rods connecting bellcranks "B" and "D", "C" and "D", linkage "A" and bellcranks "E" and "F" (and of course, the aileron system downstream of "E" and "F") were not contained in the X-24B flight control system.

<sup>20</sup>Reference 16: Kirsten, Paul W., Measured Characteristics of the X-24A Lifting Body Flight Control System, AFPTC-TD-71-12, Air Force Flight Test Center, Edwards AFB, California, October 1972.



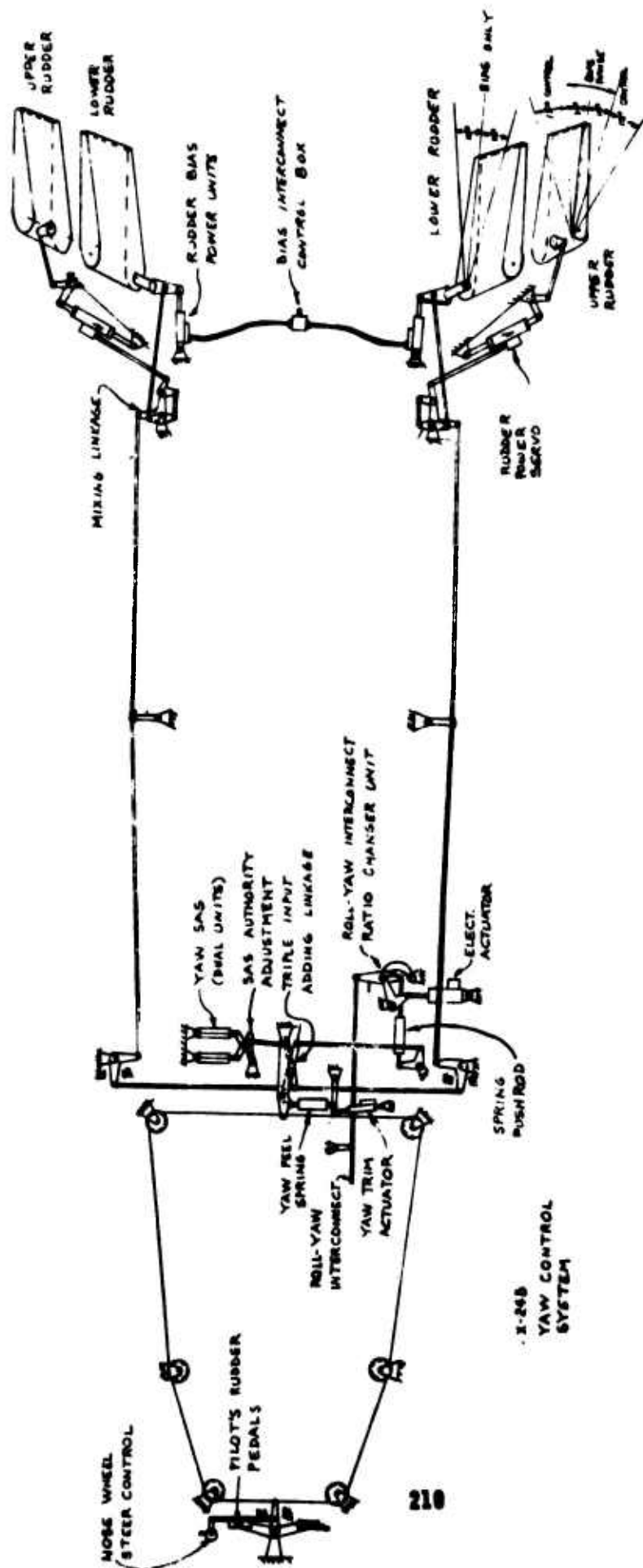


Figure D2. Flight Control System Schematic (Yaw)



The vehicle's flight controls used two hydraulic systems with one 2,750 psi and one 3,000 psi pump in each system (a total of four pumps). The two systems were independent but operated simultaneously to supply hydraulic pressure to the hydraulically dualized control surface actuators, the six SAS servo actuators (two in each axis), and the pitch/roll boost actuators. Thus, for normal operation of the aircraft, each hydraulic system provided one-half the power required to operate the control surface actuators. Also, the No.1 hydraulic system served as the sole power source for the No.1 SAS servo actuators, while the No.2 hydraulic system provided the sole power for the No.2 SAS servo actuators. During the X-24A program, it was found that two high pressure hydraulic pumps provided sufficient volume flow for most of the flight of the aircraft. This allowed the aircraft to be flown with two of the pumps off, except for the landing approach, and thereby reduced the hydraulic pump battery requirement from four to two. The X-24B was able to utilize the same procedure. From launch through most of the flight, only the high pressure pumps were operating; just prior to the landing pattern, the two remaining low pressure pumps were turned on for the landing maneuver where higher demands by the pilot and SAS system might require the additional hydraulic capability.

The X-24B was provided with stability augmentation about the pitch, roll, and yaw axis. The SAS was a simple rate feedback system used to augment vehicle damping. The system for each axis was triply redundant, thus providing fail-operational capability. The fail-operational criterion was that a single failure in any axis would not degrade the performance and authority of that axis.

Seven SAS gains were available to the pilot in each axis through rotary switches in the cockpit. Zero-gain switches were also provided in the cockpit for the purpose of disengaging each axis of the SAS. Washout filters in the pitch and yaw SAS prevented constant angular rates, as sensed by the rate gyros, from commanding constant elevator or rudder deflections and allowed the SAS servos to continually operate from a nominal centered position.

A lateral acceleration feedback ( $a_y$  feedback) was added to the SAS during the flight program to increase the aircraft's power-on stability at transonic and supersonic Mach numbers and to aid in keeping the vehicle trimmed directionally with the rocket engine on. The  $a_y$  accelerometer was located 15.5 feet forward of the reference center of gravity to include desired yaw rotational acceleration terms. It was nearly aligned with the vertical cg to minimize undesirable roll acceleration effects. The accelerometer location and gain (1.0 deg/ft/sec) were determined through AFFTC simulator studies. The accelerometer output was added to the normal yaw SAS rate-feedback signal which drove the yaw SAS servo actuator. The  $a_y$  feedback was not washed out.

Stick shaker and sideslip warning systems were added to the X-24B flight control system to alert the pilot of areas of potentially poor stability and control. The stick shaker, a standard F-104 unit, was triggered when the indicated angle of attack reached a value of 16 de-



degrees. This alerted the pilot that he was approaching a mild pitchup region. The system vibrated the control stick at a low amplitude and a frequency of 8 Hz. The sideslip warning system was installed in the aircraft prior to flight 19. The system produced an audio signal when the vehicle's sideslip angle reached a value of plus or minus 3.5 degrees. This was installed to warn the pilot of areas of poor directional stability.

The upper and lower flaps, and upper and lower rudders could be biased outward for increased stability at transonic and supersonic speeds and inward for reduced drag at subsonic speeds. The upper flaps could be biased by a low rate trim motor independently of the pilot's control stick inputs. The upper flap bias power unit also drove a lower flap bias linkage. The relationship between upper flap bias and lower flap bias was fixed mechanically by the flap bias linkage and was identified in terms of the upper flap bias position. In the manual mode the pilot was able to bias the flaps to any desired position by means of a "beeper" switch located on the landing rocket throttle handle. There was an automatic flap mode which programmed the upper flaps as a function of Mach repeater position; however this mode was never used during the X-24B program. (The Mach repeater was a device used to drive the interconnect and the upper flap bias. It could be positioned by the pilot in the manual mode or would drive from a Mach sensor in the automatic mode. The automatic mode was never used.)

A variable upper flap bias, in conjunction with variable lower flap and rudder biases (for maintaining trim), was used as a speed brake for energy management purposes in the subsonic region. (The aircraft did not have independent surfaces for speed brake usage).

A backup mode for positioning the upper flap bias was provided by the emergency flap bias mode. The emergency mode system consisted of a direct electrical signal from the upper flap bias emergency switch, through a circuit breaker, to the upper flap bias power unit, giving as simple a system as possible.

Upper and lower rudders could be biased (simultaneous inboard or outboard deflection of all four surfaces) independently of the pilot's rudder pedal inputs. Rudder pedal inputs caused movement of the upper rudders only. Automatic and manual modes were also available in the rudder bias system. Mode selection was available to the pilot through a toggle switch. In the automatic mode, the rudders were electrically biased as a function of upper flap bias position. The rudders were biased in accordance with a schedule, established using the AFFTC simulation, which gave minimum trim change as the upper and lower flap biases were changed. In the manual rudder bias mode, the pilot was able to bias the rudders to any desired position within the preset limits by means of a "beeper" switch. The automatic rudder bias mode was the standard mode used during the X-24B flight test program.

The X-24B was equipped with a mechanical aileron-to-rudder interconnect (KRA) to reduce adverse yaw tendencies during rolling maneuvers. The interconnect caused the upper rudders to be deflected in response to roll stick commands by the pilot. The sense of the interconnect was such that right stick command (positive commanded aileron) produced right rudder deflection (negative  $\delta r$ ). Roll SAS inputs were not transmitted through the interconnect. Automatic and manual modes of the KRA gain were available to the pilot through a toggle switch. In the automatic mode, the interconnect gain was programmed as a function of pilot-selected Mach repeater position and indicated angle of attack (a syncro signal from the pilot's angle of attack indicator). In the manual mode, the pilot was able to select any desired fixed interconnect gain through a "beeper" switch. The automatic KRA mode was the standard mode used during the X-24B program. This provided automatic gain scheduling as angle of attack changed, and the pilot could select the desired slope of interconnect ratio per degree angle of attack by adjusting the Mach repeater position. Two Mach repeater settings were normally used during a flight; a setting which gave a high slope of KRA versus angle of attack for use at transonic and supersonic Mach numbers, and a setting which gave a lower slope for use at subsonic Mach numbers during the approach and landing.

An emergency KRA mode was contained in the flight control system for redundancy. This mode was available to the pilot through the three-position automatic/manual/emergency switch. The automatic or manual position of the three position switch energized the primary KRA motor. The emergency position connected the "beeper" switch to the second motor. Thus, the second motor was used in a manual mode as a fully redundant system when the emergency mode was selected.

#### System Performance

Very few failures or malfunctions of the flight control system occurred during the X-24B flight test program. No significant inflight failures were experienced. This can be attributed to the fact the X-24B used, for the most part, a system whose reliability had been developed and proven during the X-24A program. Good maintenance procedures and personnel, preflight functional tests which ground checked system operation, and flight operational checks through real-time monitoring and postflight data analyses, insured that the system reliability developed during the X-24A program was maintained throughout the X-24B program. Failures or malfunctions which occurred during flight, or during preflight checks the day of a flight, are listed and discussed below. The first failure discussed (simultaneous failure of three SAS gyros) is significant from failure analysis standpoint.

1. The roll/yaw SAS failed the Spin Motor Rotation Detection (SMRD) test during the captive portion of the first flight. The SMRD test was performed before launch on every flight and verified that the SAS gyros rotated properly. The SAS gyros in the roll and yaw axis were sent to the contractor for inspection. Four of the gyros (two in roll and two in yaw) were found to be inoperative and would have caused total SAS failure in the roll and yaw axes during flight. Although the problem was felt to be caused by a combination of age and

rough handling, no evidence of damage was found by the contractor. Discoloration of grease in one gyro, and dryness and caking in another were the only abnormalities found. The gyros were the same gyros used in the X-24A and had not been used for some time (approximately two years). They had, however, been used and performed well, during the functional ground tests (such as SAS checks, limit cycle and structural resonance tests, etc.) conducted on the vehicle in preparation for first flight. They had also functioned normally during the planned captive flown prior to the failure during the attempt at a first glide flight. All gyros in the SAS system were changed as a result of this failure.

2. The stick shaker trigger point shifted from 16 degrees to 14.5 degrees during flights 2 and 3. The stick shaker system was reworked to correct for temperature sensitivity, and the problem did not reoccur on subsequent flights.

3. An amber light (indicating a single failure in the triplex system) was obtained in the yaw SAS axis during the preflight ground control system checks for flight 10. An investigation of the three yaw SAS gyros indicated different damping characteristics between the three. It was felt that the different damping characteristics could have caused the failure indication. Therefore it was decided to replace all three yaw gyros. In addition, a loading problem between one of the yaw SAS channels and the instrumentation system was discovered, which could also have been causing the failure indication. This problem was corrected. Changing the gyros and correcting the loading problem eliminated the yaw failure indication from occurring thereafter.

4. The pitch SAS amber light came on several times during pitch pulses performed with a zero gain setting in the pitch axis during flight 18. With the zero gain switch thrown, signals should not pass through the SAS electronics and logic circuitry, and a miscomparison of one of the three paths of the triplex system (indicated by the amber light) should not have occurred. The problem was found to be a failed zero-gain relay in at least one channel, so that a signal was getting through at least one of the channels and being compared with an open signal in another channel, causing a miscomparison and an amber light. All three zero-gain relays in the pitch axis were replaced, and the problem was eliminated.

5. A deadband in the left hand aileron system was first observed during flight 6, the first X-24B powered flight, and was later observed during several other powered flights. The aileron system was thoroughly checked between flights 6 and 10 in an attempt to eliminate the deadband. The rigging of the system was tightened, bushings were replaced, preload springs were lubricated, and rods and rod-end bearings were replaced. The deadband continued to occur during powered flights in spite of these efforts. Since it seemed to become larger as the mission progressed, and disappeared after the vehicle landed, it was felt the problem was temperature dependent. The liquid oxygen (LOX) vent line was just forward of the left aileron actuator bay. Also, the pressure and return hydraulic lines were routed close to the aircraft's skin, on the access door to the actuator bay, just aft of the LOX vent. It was felt that when LOX vented overboard, the left hand aileron compartment became significantly colder than the right side, thus cold-soaking some components in the left aileron system causing the deadband to occur.



In order to confirm cold-soaking as a possible cause of the deadband problem, a lab test was performed on a spare hydraulic actuator by routing one pair of pressure and return lines through a liquid nitrogen locker to demonstrate the effect of cold hydraulic fluid. As the lines were chilled, a deadband approaching the amount of deadband experienced in flight was observed.

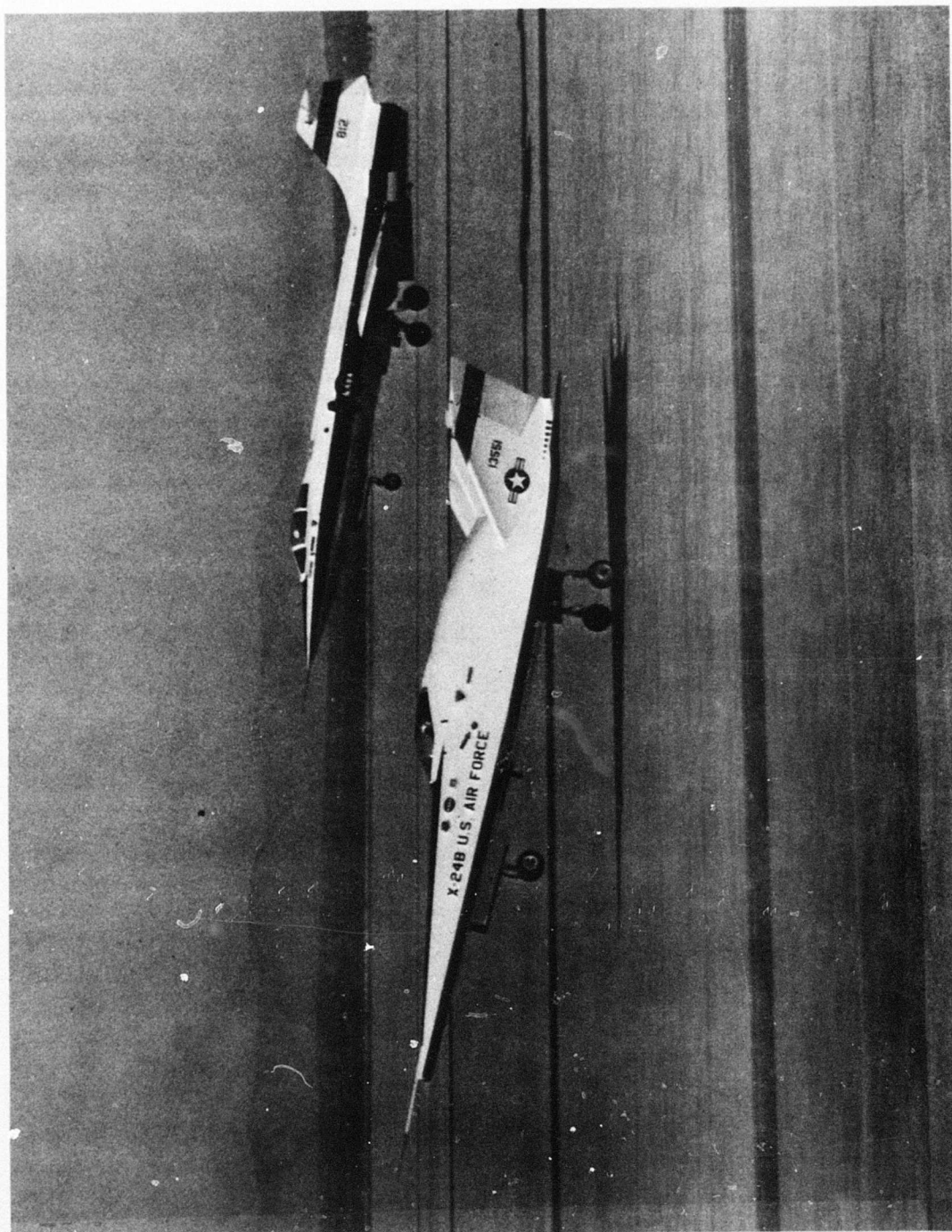
With this information, the following modifications and alterations were made to the vehicle's aileron system:

1. The hydraulic lines to the left hand aileron actuator were rerouted away from the access door and wrapped with thermal insulation.
2. The aileron actuator access door was insulated with a one inch thick polyurethane blanket.
3. Control position transducers (CPT's) were installed on the right hand and left hand aileron drive systems at three locations to determine where the deadband occurred in the system if the above two modifications did not eliminate the problem.
4. Temperature sensors were installed on the inside surface of both left and right aileron actuator access doors and in the compartment to measure air temperature surrounding the actuators.
5. Items 3 and 4 were telemetered to the control room for in-flight monitoring.

After the above modifications were made, a captive flight was flown for the purpose of verifying that the aileron deadband had been eliminated or reduced. Small, cyclic aileron inputs were initiated by the pilot at many points during the climb to the simulated launch point, and during a simulated X-24B flight (while still mated to the B-52) performed after the simulated launch point was reached. During this captive flight, it was confirmed that the left side of the vehicle did get significantly colder than the right side due to cold-soaking from the LOX vent flow. However, the relocation and insulation of the left hand aileron hydraulic lines and components reduced the deadband on this captive flight to a level which was below what had been experienced on previous powered flights. The final solution, however, was the modification of the LOX top-off procedure to minimize the amount of LOX that overflowed from the LOX vent port forward of the aileron compartment.

#### **Faired Test Data**

The flight control system data presented in this report was obtained from a complete, detailed ground test performed on the aircraft before the first flight (February 1973) and from checks on individual functions which had been changed after the February 1973 test was performed. The data presented in this report represent the fairings of the individual data points obtained from the ground tests. (Individual



NOTE: INCHES WERE MEASURED  
AT CENTER OF GRIP

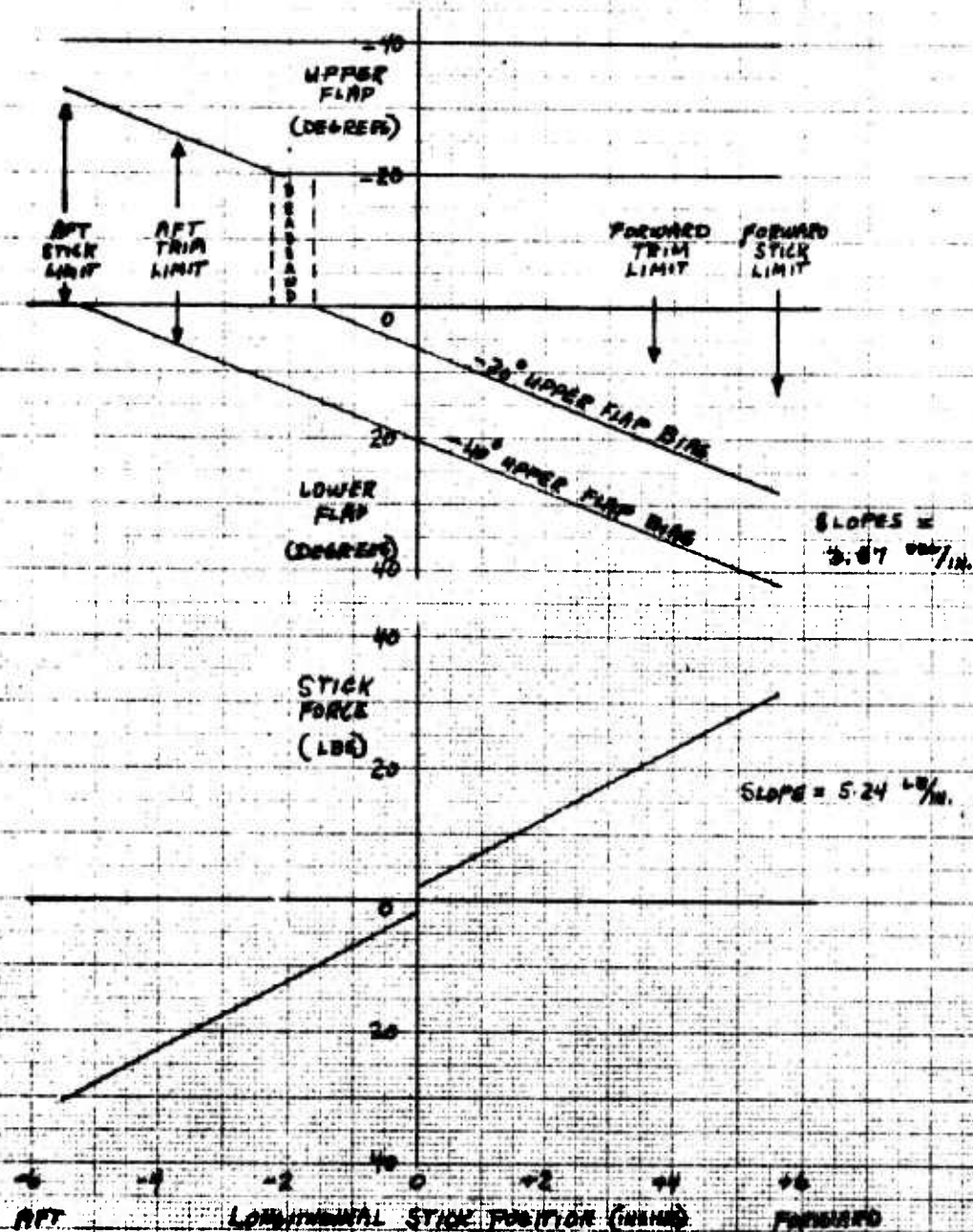


Figure 83. Longitudinal Stick Characteristics



data points will not be presented). This faired data eliminates scatter found in the individual data points, and usually represents an average of left and right side deflections of control surfaces. They do not show hysteresis effects for all cases. For the X-24B, (as was the case with the X-24A) hysteresis effects for most functions were usually very small and could be neglected.

The longitudinal stick characteristics of the X-24B are shown in figure D4. As shown in the top half of the figure, flap position versus stick deflection was a linear function whose slope was invariant with upper flap bias position. (In the X-24A, stick to surface gearing had been a function of upper flap bias position). The faired line for the -20 degree upper flap bias case shows the amount of deadband (approximately one-half inch of stick) in the crossover region between the lower and upper flaps. An attempt to reduce this deadband was made during the flight test program but was abandoned due to the fact that the proposed fix produced a more sensitive lower flap from a structural resonance standpoint. Also, very little flight time was spent with the flaps in the crossover region, and the deadband in flap motion experienced in this region apparently had very little effect upon the handling qualities of the vehicle. Pitch stick force was a single slope, linear function of stick position. Pitch force gradient was 5.24 lb/in and the pitch breakout force was  $\pm 2.0$  pounds. Hysteresis in both stick versus surface deflection and stick deflection versus force was small and immeasurable.

Lateral stick characteristics are shown in figure D5. The data which are shown for an aileron bias of 7 degrees, are valid for all bias positions. Aileron position and stick force were single slope, linear functions of stick position. Lateral stick gearing was 1.62 deg/in, the stick force gradient was 2.7 lb/in, and the breakout force was 2.0 lbs. Hysteresis in lateral stick versus surface deflection was immeasurable. There was a small hysteresis band of 1.2 pounds in lateral force versus stick deflection.

Rudder pedal characteristics, which were valid for all rudder bias positions, are shown in figure D6. Rudder position and rudder pedal force were also single slope, linear functions of rudder pedal deflection. Rudder pedal gearing was 5.75 deg/in, force gradient was 21.5 lb/in and breakout force was 11.5 lb. A hysteresis band of 2.5 pounds was present in rudder force versus rudder pedal deflection.

Rudder bias and lower flap bias were functions of upper flap bias position, rudder bias being an electrical function and lower flap bias a mechanical function. These functions are shown in figure D7 along with full pitch deflection. Limits of upper flap bias travel were -20 to -40 degrees for most of the flight test program. Rudder bias limits were set at -10 to zero degrees for most of the program. Full stick deflections produced approximately  $\pm 20$  degrees of flap motion from the lower flap bias position. Full longitudinal trim gave  $\pm 14.1$  degrees of flap motion from the bias position.

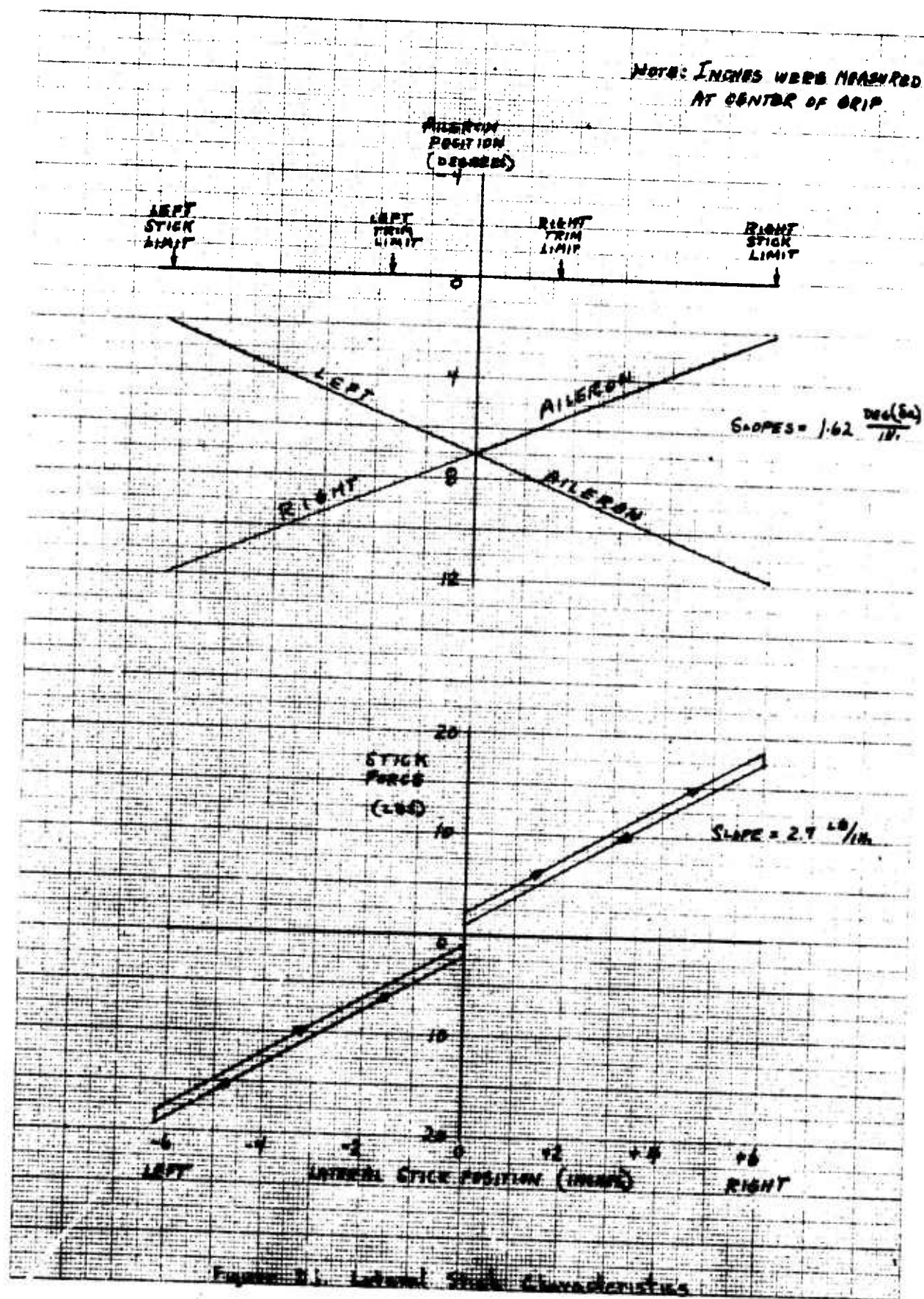


Figure 2.1. Lateral Stick Characteristics

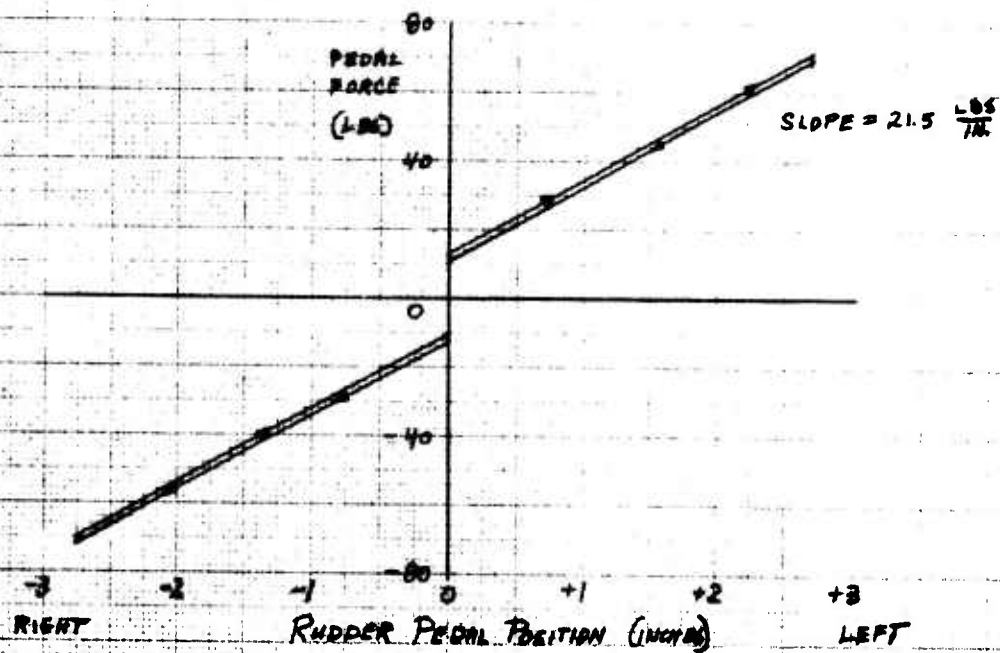
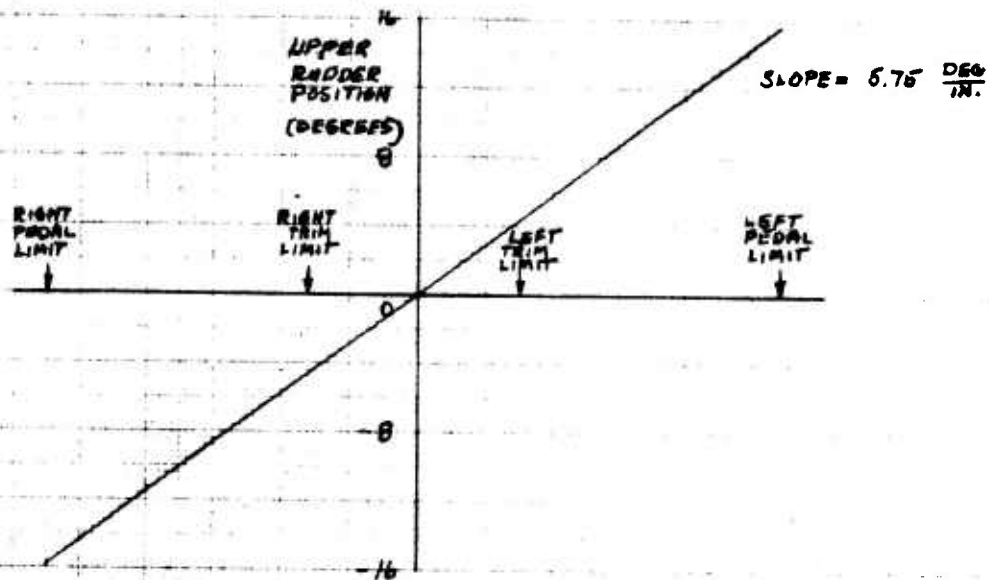


Figure D6. Rudder Pedal Characteristics



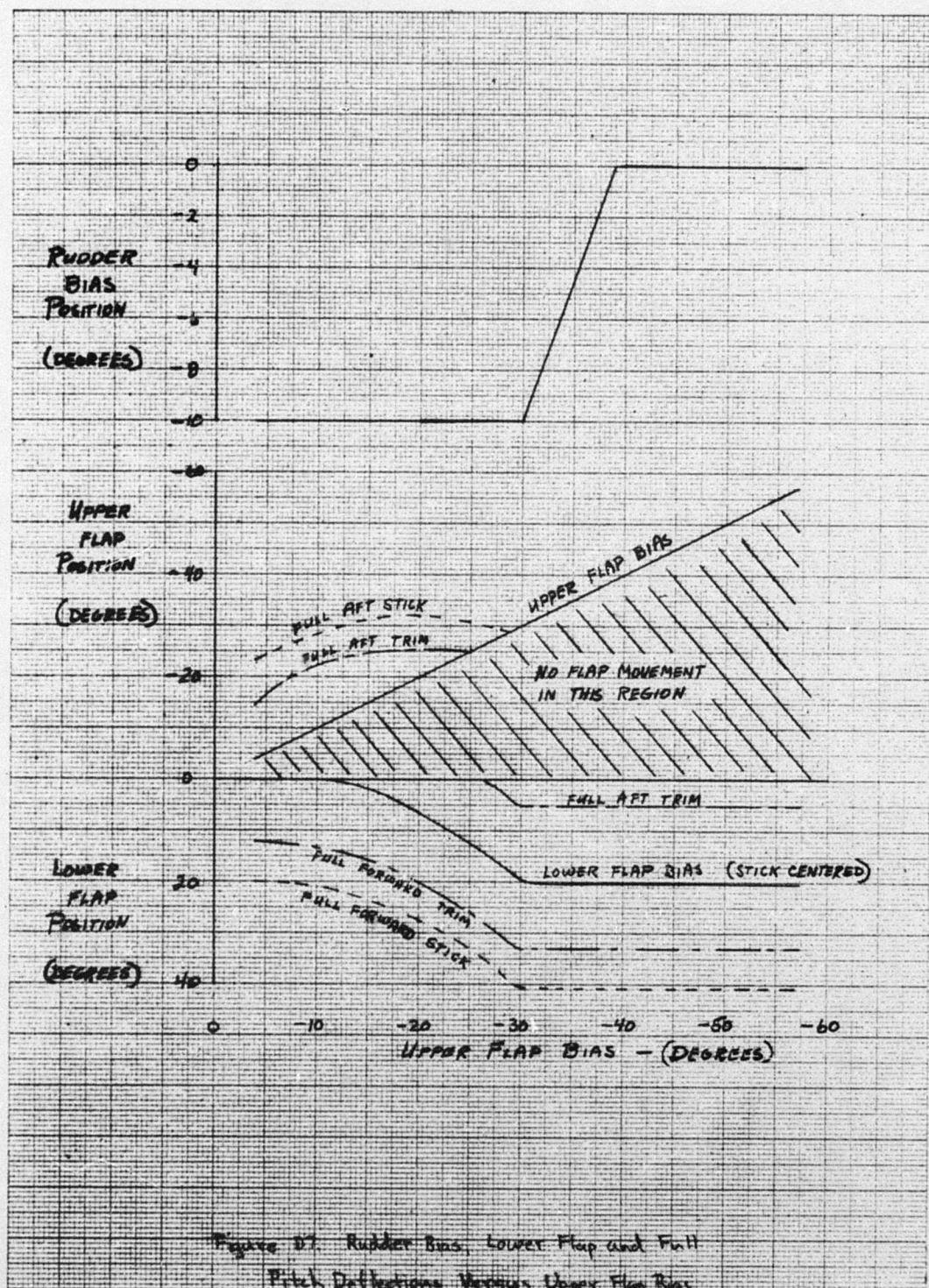


Figure 87. Rudder Bias, Lower Flap and Full Pitch Deflections Versus Upper Flap Bias

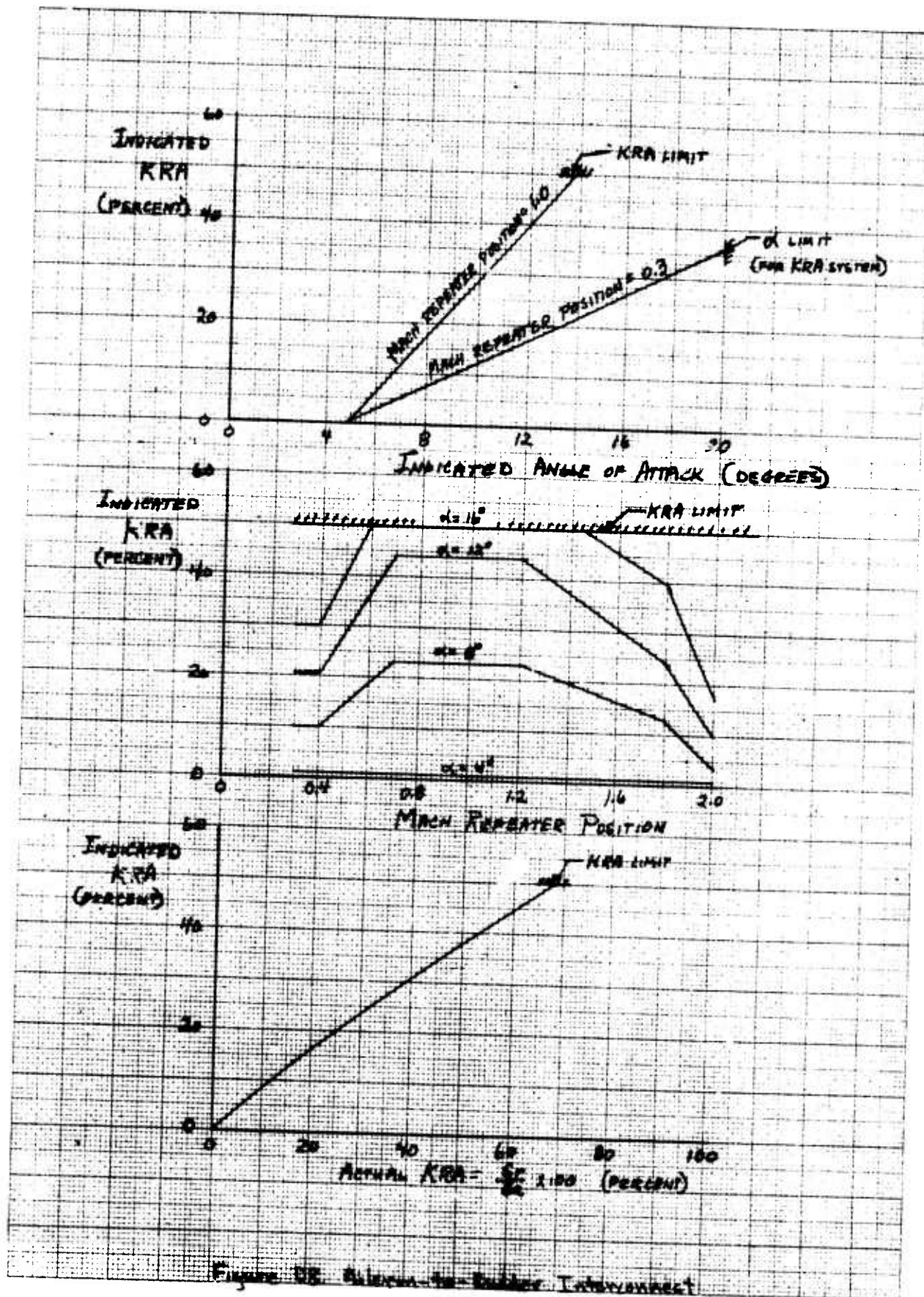
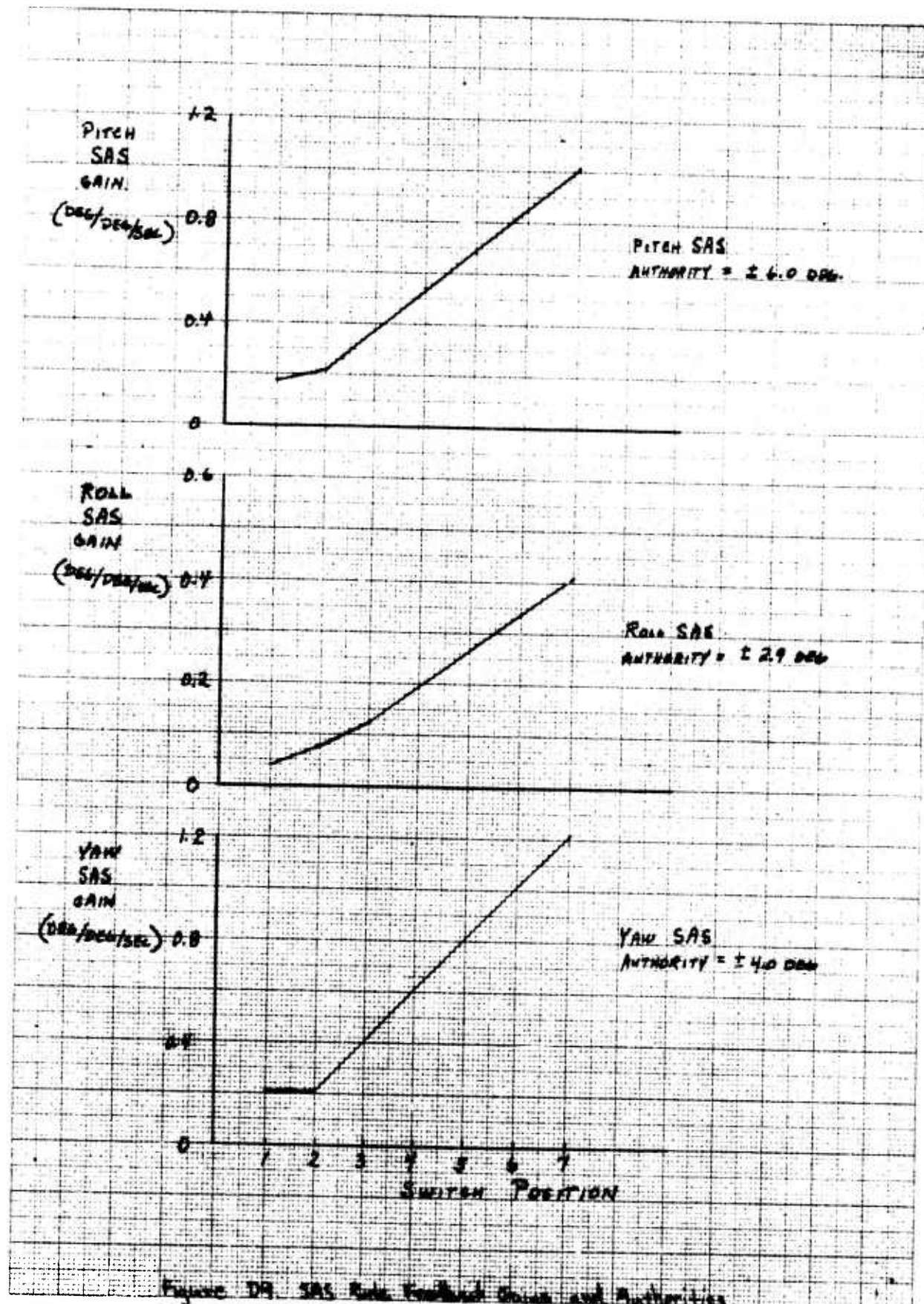


Figure 18. Radar-40 Radar Interconnect







Aileron-to-rudder interconnect ratio (KRA) was a function of indicated angle of attack and Mach repeater position (figure D8). Selection of Mach repeater position (by the pilot) gave a particular linear slope of indicated KRA versus indicated angle of attack. The two Mach repeater settings used throughout the entire program were 1.0 for transonic and supersonic Mach numbers and 0.3 at subsonic Mach numbers during the approach and landing. Percent indicated KRA versus indicated angle of attack for these two Mach repeater positions are shown in the top half of figure D8. KRA was zero below 5 degrees indicated angle of attack and varied linearly above 5 degrees as shown in the figure. Percent indicated KRA was the dial reading of the KRA indicator in the cockpit and was related to percent of KRA actuator travel. Thus, indicated KRA settings were numerical values with which the pilots were familiar and were not the ratios of rudder surface deflection to aileron surface deflection (actual KRA). The function for converting from indicated KRA to actual KRA is given at the bottom of figure D8. An KRA limit of 50 percent indicated was used throughout the program.

Stability augmentation system (SAS) gains and authorities for the pitch roll and yaw axis are given in figure D9. The seven gains in each axis which were available to the pilot during flight were obtained through seven-position rotary switches. Disengagement of the SAS in each axis was accomplished by three toggle switches. The normal SAS configurations during the flight test program were switch positions 6 in pitch, 5 in roll, and 3 in yaw for supersonic and transonic flight, and 4 in pitch, 3 in roll, and 2 in yaw for subsonic flight.

Limit cycle ground tests were performed on the X-24B aircraft in the pitch, roll, and yaw axes. A limit cycle oscillation is a sustained closed-loop oscillation of a control surface at relatively low frequencies (usually 1 to 5 Hz). The oscillation is created when the total phase lag of the loop is 180 degrees and the total gain of the loop is high. The "loop" referred to is composed of the feedback path in the flight control system from the SAS gyro to the control surface of each axis (pitch, roll, and yaw), plus the aerodynamic path from the rotational acceleration produced by the control surface to the rotational rate sensed by the SAS gyro. Approximately 90 degrees of the phase lag required for a limit cycle (180 degrees) is the aerodynamic lag between the rotational acceleration produced by the control surface deflection and the rotational rate of the aircraft as sensed by the SAS gyro. The additional 90 degrees of phase lag is created by the control system at some frequencies.

For the X-24B limit cycle ground test, a small analog computer was used to simulate the aerodynamic response of the vehicle in each axis (one axis at a time). The signal from the control surface position transducer of the aircraft was the input signal to the computer. The output of the computer was sent to the SAS gyro torquing motor in the aircraft to complete the loop required for limit cycle investigations. Limit cycle amplitudes and frequencies were then recorded as a function of total axis gain. Total axis gain was varied on the computer. A more complete discussion of flight control system instabilities is given by Paul W. Kirsten, in reference 16.

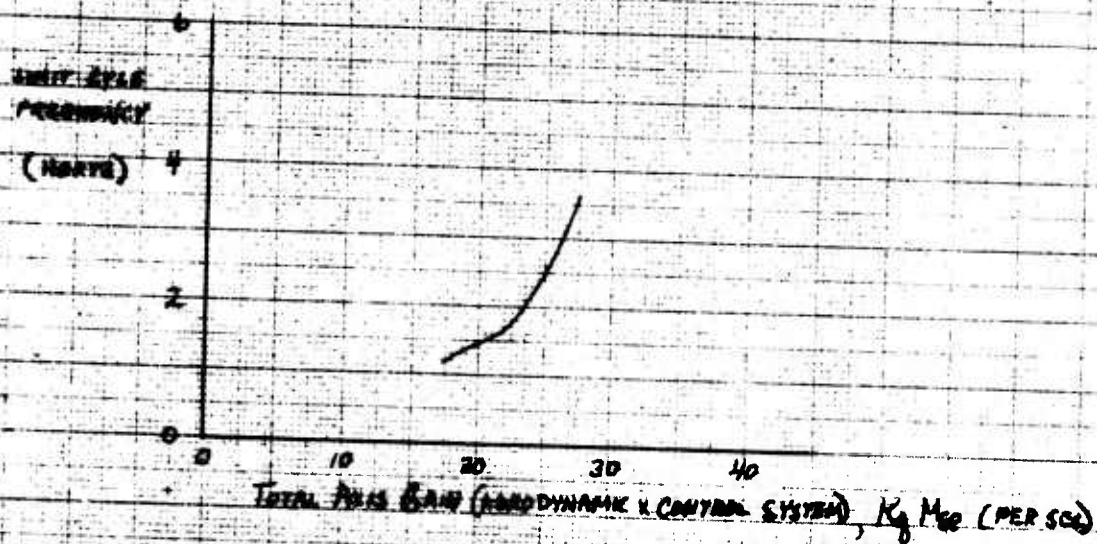
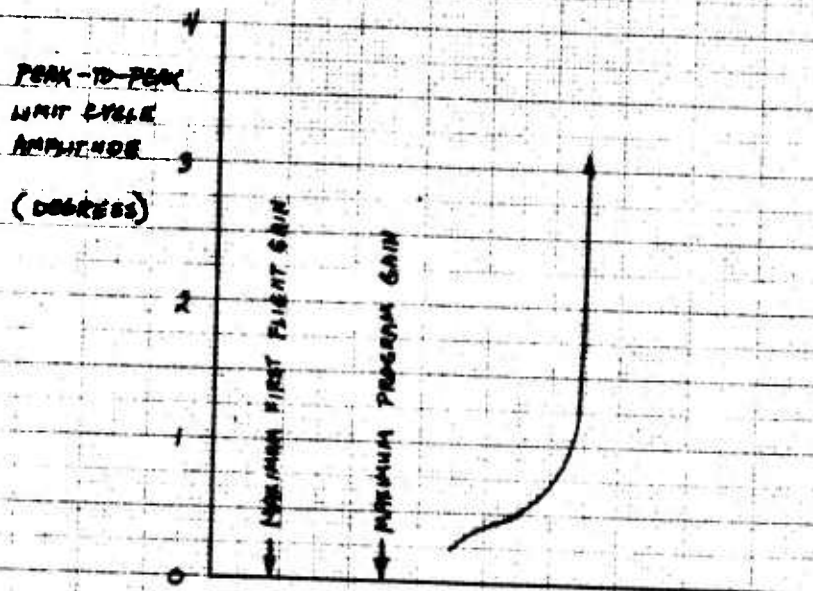


Figure D10. Pitch Limit Cycle Characteristics

Ground test limit cycle data for the X-24B are given in figures D10 through D12. These data were obtained just prior to the first flight (July 1973). Ground limit cycle test were repeated at monthly intervals for approximately six months after the first flight, or until the system was proven to be trouble-free from a limit cycle standpoint. All limit cycle ground test results obtained during the program were very similar to the July 1973 data presented in this report. Ground test limit cycle data were obtained by recording limit amplitude and frequency at each total axis gain setting (starting at low gain values). The total axis gain was increased until the value was reached at which the limit cycle oscillation diverged. These data completely define the ground limit cycle characteristics for a rate feedback system. Control system limit cycle gain margins can be established for each axis of the vehicle by comparing known or predicted flight values of total axis gain with ground test data.

Acceptable limit cycle gain margins for the X-24B were established by the following criteria:

1. The limit cycle amplitude measured during ground tests should be less than 0.5 degrees peak-to-peak at the highest total loop gain ( $K_Q M_{\delta e_L}$ ,  $K_p L_{\delta_a}$ ,  $K_R N_{\delta_r}$ ) expected in flight, and
2. The highest total loop gain expected in flight should be less than one-half of the total loop gain of the divergent limit cycle point measured in ground tests.<sup>2)</sup>

Maximum flight values of total loop gains in each axis are shown in figures D10 through D12 along with ground test limit cycle results. Maximum total loop gains for both the first flight and the entire flight test program are shown in the figures. Limit cycle gains margins in pitch, roll, and yaw for the X-24B were large, and the criteria shown above were easily satisfied. No in-flight limit cycle tendencies were observed during the entire flight test program.

Structural resonance ground tests were performed on the X-24B prior to the first flight (July 1973). Structural resonance is an oscillation of a control surface at a resonant structural frequency. It is usually caused by control system sensors (such as rate gyros) sensing small vehicle structural vibrations (caused by the surface moving) and sending these signals back to the control surface. At structural resonant frequencies (usually 10 Hz and above), these signals are amplified and a phase lag of 180 degrees may occur through the

<sup>2)</sup> These criteria were used for the first flights until flight control system characteristics and control surface effectiveness were established through flight test. If required, the margins could have been relaxed somewhat after vehicle characteristics were established.



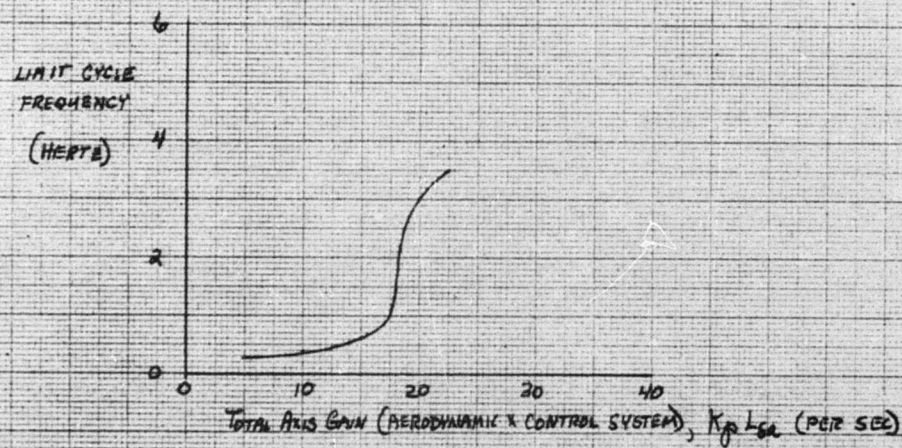
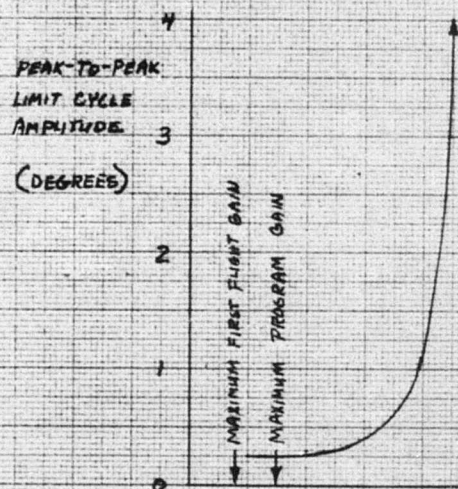


Figure 011. Roll Limit Cycle Characteristics

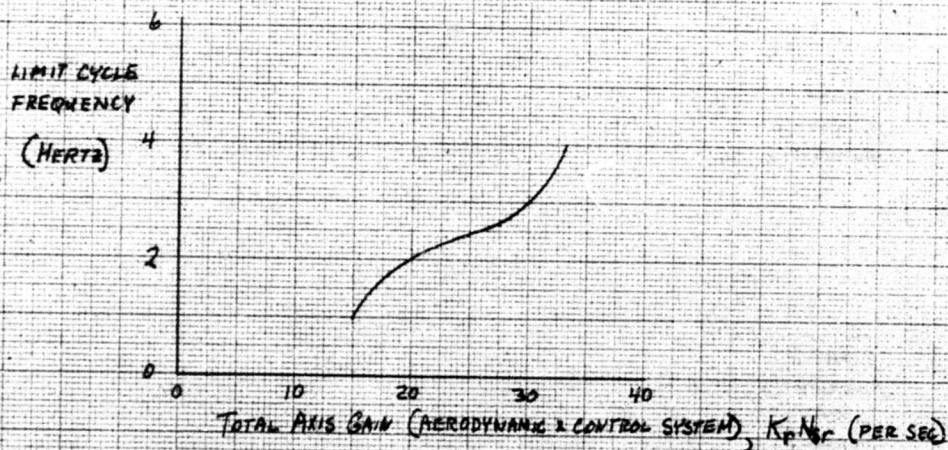
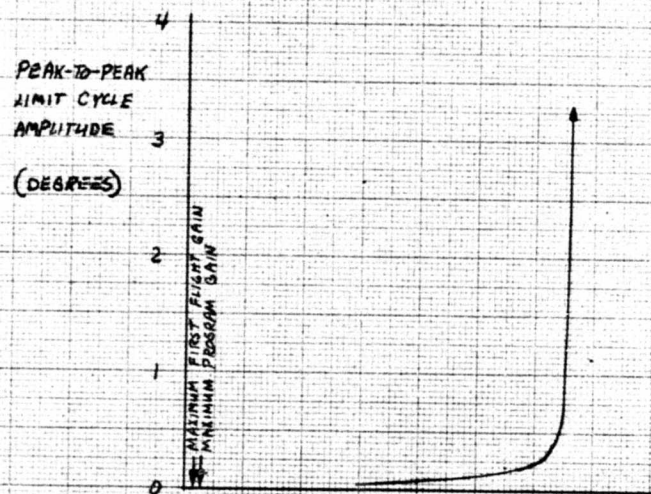


Figure D12. Yaw Limit Cycle Characteristics



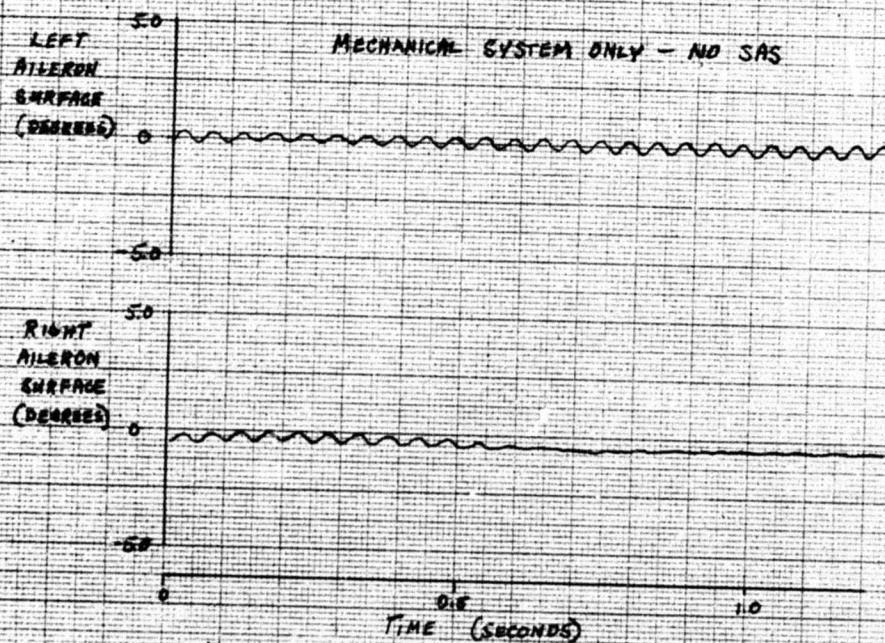


Figure D13. Aileron Mechanical Resonance

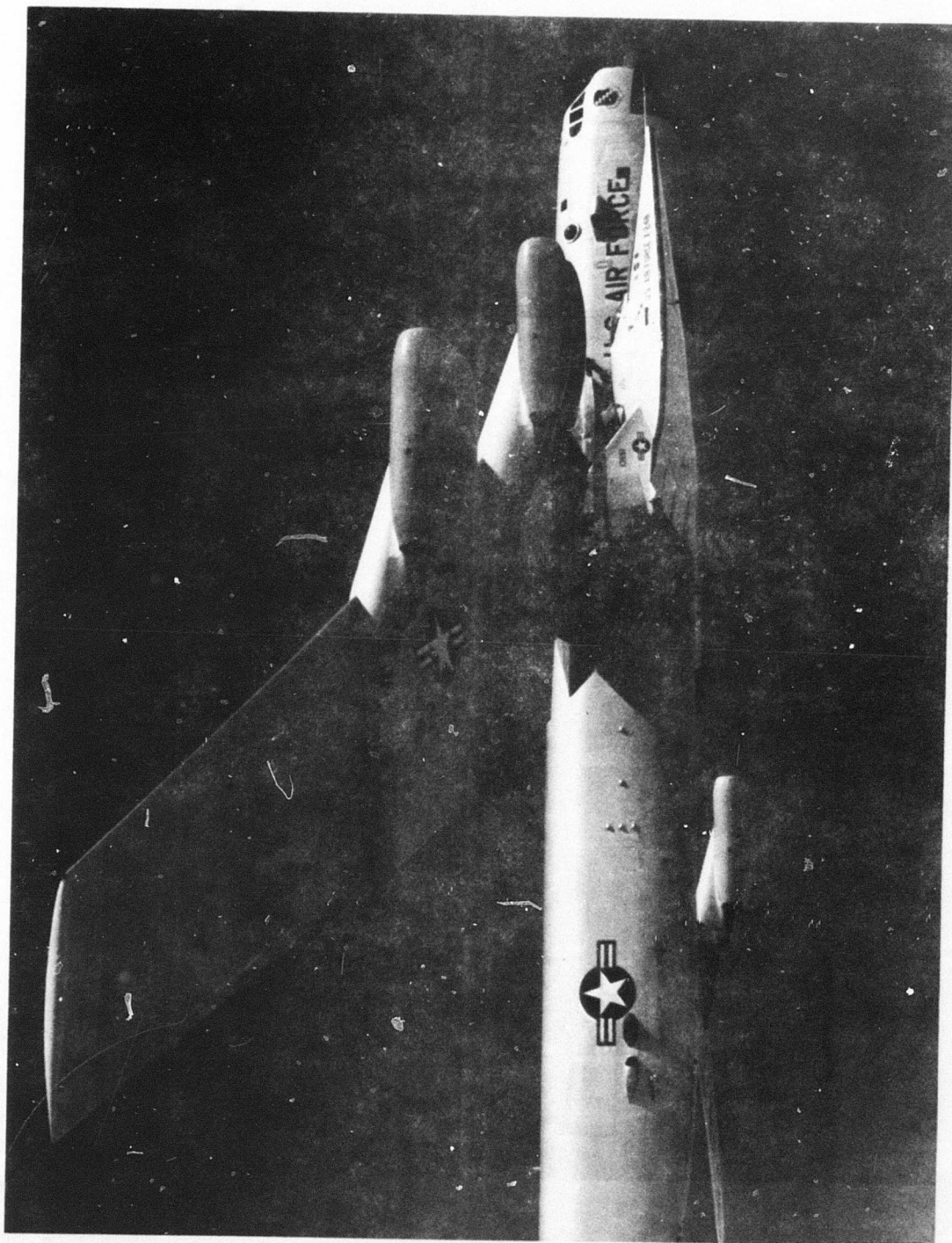


control system alone. If the phase lag from the sensor to the control surface is 180 degrees and the total system gain is high enough, the surface motion will sustain itself and structural resonance will occur. The structural resonance problem for the worst case is assumed to be independent of the vehicle flight conditions. Therefore, no aerodynamic closed-loop computations are required (it is not necessary to use an analog computer to simulate aerodynamic transfer functions).

The structural resonance ground tests consisted simply of varying the total axis flight control system gain in each feedback path (one axis at a time) and disturbing the system through the use of sharp inputs at each gain setting. The structural resonance criterion used for the X-24B was that each axis of the control system should be capable of operating on the ground at twice the maximum total axis gain to be used in flight without sustaining structural mode vibrations.

A structural resonance was found in the roll axis during ground tests. (No resonance was found in the pitch or yaw axis at gain settings up to twice the maximum gain to be used in flight). The frequency and amplitude of the resonance is shown in figure D13. The resonance was not the normal type of resonance which was sustained through the SAS feedback path. It was a purely mechanical resonance sustained solely within the aileron surface actuator and its associated linkage. (The resonance continued when the SAS was turned off). The resonance problem was eliminated by adding a mechanical damper within each aileron actuator. The damper decreased the sensitivity of actuator to high frequencies but did not significantly alter the response characteristics at the lower frequencies or reduce the maximum slew rate of the actuator.

After the mechanical resonance in the roll actuator was eliminated, structural resonance ground tests were again conducted on all three axes of the vehicle. A gain margin of a least a factor of two existed in all axes between the maximum SAS gain to be used in flight and the SAS gain at which resonance occurred during the ground tests. No in-flight structural resonance occurred during the entire flight test program.



## **APPENDIX E**



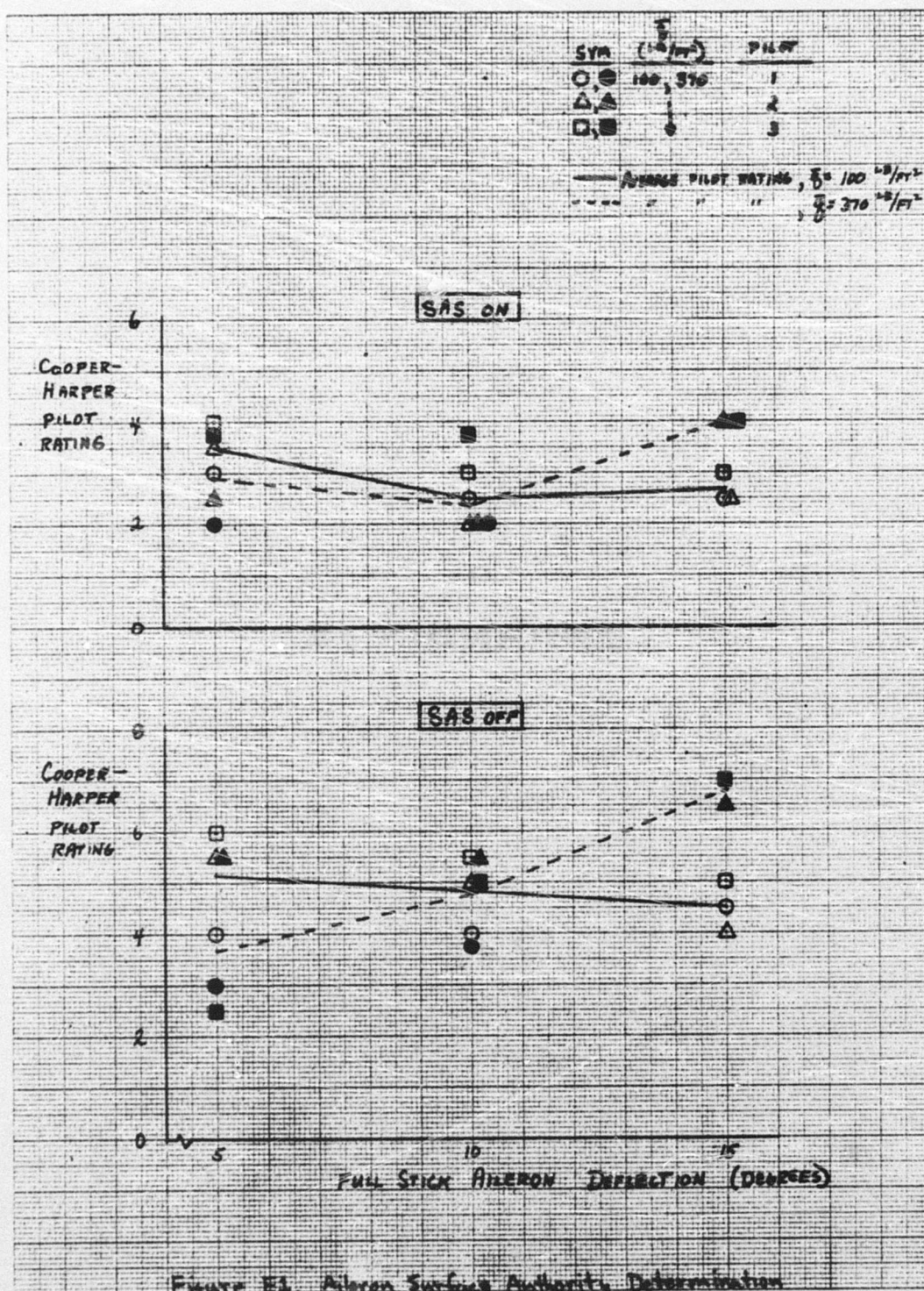


FIGURE E-1. Aileron Surface Authority Determination

## APPENDIX E

### PREFLIGHT SIMULATOR STUDIES

A thorough simulator investigation was conducted before the first flight of the X-24B to define the predicted handling qualities of the aircraft and to establish any stability boundaries that may have existed. Also, several studies were performed early in the design of the aircraft for the purpose of establishing control system parameters (such as gains, authorities, surface rate limits, etc.) for the new aileron system which differed considerably from the X-24A aileron system. Most of the preflight simulator studies concentrated on the aerodynamic environment and aircraft configurations that were to be used for the initial flights. Since these initial flights were unpowered glide flights, the Mach number region was 0.7 and below, and the primary configuration was  $\delta_{up} = +20^\circ$ ,  $\delta_{Rb} = -10^\circ$ , and  $\delta_{Ab} = 7^\circ$ .

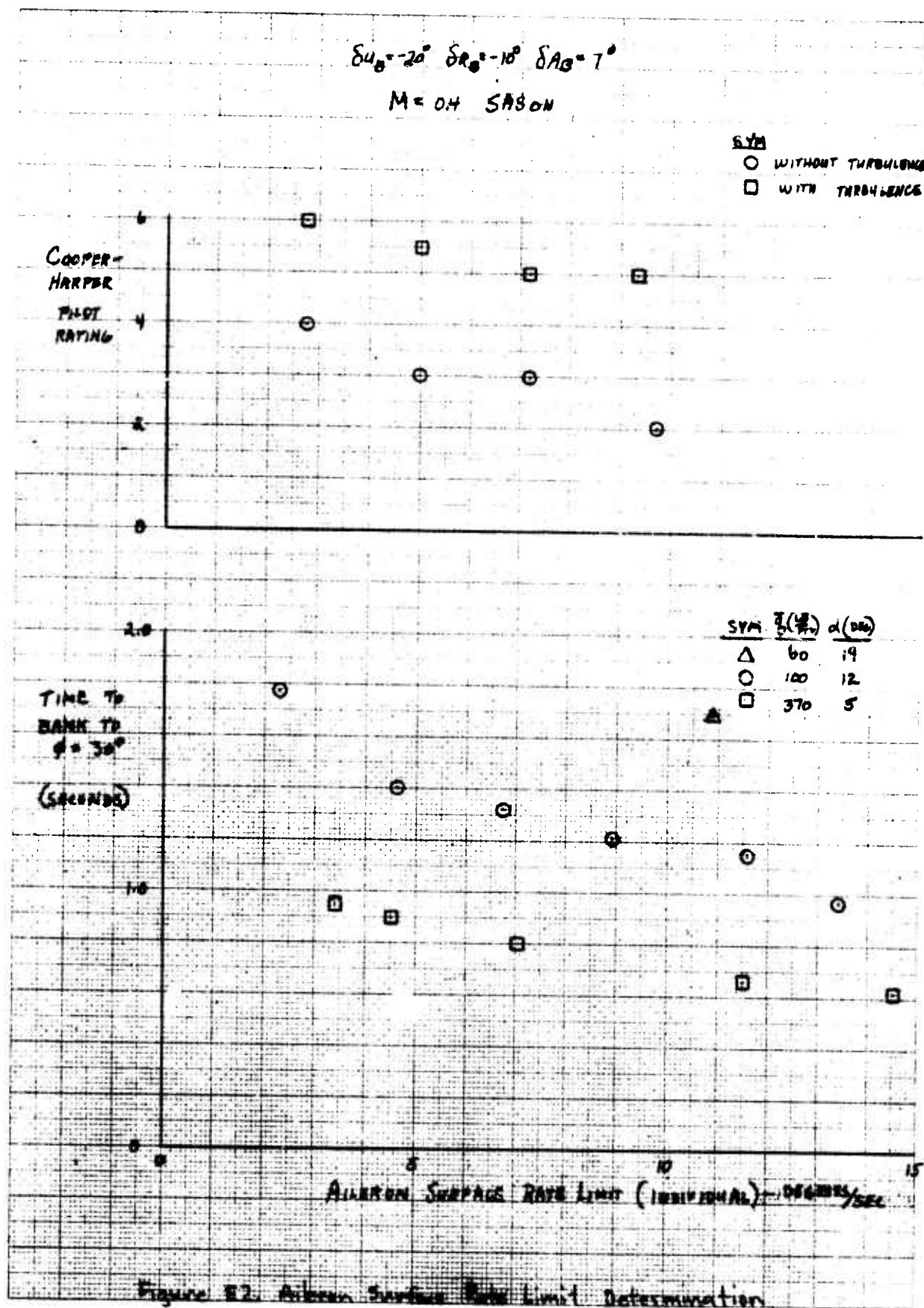
#### Aileron Authority and Rate Limit Determination

Surface rate and authority limits for the newly designed ailerons were determined through simulator studies prior to final design. Pilots were given the following tasks to perform in these studies;

1. Full deflection aileron roll from zero to 60 degrees of bank angle at zero, one and maximum "g".
2. At one g flight conditions, perform a 45 degree banked turn through 30 degrees of heading change and restabilize.
3. Repeat task 2 with the roll and yaw SAS off.

Aileron surface authorities of five, ten and fifteen degrees for full aileron stick deflection were investigated at dynamic pressures of 100 and 370 lb/ft<sup>2</sup> for SAS-on and SAS-off conditions. The Cooper-Harper pilot ratings obtained from three pilots (figure E1) indicated that, at low dynamic pressures, at least ten degrees of aileron was needed. Fifteen degrees was considered a bit sensitive by one pilot. All three agreed that the five degree authority gave insufficient roll power and sluggish aircraft response. At the high dynamic pressure the five degree authority was considered good by the pilots, while ten degrees was a bit sensitive. Fifteen degrees was conducive to PIO tendencies. Since the flight regime of the X-24B would cover both the high and low dynamic pressure conditions, the ten degree aileron deflection was selected as the optimum authority.

It was also necessary to determine the minimum acceptable aileron surface rate limits. Aileron rate limits of 5 deg/sec to 25 deg/sec were tried while performing task 2 with and without turbulence. Pilot ratings and times to bank as a function of rate limit are shown in figure E2. The lower rate limit manifested itself primarily as an apparent lack of roll power, and the lower pilot ratings were due mainly to this characteristic. Surprisingly, the simulator was controllable with aileron surface rate limits as slow as 2.75 deg/sec.





$$\delta \alpha_0 = -40^\circ, \delta \alpha_1 = 20^\circ, \delta \alpha_2 = 0^\circ$$

SYMBOL

DESCRIPTION

- Three g rolling pullout, Design 2, 3000 lb wt, 12°  $\delta \alpha_2$ , 10°  $\delta$
- Zero g roll, Design 2, 3°  $\delta \alpha_2$ , 5°  $\delta$
- △ Four g pullup, Operational 2, 1000 lb wt, 12°  $\delta \alpha_2$ , 0°  $\delta$
- Zero g pushover, Operational 2, 2°  $\delta \alpha_2$ , 0°  $\delta$

Note:

Mach	Design 2	Oper. 2
0.6	449	359
0.8	421	337
0.9	405	324
0.95	396	317
1.00	387	310
1.15	375	300
1.30	375	300

Design Requirement (Normal)  
Design Requirement (Emergency)

Hinge Moment

1000 in-lb

Mach Number

Figure E3. Aileron Design Requirements

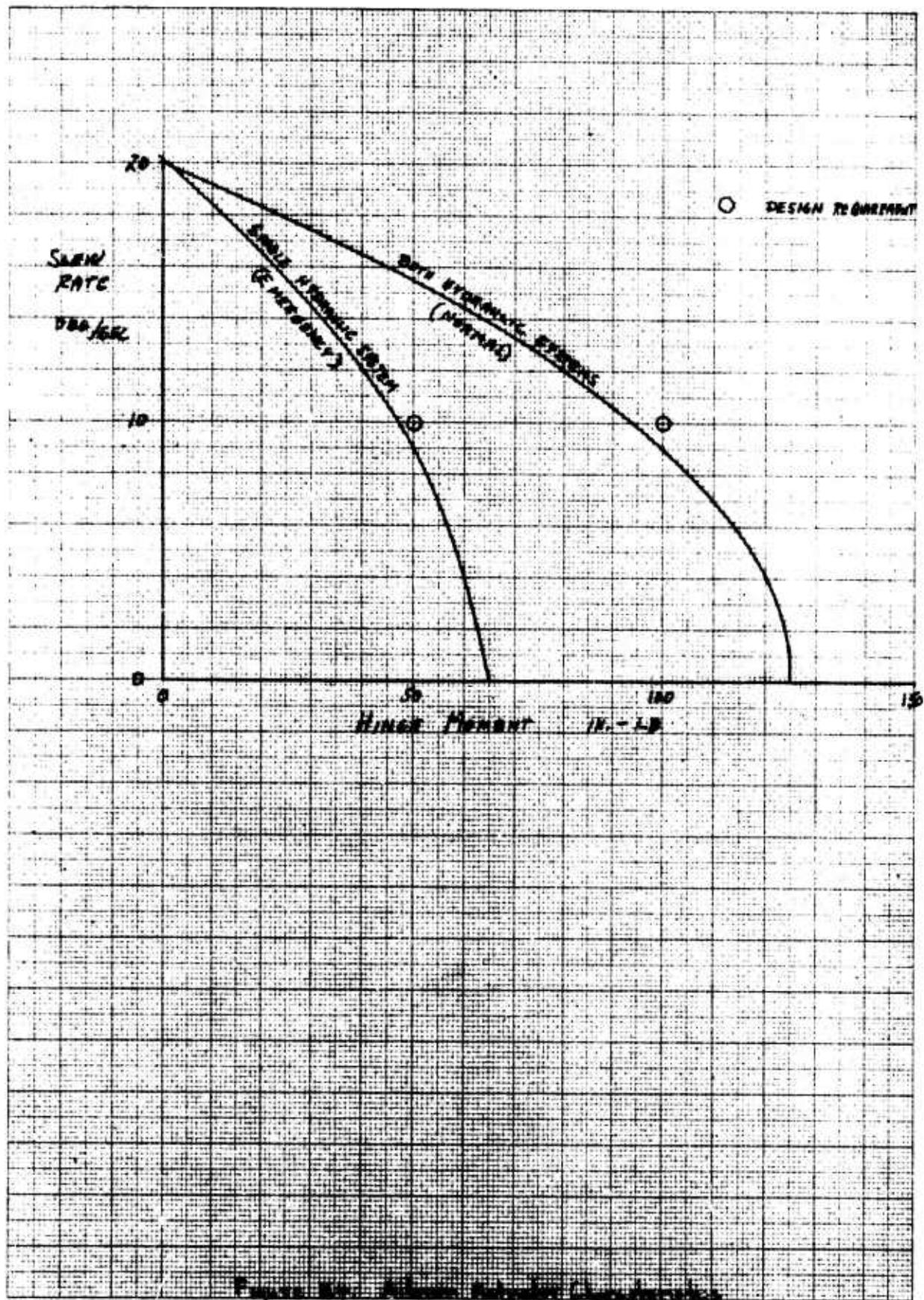


Figure 10. Sink Rate vs. Hinge Moment

Pilot ratings of 4 (smooth air) and 6 (turbulence) were recorded for this condition. The pilots could not detect any difference in handling qualities for surface rate limits above approximately 10 degrees per second. This result is primarily due to the high aileron effectiveness and relatively high level of inherent roll damping ( $C_{lp}$ ) of the X-24B.

The aileron hinge moment requirements were established by performing a series of rapid dynamic maneuvers (pullups, pushovers, rolling pullouts, etc.) on the simulator. Using the recorded transient response characteristics, in conjunction with wind tunnel predictions of surface pressure coefficients, the maximum or minimum hinge moments were determined for each maneuver and are summarized in figure E3. The actuator specifications were conservatively established at 10 deg/sec minimum rate at the highest expected hinge moment (100,000 inch pounds for the normal hydraulic system case). The load/slew rate characteristics of the selected actuator (X-15 rudder actuator) are shown along with the required specifications in figure E4.

#### Pitch Gearing

On the X-24A, pitch control gearing varied as a function of upper flap bias position (reference 16). The X-24A gearing was approximately  $\pm 30$  degrees of upper and lower flap deflection for full stick at an upper flap setting of  $-3$  degrees and  $\pm 12.5$  degrees at an upper flap setting of  $-40$  degrees (which was the supersonic setting). The X-24B had a larger transonic trim change than the X-24A, and therefore required more lower flap deflection per angle of attack supersonically (was more stable than the X-24A). To be able to achieve the desired, X-24B trim angle of attack range supersonically, it was necessary to increase the X-24A pitch control gearing of  $\pm 12.5$  degrees to a value of  $\pm 20$  degrees for an upper flap bias of  $-40$  degrees.

A simulator study was conducted to establish the best gearing for  $-20$  degrees of upper flap bias (proposed X-24B subsonic configuration). The study was conducted at Mach number of 0.4 and two values of dynamic pressure; a low value of  $q = 100$  lbs/ft<sup>2</sup> and a high value of  $q = 370$  lbs/ft<sup>2</sup>. Pilots were given the following tasks to do during the study;

1. Trim to one g; change angle of attack by  $\pm 5$  degrees and restabilize.
2. Repeat task 1 with the pitch SAS off.
3. Do one g pitch pulses SAS-on and SAS-off.

The gearings used in this study were  $\pm 10$  degrees,  $\pm 20$  degrees, and  $\pm 27.5$  degrees of elevator travel for full forward and full aft stick travel. All pilots agreed that the aircraft with the  $\pm 10$  degrees gearing was too sluggish at both high and low dynamic pressures. There seemed to be little difference between the  $\pm 20$  degree and  $\pm 27.5$  degree gearings, and the pilots indicated the aircraft was quite easy to fly at either sensitivity. Pilot ratings are shown in figure E5. The  $\pm 20$  degree gearing was chosen over the  $\pm 27.5$  degree gearing to allow a fixed gearing as a function of upper flap bias to be implemented in the aircraft. It would also tend to minimize any possible PIO tendencies which might occur at the higher gearings.



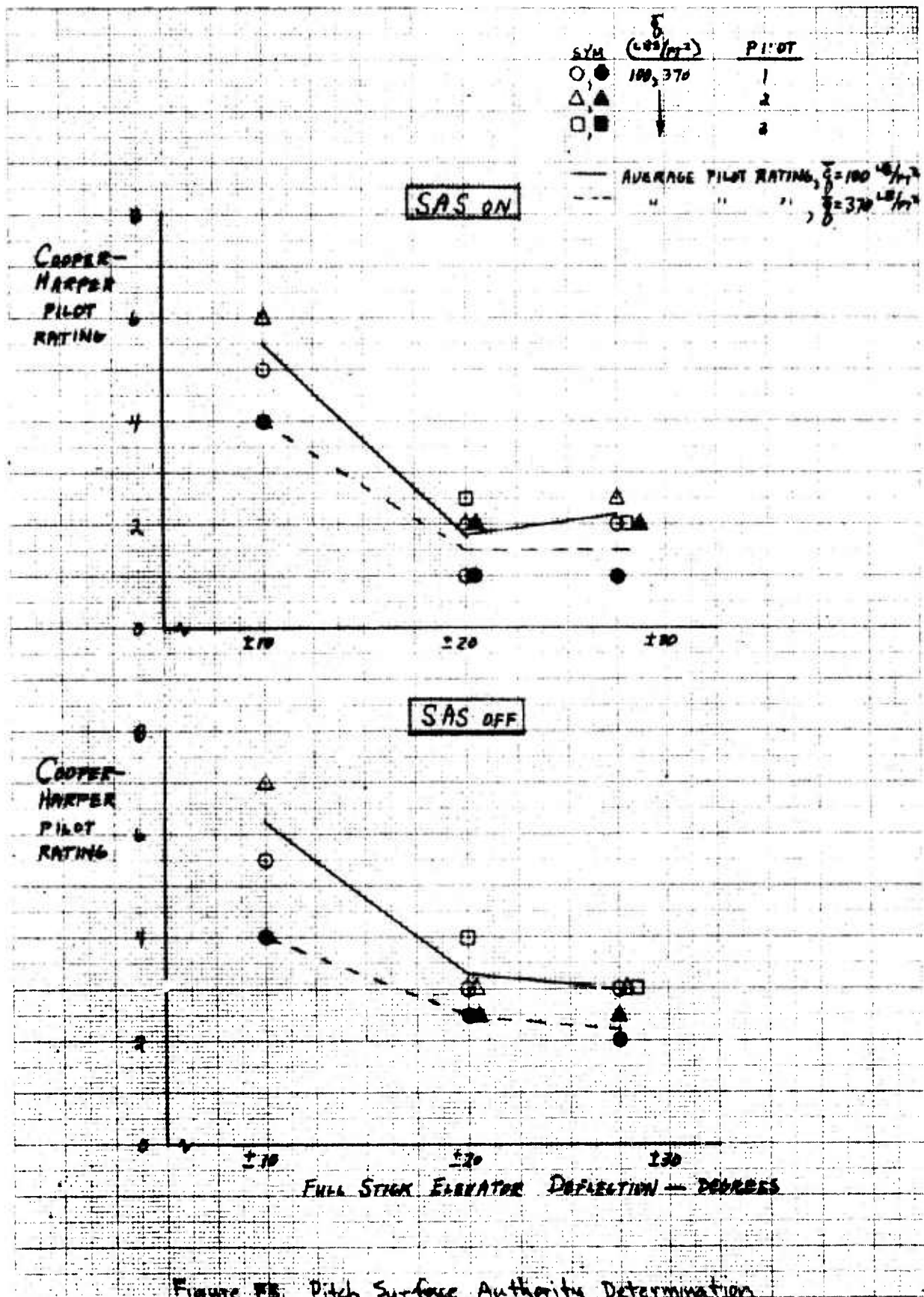


Figure 15. Pitch Surface Authority Determination

### Derivative Sensitivity

A lateral-directional handling qualities study was performed on the X-24B six-degree-of-freedom simulator. Cooper-Harper pilot ratings and times to bank were obtained at different flight conditions and flight control system configurations using both wind tunnel predicted stability derivatives and alterations applied to these derivatives to account for potential errors in wind tunnel predictions. Future X-24B pilots were used to obtain pilot ratings. Pilots performed the following maneuvers during this study;

1.  $\delta r$ ,  $\delta a$  pulses
2. Full stick aileron rolls
3. Zero to  $45^\circ$  bank angle change; hold  $\phi=45^\circ$  through a  $30^\circ$  heading change
4. General lateral-directional maneuvering

Pilot ratings and times to bank were obtained at the following vehicle configurations and flight conditions;

Flight Phase	Subsonic Glide	Approach	Post Flare	Landing (gear down)
Mach number	0.7	0.5	0.4	0.3
Velocity (KEAS)	200	300	200	180
$\alpha$ (degrees)	4, 12, 16	6	12, 16	8, 12, 16

Upper flap bias ( $\delta U_B = -20^\circ$ , Rudder bias ( $\delta R_B = -10^\circ$ , Aileron bias ( $\delta A_B = 7^\circ$

These conditions were evaluated for each of the following:

- SAS off and 0% aileron-to-rudder interconnect gain (KRA)
- SAS off and high KRA schedule
- SAS on ( $K_P=.08$ ,  $K_R=.21$  deg/deg/sec) and low KRA schedule
- SAS on ( $K_P=.08$ ,  $K_R=.81$  deg/deg/sec) and high KRA schedule

where:

$$KRA \text{ actual} = \frac{\text{degrees } \delta r}{\text{degrees } \delta a} \times 100 \text{ (percent)}$$

$\alpha$ (degrees)	low KRA schedule (%)	high KRA schedule (%)
0	0	0
4	10	22
8	22	60
12	37	102
16	54	148

Both of these schedules were refined prior to first flight (see figure D8)

$$\delta u_b = -20^\circ \quad \delta R_b = -10^\circ \quad \delta A_b = 7^\circ$$

$$M = 0.7 \quad V = 200 \text{ KEAS}$$

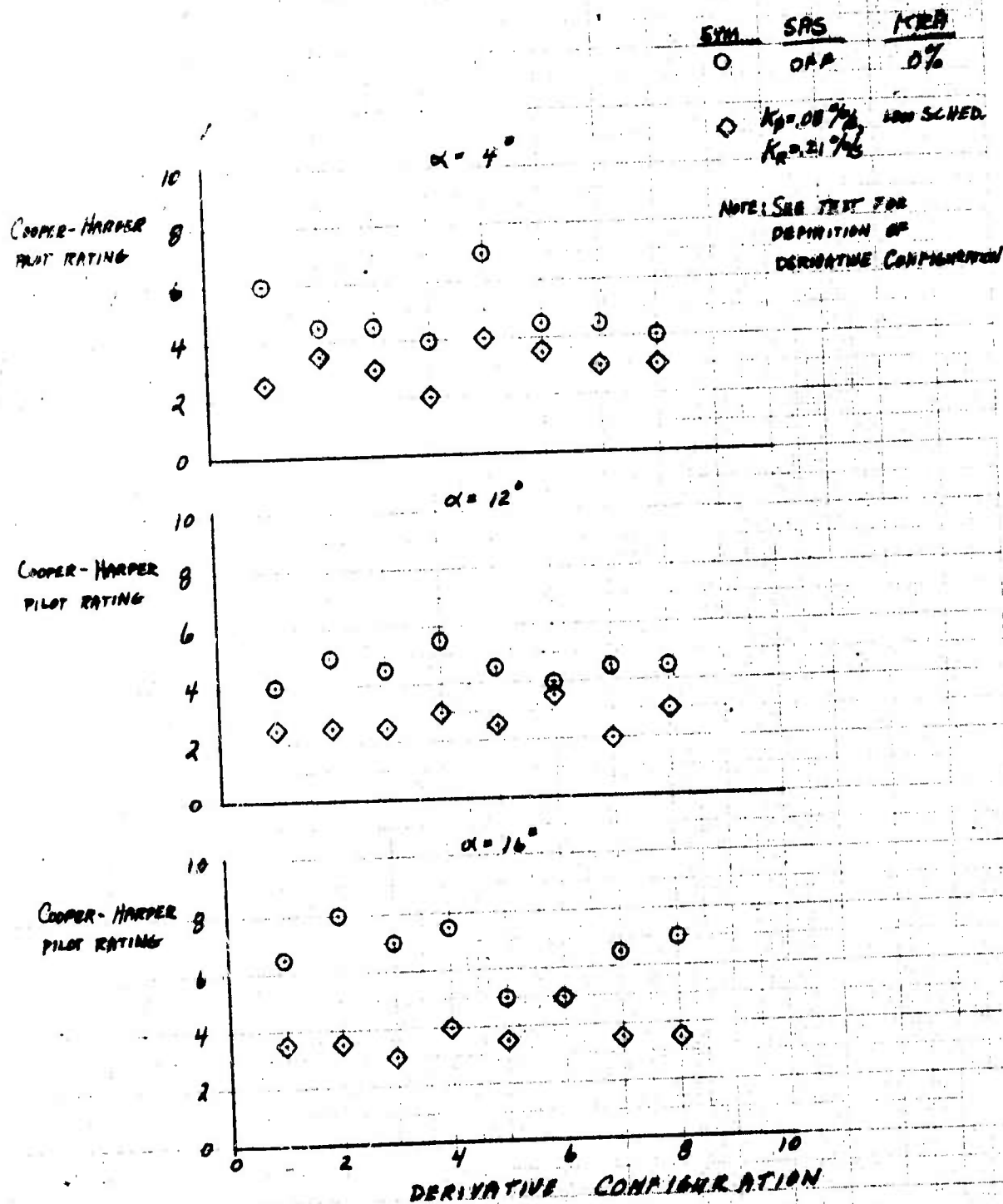


Figure E6 Derivative Sensitivity Results



A derivative sensitivity study was conducted at all of the above conditions. Derivatives were altered in the following manner:

<u>Derivative Configuration Number</u>	<u>Description</u>
1	Basic wind tunnel derivatives
2	Basic derivatives plus $\Delta C_{n\beta} = -.00053$ per deg
3	Basic derivatives plus $\Delta C_{l\beta} = +.0005$ per deg
4	Basic derivatives plus $\Delta C_{n\delta a} = -.0003$ per deg
5	Basic derivatives plus $\Delta C_{n\delta a} = +.0003$ per deg
6	Basic derivatives plus $\Delta C_{l\delta a} = -.00025$ per deg
7	Basic derivatives plus $\Delta C_{l\delta r} = +.00015$ per deg
8	Basic derivatives plus $\Delta C_{n\delta r} = +.00025$ per deg

Specification requirements shown in the data for times to bank were obtained from Preliminary Handling Qualities Requirements for Lifting Re-Entry Vehicles During Terminal Flight.<sup>22</sup>

Pilot ratings for the various flight conditions and control system configurations are plotted versus derivative configuration in figures E6 through E11. In general, simulator results indicated that the aircraft was not very sensitive to derivative variation. This is usually an indication that the basic stability of the aircraft is good, which indeed turned out to be the case during the X-24B flight test program at subsonic Mach numbers. Pilot ratings were usually good when the low KRA schedule was used. The ratings were almost always significantly worse when the high schedule was used. This was especially true in the gear down configuration at 0.3 Mach numbers. (As discussed previously, the low KRA scheduled was used in the approach and landing phase during the flight test program). Most of the adverse comments and poor pilot ratings obtained during this study were due to the fact that the simulator appeared to be PIO sensitive in the lateral-directional axis. Increasing

<sup>22</sup>Reference 17: DiFranco, Dante A. and Mitchell, John F., Preliminary Handling Qualities Requirements for Lifting Re-Entry Vehicles During Terminal Flight, AFFDL-TR-71-64, Air Force Flight Dynamics Laboratory, Wright-Patterson AFB, Ohio, August 1971.

$$\delta u_B = -20^\circ \quad \delta R_B = -10^\circ \quad \delta A_B = 7^\circ$$

$$M = 0.7 \quad V = 200 \text{ KEAS}$$

<u>SYM</u>	<u>SAS</u>	<u>KRA</u>
□	OFF	HIGH SCHED

△  $K_D = 0.08\%$ , HIGH SCHED.  
 $K_R = 0.11\%$

NOTE: SEE TEXT FOR  
 DEFINITION OF  
 DERIVATIVE CONFIGURATION

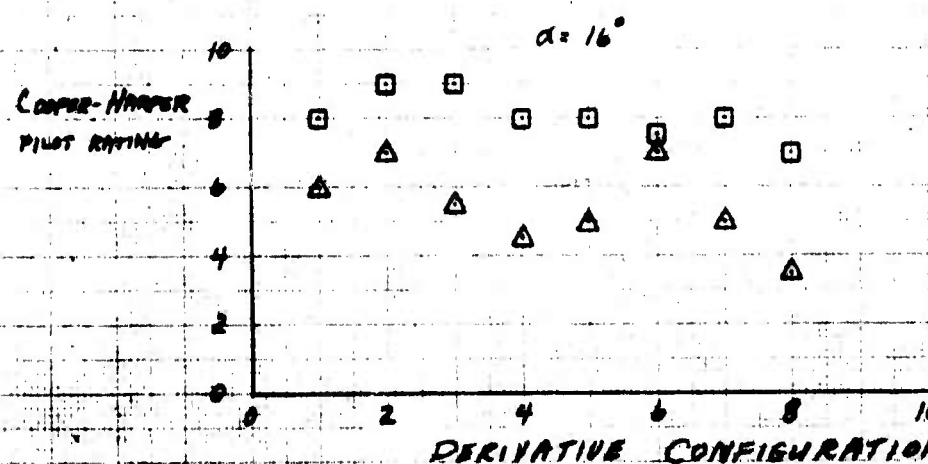
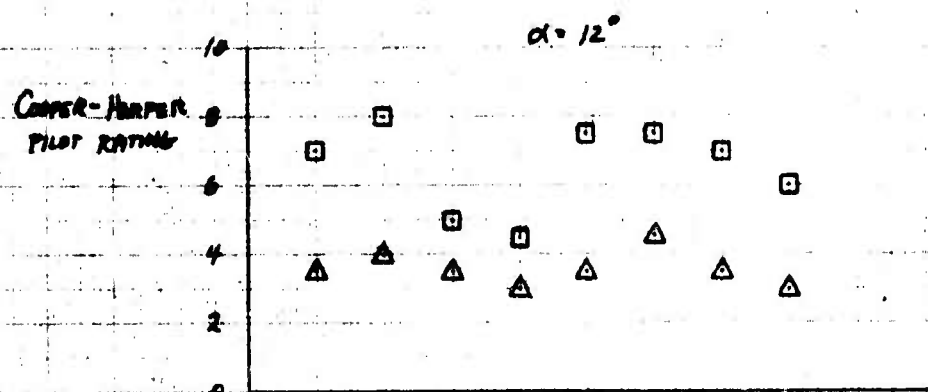
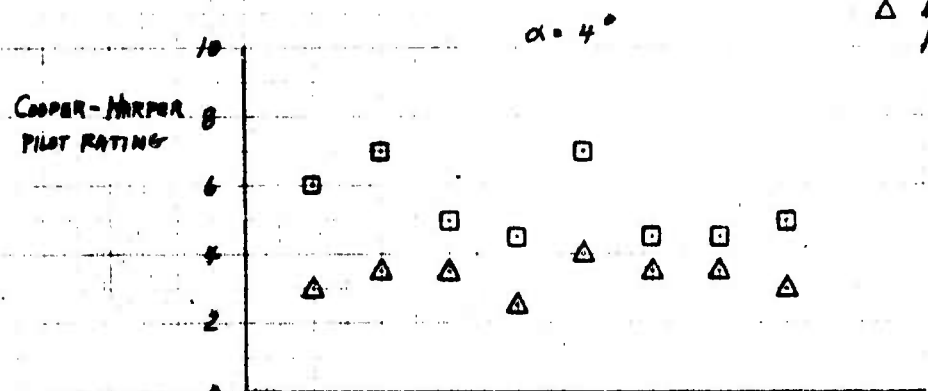


Figure E7. Derivative Sensitivity Results

A derivative sensitivity study was conducted at all of the above conditions. Derivatives were altered in the following manner;

<u>Derivative Configuration Number</u>	<u>Description</u>
1	Basic wind tunnel derivatives
2	Basic derivatives plus $\Delta C_{n\beta} = -.00053$ per deg
3	Basic derivatives plus $\Delta C_{l\beta} = +.0005$ per deg
4	Basic derivatives plus $\Delta C_{n\delta a} = -.0003$ per deg
5	Basic derivatives plus $\Delta C_{n\delta a} = +.0003$ per deg
6	Basic derivatives plus $\Delta C_{l\delta a} = -.00025$ per deg
7	Basic derivatives plus $\Delta C_{l\delta r} = +.00015$ per deg
8	Basic derivatives plus $\Delta C_{n\delta r} = +.00025$ per deg

Specification requirements shown in the data for times to bank were obtained from Preliminary Handling Qualities Requirements for Lifting Re-Entry Vehicles During Terminal Flight. 22

Pilot ratings for the various flight conditions and control system configurations are plotted versus derivative configuration in figures E6 through E11. In general, simulator results indicated that the aircraft was not very sensitive to derivative variation. This is usually an indication that the basic stability of the aircraft is good, which indeed turned out to be the case during the X-24B flight test program at subsonic Mach numbers. Pilot ratings were usually good when the low KRA schedule was used. The ratings were almost always significantly worse when the high schedule was used. This was especially true in the gear down configuration at 0.3 Mach numbers. (As discussed previously, the low KRA scheduled was used in the approach and landing phase during the flight test program). Most of the adverse comments and poor pilot ratings obtained during this study were due to the fact that the simulator appeared to be PIO sensitive in the lateral-directional axis. Increasing

22 Reference 17: DiFranco, Dante A. and Mitchell, John F., Preliminary Handling Qualities Requirements for Lifting Re-Entry Vehicles During Terminal Flight, AFFDL-TR-71-64, Air Force Flight Dynamics Laboratory, Wright-Patterson AFB, Ohio, August 1971.



$$\delta \alpha_B = -2^\circ \quad \delta R_B = 10^\circ \quad \delta A_B = 7^\circ$$

$$M = 0.5 \quad V = 300 \text{ KEAS (FOR } \alpha = 6^\circ)$$

$$M = 0.4 \quad V = 200 \text{ KEAS (FOR } \alpha = 12^\circ, 16^\circ)$$

SYM	SAS	KRA
○	OFF	0%
◇	$K_p = 0.08\%$ , LOW SCHED. $K_R = 0.21\%$	

NOTE: SEE TEXT FOR  
DEFINITION OF  
DERIVATIVE CONFIGURATION

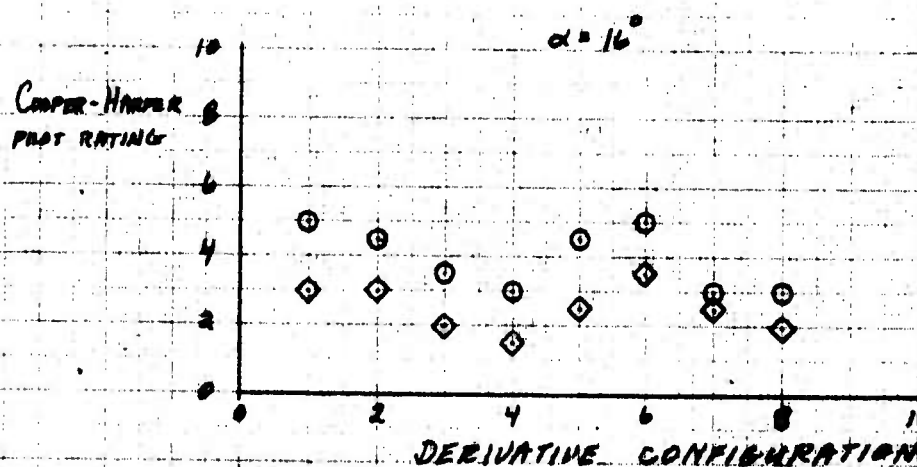
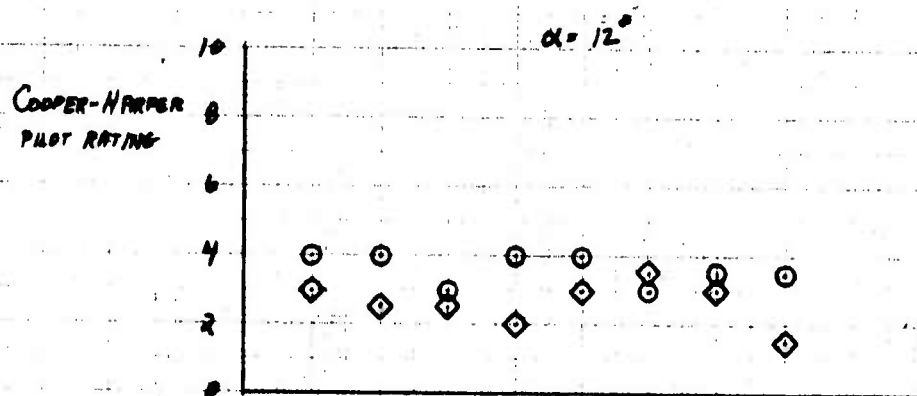
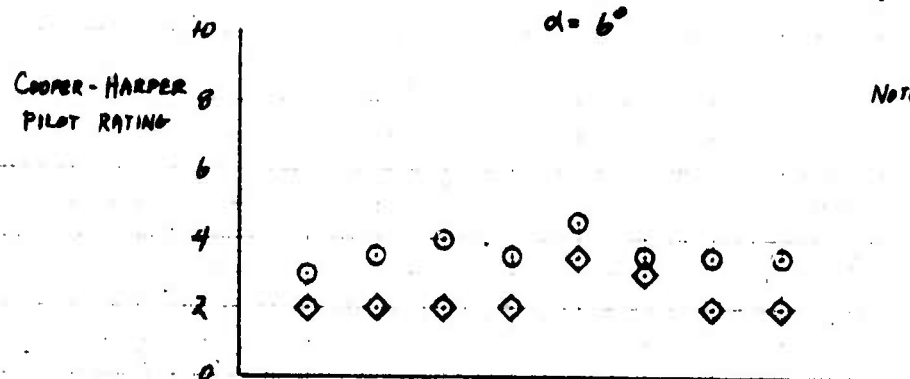


Figure E8. Derivative Sensitivity Results

$$\delta u_B = -20^\circ \quad \delta R_B = -10^\circ \quad \delta A_B = 7^\circ$$

M = 0.5 V = 300 KEAS (FOR  $\alpha = 6^\circ$ )

M = 0.4 V = 200 KEAS (FOR  $\alpha = 12^\circ, 16^\circ$ )

SYM    SAS    KBA  
☐    OFF    HIGH SCHOOL

$\Delta$  K<sub>0</sub> = 20%, HIGH SCHOOL,  
K<sub>0</sub> = 21%

NOTE: SEE TEXT FOR  
DEFINITION OF  
DERIVATIVE CONFIGURATION

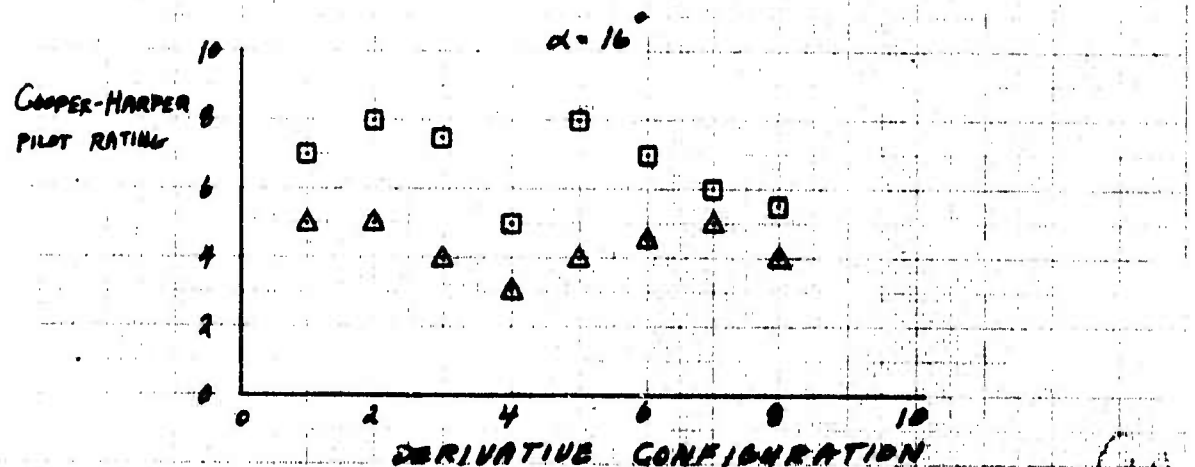
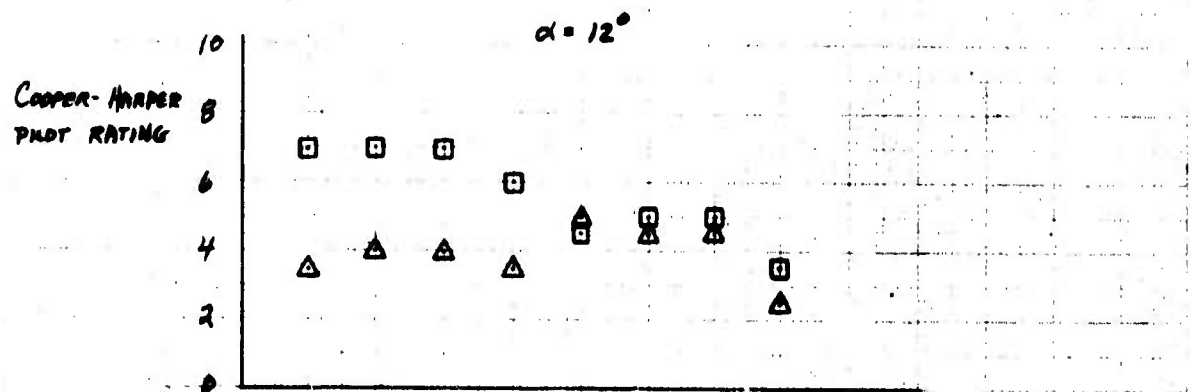
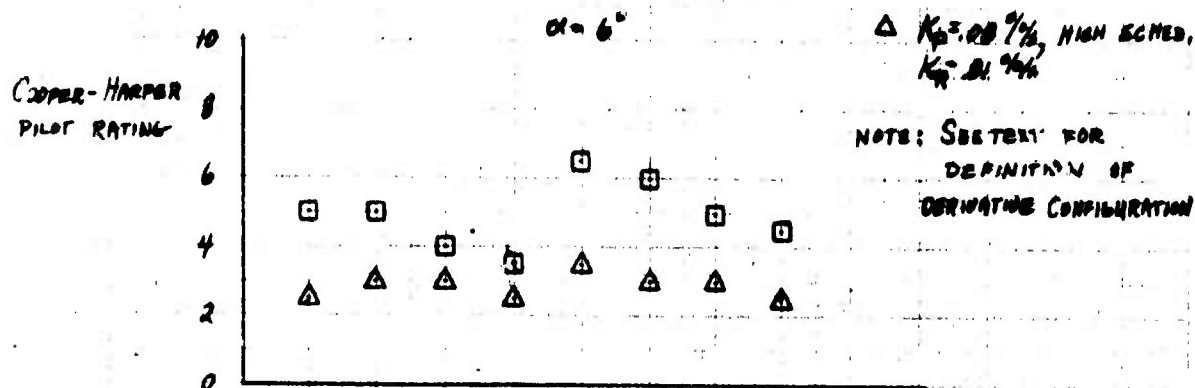


Figure E9. Derivative Sensitivity Results

$$\delta H_D = -20^\circ \quad \delta R_D = -10^\circ \quad \delta A_D = 7^\circ$$

$$M = 0.3 \quad V = 100 \text{ KEAS}$$

GEAR DOWN

SYM	SAS	KRA
○	OFF	0%

◇  $K_P = .08\% / \text{sec}$  LOW SPEED  
 $K_R = .21\% / \text{sec}$

NOTE: SEE TEXT FOR  
 DEFINITION OF  
 DERIVATIVE CONFIGURATION

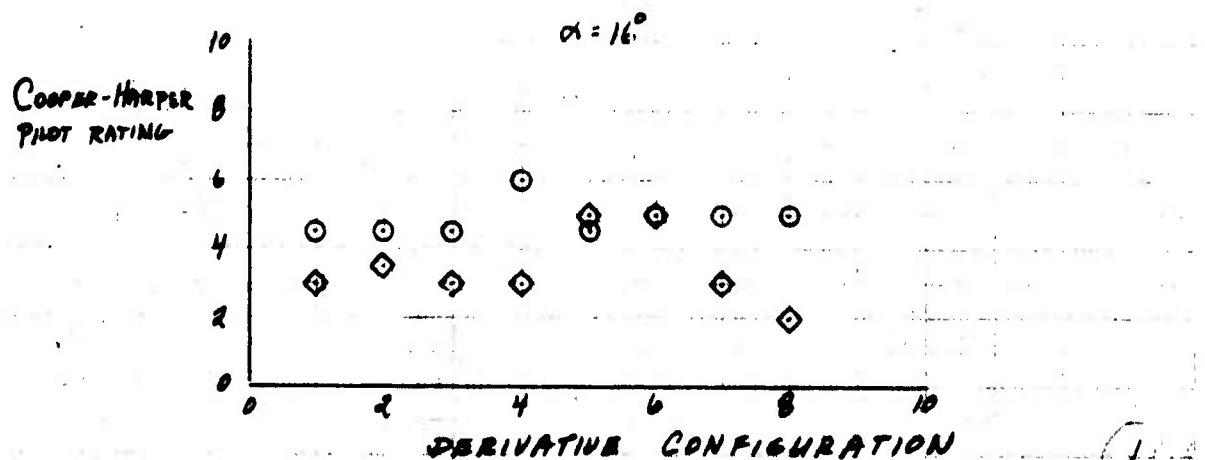
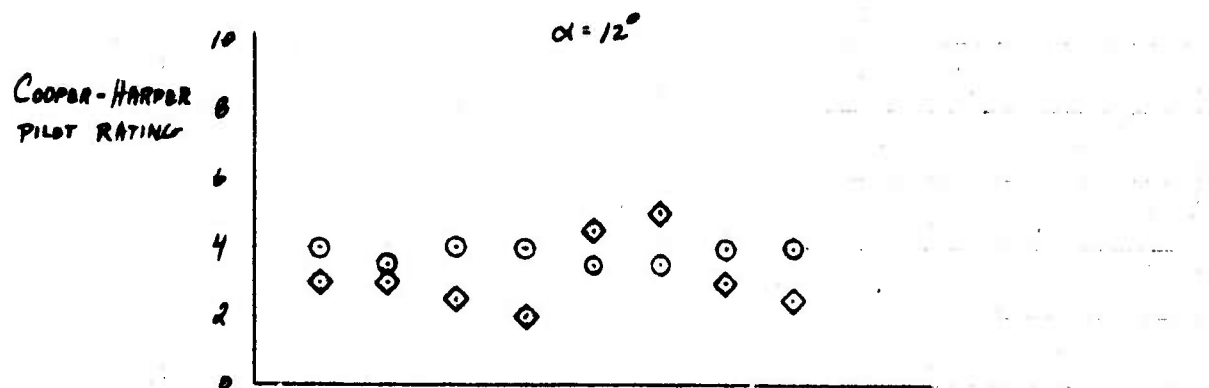
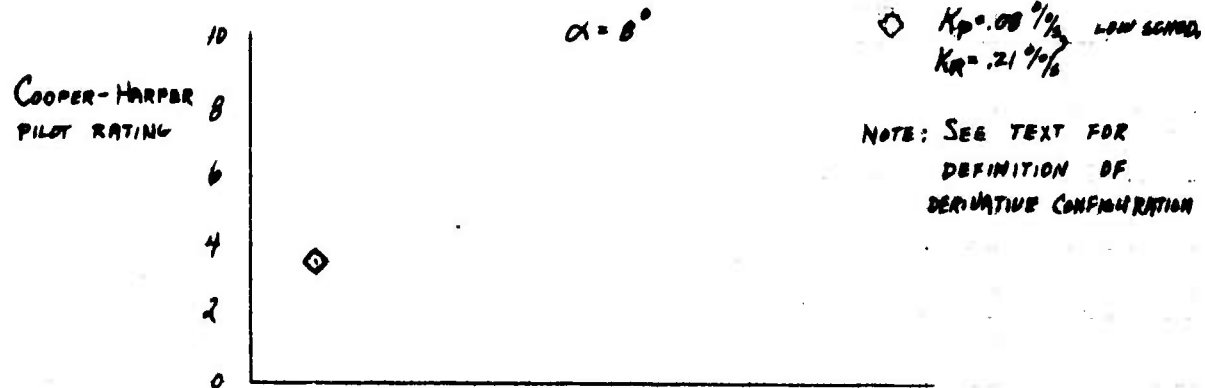


Figure E10. Derivative Sensitivity Results



$$\delta u_0 = -20^\circ \quad \delta R_0 = -10^\circ \quad \delta A_0 = 7^\circ$$

$$M = 0.3 \quad V = 180 \text{ KEAS}$$

GEAR DOWN

SYM SAS KRA  
 □ OFF HIGH SCHOOL  
 △  $K_D = .007\%$  " "  
 $K_R = .01\%$

NOTE: SEE TEXT FOR  
 DEFINITION OF  
 DERIVATIVE CONFIGURATION

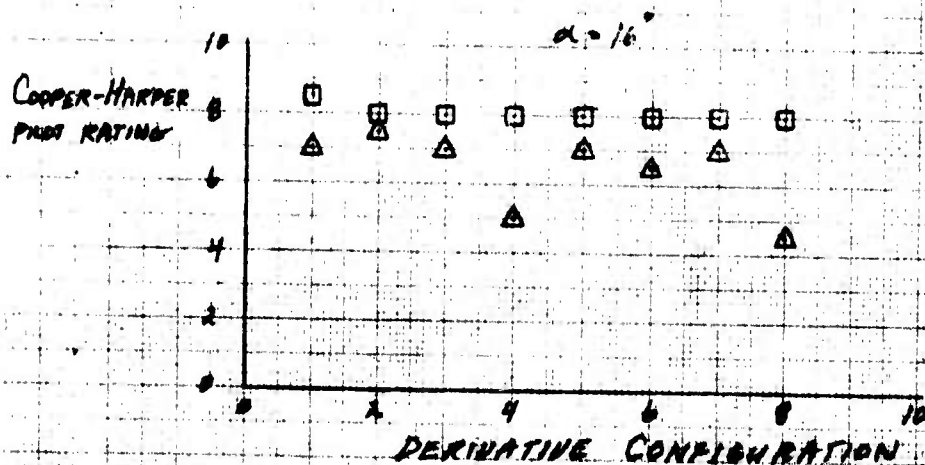
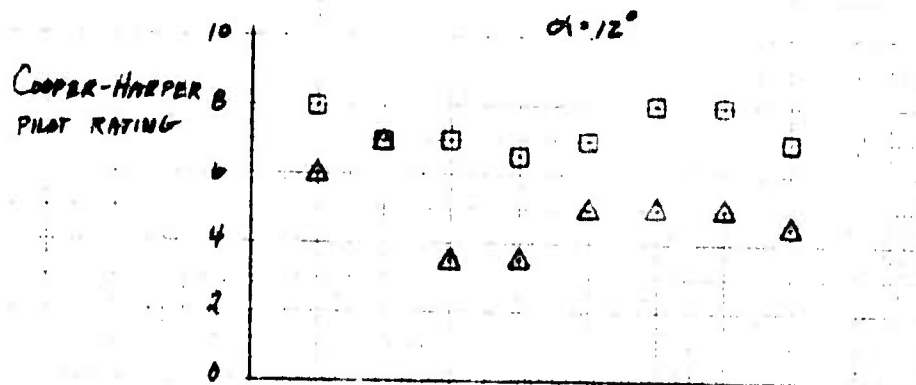
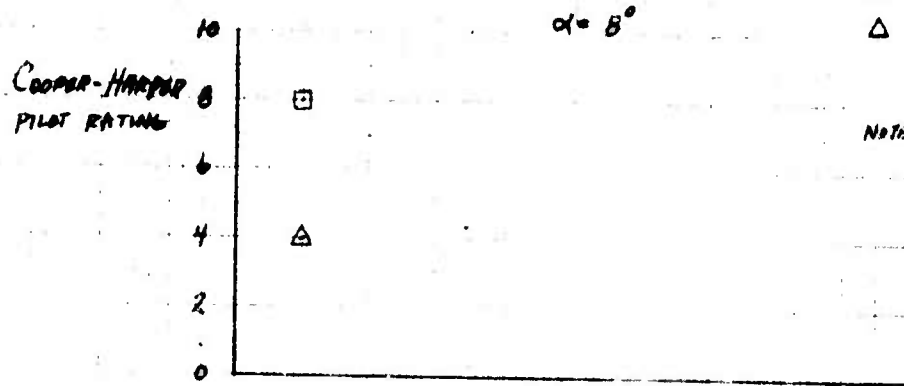


Figure E11. Derivative Sensitivity Results

the KRA gain aggravated the PIO tendency and hence made the pilot ratings worse. During the actual flight test program, the aircraft did not demonstrate this PIO tendency. A possible explanation for this discrepancy between simulator and flight results is given in the section entitled "Lateral-Directional PIO Sensitivity".

Times to bank to 45 degrees for the various flight conditions and derivative configurations are plotted versus angle of attack in figures E12 through E14. The times shown are for full roll stick inputs. The results obtained usually met level 1 or level 2 of the proposed military specification requirements for lifting re-entry vehicles during terminal flight (reference 17). Also, the times were amazingly consistent and did not vary significantly with angle of attack flight condition, SAS gain, or KRA gain.

#### Lateral-Directional PIO Sensitivity

A lateral-directional pilot-induced-oscillation study was performed on the X-24B six-degree-of-freedom simulator in conjunction with a digital computer program. Although agreement between these two methods was excellent, final conclusions were taken from the simulator because the non-linear effects of the flight control system and the math model were included in the simulator results. The PIO tendencies were determined by replacing the pilot's roll stick signal by either bank angle or roll rate feedback. This established a transfer function for the pilot of aileron input directly proportional to either bank angle or roll rate. Two pilot gains developed from the X-24A program were investigated for each feedback parameter. Since it was uncertain as to what the actual inflight lateral-directional pilot transfer function would be for the X-24B, it was felt that using both transfer functions would adequately cover the range of inflight possibilities. After the loop had been closed by substituting bank angle or roll rate for pilot roll command in the simulator, the PIO tendencies were determined by disturbing the simulator with sharp inputs in the lateral-directional axis. If the oscillations damped after the input was applied, that was an indication that no PIO tendencies existed; if they did not damp, it was an indication that the vehicle was PIO sensitive. The PIO boundaries shown in figures E15 and E16 were determined very quickly, at each Mach number, by varying angle of attack until the angle of attack at which the oscillations were neutrally damped (if any) was found.

The PIO study was performed for the following conditions;

Flight Phase	Subsonic Glide	Approach	Post Flare	Landing (gear down)
Mach number	0.7	0.5	0.4	0.3
Velocity (KEAS)	200	300	200	185
$\delta U_B = -20^\circ$ $\delta R_B = -10^\circ$ $\delta A_B = 7^\circ$ c.g. = 65%				

The aileron-to-rudder interconnect gain (KRA) schedules used were:

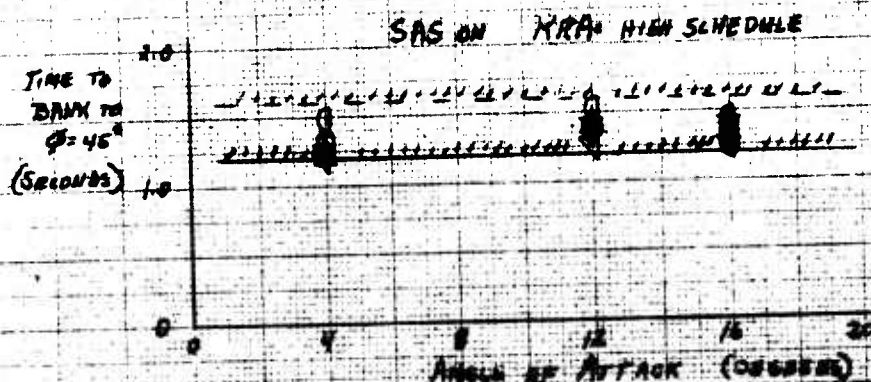
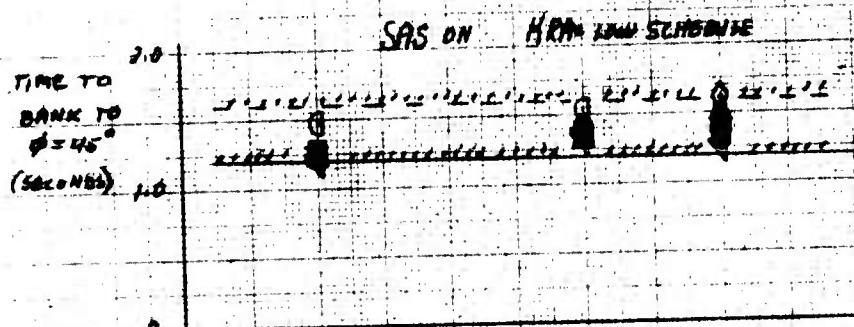
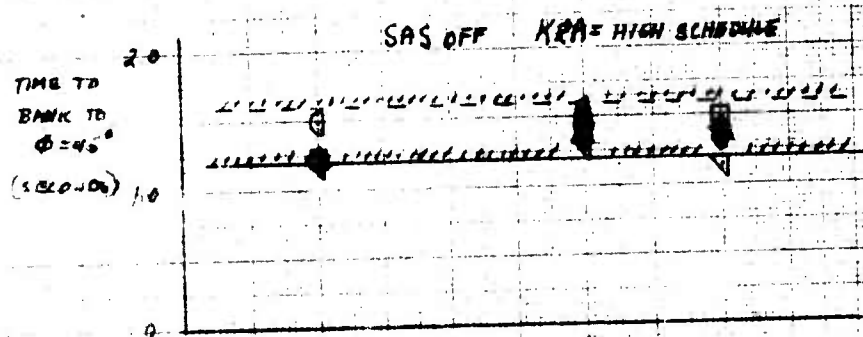
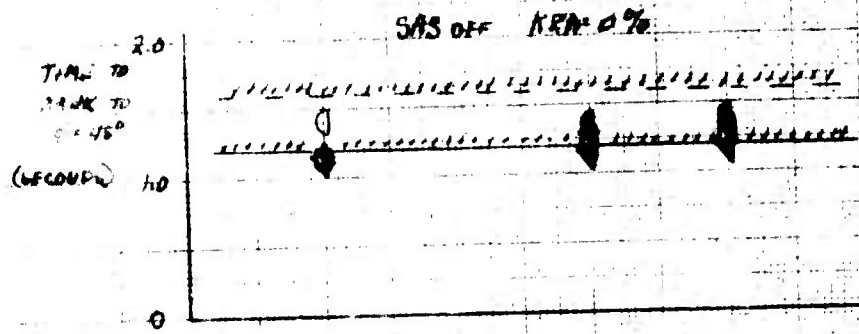
$$\text{KRA actual} = \frac{\text{degrees } \delta r}{\text{degrees } \delta a} \times 100 \text{ (percent)}$$

$\delta u_0 = -20^\circ$   $\delta a_0 = -10^\circ$   $\delta a_0 = 7^\circ$   
 $M = 0.7$   $V = 200 \text{ Kts}$

NOTE: 1) TIMES ARE FOR FULL  
 ROLL STICK INPUT

2) SYMBOLS REPRESENT  
 VARIOUS DERIVATIVE  
 CONFIGURATIONS. SEE  
 TEXT FOR DEFINITION.

LEGEND: ORIGIN: A, B-LEVEL  
 L: C-LEVEL, A, B-LEVEL



SYM	CONFIGURATION
○	1
△	2
□	3
◇	4
▽	5
○	6
◇	7
▽	8

Figure E-12 Predicted Roll Performance



$$\delta \alpha_B = -20^\circ \quad \delta \alpha_B = -10^\circ \quad \delta \alpha_B = 7^\circ$$

$$M = 0.5 \quad V = 300 \text{ Kts (FOR } \alpha = 4^\circ)$$

$$M = 0.4 \quad V = 200 \text{ Kts (FOR } \alpha = 12, 16^\circ)$$

NOTE: 1) TIMES ARE FOR FULL  
ROLL STICK INPUTS.  
2) SYMBOLS REPRESENT  
VARIOUS DERIVATIVE  
CONFIGURATIONS. SEE  
TEXT FOR DEFINITION.

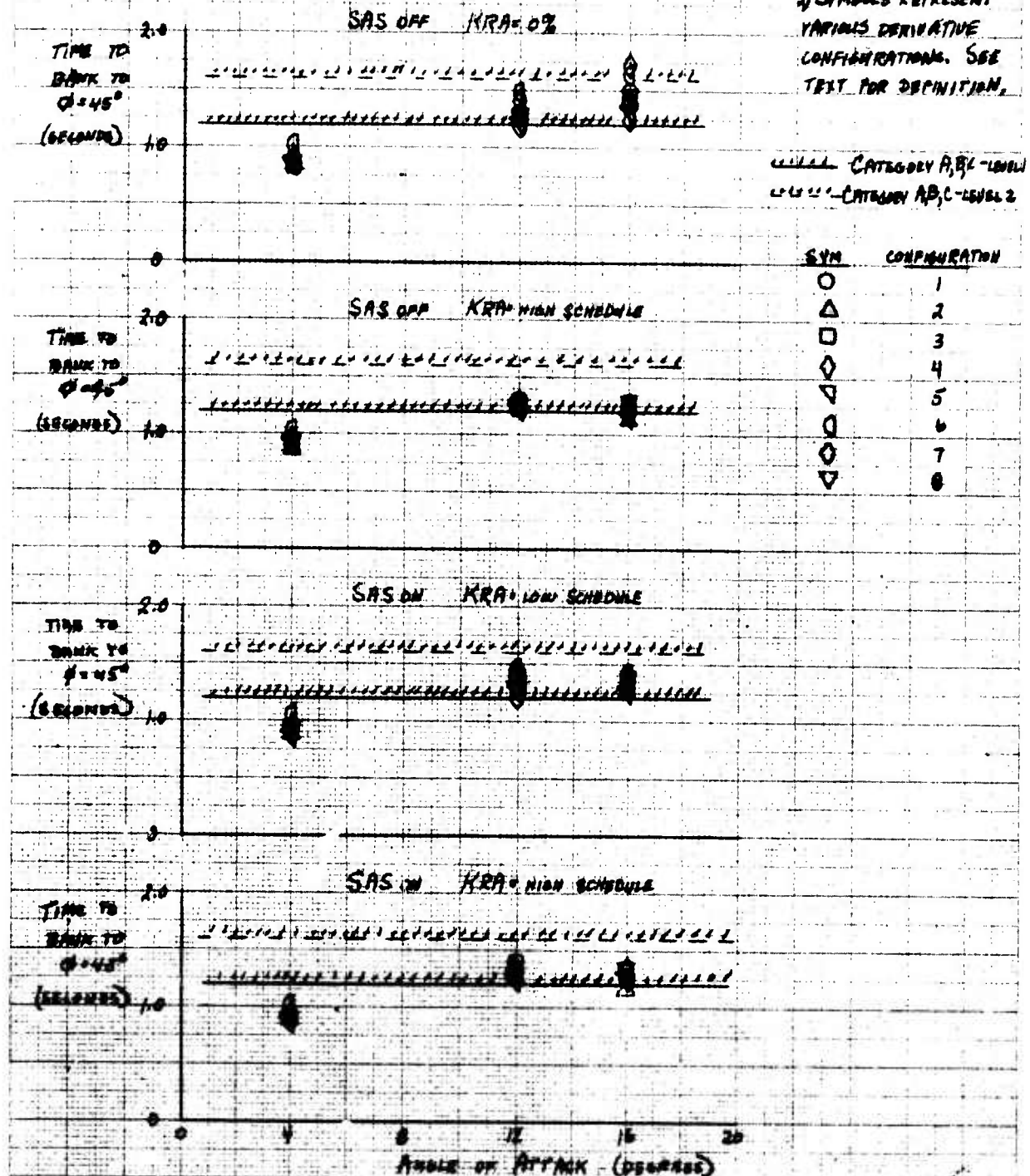
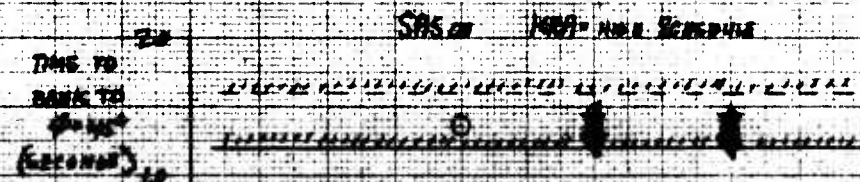
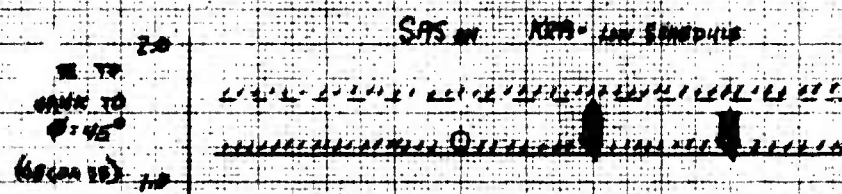
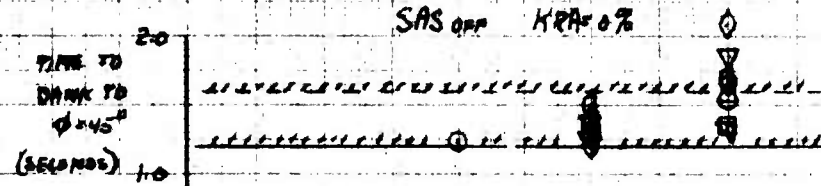


FIGURE E.18 Predicted Roll Performance

$\delta u_B = 20^\circ$   $\delta \alpha_B = -10^\circ$   $\delta \beta_B = 7^\circ$   
 $M = 0.9$   $V = 180 \text{ KTS}$   
 GEAR DOWN

NOTE: 1) TIMES ARE FOR FULL  
 ROLL STICK INPUTS  
 2) SYMBOLS REPRESENT  
 VARIOUS DERIVATIVE  
 CONFIGURATIONS. SEE  
 TEXT FOR DESCRIPTION.

CATEGORY C-LEVEL 1  
 CATEGORY C-LEVEL 2

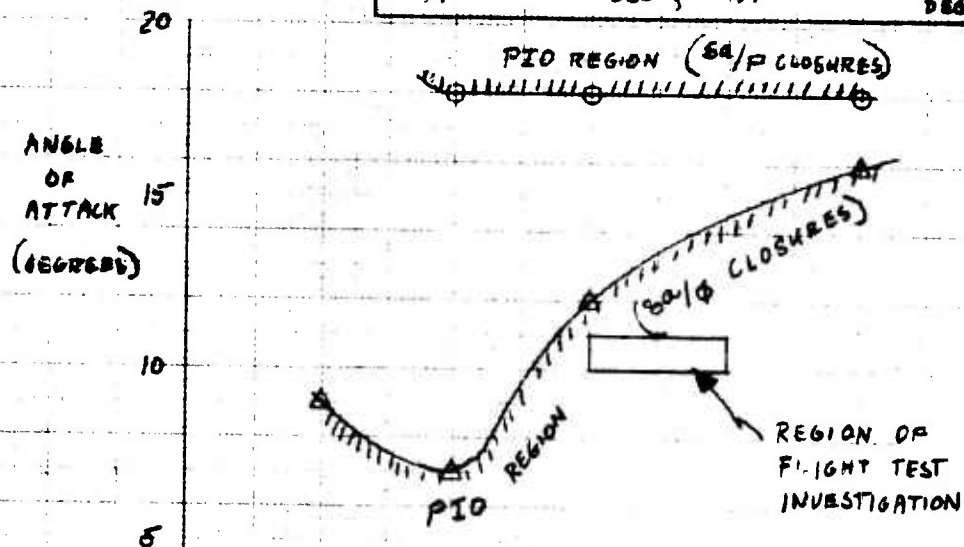


SYM	CONFIGURATION
○	1
△	2
□	3
◇	4
▽	5
○	6
◇	7
▽	8

Figure E14. Predicted Roll Performance

$\delta u_0 = -20^\circ$   $\delta R_0 = -10^\circ$   $\delta A_0 = 7^\circ$  KRA GAIN SCHEDULED (SEE TEXT)

$\delta a/p \text{ GAIN} = 0.2 \frac{\text{DEG}}{\text{DEG}}$ ,  $\delta a/p \text{ GAIN} = 0.1 \frac{\text{DEG}}{\text{DEG}}$



$\delta a/p \text{ GAIN} = 0.5 \frac{\text{DEG}}{\text{DEG}}$ ,  $\delta a/p \text{ GAIN} = 0.3 \frac{\text{DEG}}{\text{DEG}}$

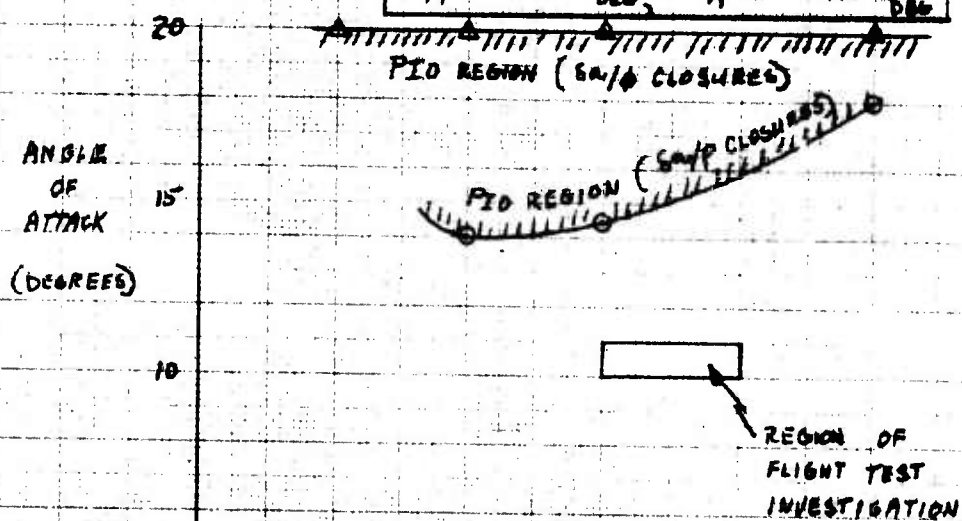


FIGURE EES PREDICTED LATERAL-DIRECTIONAL PIO BOUNDARIES (SAS OFF)



$\delta\alpha_0 = -20^\circ$   $\delta\alpha_0 = -10^\circ$   $\delta\alpha_0 = 7^\circ$  KRA GAIN SCHEDULED (SEE TEXT)  
 $K_p = 0.12, K_r = 2.1$   $\frac{deg}{deg}$

$\delta\alpha/p \text{ GAIN} = 0.2 \frac{deg}{deg}$ ,  $\delta\alpha/p \text{ GAIN} = 0.1 \frac{deg}{deg}$

ANGLE  
OF  
ATTACK  
(DEGREES)

NO PIO OCCURRED  
FOR  $\delta\alpha/p$  OR  
 $\delta\alpha/p$  CLOSURES

$\delta\alpha/p \text{ GAIN} = 0.5 \frac{deg}{deg}$ ,  $\delta\alpha/p \text{ GAIN} = 0.5 \frac{deg}{deg}$

ANGLE  
OF  
ATTACK  
(DEGREES)

NO PIO OCCURRED  
FOR  $\delta\alpha/p$  CLOSURES

PIO REGION ( $\delta\alpha/p$  CLOSURES)

PILOT NUMBER

FIGURE 1-10 TRACKED LATER DISTANCE PIO ISOLATION (SAS ON)

Angle of Attack (degrees)	Low KRA Schedule (%)	High KRA Schedule (%)
5° and below	0	0
8°	8	18
12	18	52
16	33	93
20	50	140

This was the same schedule used during the flight program except that KRA values were limited to 68% actual (figure D8).

The PIO boundaries predicted by this study are shown in figures E15 and E16 for different pilot transfer functions and gains, and SAS-off and SAS-on conditions. For the SAS-on conditions, a PIO occurred only for the high gain ( $0.5 \frac{\text{deg}}{\text{deg}}$ ) aileron to bank angle pilot transfer function at the higher angles of attack. With the SAS-off, the simulator predicted the vehicle to be PIO sensitive over much of the Mach region studies ( $<0.7$ ) using an aileron to bank angle pilot transfer function. If an aileron to roll rate transfer function was used, the PIO tendencies existed only at the very high angles of attack. As was stated in the previous section, pilot comments obtained during the derivative sensitivity handling qualities study indicated that the simulator was PIO sensitive in the lateral-directional axis especially with the SAS off. Their comments generally verified the results obtained using the automatic aileron to bank angle pilot closure technique, which would indicate that pilots tend to respond to bank angle while flying a fixed-based simulator.

The actual SAS-off lateral-directional PIO tendencies of the vehicle were investigated during the flight test program. The flight conditions at which the investigation occurred are shown in figure E15. The pilots found no PIO tendencies whatsoever during flight. This tends to confirm the simulator results obtained from the automatic closure technique using aileron to roll rate pilot transfer functions and indicates that he responded to roll rate in flight. In other words, because of motion cues, the pilots responded more quickly during actual flight than they did when using a fixed base simulator in a normal manner.

For this aircraft, simulator results obtained in the normal manner with the pilot in the loop were conservative in that the PIO tendencies shown on the simulator did not occur in flight (because the pilots responded to roll rate inflight and bank angle on the simulator). If the tendencies had been reversed such that the aircraft were PIO sensitive to  $\delta a/P$  transfer functions and not PIO sensitive to  $\delta a/\phi$  transfer functions (such might be the case with a vehicle with a high  $C_{L\beta}$  to  $C_{n\beta}$  ratio), a fixed-base simulator with a pilot in the loop would probably not predict PIO tendencies which might occur in flight. This had been experienced previously during the X-24A program. The X-24A fixed-base simulator, when used in a normal piloted manner (with the pilot generally responding to bank angle), indicated that the vehicle was not PIO sensitive. However, the actual vehicle was found to have PIO tendencies during flight. Lateral-directional PIO's were experienced on several occasions. The recorded data of these oscillations showed that the pilot was responding

SAS OFF  $V_E = 200 \text{ Kts}$

### AILERON ROLL REVERSAL

ANGLE  
OF  
ATTACK  
(DEGREES)  $\alpha$

NO AILERON ROLL REVERSAL OCCURRED AT ANY VEHICLE  
CONFIGURATION OR ANY FLIGHT CONDITION WITH  
ZERO PERCENT AILERON-TO-RUDDER INTERCONNECT,  
INCLUDING THE CONDITIONS LISTED BELOW.

#### UNALTERED WIND TUNNEL DERIVATIVES

"	"	"	"	PLUS $\Delta C_{l_{\delta a}} = -0.004 / \text{deg}$
"	"	"	"	PLUS $\Delta C_{l_{\delta a}} = -0.004 / \text{deg AND}$
"	"	"	"	$\Delta C_{l_{\delta a}} = -0.002 / \text{deg}$
"	"	"	"	PLUS $\Delta C_{l_{\delta a}} = -0.004 / \text{deg,}$
"	"	"	"	$\Delta C_{l_{\delta a}} = -0.002 / \text{deg, AND}$
"	"	"	"	$\Delta C_{l_{\delta a}} = +0.005 / \text{deg}$

### RUDDER ROLL REVERSAL (SMALL DERIVATIVES ONLY)

ANGLE  
OF  
ATTACK  
(DEGREES)  $\alpha$

---  $\delta u_0 = -20^\circ, \delta \alpha_0 = -10^\circ, \delta \alpha_0 = 7^\circ$   
 —  $\delta u_0 = -40^\circ, \delta \alpha_0 = 0^\circ, \delta \alpha_0 = 7^\circ$

NORMAL  
CONTROL

RUDDER  
ROLL  
REVERSAL

MACH NUMBER

FIGURE E-1 PREDICTED ROLL REVERSAL BOUNDARIES



to roll rate. Analysis using the automatic feedback technique showed the X-24A simulator to be PIO sensitive when roll rate was applied to the roll stick signal.

#### Aileron and Rudder Roll Reversal

Roll reversal studies were also performed on the six-degree-of-freedom flight simulator prior to first flight. Predicted roll reversal boundaries were defined to Mach = 1.3 using both aileron stick inputs and rudder pedal inputs for roll control. The results of these studies are shown in figure E17.

No aileron roll reversal was predicted over the entire flight envelope at the conditions investigated, which included a zero KRA gain and all of the stability derivative variations shown on figure E17. The simulator was, however, sluggish in roll at high angles of attack with a KRA gain of zero. Aileron roll reversal was not encountered during the flight test program.

Roll reversal boundaries obtained using the rudder pedals only for roll control are also shown in figure E17. These boundaries were not expected to cause a problem during the flight test program since the rudder pedals were not normally used for maneuvering during flight. However, rudder roll investigations conducted in flight at 0.65 Mach number and 10° angle of attack showed rudder-only roll response similar to swept wing fighters.

#### Handling Qualities Study in the Gear Down Configuration

Wind tunnel tests conducted in the Air Force Institute of Technology (AFIT) low speed tunnel at Wright-Patterson AFB used an eight percent scale model of the X-24B with and without landing gear. A comparison of the AFIT and Cornell data in the gear up configuration (see figure A27) revealed significantly lower values of  $C_{n\delta}$  (50 to 60 percent in the  $\alpha = 4$  to 16 degree range) from the AFIT tunnel. Lower values of  $C_{m\alpha}$  (30 to 40 percent) as well as lesser changes in other aerodynamic coefficients were also predicted in the AFIT tunnel. (No aileron or rudder derivatives were obtained in the AFIT tunnel.) A comparison of the gear up and gear down AFIT data showed a large reduction in  $C_{n\delta}$  (-0.00055 per degree), a small change in  $C_{L\delta}$  and  $C_{Y\delta}$ , and insignificant changes in  $C_m$  and  $C_N$  with the landing gear extended. Further wind tunnel tests indicated that the nose gear doors were a major contributor to the reduced gear down values of  $C_{n\delta}$ .

As a result of these tunnel data, a five-degree-of-freedom simulator study was conducted to assess the effect of the landing gear (and doors) on the handling qualities of the vehicle. Four sets of aerodynamic data were used in the simulator for this study;

1. Gear up Cornell wind tunnel data without any modifications.
2. Gear down Cornell data, which was gear up Cornell data with  $C_{n\delta}$  reduced by a value of -0.00055 per degree (the incremental value between the gear up and gear down AFIT data).

$$\delta u_B = -20^\circ \quad \delta r_B = -10^\circ \quad \delta a_B = 7^\circ \quad C_g = 66\%$$

NOTE: KRA GAIN WAS LINEAR - ZERO PERCENT  
AT  $\alpha = 0$  DEG AND 120% AT  $\alpha = 16$  DEG

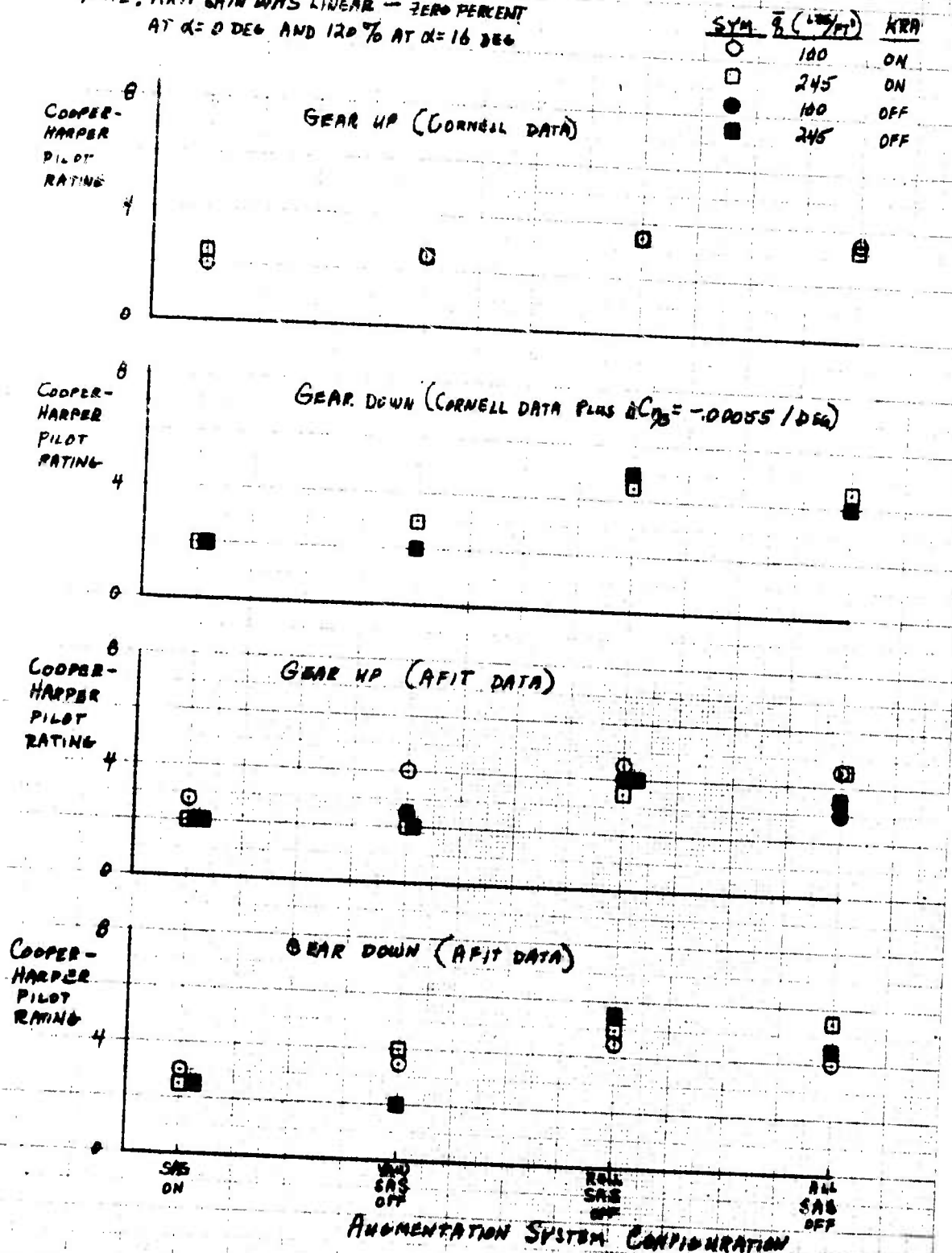


Figure E1. Landing Gear Effects on Handling Qualities

3. Gear up AFIT data in which the gear up values of  $C_{n\beta}$ ,  $C_{l\beta}$ ,  $C_{y\beta}$ ,  $C_m$ , and  $C_N$  obtained from the AFIT tunnel were used.

4. Gear down AFIT data in which the gear down values of  $C_{n\beta}$ ,  $C_{l\beta}$ ,  $C_{y\beta}$ ,  $C_m$ , and  $C_N$  obtained from the AFIT tunnel were used.

In all four cases, the rudder and aileron derivatives obtained from Cornell data were used. All data were for a control system configuration of  $\delta U_B = -20$  degrees,  $\delta R_B = -10$  degrees, and  $\delta A_B = 7$  degrees, and cg of 66 percent.

The pilots were given several tasks to perform on the simulator;

1. Roll and yaw pulses with the SAS on and off at one g flight conditions.
2. Zero to 45 degree bank angle change; hold  $\phi=45$  degrees through a 30 degree heading change and then restabilize wings level. (SAS on and off at one g flight conditions.)
3. Repeat task 2 with roll SAS off only and yaw SAS off only.
4. Check lateral PIO tendency by tracking bank angle.

Two airspeed conditions were investigated;

1.  $V_e=270$  Kts,  $\bar{q}=245$  psf,  $\alpha=6$  degrees maximum expected airspeed condition at gear extension). KRA actual=45 percent.
2.  $V_e=170$  Kts,  $\bar{q}=100$  psf,  $\alpha=12.3$  degrees (approximate touch-down condition). KRA actual=92 percent.

The results of the simulator study are summarized by the pilot ratings shown in figure E18. The poorest rating with the SAS on was 3.0 and with the SAS off was 5.5. The SAS-off rating was due to the tendency toward a lateral-directional PIO. In all cases the simulator was adequately controllable and deemed acceptable by the pilots. As was discussed previously, the actual flight vehicle proved to have very good SAS-on handling qualities during the landing flight phase.

#### Aileron-To-Rudder Interconnect (KRA) Determination

The six-degree-of-freedom flight simulator was used prior to first flight to establish the KRA gain schedule to be used in the actual vehicle. The X-24B pilots were asked to select which KRA gain they preferred at angles of attack of 4, 8, 12, and 16 degrees and at the following flight conditions:



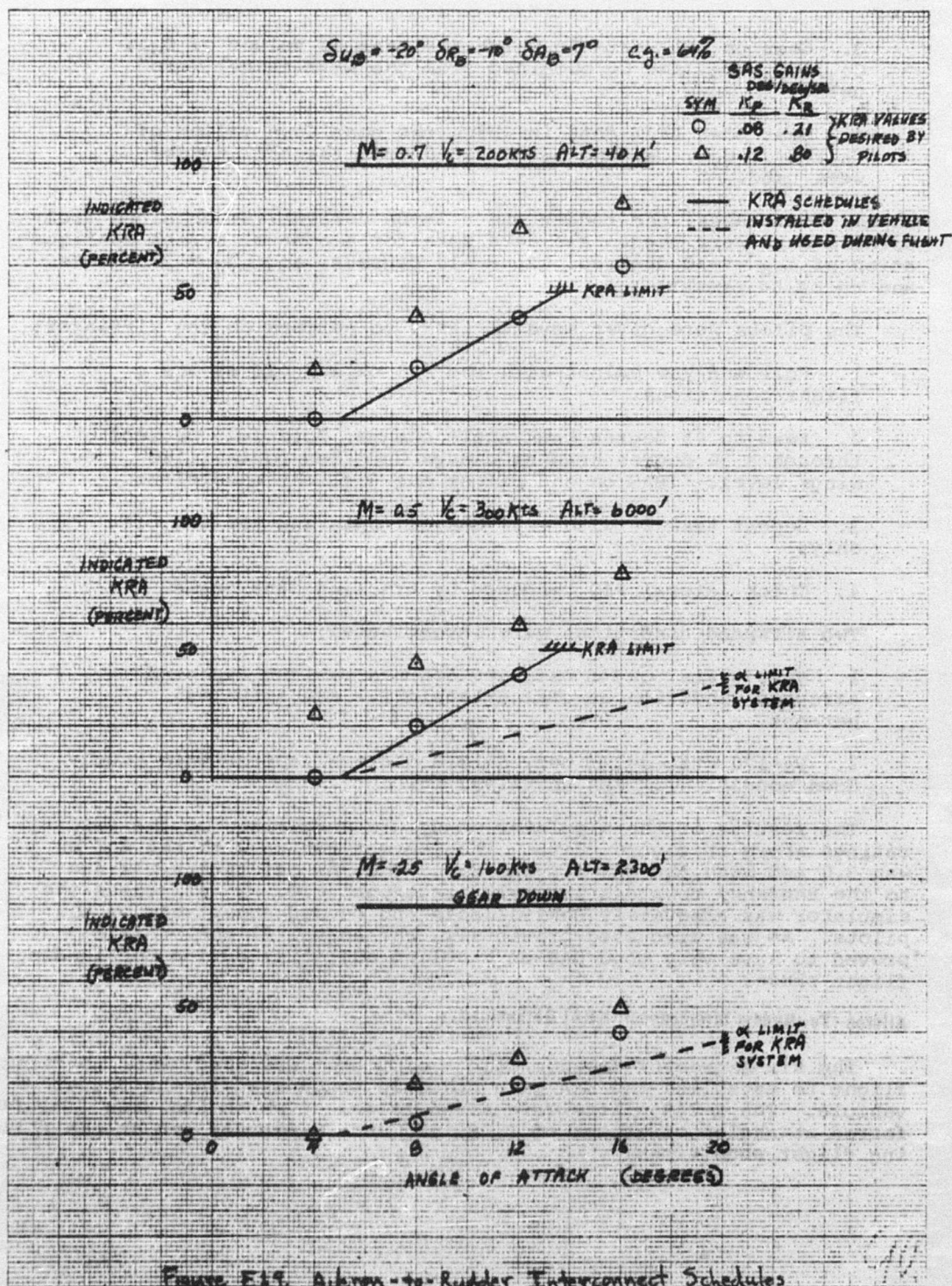


Figure E-9. Aileron-to-Rudder Interconnect Schedules

	Subsonic Glide	Approach	Landing (gear down)
Mach	0.7	0.5	0.25
$V_0$ (KB)	200	300	160

All of the conditions were for  $\delta U_B = -20$  degrees,  $\delta R_B = -10$  degrees,  $\delta A_B = 7$  degrees, and a cg of 64 percent. Two SAS gains in roll and yaw were used in the study.

The KRA gain values which pilots selected for each of the above conditions are shown as symbols in figure E19. The data indicated the pilots preferred a higher slope of KRA versus  $\alpha$  for the Mach 0.7 glide condition and the Mach 0.5 approach condition, and a lower slope during the landing flight phase. The approach phase was not extremely critical to interconnect gain, so that during the actual flight test program, the change to the lower slope was made at the beginning of approach. The data also showed that a lower interconnect gain was preferred with the lower yaw SAS gains. Since it was decided to use a yaw gain of 0.21 deg/deg/sec during flight, the data shown in figure E19 for  $K_y = 0.21$  deg/deg/sec were used to establish the KRA schedule. Based on these results, two schedules were programmed in the aircraft, a low slope of KRA versus  $\alpha$  to be used during the landing phase, and a higher slope to be used in all other regions of the flight envelope. (The higher slope determined during this study was later verified to be adequate at Mach numbers greater than 0.7.) The schedules which were selected, and which represent a best compromise of all the data obtained from the study, are shown in figure E19. A limit of 50 percent was installed in the vehicle to minimize the effect of a potential hard over of the KRA actuator on the handling qualities of the vehicle. (A high value of KRA was predicted to strongly increase the lateral-directional PIO tendencies especially at the low angles of attack.)

KRA schedules established during the simulator study proved to be adequate and were not changed.

#### SAS Gain Determination

Seven SAS switch positions were available on the X-24B in each of the three axis. These seven switch positions provided linear voltage outputs which were to be used for SAS gain values. Since the control surfaces for pitch and yaw were identical to those on the X-24A, it was assumed that the X-24A range of SAS gains would be adequate. The new ailerons, however, dictated that a simulator study be conducted to determine the range of roll SAS gain values to be used. Both maximum and minimum gain values were considered in the study. Maximum values were established by considering lateral-directional handling qualities and damping characteristics. Minimum roll SAS gains were desired for test maneuvers for stability derivative extraction, and the potential need for eliminating any control system instabilities, such as limit cycling or structural resonance which might occur.

The study was performed using the AFMTC six-degree-of-freedom flight simulator and the NASA-DPFC all-digital CONTROL program. Flight conditions investigated were;

$$\delta u_B = -40^\circ \quad \delta R_B = 0^\circ \quad \delta A_B = 7^\circ$$

$$M = 0.95 \quad \dot{\gamma} = 157 \text{ } ^\circ/\text{sec} \quad V = 920 \text{ ft/sec}$$

NOTE:

DATA IS FROM  
NASA-DTRI  
CONTROL PROGRAM

DUTCH ROLL MODE

$$\alpha = 4^\circ$$



SVA	$K_p$	$K_r$
○	0	.8
△	.1	
□	.2	
◇	.3	
▽	.4	
◻	.5	
○	.6	
○	∞	

SAS GAINS (1000/Sec)

↓

$$\alpha = 12^\circ$$



$$\alpha = 20^\circ$$

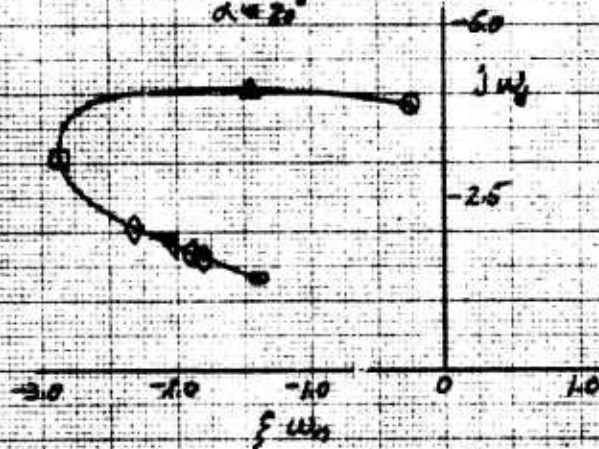


Figure E20. Dutch Roll Root Locus Characteristics



<u>Mach number</u>	<u><math>\alpha</math> (degrees)</u>	<u>Velocity (KEAS)</u>
0.5	4, 12, 16	200, 250, 300
0.8	4, 12, 16	200, 250
0.95	4, 12, 16	175, 200, 250
1.3	4, 12, 16	200, 250

The pilots performed the following tasks in this study;

1. Rudder and aileron doublets - to measure frequency and damping
2. Full aileron rolls - to measure times to bank.
3. General lateral-directional maneuvering - from which qualitative comments with regard to sensitivity, sluggishness, etc., were obtained.

Typical dutch roll mode frequency and damping characteristics as a function of roll SAS gain are shown in figure E20 for a Mach number of 0.95 and an angle of attack of 12 degrees. The migration of the roots shown in the figure was typical of most cases investigated. It showed that the roll damping increased as the gain was increased to values between 0.2 and 0.3 deg/deg/sec. Increasing the gain above these values generally tended to decrease the damping and frequency slightly.

Times to banks obtained from the full roll stick inputs were not a strong function of roll SAS gain, at least up to a gain value of 0.26 deg/deg/sec which was the maximum value investigated.

The most desirable roll gain value obtained from pilot comments for general maneuvering in the flight simulator was between 0.1 and 0.2 deg/deg/sec for all cases investigated. Increasing the gain above 0.2 deg/deg/sec did not seem to help the damping significantly. At a gain of 0.3 deg/deg/sec, the roll response appeared to be getting a bit sluggish for most cases. This roll SAS gain value was felt to be an adequate maximum for the X-24<sub>1</sub> flight envelope. The simulator indicated that the vehicle was somewhat PIO sensitive with the roll SAS off or at low values of 0.05 deg/deg/sec or less. The tendency was eliminated at gains above this value however. Thus from a handling qualities standpoint, a gain value of approximately 0.05 deg/deg/sec appeared to be an acceptable minimum. To satisfy these requirements, the roll SAS gain schedule as a function of switch position shown in figure D9 was installed in the vehicle. This gain schedule proved to be adequate for the entire flight test program and was never changed.

The pitch SAS gain chosen for the initial flights was based on a parametric study performed on the six degree of freedom simulator. Pitch tasks were evaluated at conditions of subsonic glide (.7M/200KEAS), final approach (.5M/300KEAS), speed overshoot on final approach (.5M/330KEAS) and landing (.3M/190KEAS). A pitch SAS switch position of 4 was chosen based on the best compromise between obtaining satisfactory limit cycle gain margins and achieving acceptable aircraft damping.

This gain worked well and was used for the entire research program during the landing phase. At the higher speeds attained during powered flight, increased damping was required to offset the higher pitch natural frequency. A simulator study indicated that the highest switch position would be desired. The first powered flight was flown with a switch setting of 7. For the remaining flights the setting was reduced to 6 to provide an adequate limit cycle margin in the .95 Mach area where the lower flap effectiveness was considerably greater.

Yaw rate feedback was relatively ineffective in providing dutch roll damping. Hence a yaw rate gain was chosen in conjunction with the aileron-to-rudder interconnect. High yaw SAS gain values tended to negate the KRA and produce poor turn coordination. A yaw SAS switch setting of 2 was found during simulator studies to be satisfactory for initial flights. However, prior to the first powered flight, studies on the simulator indicated that increasing the yaw gain switch setting to 3 would provide more optimum yaw damping at the higher Mach numbers and lower dynamic pressures to be experienced during the boost. This proved to be a proper selection in that the setting was used for this phase of flight throughout the program.

## list of symbols

SYMBOL	DESCRIPTION	UNITS
AEDC	Arnold Engineering Development Center	---
AFFDL	Air Force Flight Dynamics Laboratory	---
AFFTC	Air Force Flight Test Center	---
AFIT	Air Force Institute of Technology	---
$a_y$	Lateral Acceleration	g's
$b$	Reference span (19.0)	ft
$\bar{c}$	Reference chord (37.5)	ft
$cg$	Center of gravity (reference 66%)	inches or % $\bar{c}$
$C_L$	Lift coefficient	---
$C_l$	Rolling moment coefficient	---
$C_{lp}$	$\partial C_l / \partial \frac{Pb}{2V}$	per radian
$C_{lR}$	$\partial C_l / \partial \frac{Rb}{2V}$	per radian
$C_{l\beta}$	$\partial C_l / \partial \beta$	per degree
$C_{l\delta a}$	$\partial C_l / \partial \delta a$	per degree
$C_{l\delta r}$	$\partial C_l / \partial \delta r$	per degree
$C_m$	Pitching moment coefficient	---
$C_{mQ}$	$\partial C_m / \partial \frac{QC}{2V}$	per radian
$C_{m\alpha}$	$\partial C_m / \partial \alpha$	per degree
$C_{m\delta AB}$	$\partial C_m / \partial \delta AB$	per degree
$C_{m\delta e_L}$	$\partial C_m / \partial \delta e_L$	per degree
$C_{m\delta e_U}$	$\partial C_m / \partial \delta e_U$	per degree
$C_{m\delta RB}$	$\partial C_m / \partial \delta RB$	per degree
$C_N$	Normal force coefficient	---
$C_{N\alpha}$	$\partial C_N / \partial \alpha$	per degree
$C_{N\delta e_L}$	$\partial C_N / \partial \delta e_L$	per degree
$C_n$	Yawing moment coefficient	---



SYMBOL	DESCRIPTION	UNIT
$C_{Np}$	$\partial C_N / \partial \frac{Pb}{2V}$	per radian
$C_{NR}$	$\partial C_N / \partial \frac{Rb}{2V}$	per radian
$C_{N\beta}$	$\partial C_N / \partial \beta$	per degree
$C_{N\beta}^*$	Dynamic $C_{N\beta}$	per degree
$C_{N\delta a}$	$\partial C_N / \partial \delta a$	per degree
$C_{N\delta r}$	$\partial C_N / \partial \delta r$	per degree
CPT	Control position transducer	---
$C_Y$	Lateral force coefficient	---
$C_{Y\beta}$	$\partial C_Y / \partial \beta$	per degree
$C_{Y\delta a}$	$\partial C_Y / \partial \delta a$	per degree
$C_{Y\delta r}$	$\partial C_Y / \partial \delta r$	per degree
g	Acceleration of gravity (32.17405)	ft/sec <sup>2</sup>
$I_x$	Rolling moment inertia	slug-ft <sup>2</sup>
$I_{xz}$	Product of inertia	slug-ft <sup>2</sup>
$I_y$	Pitching moment inertia	slug-ft <sup>2</sup>
$I_z$	Yawing moment inertia	slug-ft <sup>2</sup>
j	Imaginary axis unit vector	---
$K_p$	Roll SAS gain	deg/deg/sec
$K_Q$	Pitch SAS gain	deg/deg/sec
$K_R$	Yaw SAS gain	deg/deg/sec
KRA	Aileron to rudder interconnect gain	deg/deg
LOX	Liquid oxygen	---
$L_{\delta a}$	$\frac{\bar{q}_{sb}}{I_x} C_{l\delta a}$	rad/sec <sup>2</sup>
M	Mach number	---
MMLE	Modified Maximum Likelihood Estimator	---
$M_{\delta eL}$	$\frac{\bar{q}_{sc}}{I_y} C_{m\delta eL}$	rad/sec <sup>2</sup>

SYMBOL	DESCRIPTION	UNIT
NASA-DFRC	National Aeronautics and Space Administration Dryden Flight Research Center	---
$N\delta_r$	$\frac{\bar{q} S b}{I_z} C_{n\delta_r}$	rad/sec <sup>2</sup>
P	Roll rate	deg/sec
PIO	Pilot induced oscillation	---
Q	Pitch rate	deg/sec
$\bar{q}$	Dynamic pressure	lb/ft <sup>2</sup>
R	Yaw rate	deg/sec
S	Reference area (330.5)	ft <sup>2</sup>
SAS	Stability augmentation system	---
SMRD	Spin Motor Rotation Detector	---
$V_t$	True airspeed	ft/sec <sup>2</sup>
$V_e$	Equivalent airspeed	knots
W	Weight	lb
$\alpha$	Angle of Attack	degrees
$\beta$	Angle of sideslip	degrees
$\Delta$	Prefix indicating increment	---
$\delta A_B$	Aileron bias position	degrees
$\delta a$	Aileron position	degrees
$\delta e_L$	Lower flap position	degrees
$\delta e_U$	Upper flap position	degrees
$\delta R_B$	Rudder bias position	degrees
$\delta r$	Rudder position	degrees
$\delta U_B$	Upper flap bias position	degrees
$\zeta$	Damping ratio	---
$\theta$	Pitch angle	degrees
$\phi$	Bank angle	degrees

SYMBOL	DESCRIPTION	UNITS
$\omega_d$	Damping frequency	rad/sec
$\omega_n$	Natural frequency	rad/sec
$\omega_o$	Break or corner frequency	rad/sec